AMERICAN UNIVERSITY OF BEIRUT

MACHINE LEARNING BASED MODELS COUPLED WITH DATA ASSIMILATION TECHNIQUES FOR PAVEMENT RUTTING PREDICTION

by
ANGELA JOSEF HADDAD

A thesis
submitted in partial fulfillment of the requirements
for the degree of Master of Engineering
to the Department of Civil and Environmental Engineering
of the Maroun Semaan Faculty of Engineering and Architecture
at the American University of Beirut

Beirut, Lebanon
September 2020

AMERICAN UNIVERSITY OF BEIRUT

MACHINE LEARNING BASED MODELS COUPLED WITH DATA ASSIMILATION TECHNIQUES FOR PAVEMENT RUTTING PREDICTION

by

ANGELA JOSEF HADDAD

Approved by:

Ghassan Chehab

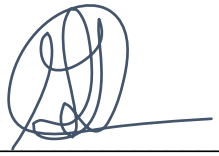

Dr. Ghassan Chehab, Associate Professor — Advisor
Department of Civil and Environmental Engineering

George Saad

Dr. George Saad, Associate Professor — Co-Advisor
Department of Civil and Environmental Engineering

Hazem Hajj

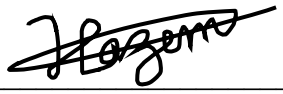

Dr. Hazem Hajj, Associate Professor — Member of Committee
Department of Electrical and Computer Engineering

Date of thesis/dissertation defense: September 4, 2020

AMERICAN UNIVERSITY OF BEIRUT

THESIS RELEASE FORM

Student Name: Haddad (Last) Angela (First) Josef (Middle)

● Master's Thesis ○ Master's Project ○ Doctoral Dissertation

☐ I authorize the American University of Beirut to: (a) reproduce hard or electronic copies of my thesis, dissertation, or project; (b) include such copies in the archives and digital repositories of the University; and (c) make freely available such copies to third parties for research or educational purposes.

☑ I authorize the American University of Beirut, to: (a) reproduce hard or electronic copies of it; (b) include such copies in the archives and digital repositories of the University; and (c) make freely available such copies to third parties for research or educational purposes
after:

One ---- year from the date of submission of my thesis, dissertation, or project.

Two ---- years from the date of submission of my thesis, dissertation, or project.

Three ☑ years from the date of submission of my thesis, dissertation, or project.

September 7, 2020

Signature Date

ACKNOWLEDGMENTS

I would like to extend my deepest and most sincere gratitude to my advisor Professor Ghassan Chehab and my co-advisor Professor George Saad for their continuous support, guidance, encouragement, and invaluable advice. Throughout my time under their supervision, they were more than generous with sharing their expertise and precious time without which this thesis would not have come forth. I have been fortunate to be their student as they consistently pushed me to improve and grow professionally and academically.

I would also like to thank my committee member Professor Hazem Hajj for investing his valuable time in reviewing my work and for his insightful advice and valuable suggestions.

I wish to thank all the people who have been with me every step of the way. This includes my family for their unparalleled love and endless support. Most importantly, I am grateful to my sister Jenny for always being there for me. Special thanks to Jad El Helou for always pushing me to explore new directions in life and aim for the best.

I would also like to express my appreciation to my friend and colleague Yara Hamdar for sharing her experience and helpful advice, as well as her emotional support when times got rough. Additionally, many thanks to my friends Hala, Ghadeer, Farah, and Amir for continuously motivating me. Achieving this milestone would not have been possible without the help of all these people.

AN ABSTRACT OF THE THESIS OF

Angela Josef Haddad for Master of Engineering
Major: Civil Engineering

Title: Machine Learning Based Models Coupled with Data Assimilation Techniques for Pavement Rutting Prediction

Rutting is one of the critical distresses affecting the safety and serviceability of flexible pavements. Modeling the progression of rutting remains a challenge due to its numerous interacting factors. There exist many empirical and probabilistic models for predicting rutting propagation in the literature. However, these models are limited by their ability to accurately simulate local conditions, their high input requirements, and their local calibration requirements. Provided the significance of predicting rutting to ensure timely and strategic maintenance interventions, this study aims at developing a framework that achieves accurate rut depth predictions and quantifies the relative contribution of the different factors. This framework is characterized by low input requirements that can accommodate data scarcity and resource limitations in local road agencies, mainly in developing countries, that are initiating their pavement management systems.

For the scope of this research, historical rutting time-series, climate, traffic, and pavement design and materials data are acquired from the Long-Term Pavement Performance database (LTPP) and employed in training a Deep Neural Network (DNN). Ultimately, a model requiring twenty-nine inputs was determined. The findings show that the developed DNN model has significantly superior performance as compared to a multiple-linear regression model developed using the same dataset, the mechanistic-empirical rutting prediction model provided in Pavement-ME, and the world bank's HDM-4 models. The model estimations were further used to capture and rank the relative importance of the different variables, which confirmed the high influence of traffic and climatic conditions. Generic family performance curves that correspond to certain traffic, climate, and mix design combinations are developed to further simplify the problem and assist road agencies that cannot acquire the data required for utilizing the DNN. Family curves introduce additional inaccuracies due to the mathematical simplifications; therefore, an Ensemble Kalman Filter (EnKF) framework is proposed to probabilistically calibrate the family models as new measurements become available.

CONTENTS

ILLUSTRATIONS

Figure Page

TABLES

LIST OF ABBREVIATIONS

AADT	Average Annual Daily Traffic
AASHTO	The American Association of State Highway and Transportation Officials
AC	Asphalt Concrete
ASTM	American Society for Testing and Materials
ATB	Asphalt Treated Base
AV	Air Voids
C.O.V.	Coefficient of Variation
DGAB	Dense Graded Aggregate Base
DOT	Department of Transportation
EnKF	Ensemble Kalman Filter
ESAL	Equivalent Single Axle Load
FHWA	Federal Highway Administration
GPS	General Pavement Studies
GR	Traffic Growth Rate
GUI	Graphical User Interface
HDM-4	Highway Development Model
LOESS	Locally Weighted Regression
LTPP	Long-Term Pavement Performance
MAAT	Mean Annual Air Temperature
MAE	Mean Absolute Error
MAPE	Mean Absolute Percentage Error

M-E	Mechanistic-Empirical
MEPDG	Mechanistic Empirical Pavement Design Guide
MERRA	Modern-Era Retrospective analysis for Research and Application
MLR	Muli-linear Regression
MMAT	Standard Deviation of the Monthly Mean Air Temperature
M&R	Maintenance and Rehabilitation
M_R	Resilient Modulus
MSE	Mean Squared Error
NCHRP	National Cooperative Highway Research Program
NN	Neural Network
NONBIT	Non-bituminous treated base
R^2	Coefficient of Determination
PATB	Permeable Asphalt Treated Base
P_b	Asphalt Binder Content
PMS	Pavement Management System
RD	Rut Depth
RELU	Rectified Linear Unit
SPS	Specific Pavement Studies

CHAPTER 1

INTRODUCTION

1.1 Background

Transportation infrastructure is critical for the economic prosperity of all nations [1]. Thousands of kilometers of paved roads are traveled daily to transport people and goods, where a total of 3.2 trillion miles were traveled on the United States (U.S.) roads in 2016 [2], [3]. Currently, more than 32% of the U.S.'s pavements are in poor or mediocre conditions costing users more than $120 billion for vehicle repair and extra operating costs [3]. The Federal Highway Administration (FHWA) estimates that a total of $170 billion in capital investment is required to maintain and improve all U.S. highways to adequate performance levels [4]. With continuous budgetary constraints and downsizing, highway maintenance and preservation is foregone for achieving short-term savings where only 60% of the annual funding requirements are being invested for these purposes [1], [5]. As a consequence, pavement management systems (PMS) have been on the rise as governments and departments of transportation (DOTs) realize the need for strategic, efficient, and cost-effective pavement maintenance and rehabilitation practices. Such practices will optimally preserve the national highway networks while minimizing the negative impacts on motorists and the overall economy [6], [7].

Traditionally, highway agencies relied on present pavement conditions and certain priority schemes in deciding their immediate maintenance needs [7]. However, with the increased maintenance costs, decreased availability of funds, shortages in energy and materials, and growth of awareness in management methods, agencies are

becoming more interested in developing strategic and systematic decision support systems that are capable of managing, planning and allocating budgets based on advanced economical and engineering concepts [6], [7].

In order to achieve such objectives, developed pavement management systems must rely on reliable data collected from continuous evaluation and monitoring of the roadway networks as well as future condition prediction processes to forecast pavement needs before the pavement fails [2], [7]. The use of such systems was further emphasized by the Moving Ahead for Progress in the 21st Century Act (MAP-21), which requires all states to develop asset management systems capable of providing supporting information that justifies proposed investments [8], [9]. MAP-21 provided the legislative platform that mandates transportation asset management systems to include consistent data collection methodologies, deterioration models, potential work types and their effect on performance and management strategies to minimize life-cycle costs [10]. Thus, deterioration modeling and condition data collection in the context of pavement management are crucial for establishing effective PMS.

With time, the pavement performance deteriorates mainly due to traffic loading and weather conditions [6]. As such, a good PMS should have the capacity of forecasting deterioration as a function of age or accumulated traffic as well as other relevant variables. The latter will ensure timely maintenance interventions, preserve the required level of performance of the pavement network, and guarantee significant budget savings [11], [12]. In addition to their pivotal role in PMSs, accurate performance prediction models allow for quantifying the contribution of relevant variables on pavement deterioration, which in turn has significant implications on road pricing and regulation [11], [13].

Evident signs of pavement deterioration include the manifestation and development of distresses such as cracking and rutting that reflect a reduction in the functional or structural performance [14]. Repeatable measurements and collection of pavement distresses such as cracking and rutting, as well as structural properties are indispensable since current and historical performance trends are required for developing deterioration prediction models. These models either predict an overall condition index or individual distress indices [6], [14]. While forecasting the progression of specific distresses is more complex, it introduces further insights about the specific corrective actions required based on the prevailing defects [11], [15].

Asphalt rutting is one of the most critical distresses affecting the performance of asphalt concrete (AC) pavements. Rutting results from the accumulation of permanent deformations or depressions along the wheel-path. The rutting behavior is characterized by three distinct stages; primary, secondary, and tertiary. The primary stage corresponds to the rapid densification of newly constructed asphalt layers followed by a reduction in the rate of rutting during the secondary stage, after which high rutting progression rates corresponding to shear failure are observed in the tertiary stage [16]. Rutting is a major concern due to its impacts on road safety and serviceability [16]. The presence of rutting endangers the safety of road users due to its hydroplaning potentials, where water accumulates in the ruts resulting in the loss of contact between the pavement and the vehicle tires, as well as steering problems [17], [18]. In addition to the safety concerns, rutting is a major economic burden on road agencies since it cannot be addressed by low-cost preventive maintenance activities. Therefore, substantial costs are incurred when rutting occurs in in-service pavements due to the need for major maintenance and rehabilitative treatments [19].

Provided its significance, PMSs rely heavily on rutting depth prediction. The prediction of asphalt rutting through accurate deterioration models is essential for forecasting the progression of rutting and developing maintenance and rehabilitation plans for transportation networks [20]. As a result, transportation agencies have been widely calibrating or developing deterioration models that aid in maintenance and rehabilitation planning, and fund allocation [21].

1.2 Problem Statement

Models have been developed by several DOTs such as those of Mississippi, Minnesota, North Dakota, and Oklahoma [21], [22]. In the current state of practice, performance models are commonly developed based on deterministic or probabilistic approaches. The former is further subdivided into empirical and mechanistic-empirical (M-E) models [23]. Empirical models are data-intensive techniques relating pavement performance (e.g., rut depth) to a set of variables (e.g., age, traffic, temperature, and pavement structure) [21]. They are typically based on regression analysis where the mathematical form of the model is predefined, which may not be practical due to the lack of knowledge on the interaction between inputs. M-E approaches can also be used to relate pavement mechanical responses such as strains and deflections to distresses using empirical transfer functions. The most commonly accepted M-E rutting prediction model is the plastic strain relationship, which emerged from the NCHRP Project 1-37A [16]. However, the globally calibrated model tends to over-predict rutting resulting in additional local calibration requirements [24]. While these models can be refined and used for pavement management, they require a daunting set of inputs that may not be available or are of poor quality in regions outside the United States due to the lack of

budgets and expertise. Furthermore, local calibration may not be feasible in developing countries where historical data is unavailable. Neural Networks (NNs) have also been studied to deal with the challenges imposed by the predetermined mathematical models and calibration requirements of the deterministic models [25]–[27]. However, these models were not trained using large datasets, and their applicability is restricted to the locality of their development.

Although much research has been conducted on rutting deterioration models and several models have been proposed, their application in PMS remains complicated, tedious, and suffers from inherent inaccuracies [2], [6]. Modeling asphalt rutting faces profound challenges due to its sensitivity to the local microclimate and a large number of interacting factors. Additionally, developing such models requires large sets of field data that take into account the uncertainties of the input variables [17], [18]. As such, accurate prediction models with sufficient generalization abilities, that allow the identification of significant milestones in the pavement's life, are still not available [28]. This is particularly challenging for transportation agencies in developing countries that lack adequate technical and financial resources for collecting materials, traffic, and climate properties that affect pavement performance. Additionally, with the absence of extensive datasets holding historical pavement condition data, initiating PMS with reliable deterioration models remains a difficult task.

1.3 Research Objective

To address the previously discussed limitations, this thesis aims to develop an accurate rutting prediction model that requires a limited number of input parameters

without the need for local calibration. Within this context, the specific objectives of this thesis are as follows:

1. Develop universal regression models using Neural Network techniques that predict rutting depth along with the pavement's lifespan. Employing such models alleviates the need for the pre-specification of the mathematical form of the model and implicitly takes into account the interaction between the different features. These models are also developed using a low number of input features to accommodate data scarcity and resource limitations in developing countries that are initiating their pavement management systems. For the scope of this study, the data used to develop the models is extracted from the Long-Term Pavement Performance (LTPP) database.
2. Identify the relative importance of the different features on rutting prediction to assist road agencies in planning and minimizing the expenses associated with data collection.
3. Develop a framework that updates and improves the developed rutting models to minimize the mismatch between predicted and measured rut depths. This particularly targets road agencies that are initiating their PMS and do not have sufficient information to utilize the model developed as part of the first objective. This involves employing an Ensemble Kalman Filtering (EnKF) approach as local field experiments and new data become available.

1.4 Thesis Organization

This thesis is divided into eight chapters.

- Chapter 2 provides background information about PMSs, pavement condition evaluation, and rutting development mechanisms. It also discusses and evaluates the current state of practice regarding rutting deterioration models.
- Chapter 3 presents a brief overview of the LTPP database as well as the modeling and analysis methods that contribute to the study objectives.
- Chapter 4 details the methodology followed to synthesize the dataset, develop the required models, and introduce the EnKF updating framework.
- Chapter 5 discusses all the pilot studies and troubleshooting efforts that are required to achieve the final results.
- Chapter 6 presents the final model results and discusses the sensitivity of the model to the input variables. It also examines the requirements and outcomes of the EnKF framework.
- Chapter 7 showcases the graphical user interface (GUI) that was developed to deploy the NN model.
- Chapter 8 summarizes the research contributions, results, limitations, and recommendations for future research.

CHAPTER 2

LITERATURE REVIEW

2.1 Pavement Management Systems

2.1.1 Overview on Pavement Management Systems

The twentieth century was characterized by the shift of transportation agencies from the emphasis on expanding the roadway networks to managing the existing infrastructure [6]. The concept of pavement management has been studied and expanded since the 1970s; however, practical employment of such management processes remained limited [29]. Much of the interest in pavement management originated from the realization of road agencies that the investment of billions of taxpayer dollars on the maintenance of pavements requires sound management to achieve cost-effective solutions that maximize long and short-term benefits of the limited funds [7], [30]. Emphasis has increased over the last few decades as budgets became more limited and incapable of attending to the rapidly deteriorating performance, and as accountability in transportation investments became stricter [31].

An additional factor that promoted the application of performance-based management practices, specifically in the United States, is the requirement to adopt strategic and systematic methods for operating, maintaining, and improving transportation assets to sustain adequate performance at minimum cost for pavements and bridges on the National Highway System (NHS). This requirement was enforced in 2012 through The Moving Ahead for Progress in the 21st Century Act (MAP-21) [8].

The American Association of State Highway and Transportation Officials (AASHTO) defines pavement management as the set of tools that aim at providing optimum strategies for maintaining the serviceability of pavement conditions over time and supporting road agencies in the decision-making process. In a broad sense, PMSs encompass all the functions involved in assessing past, current and future pavement conditions, optimizing funds allocation in terms of planning pavement maintenance and rehabilitation, estimating and justifying funding needs, and evaluating the outcomes of different alternatives. These functions contribute to more economically efficient management strategies [29].

2.1.2 Pavement Management System Levels

Pavement Management Systems are used to assist in decision making at three levels: strategic, network, and project levels [7], [29]. The strategic level involves the least detail and is utilized by policymakers to devise long-term strategic decisions regarding performance targets, funding allocations, and performance preservation strategies [7], [29]. Network-level management involves more detailed analyses of current and future network conditions and overall network needs in order to evaluate different investment strategies and develop multi-year network improvement plans [7], [29]. Project level analysis focuses on short-term decisions for a specific part of the network. Decisions made at this level are based on more sophisticated and reliable data collection activities to evaluate material properties, traffic levels, and environmental factors. The obtained information is used to recommend immediate maintenance treatments, perform required pavement design for rehabilitation projects, and select maintenance material types [7], [29], [32].

2.1.3 Pavement Management System Components

A PMS is comprised of three key modules including, but not limited to, an inventory or database module, an analysis module, and a reporting module. The inventory module stores all the related pavement information such as road network details, traffic data, pavement design, maintenance history, and historical pavement condition data. This database serves as a basis for the analysis module [29]. The analysis component involves predicting future pavement conditions for the entire network or a specific project based on pre-defined deterioration models, evaluating the effect of different pavement treatments, making decisions based on objective rules, and quantifying the economic and financial requirements of different strategies [10], [29], [32], [33]. The outcome of these tasks including the different funding levels, maintenance recommendations, and future condition estimates are reported and used to backup future projects and funding requests. The final component includes a feedback process to keep the databases up-to-date in response to any changes in the network, update and recalibrate deterioration models, and adjust the unit costs of the treatment activities [10], [29], [32], [33].

2.2 Overview of Pavement Performance Indicators

Defining pavement performance deterioration is fundamental for managing pavement networks and identifying treatment needs. The overall pavement condition is typically a combination of structural and functional characteristics [29]. Pavement conditions that directly influence the safety and serviceability of a roadway network reflect the pavement's functional performance, while the extent of pavement damage that limits its capacity to carry traffic loads is considered a structural characteristic [34].

Pavement performance is evaluated based on four key aspects including surface roughness, surface distresses, structural capacity, and safety [29], [35]. The extent of data collection for evaluating pavement conditions varies between network and project levels. Functional characteristics do not provide sufficient information to describe the overall pavement condition, therefore the structural performance is required for project-level decisions [36], [37].

Pavement roughness strongly correlates to motorists' comfort and satisfaction with the ride quality. Pavement roughness refers to the unevenness of the pavement's longitudinal profile arising from construction imperfections or performance-related distortions that result in a rough pavement-vehicle interaction [29], [35]. The International Roughness Index (IRI) is the most internationally used index to reflect pavement roughness [29], [35], [38].

Pavement surface distresses are indispensable factors for evaluating pavement performance and selecting maintenance treatments [35]. Each distress type is a visible damage on the pavement surface that reflects the existence of performance problems [29]. Information regarding prevalent distresses on a pavement's surface are measured through visual manual or automated surveys [29], [32], [35]. Distresses on AC pavements include different types of cracks, ruts, potholes, patches, and other surface defects [39]. There exists no universal approach for characterizing pavement performance as affected by prevalent distresses [29]. As a result, pavement performance can be evaluated in terms of the extent and severity of each distress, individual distress indices that are linked to general treatment categories (i.e. distresses that prompt the same treatment are included), and overall indices such the Pavement Condition Index

(PCI), the Surface Distress Index (SDI), and the Pavement Surface Evaluation and Rating (PASER) [21], [35].

The structural capacity is described as the pavement's ability to carry traffic loads and is obtained through destructive (e.g., material sampling) and non-destructive testing (e.g., Falling Weight Deflectometer). Current structural capacity indices describe the maximum load-carrying capacity of a pavement or its remaining service life [35].

Pavement safety aspects are described by the condition of the surface texture and skid resistance. The interaction between the pavement surface and tires and its impact on safety is measured using several indices such as the Friction Number (FN) or the Skid Number (SN) [29], [35].

Pavement condition can also be summarized by a single overall index that combines roughness, distresses, structural capacity, and safety factors. Overall indices are agency-specific and reflect its information needs and experiences to provide high-level performance indications to be used at the network and strategic levels [21], [35].

2.3 Rutting as a Pavement Distress

2.3.1 Rutting Overview

The pavement community's concern with the importance of the safety and serviceability impacts of rutting originated in the mid-1950s as part of the AASHO road test project [40]. Rutting is characterized by surface depressions in the wheel-path stemming from the accumulation of permanent deformations in the asphalt concrete (AC) and/or the subgrade layers as a function of load repetitions. As such AC

pavements are prone to the development of two types of rutting referred to as subgrade or base rutting and asphalt rutting [18], [41].

Rutting in the subgrade arises from structural deficiencies due to the absence of proper drainage measures, under-design in layers thicknesses for the existing traffic volume and loads, insufficient compaction, or inappropriate construction processes. These deficiencies render the pavement's structure unable to support vertical stresses on top of the subgrade and consequently result in the densification of the base, sub-base, or subgrade layers. Subgrade rutting can be avoided by increasing pavement thickness, improving the stiffness of the materials constituting the various layers, stabilizing the subgrade layer, as well as improving drainage conditions [18]. Since the causes and solutions of this type of rutting are well defined and easily tractable, it is typically successfully addressed in the design process. Consequently, it is not a major concern for pavement managers and maintenance decision-makers [18], [41].

On the other hand, asphalt rutting reflects deformations in the asphalt layers and appears as longitudinal depressions in the wheel-paths accompanied by small upheavals to the sides resulting from a combination of densifications and shear deformations [42]. Unlike subgrade rutting, asphalt rutting is the result of a more complex mechanism that is affected by the local microclimate, material variability, as well as other interacting factors. Hence, asphalt rutting remains one of the most important, challenging, and common distresses making it the focus of this study [17], [18]. The following chapters will focus on the asphalt rutting mechanism.

The behavior of permanent deformation is characterized by three distinct stages (Figure 1) [43]. The first phase is referred to as the primary stage and is characterized

by the rapid accumulation of permanent deformation which reflects unrecoverable strain caused by volumetric change due to densification. Initially, this phase starts with a high strain rate that decreases as the permanent strain approaches the secondary stage where it remains constant [43]. Volumetric changes continue in the secondary stage; however, shear deformations are also observed [44]. In the tertiary stage, permanent deformation accumulates at an increasing rate, reflecting excessive shear deformations in the absence of volume reduction [44]. The number of load repetitions to reach the tertiary zone is referred to as the "Flow Point" or "Flow Number" and it represents the cumulative traffic loading required for failure [43]–[45].

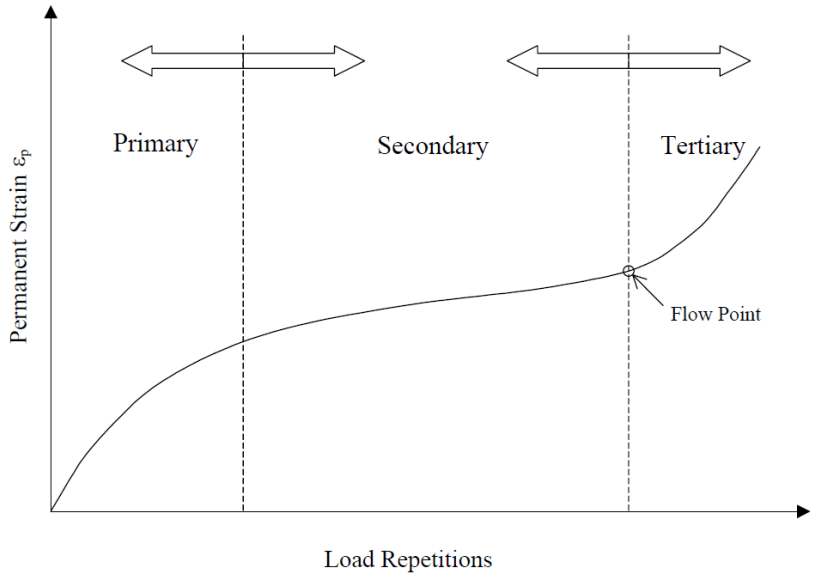

Figure 1: Typical Permanent Deformation Behavior of Pavement Materials as a Function of Repeated Loads [43].

2.3.2 Factors Affecting Asphalt Rutting

The sensitivity of the rutting mechanism to different variables has been studied through laboratory experiments and analysis of field data over several decades. More than thirty interacting factors that influence rutting with varying levels have been identified [17]. These inputs fall under three categories: material properties, traffic loading, and climatic conditions. A study conducted on data collected from Iowa's DOT concluded that temperature has the highest effect on rutting, followed by pavement thickness and age [46]. Other studies conducted on data collected in China found that age and maintenance information significantly affect rutting predictions, while traffic had a lower impact [27]. Random forest analysis proved that air voids, traffic, precipitation, thickness of the base, and percentage of aggregates retained on the 3/8-inch sieve are among the most influencing factors [47]. Schwartz et al. established that asphalt mix dynamic modulus, binder performance grade, pavement thickness, and traffic are the most influential contributors to rutting [48]. Results of an earlier study on LTPP data revealed that presumably thin pavements exhibit more rutting. However, the effect of base layers properties, climatic conditions, and subgrade types was found to be insignificant [49]. Results of laboratory testing using the Hamburg-Wheel tester and the Asphalt Pavement Analyzer (APA) were also studied in [50], [51]. Based on these analyses, asphalt mixture properties such as the dynamic modulus, percentage of air voids, asphalt content, asphalt binder grades followed by temperature, and traffic conditions were identified to impact rutting. Most of the reviewed studies exhibited inconsistent conclusions regarding the main factors that need to be considered to predict rutting accurately. Additionally, there is a lack of consensus in the literature regarding

the extent of the contribution of each variable and its effects on the performance of prediction models.

2.3.3 Rutting Indices

Several indices were developed to characterize and quantify rutting [52]. Two primary categories of indices that characterize rutting either in terms of area or depth were calculated as part of the Long-Term Pavement Performance Program (LTPP) [52]. The positive and negative area indices represent the areas above and below a straight line connecting the transverse profile's start and end points. The fill area index represents the total area delineated by straight lines connecting the peak elevations along with the transverse profile. The main advantage of the latter index is that it reflects the material quantity requirements for rut filling projects. The water depth index reflects the direct safety implications of rutting related to water ponding and corresponding accident potential. Finally, the rut depth (RD) is the most universally applied index. RD is the maximum vertical distance between the bottom of the rut and wireline or a straightedge as defined by ASTM E1703 [42], [52].

2.4 Rutting Considerations for Pavement Management

2.4.1 Maintenance Thresholds

Rut depth intervention levels or threshold values refer to the rut depths that trigger relevant maintenance treatments [53]. These values are commonly used by DOT personnel, specifically maintenance decision-makers; however, to-date, there does not exist a consensus regarding the assessment of rutting severity and its implications on

maintenance and pavement management in general. In fact, most highway agencies classify rutting severity based on their respective experience [54].

Regardless of the exact values, information regarding current and forecasted rut depths is crucial for efficient maintenance planning and scheduling [55]. The Mechanistic-Empirical Pavement Design Guide (MEPDG) suggests a maximum allowable rut depth of 10 mm for interstates and 13 mm for primary roads, while Austroads considers a terminal rut depth value of 20 mm [56], [57]. Rut depths exceeding these limits compromise road user safety due to elevated hydroplaning risks. Additionally, the FHWA encourages State DOTs to take action even before these limits are reached [55]. For example, AASHTO's Guide Specifications for Highway Construction suggests that a rut depth of 6 mm prompts milling and resurfacing, while a depth of 13 mm requires removing the entire distressed area [58]. On the other hand, maintenance is triggered for rut depths exceeding 25.4 mm in Caltrans [59].

Some DOTs base their maintenance decisions on the rutting severity instead of a fixed trigger value. In the current state of practice, three rut depth severity levels are developed and defined in ASTM D6433 regardless of maintenance [60]. The low severity category includes rut depths between 6 and 13 mm, medium severity encompasses rut depths between 13 and 25 mm, and high severity rutting is attributed to rut depths that exceed 25 mm. However, ruts that are shallower than 6 mm are not typically counted as pavement distresses [61]. There are significant discrepancies in the severity level classifications as presented in Table 1. In addition to rating levels in practice, critical rut depth values were studied by numerous researchers. Most studies concluded that a rut depth greater than 12.7 mm poses safety risks on travelers, while others stated that a depth of 5 mm is sufficient for creating hydroplaning threats [53].

Table 1: Rutting severity levels used in international practice.

Road Agency	Rutting Severity Levels	References
Illinois DOT Maryland DOT NC DOT	Low: <12.7 mm Medium: 12.7 – 25.4 mm High: >25.4 mm	[62] [63] [64]
Nevada DOT	Low: <5 mm Medium: 5 – 10 mm High: >10 mm	[65]
Texas DOT	Shallow: 6 – 13 mm Deep: 13 – 25 mm Severe: 25.4 – 50.8 mm Failure: > 50.8 mm	[66]
Washington DOT	Low: 6.3 – 12.7 mm Medium: 12.7 – 19.1 mm High: >19.1 mm	[67]
Arizona DOT	Low: 0 – 6.3 mm Medium: 6.3 – 12.7 mm High: >12.7 mm	[68]
British Colombia Ministry of Infrastructure	Low: 3 – 10 mm Medium: 10 – 20 mm High: >20 mm	[69]
Ontario Ministry of Transportation	Very Slight: 3 – 6 mm Slight: 7 – 12 mm Moderate: 13 – 19 mm Severe: 20 – 25 mm Very Severe: >25 mm	[70]

2.5 Pavement Performance Modeling

2.5.1 Overview and Significance of Pavement Performance Models

Pavement performance modeling, also referred to as pavement deterioration prediction serves as an essential pillar in the pavement management process. Performance prediction is considered a prerequisite for establishing most PMS outputs including maintenance treatment strategies and priority programming [71]. Pavement performance models are defined as mathematical representations to forecast the change in pavement conditions as a function of traffic and environmental conditions [72].

Pavement management systems which originally did not include a predictive component, have historically evolved to include simplistic models that are based on engineering judgment. Later, complex models that relate pavement performance to multiple variables based on condition survey data and regression analyses were utilized. However, achieving reliable models is complicated due to the involvement of a large number of parameters [71]. Currently, research is shifting towards employing artificial intelligence concepts to improve pavement performance modeling and overcome the existing challenges [72].

Deterioration models can be developed to predict several aspects of pavement performance including distresses, individual indices, or overall composite indices as described in section 2.2. A decision regarding which index to predict depends on the objective of the model and the management level (project or network). While predicting overall indices provides a general overview of pavement performance, it does not provide sufficient information to develop maintenance and rehabilitation strategies since different distress combinations can produce the same value of the index. On the other hand, predicting the extent and severity of each distress is a highly complicated and data-intensive approach. A more realistic approach involves predicting individual indices that reflect a combination of severities to allow pavement managers to estimate future maintenance needs and action times [21], [29].

2.5.2 Rutting Deterioration Models

The models used to predict and assess pavement performance are classified into three main categories: deterministic, probabilistic, and neural network models

(Wolters and Zimmerman, 2010). This section includes a review of the different modeling techniques used in the context of rutting prediction.

2.5.2.1 Deterministic Models

Initial attempts for rutting prediction were heavily based on deterministic models that use regression analysis to generate linear relationships between rutting and its influencing factors [21]. Among the most used models are the Highway Development and Management models (HDM-4), which were developed by the World Bank to assist developing countries in implementing PMS and optimizing maintenance strategies [6], [73]. The main inputs required by these models include strength related parameters, thickness, traffic, speed, construction quality, and calibration factors [74]. These models were derived from a sample of 2,546 data points obtained from a UNDP study conducted in Brazil. Therefore, they require local calibration to provide reliable predictions [75]. However, local calibration requires time-series rutting data from field surveys because the HDM-4 does not take asphalt material properties directly into account [73], [76]. Such data is not typically available in transportation agencies, especially in developing countries. Other empirical models implementing multi-linear or non-linear regression were later developed to predict rutting for several DOTs in North America, such as that of Arkansas, Mississippi, Minnesota, and Oklahoma [21], [22], [77]. The Mississippi DOT developed a power regression model to predict rutting based on three years of field data stored in its inventory. The resulting models did not yield satisfactory predictions and were not able to capture the effect of material properties on rutting [22]. Similar efforts were also conducted by Arkansas DOT that applied linear regression using only age as an explanatory variable. This model also resulted in poor

predictive performance [77]. In addition to the United States, deterministic models that predict the accumulation of rutting over time as a function of traffic, the Thornthwaite Moisture Index, and the subgrade strength were developed by Austroads for the Australian pavement network [78].

To improve the existing empirical approaches that were not able to achieve satisfactory results, the Mechanistic-Empirical Pavement Design Guide (MEPDG) was developed [16]. The MEPDG uses a Mechanistic-Empirical (M-E) model for rutting prediction that empirically correlates mechanistically calculated pavement responses (stresses, strains, and deflections) to field manifested distresses (i.e., rutting) [16]. The corresponding model uses a thorough set of inputs representing three main influencing criteria: climate, traffic, and material properties [6]. Although this model was able to achieve better results than the previous empirical models, studies have shown that it requires significant calibration efforts to adhere to site-specific conditions [24]. Also, it requires many inputs that are either not available or difficult to collect since they require advanced testing [79]. As for any regression model, and in addition to the previous limitations, the effectiveness of both the empirical and M-E models depends heavily on the engineer's ability to comprehend the mathematical form beforehand. Moreover, due to the large number of variables and the complex way in which they affect one another, simple regression is insufficient to recognize the trends in empirical data resulting in underestimated errors [80]. The MEPDG model, however, remains the most commonly used for rut depth prediction because it is the only model that allows generalization in opposition to other models developed for specific DOTs and because it is available to the public through a software package.

2.5.2.2 Probabilistic Models

Inaccuracies in the M-E models may be attributed to the variability in parameters and the uncertainties in the model itself. This problem was addressed by introducing probabilistic models, which consider pavement conditions to be random variables [6], [23]. Markov models have been used extensively in pavement deterioration applications [23], [81]. These models rely on transition probability matrices (TPM), which describe the probability of deteriorating from one condition to another [23]. These probabilities are obtained from historical field condition data or may be based on expert knowledge. Saha et. al. have used a discrete-time Markov process to develop rutting prediction models for low-volume roads in Colorado based on five years of field data. This model performed better than the previous deterministic models [82]. However, this modeling approach does not consider the time dependency of the rate of rutting progression along the analysis period. The time dependency of the deterioration rate was considered in [83] through using five-year staged time-periods having different TPMs. However, implementing the latter approach entails more complexity and requires more data [23]. Additionally, Markov models have several shortcomings related to the requirement of discretizing rutting depth and the restricted generalization ability as they do not explicitly consider how different predictors (e.g., levels of traffic, environmental exposure, pavement materials, or structural deficiencies) affect rutting. These restrictions limit the use of probabilistic models for developing rutting prediction models.

2.5.2.3 Neural Network Models

More recently, the application of machine learning, specifically artificial neural networks (ANN) in pavement applications has been explored [84]. Yang et al. were among the first to develop an ANN model to forecast pavement surface conditions (i.e., crack, ride, and rut indices) for different time intervals for the Florida highway network [27]. Although the proposed model showed more accurate predictions than traditional linear regression models, it presented several shortcomings. The rutting index could only be forecasted up to a 5-year interval, and the model required knowledge of the current and all past values of this index. Similarly, an ANN model was developed in [26] to predict rutting for low volume roads in India. The model utilizes the current rutting depth (at the time of prediction) as an input to forecast the rut depth at the next time-step. The comparison with the previously calibrated HDM-4 model in India reveals the superiority of the new ANN model [85]. However, the model only considered subgrade material properties, while other features related to the asphalt and base layers that are key contributors to rutting were neglected. In [25], data corresponding to eleven expressways in China was used to develop a rutting prediction model. The model fails to account for environmental and subgrade conditions since these factors were similar for all the studied roads. Deep neural network models were developed in [47] based on a broad set of input variables (i.e., material, climate, traffic parameters, and pavement deformations). Compared to the predictive performance of a multi-linear regression model developed using the same dataset, the deep NN model achieved significant improvements in terms of mean squared errors of up to 50% [47]. However, because of their limited dataset, the authors did not have a hold-out set for testing, and they only relied on four-fold cross-validation [47]. Therefore, the generalization performance of

the model is not well proven, and the model's ability to achieve superior prediction accuracy without overfitting is questioned.

2.5.2.4 Updating Existing Pavement Deterioration Models

Several inevitable issues regarding the unobserved heterogeneity of pavement performance data, inherent variability in the measurement of distresses, the small number of available observations, and uncertainties within the adopted mathematical models have detrimental effects on the reliability and applicability of pavement deterioration prediction models [86], [87]. Consequently, AASHTO's Pavement Management Guide emphasizes the importance of periodically reviewing the adopted models to ensure a proper representation of the prevalent deterioration trends and the continuous improvement in the efficiency of the management system [29]. Since highway agencies with well-developed PMS or those initiating pavement management collect pavement condition data on an on-going basis, the newly available data could be used to update and enhance the existing models [23]. Bayesian approaches have been adopted by several researchers to perform model updates. One of the earliest implementations of such frameworks was conducted by Li in 1997 to update transition probability matrices used to predict deterioration using a Markov process at the end of each year [88]. An enhancement of the AASHO deterioration model was also introduced through the application of a Bayesian updating approach [89]. Park et al. also proposed a Bayesian data analysis tool that provides a sound engineering and statistical framework for updating distress prediction [87]. A case study was conducted on highways in Texas, where generic deterioration curves were updated when road-specific data were obtained [87].

CHAPTER 3

THEORETICAL BACKGROUND

3.1 Data Sources

The Long-Term Pavement Performance (LTPP) database is the most comprehensive database that encompasses a wide range of pavement distress, material, climate, and traffic data. It was founded in 1991 by the Federal Highway Administration (FHWA) as part of the Strategic Highway Research Program (SHRP) [55]. The purpose behind the development of the LTPP program was to support pavement and transportation researchers' needs for data while reducing the time required for data collection. Additionally, the LTPP program was also established to evaluate the long-term performance of pavements provided different structural designs, materials, maintenance activities, traffic loads, and climatic conditions [90].

The total number of pavement sections that are monitored by the LTPP program exceeds 2,500 sections located in North America [91]. The LTPP hosts two types of experiments, generally known as the general pavement studies (GPS) and the specific pavement studies (SPS) that cover asphalt concrete (AC) and Portland cement concrete (PCC) pavements. SPS sections are specifically constructed for monitoring purposes and for evaluating the effects of different engineering factors. In contrast, the GPS sections include existing roadway sections that have been incorporated into the LTPP program or SPS sections that underwent maintenance and rehabilitation. The SPS category consists of a total of ten different experiments that study the influence of structural factors, preventive maintenance, rehabilitation, environmental factors,

Superpave specifications and mix design, and warm mix asphalt overlays on the performance of flexible and rigid pavements. For each of the latter experiments, the pavement performance is examined by collecting data on distress, roughness, structural capacity, traffic, and other variables [91]. Typically, SPS project sites include several coexisting test sections, each having different characteristics depending on the factor whose effect is being tested. On the other hand, GPS project sites include only individual test sections. The typical layout of SPS and GPS sections is illustrated in Figure 2.

3.2 Data Analytics and Modeling

3.2.1 Overview of Neural Networks

Artificial neural networks are models inspired by the biological neuron system and are currently being used to solve problems in all fields [92]. Artificial Neural Networks (ANN) are nonlinear statistical data modeling techniques capable of capturing

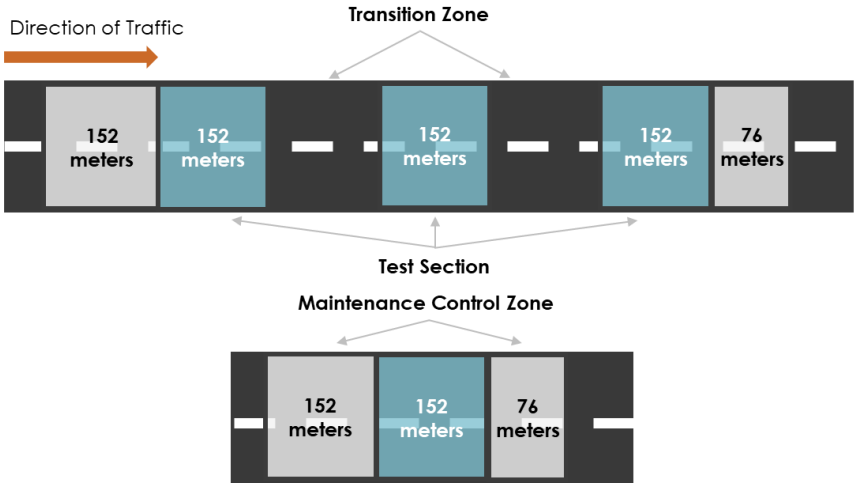

Figure 2: SPS and GPS site layout.

complex relationships between inputs and outputs. As a result, ANN models have the ability to identify meaningful patterns from noisy data commonly encountered when developing performance models [93]. NN's are defined as an assembly of interconnected processing units. These units are driven by the weights of the connections between them, and their functionality is determined by the learning method, architecture, and the neuron activation function [94]. Two main classes of neural networks are distinguished: feedforward NN, which presents the output as a non-linear function of the inputs, and recurrent NN, which are used to model time sequence data where the output is also a function of its past values [95]. Feedforward networks are commonly used to solve most engineering problems [96].

Training the NN is achieved by altering the weights of the connections between the units to minimize model errors using the backpropagation approach. Supervised learning through backpropagation consists of a forward pass, which involves processing inputs in the network based on random weighting factors to calculate the outputs. It also includes a backward pass that handles the predicted outputs compared to the actual ones provided by the training data to adjust the weights and minimize errors in the prediction [97]. The network's architecture refers to the number of inputs, outputs, hidden neurons, and layers whose interconnection contributes to the computational power of the NN. On the receiving end of each neuron, weighted signals are summed to contribute to its activation through predefined activation functions. Activation functions ensure a non-linear relationship between the input and output neurons. Applying non-linear activation functions can help the network learn complex patterns and provide more accurate predictions. The most common activation functions used in feedforward network analyses are the sigmoid function $logh(z)$, the rectified linear activation

function $ReLu(z)$ and the hyperbolic tangent function $\tanh(z)$, which are mathematically described as [98]:

$$logh(z) = \frac{1}{1 + e^{-z}} \quad \textbf{(1)}$$

$$ReLu(z) = \max(0, z) \quad \textbf{(2)}$$

$$\tanh(z) = \frac{e^{z} - e^{-z}}{e^{z} + e^{-z}} \quad \textbf{(3)}$$

Where z is the output from the previous layer.

The number of neurons in the hidden layer and the number of layers are generally determined by trial and error, where the network that achieves an optimal performance is selected [99]. The performance of regression models is evaluated by the coefficient of determination (R^2), the mean square error (MSE), the mean absolute error (MAE), and/or the mean absolute percentage error (MAPE) [99]. One hidden layer could be highly efficient in modeling complex functions if the number of selected neurons was large enough and depending on the complexity of the problem at hand. Increasing the depth of the NN becomes essential as the complexity of the problem increases. However, the bigger the number of hidden layers, the higher the risk of overfitting the data [100]. Once the network training is completed, an independent out-of-the-bag testing dataset is used to validate the model's generalization potential [99].

3.2.2 Feature Engineering and Feature Importance

Although NN models exhibit superior performance compared to traditional modeling techniques, they are referred to as black-box models that lack interpretability and understanding regarding the contribution and the influence of variables [101].

However, several methods exist for quantifying the importance of variables within networks either at the feature selection stage or after modeling for interpreting the results. The variables used in machine learning models have a significant impact on their performance [102]. As such, the accuracy of developed models is strictly tied to the selection of a proper feature subset. Feature selection techniques can be divided into three categories: filter, wrapper, and embedded methods [102]. Filter algorithms are typically used as a data preprocessing step to evaluate the intrinsic properties of each feature separately, and they are independent of the models. Examples of filter techniques include correlation analysis, Chi-Squared statistical test, and linear discriminant analysis [102], [103]. Filter methods are very efficient; however, they do not take into account the importance of the features on the overall model [104]. Wrapper methods, also known as greedy algorithms, overcome this disadvantage by aiming to find the best feature subset that results in the best model performance [102], [104]. These algorithms entail either forward selection, backward selection, or a variation of both [102]. In forward selection, a null model is evolved iteratively by adding features that improve the overall performance. Backward selection algorithms begin with a full model and iteratively remove features that result in performance improvements [102]. Additional implementations of wrapper methods include permutation importance and drop-column importance algorithms where feature importance is examined based on the change in the performance when a model is tested based on a permuted dataset or a dataset with missing features [105]. In addition to feature selection, the latter methods can be used to quantify the contribution of different features to the output and consequently provide further insight into the developed models. On the downside, the requirement of developing and evaluating many models

that require parameter tuning, drastically increases computation time [102]. Embedded techniques incorporate feature selection in model training such as regularization methods and decision tree-based feature importance methods. These methods balance the advantages and disadvantages of the filter and wrapper feature selection algorithms [102], [104].

3.2.3 Sequential Data Assimilation

Sequential data assimilation (filtering) techniques are applied in situations where the forward propagation of a system's state in time is required. The main goal of this method is to rectify the current model state estimate obtained from physical models as observations become available. Then future states are forecasted based on the inferred information [106]. This technique has been widely used in damage detection and on-line health monitoring of systems [107]. The two sequential data assimilation approaches that are mostly used include the Bayesian probabilistic approach and the Kalman filtering approach [108].

The traditional Kalman filter approach provides an optimal solution to linear systems subject to Gaussian noise perturbations, and therefore, it is only applicable for limited problems. Variants of the traditional KF, such as the extended Kalman filter (EKF), allow performing sequential data assimilation in a broader range of complex and non-linear systems [109]. However, the extended Kalman filter suffers from several shortcomings due to its impracticality, high computational requirements, bias, and possible divergence potential [109], [110]. The Ensemble Kalman filter (EnKF) overcomes the previous limitations and outperforms other adaptations of the traditional

KF [110]. EnKF algorithms are attractive due to their applicability to complex non-linear models and non-gaussian noise, simplicity, and low computational cost [110].

3.2.3.1 Mathematical Formulation of Ensemble Kalman Filters (EnKF)

The Ensemble Kalman filter (EnKF) provides a sub-optimal Monte Carlo estimation of the traditional KF. The probability distribution of the model states is randomly sampled to obtain an ensemble of model states. The EnKF algorithm includes two phases, the first phase consists of the prediction or forecasting step, and the second phase is the update or analysis step. The prediction step entails propagating an ensemble of realizations at time t forward in time; then, updating or correcting the variables at time $t+1$ when actual measurements are collected. The EnKF algorithm is presented below [111], [112]:

1.	**Initial/Previous State (t):**		
1.1	Model State Vector:	X_0	$\in R^n$
1.2	Initial Ensemble Matrix:	$A = (x_1, x_2, \dots, x_N)$	$\in R^{n \times N}$
Where N is the number of ensemble members, n is the model state vector size, and x_i is the i[th] ensemble member			
2.	**Forecast Step (t+1):**		
2.1	Predicted State Ensemble Matrix:	$A_{t+1}^f = f(A_t^a) + \varepsilon_i$	$\in R^{n \times N}$
2.2	Ensemble Mean:	$\overline{A_{t+1}^f} = A_{t+1}^f 1_N$	$\in R^{n \times N}$
2.3	Ensemble Perturbation:	$A_{t+1}^{f\,\prime} = A_{t+1}^f - \overline{A_{t+1}^f} = A(I - 1_N)$	$\in R^{n \times N}$
2.4	Ensemble Covariance Matrix:	$P_e = \frac{A_{t+1}^{f\,\prime}\left(A_{t+1}^{f\,\prime}\right)^T}{N-1}$	$\in R^{n \times n}$
Where f is the mathematical representation of the forward model, ε_i is the process noise, $1_N \in R^{n \times N}$ with all elements equal to 1/N, and I is an identity matrix			
3.	**Update Step (t+1):**		
3.1	Observation Vector:	d_{t+1}	$\in R^{m \times N}$
3.2	Ensemble of Observations:	$D_{t+1} = \mathrm{d_{t+1}} + \varepsilon_j$	$\in R^m$
3.3	Ensemble Perturbations:	$\Upsilon = (\epsilon_1, \epsilon_2, \dots, \epsilon_N)$	$\in R^{m \times N}$
3.4	Measurement Error Covariance:	$R_e = \frac{\Upsilon(\Upsilon)^T}{N-1}$	$\in R^{m \times m}$
3.5	Kalman Gain Matrix:	$K_{t+1} = \mathrm{P_e}.H^T(H\mathrm{P_e}H^T + \mathrm{R_e})^{-1}$	$\in R^{n \times m}$
3.6	Analysis Matrix:	$A_{t+1}^a = A_{t+1}^f + K_{t+1}\,(D_{t+1} - HA_{t+1}^f)$	$\in R^{n \times N}$
Where m is the number of measurements, ε_j is the measurement noise, and $H \in R^{m \times n}$ is an observation matrix			

CHAPTER 4

RESEARCH METHODS

The research methodology to achieve the study objectives is presented in the flowchart in Figure 3 and elaborated in the following subsections. The work is divided into three main components covering the data acquisition process, the development of rutting prediction models based on NN, and the development of a model calibration framework using an EnKF approach.

4.1 Synthesis of the Analysis Dataset

4.1.1 Data Mining and Transformation

The decision about the data to be extracted from the LTPP database is based on the factors that are expected to affect rutting as established by common engineering practice and the results of the literature review. Features that do not require advanced testing and that are easily attainable in data-scarce locations are considered. Data availability is also considered throughout the selection process since a large dataset is needed for training a NN model. This results in a set of inputs reflecting climatic and traffic conditions as well as material and structural properties for the asphalt, base and subgrade layers. The following subsections explore the criteria behind the selection of the different input factors, as well as the LTPP data sources that are used to extract and populate the dataset to be used for modeling. Table 5 lists all the extracted data items and their corresponding sources in the LTPP database.

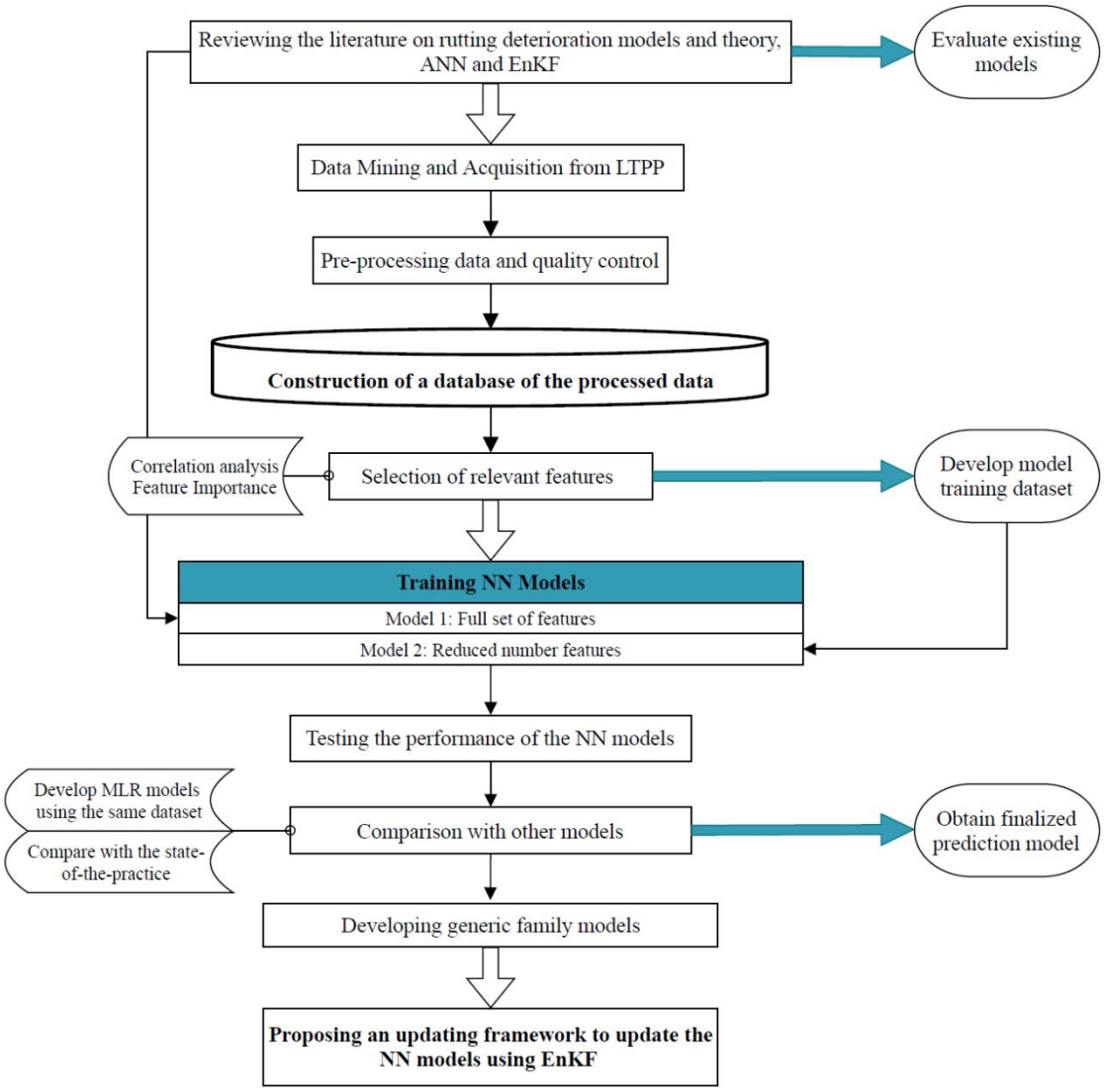

Figure 3: Research methodology flowchart.

4.1.1.1 LTPP Experiment Selection Criteria

This study aims at predicting the accumulation of rutting in flexible pavements while excluding the effects of maintenance. Therefore, SPS sections corresponding to new AC pavements were given the highest priority. In order to further expand the available sections, SPS and GPS sections corresponding to asphalt pavements that were subjected to major rehabilitation involving milling and overlaying with more than 1.5

inches of asphalt are considered. GPS sections other than those experiencing rehabilitation are excluded since their maintenance history might not be complete [91]. Table 2 lists the LTPP experiments used in this study and their description.

The outcome is a dataset corresponding to rutting measurements from different regions that accounts for the variability in factors affecting rutting, mainly climatic conditions, and soil types. Thus, ensuring the generalization abilities of the model.

4.1.1.2 General Section Information

Relevant general section information includes section SHRP ID, section location, construction year, opening dates to traffic, and project ID which correlates co-located test sections having the same material properties. The IDs and location of the available test sections are essential for extracting the remaining data from the other LTPP modules. The construction and traffic opening dates were also extracted and used to calculate the pavement age corresponding to the date of each distress survey. The tables and fields required to obtain the latter information are detailed in Table 5.

Table 2: LTPP Experiments included in the analysis dataset.

LTPP Experiment	Description
SPS 1	Strategic Study of Structural Factors for Flexible Pavements
SPS 5	Rehabilitation of Asphalt Concrete Pavements
SPS 8	Study of Environmental Effects in the Absence of Heavy Loads
SPS 9	Validation of Strategic Highway Research Program Asphalt Specification Mix Design (Superpave)
GPS 6	Asphalt Concrete Overlay of Asphalt Concrete Pavement

4.1.1.3 Maintenance and Rehabilitation History

The maintenance and rehabilitation (M&R) history for the test sections were extracted from the MNT_IMP, RHP_IMP, and the EXPERIMENT_SECTION tables. The CN_ASSIGN_DATE and CN_CHANGE_REASON fields include the date at which any M&R activity took place. However, some activities were not reported in this table and alternatively were mentioned in the MNT_IMP or RHB_IMP tables. This prompted the use of the three tables collectively to determine the timings when M&R activities that could influence rutting took place. Treatments expected to affect rutting included activities in the following categories: reconstruction, overlays, different types of patching, and surface treatments and coatings. Rutting data reported after the implementation of these activities were discarded from the analysis.

4.1.1.4 Rut Depth Data

4.1.1.4.1 Data Sources

For each test section, rutting depth is monitored for several years at different locations along its length. A measurement is performed at 15.2-meter (50 ft) intervals on both the left and right halves of the wheel-path, as shown in Figure 4. This results in a total of 22 measurements for each section during each data collection survey. Rut depth values are reported using two measurement methods. The first is based on the 1.8-m straight edge reference method and the second corresponds to the wireline reference method. The rutting shape affects the rut depth measurement corresponding to each method, while the wireline reference method is the most used in the literature [41]. For this reason, rut depths obtained from the wireline method were used in this study. Only

test sections having three or more distress surveys were extracted as considered in [113].

In the LTPP, time-series rutting data is reported on a station basis with two measurements every 50-ft, as available in the MON_T_PROF_INDEX_POINT table, or as a representative section average value, as reported in the MON_T_PROF_INDEX_ SECTION table. The required rutting data is extracted from the former table in order to quantify the construction variability within individual sections. In controlled laboratory experiments, the same rut depth should be obtained at all stations because they have the same characteristics and are subjected to the same climatic and traffic conditions. However, for in-service road conditions, construction techniques and other uncontrolled variables result in construction variability along the section. Since the pavement material properties are reported per section and not per station, the effect of the construction variability is not readily quantifiable. Therefore, the construction variability is calculated, for each road section, as the coefficient of variation (C.O.V.) of the varying rut depths at different stations.

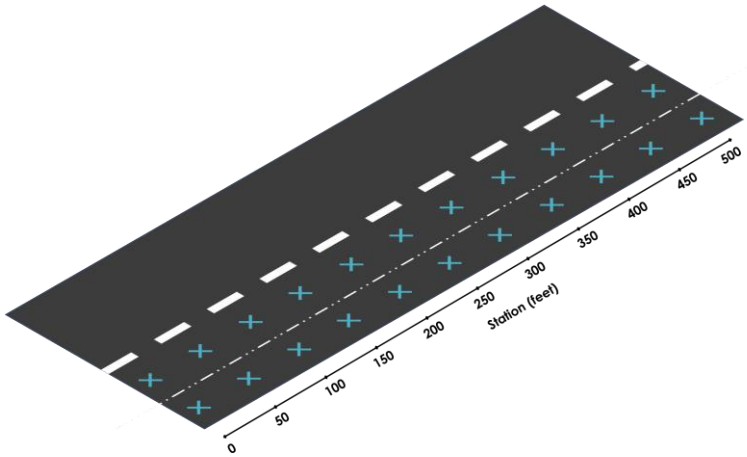

Figure 4: Rutting data collection layout.

4.1.1.4.2 Data Quality Control

Even after eliminating the effect of maintenance, the extracted data revealed frequent fluctuations in the measured rut depth across different surveys where the rut depth decreases with time. Such fluctuations have been examined previously in the literature and attributed to several measurement and climatic factors [42]. Frost heave or swelling soils can cause the rut depth to increase or decrease with time. Additionally, in some situations, the PASCO RoadRecon unit and the Dipstick were used to collect rutting data causing variability in the measurements. Fluctuating depths can also be caused by errors in locating the data collection stations over the years. Instrument errors associated with the data collection technologies can also contribute to introducing additional noise to the measurements where an average error of ±2 to 3 mm is expected [42]. In such instances, an increasing rut depth is forced for each station and wheel-path individually by selecting the higher value when the depth decreases with time.

Another limitation present in the dataset is the unavailability of rutting measurements over the first few years after the construction of the test sections. This issue will restrict the capability of the developed models to predict rutting at an early age. The depth of rutting is interpolated over 0.5-year increments between age of zero and that corresponding to the first data point. The age of the pavement at which the first rutting measurement was collected is very critical for estimating the missing trend and determining whether it should be smooth or steep (Figure 5 and Figure 6). For practicality purposes, this rationale is executed by reviewing the depth of rutting for the first two collected observations. If the latter values do not vary significantly, it can be concluded that the rutting trend is stable. Consequently, the trend to be estimated should increase steeply in the beginning and then flatten as it approaches the values of the

actual measured data, as illustrated in Figure 5. On the other hand, a significant increase in the rut depth between the first two observations indicates that the progression of rutting is in a steep phase, which should be reflected by the estimated trend (Figure 6). These considerations are achieved through interpolating the missing early age rutting data for each test section individually using second-degree polynomials and the rutting depth of the first two measurements. Examples of this process are presented in Figure 5 and Figure 6, which show a case that requires a steep trend and another that requires a smoother one. In some instances, the second-degree polynomial estimation does not result in a good fit and is substituted with linear interpolation.

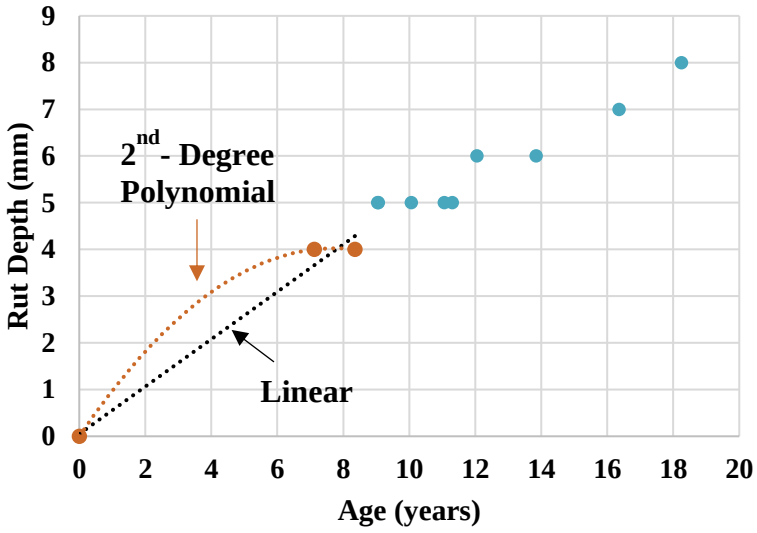

Figure 5: Plot illustrating a smooth estimated trend for missing rutting depths.

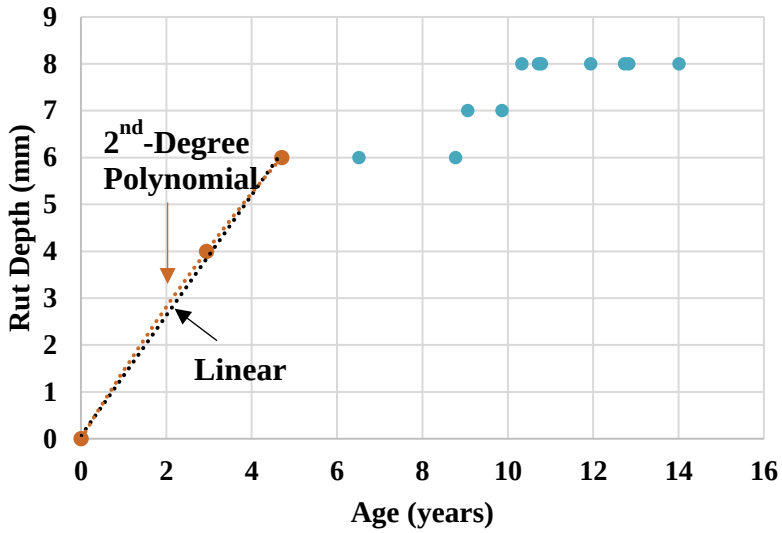

Figure 6: Plot illustrating a steep estimated trend for missing rutting depths.

4.1.1.4.3 Data Smoothing

The use of point-based observations proved to be impractical since no information is available regarding the spatial variability of input variables along the length of the road. In other words, the 22 rut depth values under each wheel-path and each station, all of which having identical input features, cannot be used. Instead, an average representative rut depth is used to represent the performance of a test section during each data collection survey.

Several techniques were examined to achieve the latter. This includes using the average value of measurements for every year, fitting a regression for rut depth versus age for each road, or performing Locally Weighted Regression (LOESS). The use of average values of measurements has several limitations as it results in unsmooth curves and un-reasonable trends in numerous cases. Rut depth is expected to increase with time and traffic repetitions; however, the average method resulted in constant rutting values

over time in some instances, as shown in Figure 7 (grey line). On the other hand, using regression analysis is disregarded as well because reasonable fits that represent the data with minimal errors were unattainable due to the complex trends in the data. This limitation is overcome with LOESS analysis, a non-parametric technique used to obtain smooth lines through scatters of data [114]. Unlike regression analysis, this method works because it does not require stringent specifications about the mathematical structure that may exist within the data. The rut depth is smoothed as a function of age in a moving fashion analogous to moving average computations [114]. The LOESS technique is adopted to smoothen the data and get rutting depths at 0.5-year increments. Obtaining the data at equal time intervals provides several advantages, especially if it were to be used in time-series analysis.

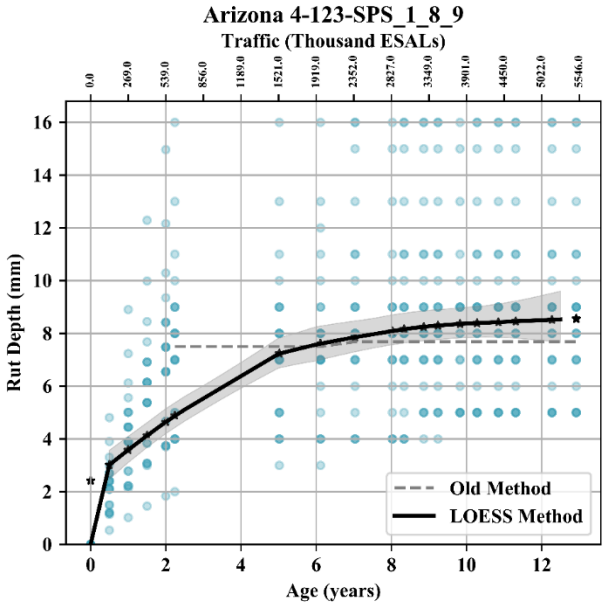

Figure 7: Rutting depth as a function of age using the average and LOESS methods.

4.1.1.5 Climate Data

The LTPP provides two sources for climatic data. These sources include data obtained from weather stations in the vicinity of LTPP test sections and data obtained from the Modern-Era Retrospective Analysis for Research and Applications (MERRA) database that was developed by NASA through the analysis of ground, satellite, ocean, and atmospheric observations [91]. The MERRA data was selected since its availability is not restricted to the United States.

To account for climatic effects, variables required to calculate the effective temperature conditions were used. The concept of the effective temperature was introduced to provide a single temperature that accounts for seasonal fluctuations while inducing similar cumulative damage [115]. In its latest form, T_{eff} is calculated using Equation 4.

$$T\_eff = 14.62 - 3.361 \ln(Freq) - 10.940(z) + 1.121(MAAT) + 1.718(\sigma_{MMAT}) - 0.431(Wind) + 0.333(Sunshine) + 0.08(Rain) \quad \textbf{(4)}$$

Where:

- T_{eff} is the effective temperature in (^{o}F)
- z is the critical depth (inches)
- $Freq$ is the loading frequency (Hz)
- $MAAT$ is the mean annual air temperature (^{o}F)
- σ_{MMAT} is the standard deviation of the mean monthly air temperature (^{o}F)
- $Wind$ is the mean annual wind speed (mph)
- $Rain$ is the annual cumulative rainfall depth (inches)
- $Sunshine$ is the annual percentage of sunshine (%)

The individual variables required to calculate the effective climatic conditions were extracted to be used as inputs into the model from the sources detailed in Table 5.

Yearly could cover, wind velocity, precipitation, freezing index, and temperature measurements are extracted and used to compute annual averages from at least 20 years of data. Monthly temperature measurements were also obtained to evaluate the monthly standard deviation. The average of the monthly temperature standard deviation (σ_{MMAT}) associated with more than 20 years of measurements was calculated for all the test sections.

4.1.1.6 Traffic Data

4.1.1.6.1 Traffic Inputs and Data Sources

Traffic is one of the most influencing factors in predicting rutting which is a load-related distress. Several measures may be used for reflecting the amount of traffic experienced by a pavement including the Average Annual Daily Traffic (AADT), the Equivalent Single Axle Load (ESAL), and the elaborate traffic load spectra [116]. The traffic load spectra measure provides the most detailed and accurate representation of traffic as it records the number of axles, configuration, and weight of each vehicle. However, this method involves high complexity and a large number of variables; therefore, it could not be used for the fulfillment of the objectives of this study. On the other hand, AADT, which approximates the average daily traffic volume traversing a roadway, does not correlate traffic to the associated pavement damage. Consequently, the number of ESALs is used as a metric to overcome the complexity of using load spectra while taking into account the corresponding pavement damage potential [116],

[117]. The number of ESALs is the equivalent number of 18-kip single axle loads that result from a combination of different axle loads, configurations, and pavement characteristics. The damage caused by different axle loads and configurations is related to that of a standard axle by Equivalent Axle Load Factors (EALF) that were developed in the 1993 AASHTO guide. This guide lists the numerical values of EALF for single, tandem, and tridem axles of varying weights. Additionally, several DOTs provide estimates of EALF as a function of FHWA's truck classification criteria. Since the ESAL simplifies the complexity of the load spectra in one value while providing DOTs with sufficient flexibility to make assumptions and estimations when data is not complete, it is considered the most appropriate traffic metric for the objective and scope of this research [116], [117].

Annual ESAL data are available in two tables in the LTPP. The TRF_MON_EST_ESAL table includes ESAL estimates provided by highway agencies over several years, while the TRF_ESAL_COMPUTED table includes ESAL values obtained from instrumented sections. The evaluation of data availability revealed that data in the TRF_ESAL_COMPUTED table is limited as it is either unavailable for many sections or it does not cover the years of the rutting surveys. Therefore, the bulk of data were extracted from the TRF_MON_EST_ESAL table and the use of the TRF_ESAL_COMPUTED table was restricted to cases where data was unavailable in the former.

4.1.1.6.2 Cumulative Traffic Calculation

The ultimate objective is to obtain the cumulative value of ESALs at every point in the pavement timeline corresponding to rut depth measurements. The cumulative ESALs is calculated using Equation 5.

$$CESAL_i = \sum_{n=0}^{i} ESAL_n \quad \textbf{(5)}$$

Where:

- $CESAL_i$ = cumulative traffic at the end of year i.
- $ESAL_n$ = annual traffic at the end of year n.

However, the persistent unavailability of $ESAL_n$ information for some years of the pavement's life introduced several challenges to the calculation process. Consequently, several methodologies were assessed to estimate the annual ESALs and calculate the cumulative traffic. These methodologies require the calculation of the growth rate which is then used to estimate the number of ESALs for the missing years. The GR is calculated using Equations 6 and used to estimate the missing values based on Equation 7.

$$GR_{\mathrm{i}} = \left(\frac{\mathrm{ESAL_j}}{\mathrm{ESAL_i}}\right)^{\left(\frac{1}{\mathrm{j-i}}\right)} - 1 \quad \textbf{(6)}$$

Where:

- GR_{i} = growth rate at year i.
- $\mathrm{ESAL_{i/j}}$ = traffic at the end of year i/j.
- $\mathrm{j - i}$ = the analysis period in years.

$$ESAL_i = ESAL_0(1 + GR)^i \quad \textbf{(7)}$$

Where:

- $ESAL_i$ = annual traffic at the end of year i.
- $ESAL_0$ = traffic at the construction year.

- **Method 1:**

This procedure involves obtaining the initial ESALs corresponding to the construction year and calculating the GR for consecutive measurements. It is worth noting that the consecutive measurements are not necessarily done at equal time intervals. This results in a set of GR values corresponding to the list of available years. The average GR and the ESALs at construction are obtained and used to populate the traffic data at one-year intervals between the construction year and the year corresponding to the last rut depth measurement (Equation 6 and Equation 7). The cumulative ESALs are then acquired by applying Equation 5.

This method exhibited significant shortcomings due to its sensitivity to the annual fluctuations in the reported ESALs. The corresponding limitations are illustrated in the following example where traffic data over fifteen years for an SPS 5 section in Alabama were extracted and analyzed (Table 3). A spike in the reported ESALs is experienced in year 9, where the number of annual ESALs increases from 82,000 to 290,000. This increase is equivalent to a growth rate of 254% which skews the average and results in a significantly high GR (Table 3). Computing the annual ESALs based on the calculated average GR of 19% and the annual value of 65,000 ESALs leads to unrealistic estimates of annual ESALs. For example, at year 4 the outcome will be 129,000 ESALs, which is much higher than the actual value of 73,000 ESALs (Table 3).

Following deliberate evaluation of the entire dataset, it was concluded that using this method can result in erroneous calculations and therefore it is not suitable for estimating the ESAL values for missing years.

Table 3: Example of traffic data processing.

Year	0	1	2	3	4	5	6	7	8	9	10	11	12	13	14	15
kESAL	65	67	69	71	73	75	78	80	**82**	**290**	293	290	287	288	298	294
$kESAL_0$	65															
Annual GR	3	3	3	3	3	4	3	3	**254**	1	-1	-1	0	3	-1	-
Average GR	19%															
Estimated ESAL	65	77	91	108	129	152	181	214	254	301	357	424	502	596	706	838

- **Method 2:**

Method 2 was introduced to account for the limitations of method 1. Instead of using an average GR to repopulate all the traffic data, all the growth rates corresponding to consecutive traffic observations are used to estimate the annual ESALs for the missing years only. This approach involves extracting the construction date and the date of the last rut depth measurements for each section and listing all the years between these dates at one-year intervals. Annual ESALs obtained from the database tables are matched with the listed years and the years with missing data are identified. The GR values between each two consecutive traffic measurements are calculated using Equation 6. It should be reiterated that consecutive traffic measurements are not necessarily reported at one-year intervals causing gaps in the available data. The missing ESAL values are subsequently estimated on a case-by-case basis based on two considerations:

- In case the missing years belong to the upper bound of the available data (e.g., years 13, 14, and 15 in Table 3), the average GR of the last few available years is used to estimate the missing information. This can only be done provided that the data was consistent over the last few years. As such, a GR of 0.25% is applied to a value of 287,000 ESALs (year 12) to estimate future traffic using Equation 7 (Table 3). Conversely, if the GR values fluctuate significantly, the general growth trend over all the available years is evaluated.
- In case there were gaps in the reported traffic data (i.e. $j - i > 1$), the value of ESALs for the missing years are obtained based on the GR value corresponding to the relevant range of years. For example, if traffic data was not available for year 4 (Table 3), the GR value between years 3 and 5 is calculated, using Equation 6, and used to calculate the annual ESAL at year 4.

The completed set of annual traffic data is utilized to obtain the cumulative traffic each year. The final stage includes coupling the cumulative traffic values with the exact rutting survey dates. Rutting surveys are not specifically conducted at the end of the year; consequently, the end of year cumulative ESALs that are obtained from Equation 5 need to be corrected. The adjustment is achieved by subtracting the ESALs that are expected to traverse the road after the date of the survey according to Equation 8.

$$Corr_{CESAL\,i} = CESAL_i - \left(\frac{No.\,days\ until\ survey\ day}{Days\ in\ a\ year}\right) ESAL_i$$
$$= CESAL_i - \left(\frac{(Month - 1) \times 30 + Day}{365}\right) ESAL_i \quad \textbf{(8)}$$

Where:

- $Corr_{CESAL\,i}$ = corrected cumulative ESALs at rutting measurement date i.
- $CESAL_i$ = calculated cumulative ESALs at the end of the year corresponding to rutting measurement date i.
- $ESAL_i$ = annual ESAL at the end of the year corresponding to rutting measurement date i.

4.1.1.7 Layer Thickness and Material Data

Layer thickness and material type information are extracted for all layers that are reported in the SECTION_LAYER_STRUCTURE table for the required road sections. It is worth noting that the number of layers is not consistent across all the test sections. This becomes challenging while inputting the properties for the different layers into the NN model since it only accepts a fixed number of inputs. Consequently, a manipulation process was performed based on the maximum possible number of layers within each layer category (e.g., original surface layer, binder layer, etc.), in order to have the same number of layers for all test sections.

4.1.1.7.1 Asphalt Concrete Layers

A surface layer and a binder layer are typically present in any pavement structure. Volumetric information as well as binder and mix properties are extracted for these layers. The thicknesses of the layers are extracted from the SECTION_LAYER_ STRUCTURE table. The extracted volumetric information includes bulk and maximum specific gravities, percentage of air voids, percentage of asphalt content, and the aggregate gradation. Volumetric data is available for every core taken on a specific test section in and out of the wheel path. After investigating the data, the difference between the two was obtained to be insignificant, therefore all available values were averaged for every layer. Additionally, the gradation data is used to calculate the Nominal Maximum Aggregate Size (NMAS). The mixture volumetric information is scattered over multiple TST, SPS, INV, and RHB LTPP tables. TST tables were given the highest priority as they contain the most data. When the required information is missing from the TST tables, the SPS, RHB, and INV tables were checked. Details about the specific tables and fields are available in Table 5.

The penetration value at 25 ^{o}C was used to represent binder properties for the surface and binder layers. Following the preliminary statistical analysis of the extracted data, it was concluded that the penetration grade does not vary significantly between the different asphalt layers. Hence, only the penetration grade for the top layer is considered. Although the LTPP is populated with dynamic modulus data, it was not considered in this study because it only considers inputs that do not require advanced laboratory testing.

4.1.1.7.2 Base and Subbase Layers

Layer thickness, material type, and resilient modulus values were extracted from the LTPP database. General material types for the base and subbase layers were obtained from the SECTION_LAYER_STRUCTURE table and grouped into several categories in an attempt to reduce the number of variables while accounting for their different characteristics that affect pavement deterioration. As a result, five base categories were distinguished, including unbound base (DGAB), asphalt treated base (ATB), permeable asphalt treated base (PATB), nonbituminous treated base (NONBIT), and no base (NONE) [49]. Material types were classified into different categories based on Table 4.

Additionally, average resilient modulus (M_R) data was extracted for granular base materials and the average resilient modulus at 4, 25, and 40 ^oC for treated base materials if they exist. The resilient modulus of the unbound layers is stress-dependent and is measured using the triaxial test at different confining pressure and deviatoric stress states. The obtained M_R values corresponding to 15 measurements at different stress states were extracted from the TST_UG07_SS07_WKSHT_SUM table and used to fit a predictive equation. This equation serves to obtain the required resilient modulus at any stress state. NCHRP Project 1-28A recommends using Equation 9 for that purpose. This equation was solved to obtain $k1$, $k2$, and $k3$ of all the layers available in the LTPP via a MATLAB code. For pavements, the NCHRP Project 1-28A proposes using a σ_3 of 5 psi and a σ_1 of 15 psi for the aggregate base and subbase layers and a σ_3 of 2 psi and a σ_1 of 6 psi for the subgrade [118].

$$M_r = k_1 P_a \left(\frac{\theta}{P_a}\right)^{k_2} \left(\frac{\tau_{oct}}{P_a} + 1\right)^{k_3} \quad \textbf{(9)}$$

$$\theta = \sigma_1 + 2\sigma_3 \quad \textbf{(10)}$$

$$\tau_{oct} = \frac{\sqrt{2}}{3}(\sigma_1 - \sigma_3) \quad \textbf{(11)}$$

Where:

- $k1$, $k2$, $k3$ = regression constants.
- P_a = atmospheric pressure equal to 14.7 psi.
- θ = bulk stress.
- τ_{oct} = octahedral shear stress.
- $\sigma_1 \; and \; \sigma_3$ = principal stresses.

Table 4: Material code classifications for the different base categories [49].

Base Category	Base Description	Material Description
DGAB	Unbound Base	Gravel (uncrushed)
		Crushed stone
		Crushed gravel
		Crushed slag
		Sand
		Soil-aggregate mixture (fine-grained)
		Soil-aggregate mixture (coarse-grained)
		Fine-grained soils
ATB	Asphalt Treated Base	Hot mix asphalt concrete (HMAC)
		Sand asphalt
		Asphalt treated mixture
		Dense graded, hot laid, central plant mix
		Dense graded, cold laid, central plant mix
		Dense graded, hot laid, mixed in-place
		Recycled asphalt concrete, plant mix, hot laid
		Recycled asphalt concrete, plant mix, cold laid
PATB	Permeable Asphalt Treated Base	Open-graded, hot laid, central plant mix
		Open-graded, cold laid, mixed in-place
		Open-graded, cold laid, central plant mix
NONBIT	Non-bituminous Treated Base	Cement aggregate mixture
		Econocrete
		Cement-treated soil
		Includes treated soils (e.g., lime, calcium chloride

4.1.1.7.3 Subgrade Layer

Regarding the subgrade layer, the AAHSHTO soil classification was used instead of the material description provided in the SECTION_LAYER_STRUCTURE table since it provides a clear distinction among the different soil types. The data revealed that more than one soil class can coexist on a test section. In such cases, the most frequent soil class was assumed to be representative of the entire test section. The average resilient modulus of the subgrade was also extracted and calculated using Equation 9.

Table 5: LTPP database source tables and corresponding calculations.

Data Item	LTPP Database Table	Field ID	Calculated Value
General Section Information			
Section ID	EXPERIMENT_SECTION	SHRP_ID	-
State		STATE_CODE	-
Construction year		ASSIGN_DATE	Age
Project ID	SPS_PROJECT_STATIONS	PROJECT_ID	-
Climate Data			
Annual Average Cloud Cover	MERRA_SOLAR_YEAR	CLOUD_COVER_AVG	Average Annual Sunshine
Annual Average Wind Velocity	MERRA_WIND_YEAR	WIND_VELOCITY_AVG	Average Annual Wind Velocity
Annual Average Precipitation	MERRA_PRECIP_YEAR	PRECIPITATION	Average Annual Precipitation
Annual Average Freezing Index	MERRA_TEMP_YEAR	FREEZE_INDEX	Average Annual Freezing Index
Annual Average Temperature	MERRA_TEMP_YEAR	TEMP_MEAN_AVG	Average Annual Temperature
Monthly Average Temperature	CLM_VWS_TEMP_MONTH	MEAN_MON_TEMP_VG	Standard deviation of the mean monthly air temperature

Table 5: LTPP database source tables and corresponding calculations (Continued).

Data Item	LTPP Database Table	Field ID	Calculated Value
Rutting Data			
Rut Depth	MON_T_PROF_INDEX_ POINT	LLH_DEPTH_1_8 RLH_DEPTH_1_8	COV Rut Depth LOESS Rut Depth
Maintenance and Rehabilitation History			
Maintenance Dates and Types	MNT_IMP	IMP_DATE IMP_TYPE	-
Rehabilitation Dates	RHB_IMP	IMP_DATE IMP_TYPE	-
Construction No. Change Date and Reason	EXPERIMENT_SECTION	CN_ASSIGN_DATE CN_CHANGE_REASON	-
Traffic Data			
Equivalent Single Axle Loads	TRF_ESAL_ESTIMATED	ANL_KESAL_LTPP_LN_YR	Cumulative ESALs
	TRF_ESAL_COMPUTED	KESAL_YEAR	
Thickness and Material Data			
Layer Number	SECTION_LAYER_ STRUCTURE	LAYER_NO	-
Layer Type		DESCRIPTION	-
Thickness (mm)		REPR_THICKNESS	-
Layer Material Type		MATL_CODE	Base Category
Group Project Layers		PROJECT_LAYER_CODE	-
Gradation for AC Layers	TST_AG04 RHB_ACO_AGGR_PROP INV_GRADATION	ONE_AND_HALF_PASSING → NO_200_PASSING	NMAS
Subgrade Material Type	TST_SS04_UG08	AASHTO_SOIL_CLASS	-
Air Voids (%)	TST_AIR_VOIDS_CALC SPS*_PMA_MIXTURE_PROP RHB_ACO_MIX_PROP INV_PMA_ORIG_MIX	AIR_VOIDS PCT_AIR_VOIDS_MEAN	Average AV
Bulk Specific Gravity		BSG BULK_SPEC_GRAVITY_MEAN	Average G_{mb}
Maximum Specific Gravity		MSG MAX_SPEC_GRAVITY	Average G_{mm}
Asphalt Binder Content (%)	TST_AC04 SPS#_PMA_MIXTURE_PROP RHB_ACO_MIX_PROP INV_PMA_ORIG_MIX	ASPHALT_CONTENT_MEAN	Average P_b

Table 5: LTPP database source tables and corresponding calculations (Continued).

Data Item	LTPP Database Table	Field ID	Calculated Value
Penetration	SPS_PMA_AC RHB_ACO_PROP INV_PMA_ASPHALT	PENETRATION_77 ORIG_PENETRATION_77	-
Resilient Modulus at 4, 25 and 40 ºC	TST_AC07_V2_MR_SUM	TEST_TEMPERATURE TOTAL_MR_AVG	-
Average Resilient Modulus for Unbound Layers	TST_UG07_SS07_WKSHT_ SUM	RES_MOD_AVG	Solve Equation 9

4.1.2 Data Pre-processing

4.1.2.1 Handling Missing Data

Following the data extraction operations elaborated in section 4.1.1, the obtained tables are combined in a complete dataset storing all the required modeling inputs and outputs in their final form after conducting transformations when applicable. The outcome is a dataset corresponding to rutting measurements from different regions that accounts for the variability in factors affecting rutting. Thus, ensuring the generalization abilities of the model and that local calibration is not crucial for meaningful results. For each road section, the collected information includes a set of 52 input features that reflect the studied factors.

Upon merging the datasets, frequent occurrences of incomplete sets of inputs were recognized. In such cases, one or more inputs are missing making the sample unsuitable for model development purposes. Data pre-processing and data imputation refer to all the operations executed to handle missing data. Three approaches

corresponding to increasing levels of interventions were performed to manage missing values and ensure a large and reliable dataset for modeling. These methods include deletion, using information of similar observations, and imputation based on logical rules [119]. The number of roads with complete data is identified after the application of each of the methods and a detailed breakdown of the number of sections corresponding to each experiment is presented in Table 6. Furthermore, Figure 8 shows the distribution of the missing data across the different input categories. The analysis of this distribution assists in identifying the most problematic variables in the LTPP.

4.1.2.1.1 Deletion Method

Deletion, also known as the do-nothing approach, involves removing all observations with missing data [119]. Filtering out all the roads with missing information was significantly disadvantageous as it resulted in the elimination of approximately 98% of all the available roads. The dataset was further examined for missing data belonging in three categories including AC layers volumetric properties, AC penetration grade, and base, subbase, and subgrade resilient moduli.

Table 6: Number of test sections available as a function of the data handling method.

Criteria	SPS 1	SPS 5	SPS 8	SPS 9	GPS 6	Total
Total No. of Available Sections	240	91	38	50	149	568
No. of Sections with complete data						
Deletion Method	2	0	8	0	5	15
Information of Similar Observations Method	15	5	14	0	21	55
Imputation Based on Logical Rules Method	191	44	27	24	84	370

All other inputs including traffic, climate, and layer thicknesses were not included as they did not have any missing information. The evaluation revealed that more than 50% of the roads had missing information on one or more of the volumetric properties which include specific gravity, air voids, binder content, and aggregate gradation (Figure 8). While approximately 70% and 85% of the roads lacked penetration and resilient modulus data, respectively (Figure 8). As a result, only 15 complete cases of that 568 test sections were available which necessitates exploring further methods for expanding the dataset (Table 6).

4.1.2.1.2 Information on Similar Observations Method

The different layers in each test section are identified by a unique layer code. In addition to the layer code, a project layer code is assigned to SPS pavement layers with the same material properties as other sections along the same site. Therefore, the unavailable information can be populated with data from SPS sections co-located on the same project site and having an identical project layer code (Figure 4). This step increased the number of available test sections (i.e., roads) from 15 to 55, which corresponds to less than 10% of the total number of available roads (Table 6). The bulk of the unavailable data belongs to the base, subbase, and subgrade properties followed by the penetration grade of AC layers. In fact, more than 60% of the roads had missing data in the latter categories (Figure 8). An additional level of data imputation is applied for the remaining layers that continue to have missing fields in order to enlarge the dataset.

4.1.2.1.3 Imputation Based on Logical Rules Method

The imputation based on logical rules method involves replacing the missing values by the average properties of other layers and sections based on specific criteria. Regarding the penetration grades of the top layers, the availability of penetration grade information for the adjacent layers of the same test section is examined. In the cases where the adjacent layers did not include the required information, the penetration grades of other roads in the same State were sought to acquire the missing information. Regarding resilient modulus values for the base, subbase, and subgrade layer, the average M_R of the same material type was used when measurements for adjacent layers of the same type were not available. If the same material type is used in the neighboring test sections in the same State, their average M_R is used. However, if that was not the case, the overall average of the specific material types in the entire LTPP dataset was used to fill the missing cells. Missing gradation data were handled according to the number of missing sieves. If the percentage of aggregates passing all sieve sizes are missing, the data is compensated from the neighboring AC layers in the same section. On the other hand, if the percentage passing some sieves are available but some are missing, the missing values are estimated by interpolation. The interpolation methodology involved searching the LTPP database for mixes having the same NMAS and similar percentages to those available for the mix that is missing some values. This methodology is explained in Figure 9. Each missing input corresponding to other AC mix volumetric properties was estimated based on the average properties of the layers below or above them on a case-by-case basis.

Imputation based on logical rules results in a significant improvement in the number of roads having complete inputs which increases to 370 (Table 6). Despite all

the assumptions, several roads were disqualified as they continued to include missing inputs. These cases occurred when the penetration grade could not be determined, the average M_R for a certain material type could not be obtained, when traffic values were unavailable or unrealistic, and as a result of some quality control measures. Quality measures targeted roads having a significantly different number of layers; for example, sections with no base layers, three base layers, or more than one sublayer. Approximately 20% of the obtained dataset had missing penetration grades which could not be estimated, in addition to another 20% corresponding to other missing variables (Figure 8).

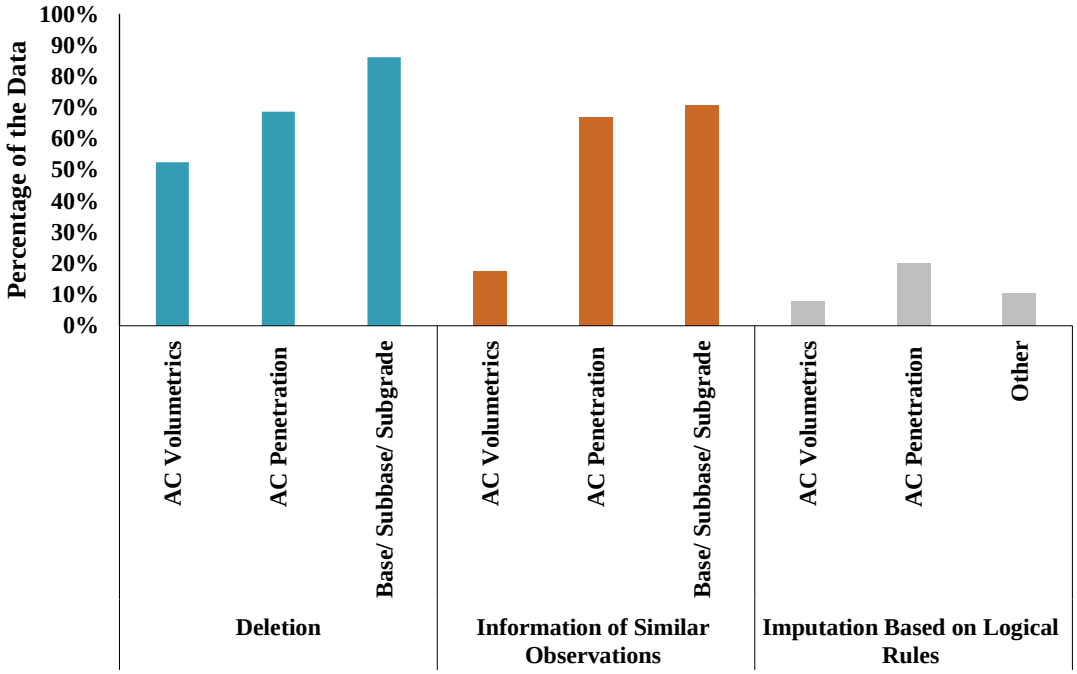

Figure 8: Distribution of the missing data based on several data handling methods.

\

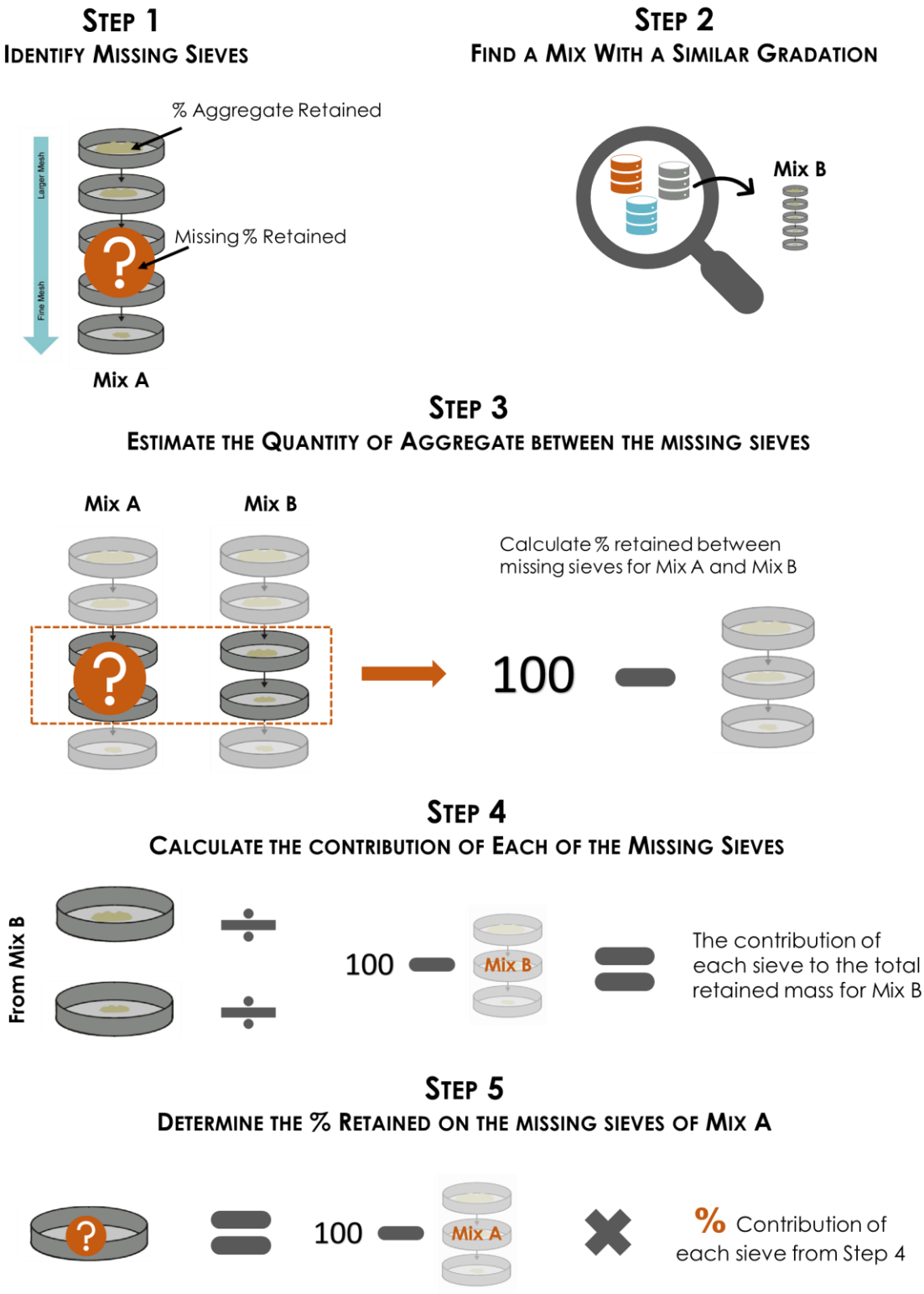

Figure 9: Missing sieve size interpolation.

4.1.2.2 Final Rutting Data

The final selection of roads includes a total of 370 test sections distributed among five different LTPP experiments. Rut depth data corresponding to several distress surveys conducted on the selected roads was extracted from the original dataset. This resulted in 75,641 data points that increased to 112,998 after being processed as discussed in 4.1.1.4.2. Ultimately, rut depth measurements obtained at 22 different locations of the test sections are smoothed to obtain a total of 8,603 data points.

4.1.3 Final Dataset

Following all the estimations and assumptions that were performed on the data, Table 7 provides the summary statistics of the data available for all the input and output parameters. Additionally, Figure 10 through Figure 12 present the data distribution of rutting and key features, including traffic and average temperatures.

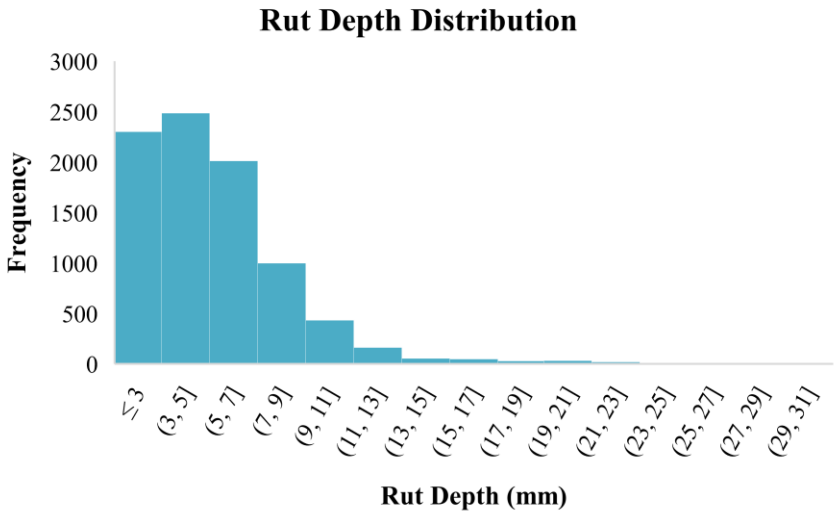

Figure 10: Rut depth distribution.

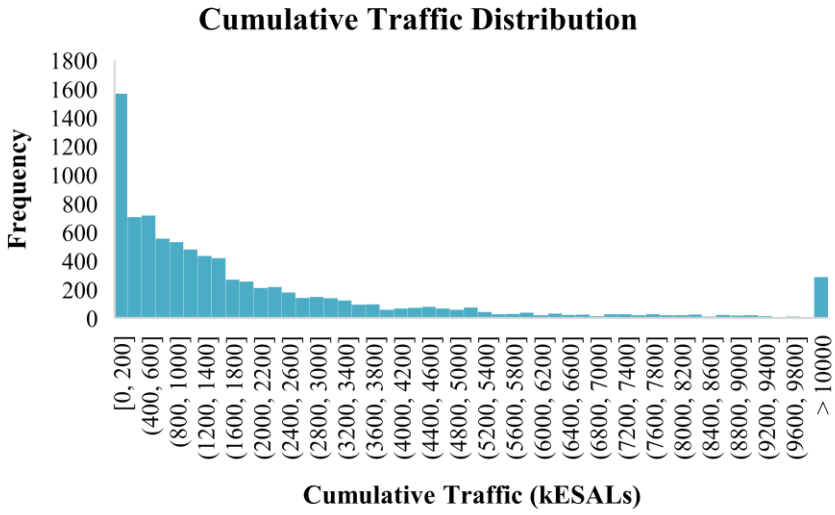

Figure 11: Cumulative traffic distribution.

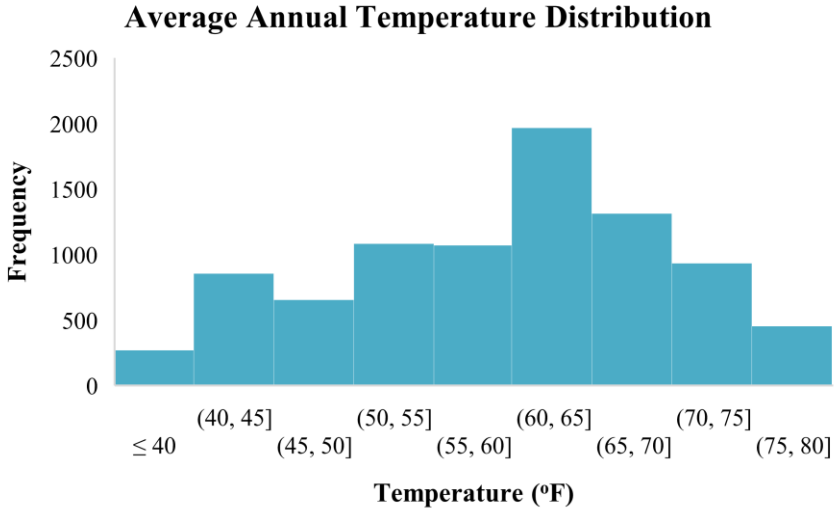

Figure 12: Average annual temperature distribution.

Table 7: Summary statistics of the adopted dataset.

Input Parameter	Mean	Standard Deviation	Min	Max
Rutting				
Rut Depth (mm)	5.02	3.40	0.00	31.00
Traffic				
1. Cumulative Traffic Range (Thousand ESALs)	2386.22	4715.70	0.00	48826.15
Climate				
2. Precipitation (inches)	35.55	14.29	6.86	64.99
3. Evaporation (inches)	29.13	11.26	6.50	50.57
4. Standard Deviation of the Monthly Mean Air Temperature (MMAT) (°F)	15.22	3.44	6.81	24.58
5. Mean Annual Air Temperature (MAAT) (°F)	58.74	10.67	34.49	75.28
6. Average Wind Velocity (mile per second)	5.69	2.54	0.00	11.51
7. Average Cloud Cover (%)	45	8	28	60
8. Average Freezing Index	218.46	340.69	0.00	1772.27
9. Average Shortwave Surface	13978.10	1535.99	10370.10	16970.62
10. Teff (°F)	76.17	7.70	51.21	89.47
Surface AC Layer				
11. Thickness (cm)	2.82	1.80	0.80	8.10
12. Bulk Specific Gravity (Gmb)	2.31	0.10	1.98	2.56
13. Maximum Specific Gravity (Gmm)	2.47	0.06	2.21	2.68
14. Air Voids (%) (A.V)	6.43	3.01	1.33	19.71
15. Asphalt Content (%) (Pb)	4.92	0.82	2.00	7.50
16. Penetration (.1 mm)	77.41	21.67	41.00	185.00
17. Nominal Maximum Aggregate Size (mm)	14.46	4.20	9.50	25.00
Gradation (% Passing)				
18. 1½”	100.00	0.13	98.00	100.00
19. 1”	99.82	1.37	84.00	100.00
20. 3/4”	96.69	3.84	71.00	100.00
21. 1/2”	91.59	9.29	40.00	100.00
22. 3/8”	81.86	10.92	26.00	100.00
23. # 4	57.03	10.63	16.00	84.00
24. #10	37.11	8.52	13.86	57.00
25. #40	19.33	5.44	8.00	40.00
26. #80	10.88	3.28	5.00	20.00
27. #200	5.60	1.41	1.00	11.60
Binder AC Layer				
28. Thickness (cm)	3.50	2.72	0.00	17.10
29. Bulk Specific Gravity	1.85	0.96	0.00	2.62
30. Maximum Specific Gravity	1.96	1.02	0.00	2.70
31. Air Voids (%)	4.36	3.57	0.00	23.79
32. Asphalt Content (%)	3.70	2.02	0.00	6.90
33. Nominal Maximum Aggregate Size (mm)	19.59	4.78	9.50	25.00

Table 7: Summary statistics of the adopted dataset (Continued).

Input Parameter	Mean	Standard Deviation	Min	Max
Binder AC Layer				
Gradation (% Passing)				
34. 1½”	78.92	40.84	0.00	100.00
35. 1”	78.73	40.76	0.00	100.00
36. 3/4”	75.11	39.22	0.00	100.00
37. 1/2”	66.02	35.44	0.00	100.00
38. 3/8”	56.89	31.16	0.00	99.00
39. # 4	39.96	22.40	0.00	79.00
40. #10	28.35	16.59	0.00	74.49
41. #40	15.55	10.44	0.00	86.31
42. #80	9.31	7.61	0.00	91.23
43. #200	4.62	2.82	0.00	11.50
Base Layer 1				
44. Thickness (in)	7.94	3.98	0.00	28.00
45. Resilient Modulus (psi)	440873.97	450871.30	0.00	2863050.12
Base Layer 2				
46. Thickness (in)	2.25	3.28	0.00	13.40
47. Resilient Modulus (psi)	118854.14	298303.27	0.00	1586135.57
Subbase Layer 1				
48. Thickness (in)	5.75	7.52	0.00	54.00
49. Resilient Modulus (psi)	8934.94	9165.28	0.00	27712.13
Subgrade				
50. Resilient Modulus (psi)	10338.60	3336.54	3606.01	30791.75
Other				
51. Equivalent Base Thickness (in)	33.31	20.20	0.00	100.75
52. Construction Quality	0.39	0.13	0.14	0.92

4.2 Rutting Deterioration Model Development

4.2.1 Correlation Analysis and Feature Selection

Correlation analysis is an efficient method for feature selection. It is crucial to identify highly correlated features as they are considered to degrade model performance [120]. Strongly correlated features are deemed redundant and non-informative and will result in a low-quality output. As a rule of thumb, a good feature subset contains features that are strongly correlated with the output but not with each other [120]. The dataset at hand is expected to include highly correlated features. Aggregate gradation, for example, includes the percentage of aggregates passing consecutive sieve sizes.

Other instances include the asphalt mixture percentage of air voids, binder content, and bulk and maximum theoretical specific gravity. Spearman's rank correlation coefficient is used to measure the correlation among the features while accounting for non-linearity. Features with correlations exceeding a predetermined threshold of 0.4 are eliminated. If features are considered important from a technical perspective, they are not removed even if they exceed the correlation threshold. This results in reducing the number of variables from 52 to 28. Table 8 lists the features based on their numbers presented in Table 7.

4.2.2 NN Model Development

The developed NN models are based on the feedforward backpropagation learning process available in the Keras library in Python. Developing the proposed NN models requires configuring the network architecture (number of hidden layers and neurons in each layer), the activation function to be used at each layer, and the optimization algorithm that will be used in training the model. For the purpose of training and tuning the model, 80% of the original dataset is used, and the remaining 20% is reserved for testing the final trained model and estimating the generalization error. In the process of model tuning, five-fold cross-validation is applied, and the performance metric used for model evaluation is the mean squared error (MSE).

Table 8: List of the selected features after correlation analysis.

Model	List of Selected Features	No. Features
Model -2-	1, 2, 4, 5, 6, 11, 13, 14, 16, 17, 23, 27, 28, 30, 31, 32, 33, 39, 43, 44, 45, 46, 47, 48, 49, 50, and 52	28

4.2.2.1 Feature Scaling

Feature scaling is performed to transform all features to a similar scale. This is necessary for all machine learning algorithms when the used features significantly differ in scale. Normalization and standardization correspond to rescaling the data to a range of [0,1] or [-1,1], and to a distribution of mean 0 and a standard deviation of 1, respectively. Both methods were examined, and the standardization method was selected as it resulted in a better performance based on the preliminary analysis.

4.2.2.2 Activation Functions

Different activation functions could be used for the hidden layers and the output layer. The results of preliminary studies on the obtained dataset justify the use of ReLU for all the hidden layers. Regarding the output layer, activation functions are not typically used for regression problems. However, predicting rutting depth introduces a constraint of having positive predictions. This can be enforced either by normalizing the rutting data to a range of [0,1] and applying a sigmoidal activation function or by applying a ReLU activation function. After experimenting with both methods, the ReLU activation function achieved better results as shown in Figure 13.

4.2.2.3 Weight Initialization

The weight initialization scheme selected has a significant impact on the training process and the model performance as it speeds up the process and prevents deadlocks. The default initialization method used by Keras is the glorot uniform

initialization [121]. However, since the RELU activation function is used, the He initialization method is recommended [122].

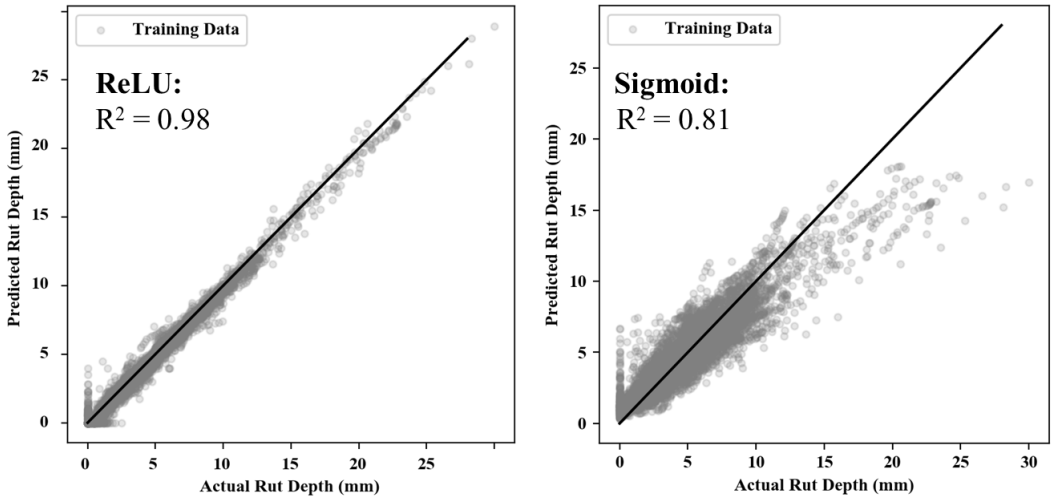

Figure 13: Effect of the output layer activation function on the model performance.

4.2.2.4 Hyperparameter Tuning

Hyperparameters are parameters that define the NN's architecture and the overall learning process [121]. These parameters cannot be learned; however, they are tuned through different approaches. In essence, all the hyperparameter tuning approaches rely on training the NN using different combinations of hyperparameters and selecting the ones that result in the best performance. Unlike other machine learning algorithms, hyperparameter tuning is very critical for deep neural networks because they have a higher dependency on the network's configuration [123]. As such, a rigorous search of the hyperparameter space is required. The considered hyperparameters include the number of hidden neurons in each layer, the batch size, the learning rate, and the

regularization penalties (L1 & L2). The traditional grid search method is typically used to search the hyperparameter space and find the best solution [100]. Since considering all combinations is very computationally expensive, tuning is performed on each parameter separately. Hyperparameter tuning starts with the number of hidden neurons and layers, then the learning rate followed by the batch size and regularization. Table 9 lists the explored space for each of the considered hyperparameters.

Table 9: Explored hyperparameter space for developing neural network models.

Hyperparameter	**Description** [121]	**Range**
No. Hidden Layers	A container of a collection of hidden neurons	1, 2, and 3
No. Hidden Neurons	Computational units that calculates the weighted sum of inputs and maps it based on the activation function	Increments of 10 $\in$ [10,1000]
Learning Rate	The size of the step taken to adjust the weights with respect to the loss gradient	0.0001, 0.0003, 0.001, 0.003, 0.01, 0.03, and 0.1
Dropout Regularization	A technique that randomly deactivates neurons during each iteration based on a predefined dropout rate or probability in order to prevent overfitting	0 and 0.2
L1	Regularization penalties that are added to the loss function to reduce the value of the weights and intimately avoid overfitting	0.0001, 0.001, 0.01, and 0.1
L2		0.0001, 0.001, 0.01, and 0.1
Batch Size	The number of training samples utilized during one iteration	32, 64, 128, 256, and 1024

4.2.3 Additional Data Filtering for Model Improvement

The feature subset is further examined to improve the obtained trained and tuned models. In this process, the model performance and errors are analyzed to identify any problematic features or values. Features that negatively impact the model performance, in terms of MSE, MAE, and MAPE, are either removed or adjusted to improve the performance. After training the model with 28 features, the errors corresponding to each individual road section are calculated. It is worth noting that the feature combinations that result in the highest MSE do not necessarily result in the highest MAE or MAPE. Mainly because MAPE is more sensitive to low values of rutting while MSE is more sensitive to large rutting depths. Therefore, all three metrics should be considered in order to identify any features or values that are deteriorating the model's performance. This is achieved by clustering the MSE, MAE, and MAPE using the Kmeans algorithm. The outcome is four clusters corresponding to low, medium, high, and extremely high errors that are clustered based on the value of the three error metrics. Finally, the distribution of values of each input within each error cluster is evaluated and illustrated using boxplots to detect problems. This method is supplemented by evaluating the correlation between the errors and the features. Features that are highly correlated with the errors would require further analysis. These procedures are depicted in Figure 14.

4.3 Feature Importance Study

The importance of the different variables is quantified to achieve the second objective of this study. Feature importance is examined using the permutation importance algorithm. In essence, the permutation importance algorithm includes

shuffling the values of each feature individually and comparing the performance to the benchmark error [124]. The permutation feature importance is calculated either as the difference between or the ratio of the estimated permutation error and the original benchmark error [124].

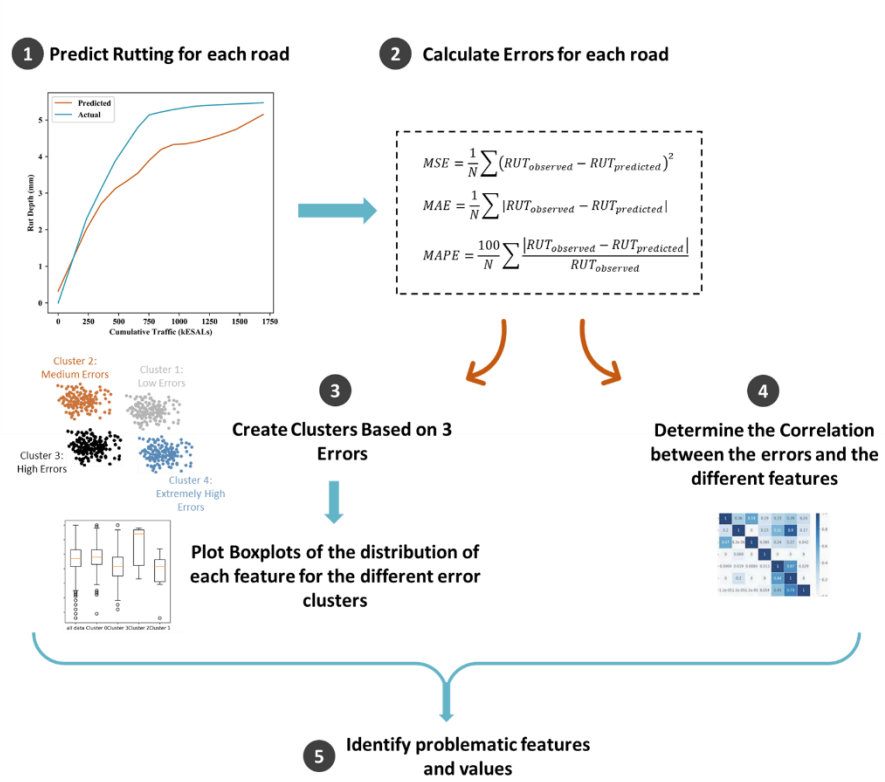

Figure 14: Process for identifying problematic features and values to improve model performance.

4.4 Sensitivity Analysis

Sensitivity analysis aims to study the influence of changes in model input values on the model output. The profile sensitivity method is used to analyze the NN model sensitivity. It aims at analyzing each input individually by varying its values

between the minimum and maximum at equal subintervals while keeping all other inputs constant [125], [126]. Inputs, excluding the one under study, are set at five levels corresponding to the minimum, first, second and third quartile, and the maximum values. The result is five values corresponding to different input parameters at each subinterval. The median is calculated and plotted with respect to the subintervals to form a profile. A profile for each input is required to evaluate the contribution of each of the variables [125]. The elasticity, which describes the percentage change in outputs as the input changes by 1%, is also calculated to quantify and rank the contribution of the different features.

4.5 Family Models

Models developed for groups of pavements are known as family models. After finalizing the NN model, family models corresponding to certain traffic, climate, and mix design combinations are obtained. The micro-climate, traffic and pavement structural and material characteristics are expected to remain unchanged within each family. The development of general family models introduces additional simplifications to agencies in data-scarce regions since it allows them to benefit from the outputs of the NN even if they do not have detailed information about the required inputs.

Family models are divided based on three distinct criteria, including traffic and climatic conditions, in addition to rutting resistance potential. The functional class for all the available roads in the LTPP database was extracted and descriptive statistics of the annual ESALs were determined. These statistics are used to obtain the limits for the local, collector, arterial and interstate roads. Additionally, the climate groups were

obtained based on the LTPP climate zoning criteria [127]. The traffic and climate classification criteria are summarized in Table 10.

The NN model is used to predict rutting over a standard 20-year analysis period for all the available roads within each traffic and climate class. Based on the predicted rutting values, the models were classified into three distinct groups. These groups represent pavements with a high, medium, or low resistance to rutting. Achieving these subgroupings requires identifying the rut depth (i.e., performance) limits for each pavement performance family. Once these limits are determined, all the predictions within that family are averaged to determine a representative family rutting curve. This is accomplished by applying an optimization algorithm that divides the data within each traffic-climate family into three performance groups in a way that minimizes the obtained family curve errors. Excel's evolutionary optimization algorithm is employed for this purpose.

Table 10: Traffic and climate grouping criteria.

Criteria	Range
Traffic	Collector: 32 – 80 Annual Thousand ESALs
	Arterial: 80 – 350 Annual Thousand ESALs
	Interstate: >350 Annual Thousand ESALs
Climate	CZ 1: Dry Freeze
	CZ 2: Dry Non-Freeze
	CZ 3: Wet Freeze
	CZ 4: Wet Non-Freeze

4.6 Ensemble Kalman Filter Application to Update the NN Model

The third objective of this study is to formulate a robust tool to achieve the most accurate rutting depth predictions. This is achieved by combining the predictions of the NN models with the EnKF. A framework that uses the EnKF technique to update the family models discussed in section 4.5 is devised to utilize new data and enhance the prediction performance. The mathematical background of EnKF is presented in section 3.2.3. Figure 15 illustrates the framework that is proposed to improve and update the generic rut deterioration models.

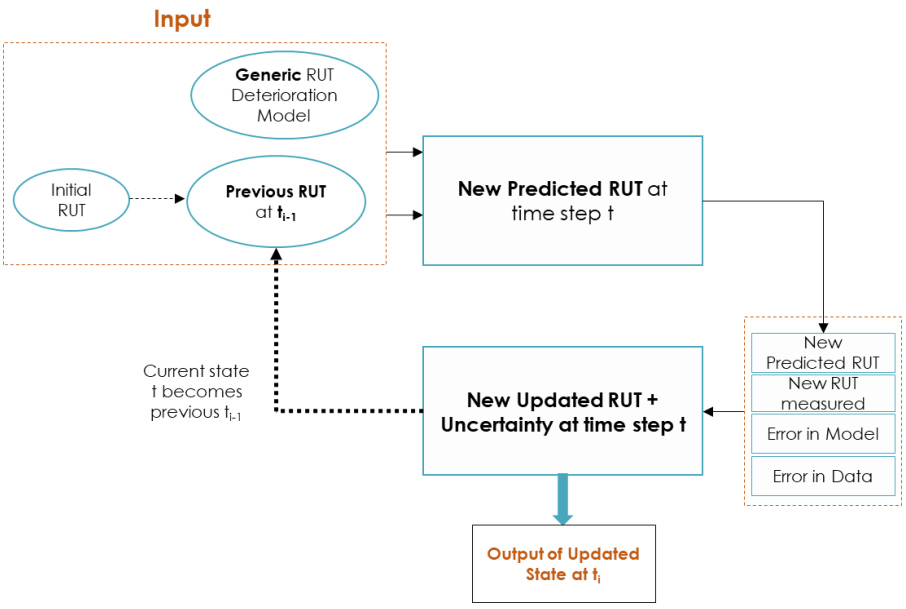

Figure 15: EnKF implementation framework.

4.6.1 EnKF Framework Formulation

The formulation of the EnKF framework includes defining the stochastic state vector. The state vector in this study incorporates the progressed rutting depth value as well as the model parameters, as shown in Equation 12.

$$A = [R\ C_1\ C_2\ C_3 \dots C_i]^T \quad \textbf{(12)}$$

Where R reflects the rutting depth state and the C_i's represent the model coefficients of the family curve that is being updated.

At the initialization stage, which corresponds to a newly constructed pavement, rutting depth (R) is expected to be zero. The model coefficients (C_i) are based on the regression-based family model obtained from the procedures of section 4.5. The initial state vector is used to obtain the initial ensemble matrix which reflects the statistical distribution of the initial guess (Equation 13). The initial ensemble matrix is obtained by perturbing the initial state vector through adding some error value.

$$A = (A_1, A_2, \dots A_N) \quad \textbf{(13)}$$

Where A is the initial ensemble matrix, A_i corresponds to the state vector of the i^{th} ensemble, and N is the ensemble size. A sensitivity analysis is typically performed to identify the optimal ensemble size.

Realizations of the state vector are propagated forward in time using the governing dynamical equations. The dynamic model is represented by an ordinary differential equation (ODE) which describes the incremental variation of rut depth as a function of time, as presented in Equation 14.

$$\frac{dr}{dt} = C_0 + C_1 t^1 + \cdots + C_i t^i \quad \textbf{(14)}$$

Where $\frac{dr}{dt}$ is the rut depth ODE, t is the time measure, and C_i corresponds to the model parameters.

The Forward Euler Discretization time integrating method is implemented to propagate the system state forward in time at a 0.01-year timestep for all the ensembles. This timestep is determined based on sensitivity analysis. The mathematical representation of the rutting propagation model is presented in Equation 15.

$$r_{t+1} = \left(r_t + \Delta t \times \frac{dr}{dt}\right) + \epsilon \quad \textbf{(15)}$$

Where r_t is the predicted rut depth at time t, Δt is the model progression timestep that is equivalent to 0.01, and ϵ represents the model error.

Field rutting measurements are used to calibrate the model parameters. The update frequency reflects typical distress survey timings, which are typically conducted on an annual basis. Each year a rutting observation is collected and used to update the model while taking into account the associated uncertainties.

4.6.2 Uncertainty Quantification

Several sources of uncertainty must be considered and quantified in prognostic formulations of naturally occurring phenomena. These uncertainties can be attributed to the adopted mathematical models and the measured data.

Uncertainty in the initial guess of the model states reflects the confidence in the selected model parameters to represent existing conditions. This error is expected to be higher when sufficient information to select an appropriate family curve is not available.

Mathematical models cannot simulate natural phenomena with absolute accuracy. Model errors arise due to simplifications associated with the adopted mathematical model or unknown details that cannot be identified and incorporated. The model error is quantified for each family model independently and it is represented as an additive Gaussian white noise with a C.O.V. equivalent to the average residual errors of the data points.

The parameters in this study are based on the fitting of field data. Parametric uncertainty arises from limitations in the amount of data available to estimate the parameters. The parametric error or process noise is represented as an additive Gaussian noise with a C.O.V. obtained from sensitivity analysis.

The sources of error associated with rut depth measurements are twofold. The first source of error is associated with the accuracy and reliability of the used instruments. The second factor resulting in measurement uncertainty includes the spatial variability of the obtained measurements. Based on the literature, instrumentation errors are estimated to have an average of 2 mm [36], [42], [128]–[130]. Therefore, instrumentation error is represented with a Uniform distribution between -2 and 2. Additionally, an additive Gaussian white noise perturbation with a C.O.V. obtained from the variability in the available data is used to simulate the spatial variability.

CHAPTER 5

EXPLORATORY PILOT STUDIES

Additional analyses on the models developed using the features selected in section 4.2.1 were conducted to identify problems. Details about the followed methodology are available in section 4.2.3. Additional issues related to the methods used to sample the testing and training data were also explored. Changing the sampling methods revealed additional complications related to the selected inputs, their values, and the model itself. This chapter discusses the complications and summarizes the lessons learned from the troubleshooting processes.

5.1 Data Sampling Methods

5.1.1 Conceptual Overview of Sampling Methods

In common practice, 80% of the entire dataset is used for training and 20% for testing. This means that the data for most of the 370 test sections are included in the training dataset. However, for each of the roads, a random portion of the points is used for testing and another for training, as presented in Figure 16a. This indicates that the model is tested on data whose features were introduced during training. This approach is not completely representative of the way the model is applied. The model is used to predict a rut depth value corresponding to a specific value of cumulative ESALs, constant climatic conditions, and pavement characteristics. Then, iteratively, the model is run again at different traffic values while keeping all other inputs the same. Ultimately, a set of rut depth predictions are obtained and used to develop a

deterioration curve (Figure 16a). This is repeated 370 times for every road with unique local conditions. Therefore, when sampling is done randomly from the dataset containing 8,603 observations, all the available values corresponding to climate and pavement features are included in the training dataset. Hence, the testing dataset is not capable of validating the model's ability to learn the effects of these properties.

A different sampling method is explored to address this limitation. Instead of randomly sampling 80% of the entire dataset (i.e. 8,603 data points), the new method involves sampling 80% of the roads (i.e. 370 feature combinations) then using their associated datapoints for training (Figure 16b). This method ensures that the model is tested on completely new features that have not been introduced in training.

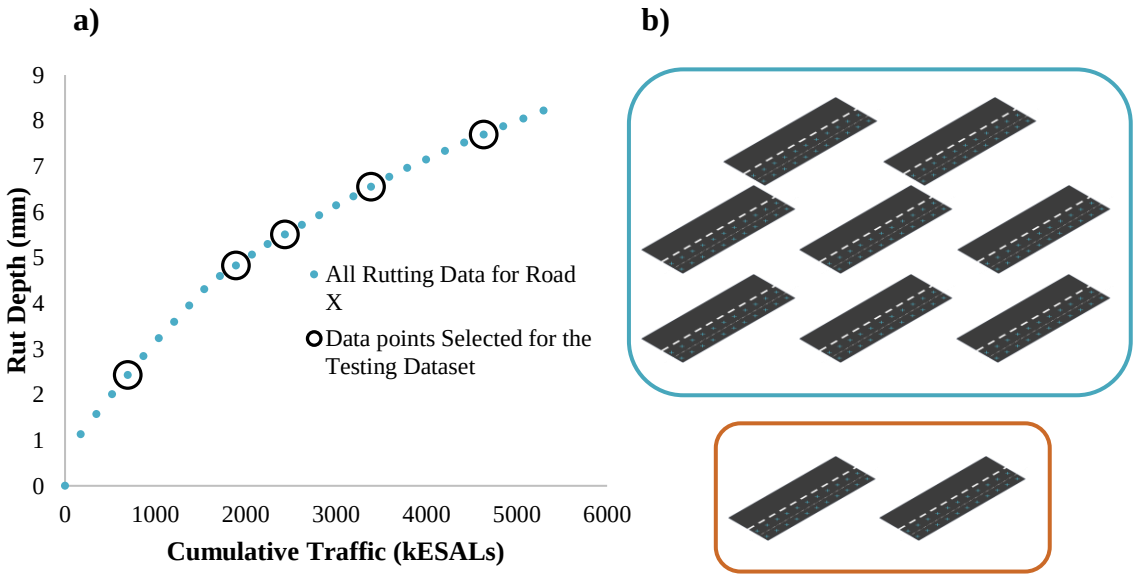

Figure 16: Training and testing dataset sampling methods illustration: a) Method 1 and b) Method 2.

5.1.2 Effect of Data Sampling on Model Performance

A model comprising of 28 inputs was tuned to obtain a configuration consisting of 3 hidden layers, 40 hidden neurons in the first layer, 40 hidden neurons in the second layer, and 10 hidden neurons in the third layer. The model uses the ReLU activation functions and has a learning rate of 0.003, and L1 and L2 regularization parameters of 0.0001. The performance of the model after being trained based on the two sampling methods is summarized in Table 11. When sampling is done using Method 2, the model overfits and the errors increase drastically relative to the original sampling method (i.e. Method 1). The model obtained using sampling Method 2 has a testing MSE of 12.58 mm^2, an R^2 of 0.1, and an MAE of 2.56 mm compared to 1.03 mm^2, 0.92, and 0.62 mm, respectively, for sampling Method 1. The high errors obtained for the model trained using sampling Method 2 are unacceptable and unjustifiable; therefore, additional in-depth examinations are crucial to rationalize the results.

5.2 Investigating the Sources of Errors

Since sampling Method 2 is more conceptually relevant in this study, detailed experiments are conducted to examine the causes of high errors by evaluating the testing and training data distributions and the procedures discussed in section 4.2.3.

Table 11: Summary of modeling results of the different sampling methods.

Sampling	**Method 1**			**Method 2**		
Metric	**MSE (mm^2)**	**MAE (mm)**	**R^2**	**MSE (mm^2)**	**MAE (mm)**	**R^2**
Training	0.88	0.56	0.93	2.11	2.01	0.81
Testing	1.03	0.62	0.92	12.85	2.56	0.1

5.2.1 Testing and Training Dataset Distributions

The first experiment involved studying the data distributions of the testing and training datasets. It is essential when splitting the data into testing and training sets to ensure that the distribution is preserved [131]. Randomly splitting the data as described in Method 2 could result in an imbalanced dataset causing an inferior model performance. The Kolmogorov-Smirnov Goodness-of-Fit (KS) Test is conducted to compare the testing and training distributions for each feature independently [132]. All the obtained p-values are greater than 0.05 indicating the training and testing datasets belong to the same distribution. The KS test is repeated for several random splits to confirm the results. Therefore, it could be concluded that the high errors are not caused by imbalances in the data distributions.

5.2.2 Investigating Features and Values

In-depth investigations of the values of each of the 28 features are performed over multiple iterations as discussed in section 4.2.3.

5.2.2.1 Iteration 1

The correlation between the errors for each combination of inputs and the features is analyzed. Ranking the correlation coefficients shows that the MSE is highly correlated to the maximum cumulative ESALs that a road encounters, the rutting depths, the volumetric properties of the binder AC layers, and the M_R of the first base layer. Table 12 lists the topmost 15 variables that are correlated with the MSE. Additionally, the errors for each road are clustered as mentioned in section 4.2.3. The boxplot in

Figure 17a shows that clusters 1 and 3 which have the highest errors correspond to roads having low traffic. This is also illustrated in Figure 17b which validates that the model is unable to predict the rutting trend for a road having a maximum traffic value of 40,000 ESALs. Therefore, roads having maximum cumulative traffic values that are less than 500,000 ESALs or greater than 30,000,000 ESALs are eliminated from the dataset. Additionally, the M_R values for the base layer are evaluated. Figure 18 reveals that the clusters corresponding to high errors have a low M_R. On average DGAB materials have an average M_R of 20,000 psi, while that of ATB is 700,000 psi. This large gap between the two types can cause intertype variability to be neglected when the data is scaled before training. Consequently, the numerical M_R value is replaced with two categories. The first is for layers having an M_R that is less than 300,000 psi corresponding to granular bases, while the second is for layers having an M_R greater than 300,000 psi corresponding to asphalt treated bases. At the end of this iteration, the number of roads decreased from 370 to 317 roads.

Table 12: Correlation coefficients for iteration 1.

Parameter	Correlation Coefficient
Maximum Cumulative ESALs	0.45
% Passing #4 for Binder Layer	0.32
MSG for Binder Layer	0.31
Rutting Depth (2nd Quantile)	0.30
Binder Layer Thickness	0.29
Rutting Depth (3rd Quantile)	0.29
Asphalt Content for Binder Layer	0.28
Surface Layer Thickness	0.28
AV for Binder Layer	0.26
Rutting Depth (4th Quantile)	0.26
Rutting Depth (1st Quantile)	0.25
Base 1 M_R	0.24
Wind Velocity	0.22
% Passing #200 for Binder Layer	0.22
NMAS for Binder Layer	0.22

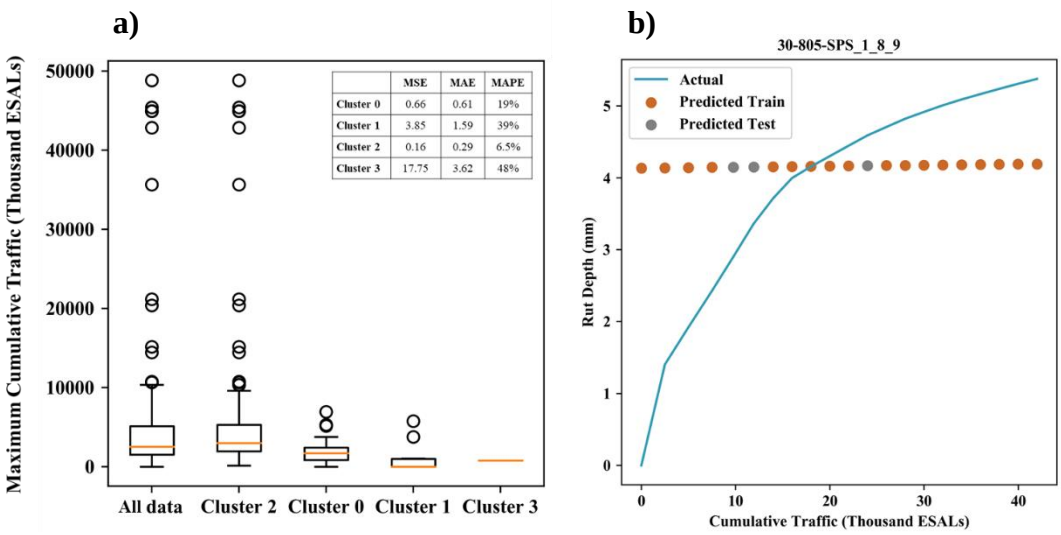

Figure 17: Effect of traffic values on the model errors.

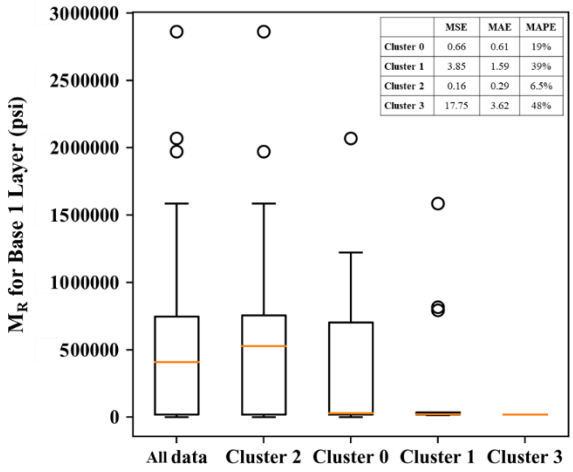

Figure 18: Effect of Base 1 resilient models on the model errors.

5.2.2.2 Iteration 2

The conclusions obtained in iteration 1 are applied and a new model is trained from the resulting dataset. The correlation analysis of the new model indicates that traffic is no longer highly correlated with the errors, while the correlation coefficients associated with the properties of the binder layer, and the third and fourth quantiles of the rutting values are still significant. The box plot in Figure 19 shows that clusters 1 and 2 having the highest errors correspond to distributions having an average rut depth of 5 and 16 mm, respectively. Therefore, the model performs poorly when predicting extremely low or high rutting values. Also, the boxplot corresponding to the 4^{th} quantile of rutting values for all the data indicates that all values exceeding 16 mm are outliers (Figure 19). Consequently, roads having maximum rut depth values that are less than 5 mm or greater than 20 mm are removed. Roads having high rut depths (i.e. exceeding 20mm) were individually evaluated to decide whether the high values are justifiable. Such cases include roads located in very hot climates, having a high percentage of air voids, or experiencing high traffic volumes.

In addition to rutting values, the properties of the binder layers are assessed. It is determined that road sections that do not have binder layers are highly correlated with the model errors. The boxplots in Figure 20 show that values of air voids and bulk specific gravity that are equivalent to zero belong to cluster 2 which has the most extreme errors. Therefore, there is a need to address roads that do not have binder layers. This problem is solved by replacing the zero values with the volumetric properties of the surface layer and by dividing the thickness of the surface layer into both AC layers. At the end of this iteration, the number of roads decreased from 317 to 282 roads corresponding to 6,946 data points.

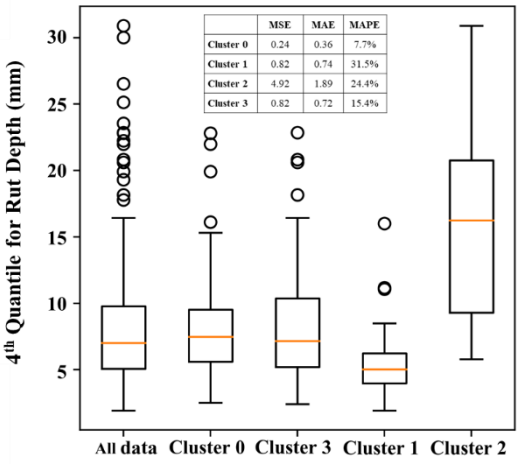

Figure 19: Effect of rutting values on the model errors.

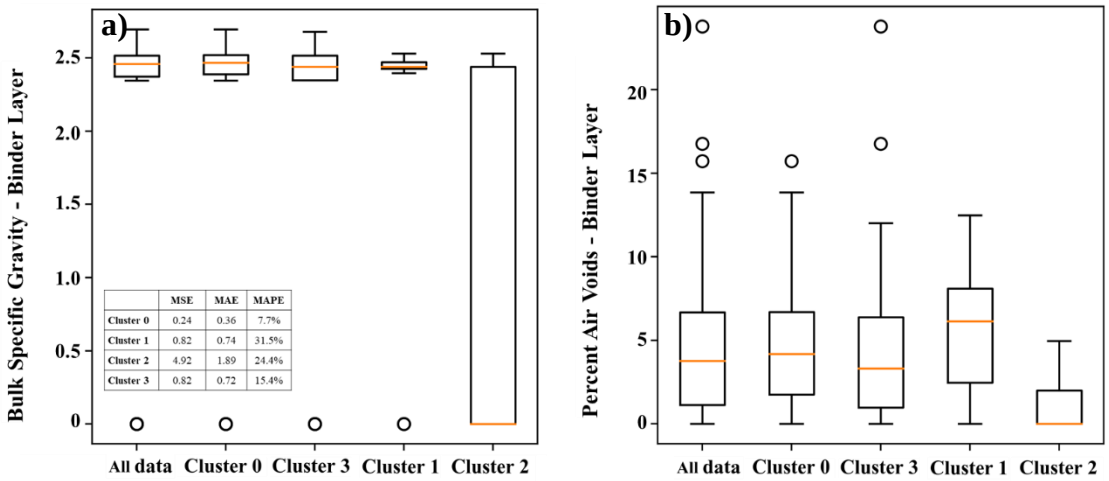

Figure 20: Effect of binder layer properties on the model errors: a) Bulk specific gravity, and b) Percent air voids.

5.2.2.3 Iteration 3

After retraining the model based on the results of iteration 2, it is concluded that no additional valuable conclusions could be drawn from correlating the values and features to the errors.

CHAPTER 6

RESULTS AND DISCUSSION

6.1 Neural Network Rutting Prediction Model

6.1.1 Model Configuration

The results of the exploratory pilot studies discussed in CHAPTER 5 are employed to obtain the final dataset used for training the final model. The second sampling method which was previously explained in section 5.1 is used for obtaining the training, validation, and testing datasets. The average MSE of the cross-validation results is obtained and used to determine the optimal network configuration that provides the best performance.

6.1.1.1 Dropout Regularization

Despite improving the model performance by conducting forensics on the dataset, the model still exhibited significant overfitting. The large cross-validation errors that are obtained due to overfitting, hinder the ability to study the effect of the different hyperparameters on the model's performance. In that case, the disparity of errors between the different validation subsets is larger than the effect of changing the hyperparameters. Therefore, it is essential to address the overfitting problem by tuning the dropout regularization parameter first. The effect of the dropout technique is studied by comparing the average validation MSE for models having one hidden layer and hidden neurons ranging between 8 and 1024. The results reveal that the inclusion of a dropout rate of 0.2 for the hidden units uniformly reduces the average validation MSE

by approximately 15% for the different numbers of hidden neurons (Figure 21). A high dropout rate was avoided to prevent underfitting. A dropout rate of 0.2 is then used for all subsequent tuning processes.

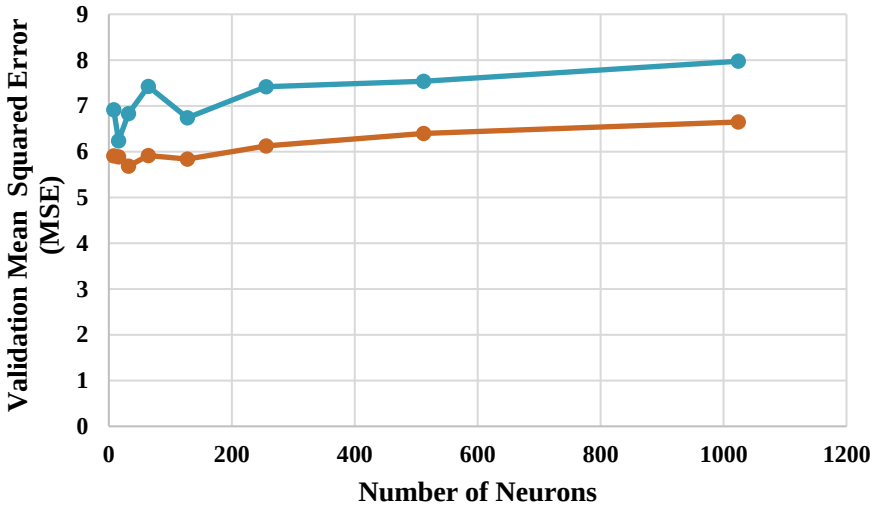

Figure 21: Effect of dropout rate on model performance.

6.1.1.2 Number of Hidden Layers and Hidden Neurons

Several numbers of hidden layers are tested, starting from one hidden layer and adding one layer at a time (Figure 24). Figure 24 shows that the standard deviation of the different cross-validation datasets is significantly high. Thus, the standard deviation should be assessed to decide on the best network architecture. Additionally, the complexity of the network is also considered in order to select the simplest network that can provide the best performance. The 10^{th} percentile of all the obtained validation MSE is calculated to be 5.07 mm^2. All architectures that result in an average MSE below the 10^{th} percentile were filtered out and compared. The minimum obtained MSE is

equivalent to 4.67 mm^2 and was achieved for a network having four hidden layers and 128 hidden neurons in the first, 32 in the second, third and fourth layers. However, if the average validation MSE values, standard deviation, and training performance are assessed for all the architectures in the lowest 10^{th} percentile, it can be concluded that their results are similar. Therefore, the network with the least complexity which is comprised of three hidden layers and has 128 neurons in the first hidden layer, 32 neurons in the second hidden layer, and 8 neurons in the third one is selected (Figure 24). This network has a mean validation MSE of 4.96 mm^2.

6.1.1.3 Learning Rate and Batch Size

Following the selection of the optimal number of hidden layers and neurons, the remaining hyperparameter space is explored to find the optimal learning rate and batch size. The learning rate is one of the most influential hyperparameters and it dictates the size of the update steps in each iteration. In conjunction with tuning the learning rate, the batch size which refers to the number of observations used to update the network at each iteration is also tuned. It is observed that the effect of the learning rate on model performance is dependent on the batch size (Figure 22). The combination of a learning rate of 0.001 and a batch size of 128 achieves the lowest average validation MSE. In fact, 0.001 is the default value for the Adam optimization algorithm being used.

6.1.1.4 L1 and L2 Regularization

Elastic Net regularization is selected as it provides a middle ground between Ridge Regression (L2) and Lasso Regression (L1). It overcomes the limitations of Lasso regression which performs poorly with the presence of multicollinearity and Ridge regression which is not effective in eliminating irrelevant variables [133]. Being a convex combination of Ridge and Lasso, Elastic Net regularization requires tuning L1 and L2 penalties. Figure 23 shows that the optimal performance is obtained at an L1 penalty of 0.0001 and an L2 penalty of 0.0001.

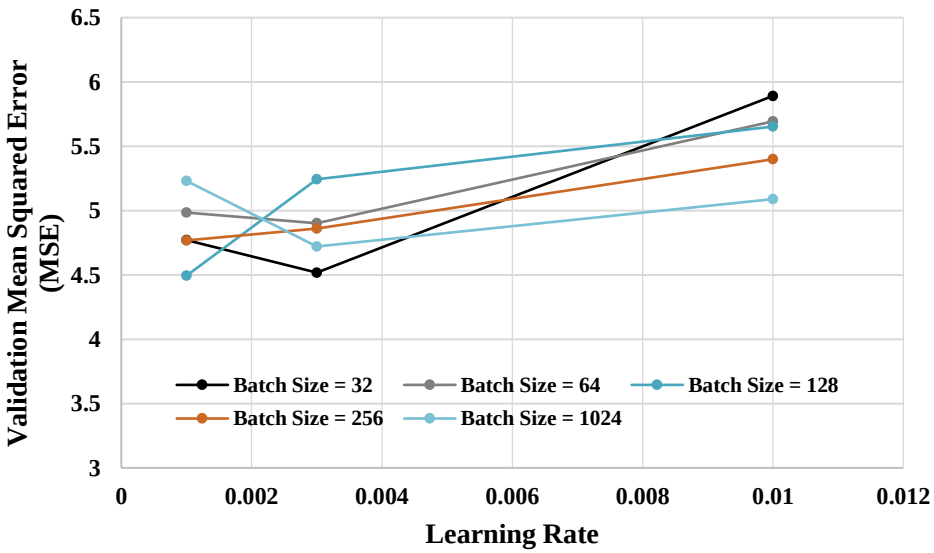

Figure 22: Effect of learning rate and batch size on model performance.

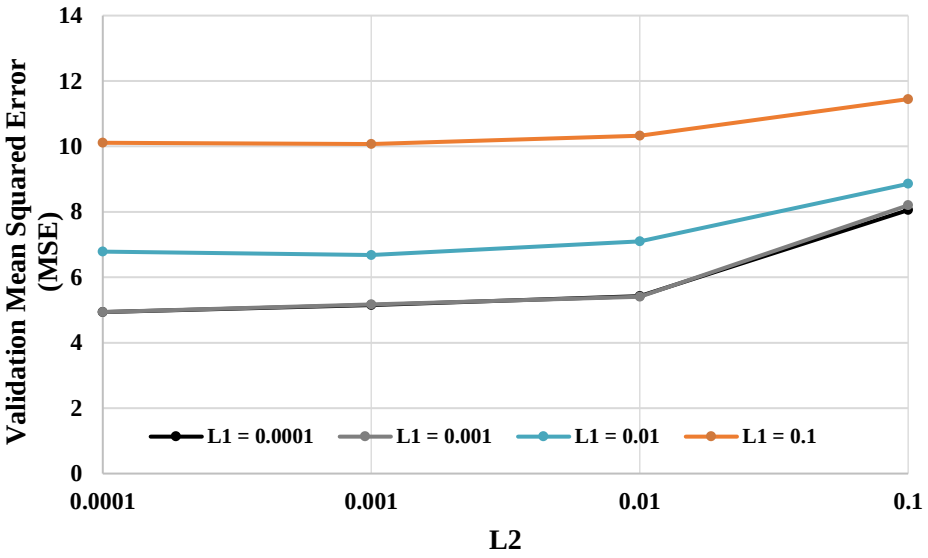

Figure 23: Effect of regularization penalties on model performance.

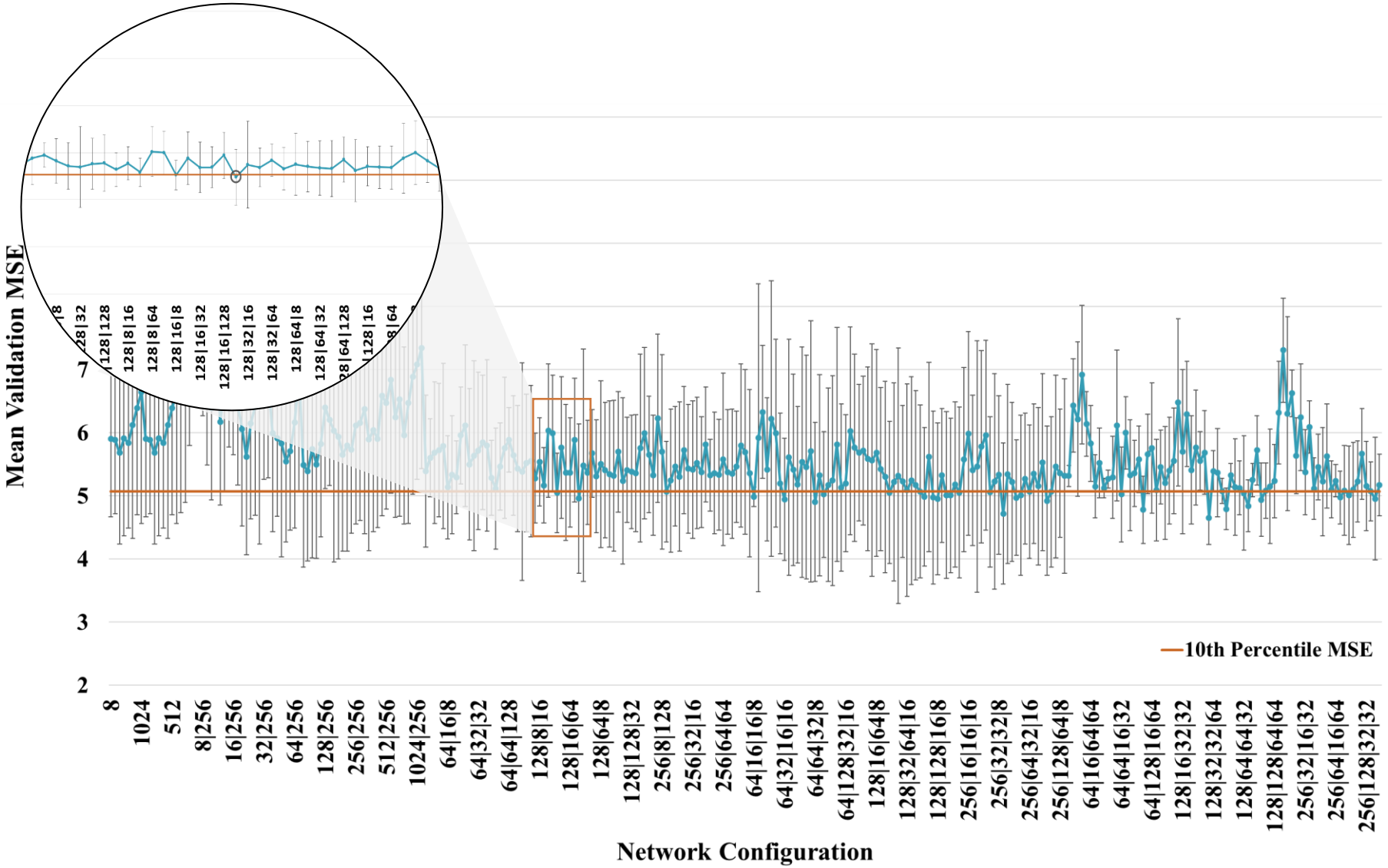

Figure 24: NN architecture tuning.

6.1.1.5 Summary

The selected hyperparameters for the model trained using the 29 inputs are summarized in Table 13.

Table 13: Results of hyperparameter tuning.

Hyperparameter	Value
No. Inputs	29
No. Outputs	1
No. of Hidden Layers	3
No. of Hidden neurons	128|32|8
Activation Function	ReLu – ReLu
Optimizer	Adam
Learning Rate	0.001
Dropout rate	0.2
L1	0.0001
L2	0.001
Batch Size	128

6.1.2 NN Model Results

The NN was fitted based on the configuration in Table 13. Table 14 presents a summary of the modeling results of the training and testing datasets.

Table 14: Summary of modeling results.

Evaluation Metric	MSE (mm^2)	MAE (mm)	R^2
Training	0.79	0.52	0.94
Testing	2.43	1.22	0.81

Figure 25a shows the mean squared error of the training and testing datasets as a function of the number of epochs. It reveals that the model converges without any overfitting problems. The model based on NN performs well with a coefficient of determination value (R^2) ranging between 0.94 and 0.81 for training and testing datasets respectively (Figure 25b and Figure 25d). The testing dataset has an MSE of 2.43 mm^2, while that of the training data is 0.79 mm^2. To further evaluate the prediction capabilities of the model, the absolute error of the testing dataset is plotted as a function of the value of rutting depth (Figure 25c). It can be observed that the largest errors occur at the high end. Higher errors are expected for large rut depths due to the low data availability in these ranges. The mean absolute error (MAE) of the NN ranges from 0.52 to 1.22 mm for the training and testing datasets. Figure 26 shows prediction examples for two roads that are part of the testing dataset.

Furthermore, the results obtained from the final model are compared to the results obtained before improving the dataset as discussed in CHAPTER 5 and before incorporating the dropout technique. The testing MSE improved by approximately 81%, the MAE by 52%, and the R^2 by 710%. This is also verified in Figure 27 that demonstrates the predicted versus measured rut depths for the testing dataset before and after incorporating the improvements. It is evident that the trend is less scattered and most of the data are concentrated around the line of equality.

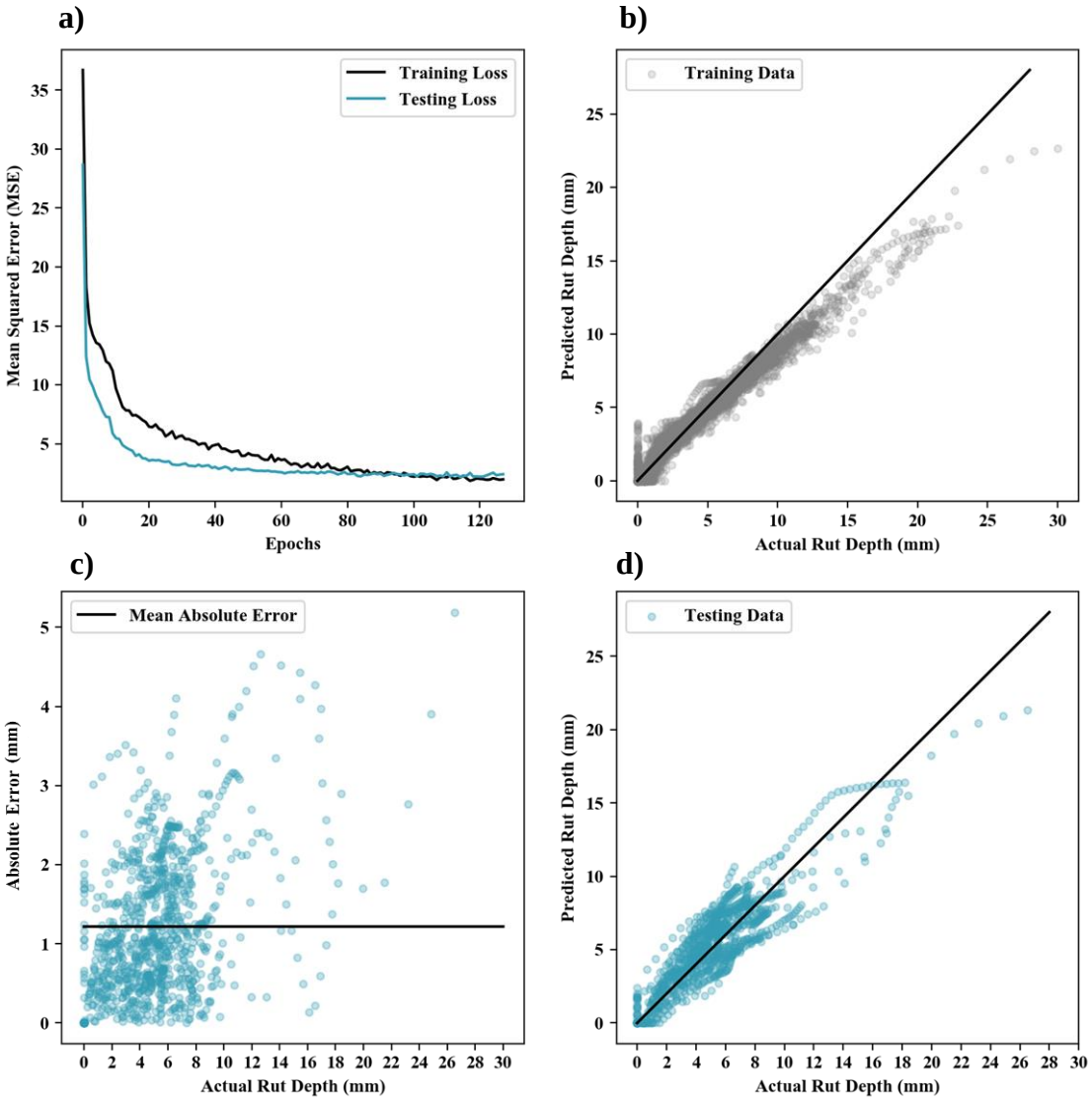

Figure 25: Modeling results: a) Learning curve, b) Measured vs. predicted rut depth regression plot for the training dataset, c) Absolute error vs. measured rut depth, and d) Measured vs. predicted rut depth regression plot for the testing dataset.

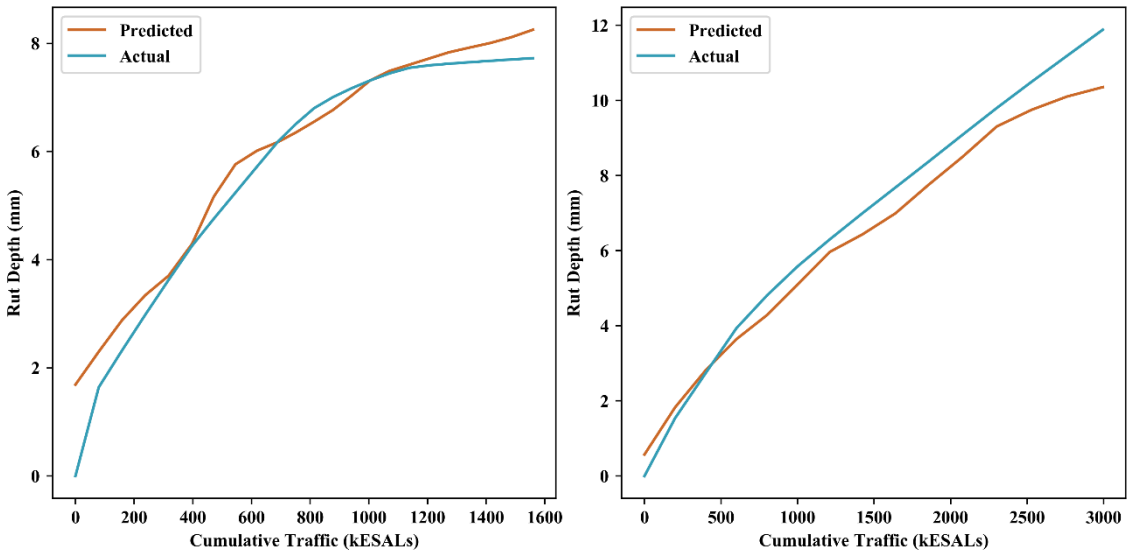

a) New Mexico 35-103 **b) Texas 48-120**

Figure 26: Examples of prediction results from: a) New Mexico SHRP section 103 and b) Texas SHRP section 120.

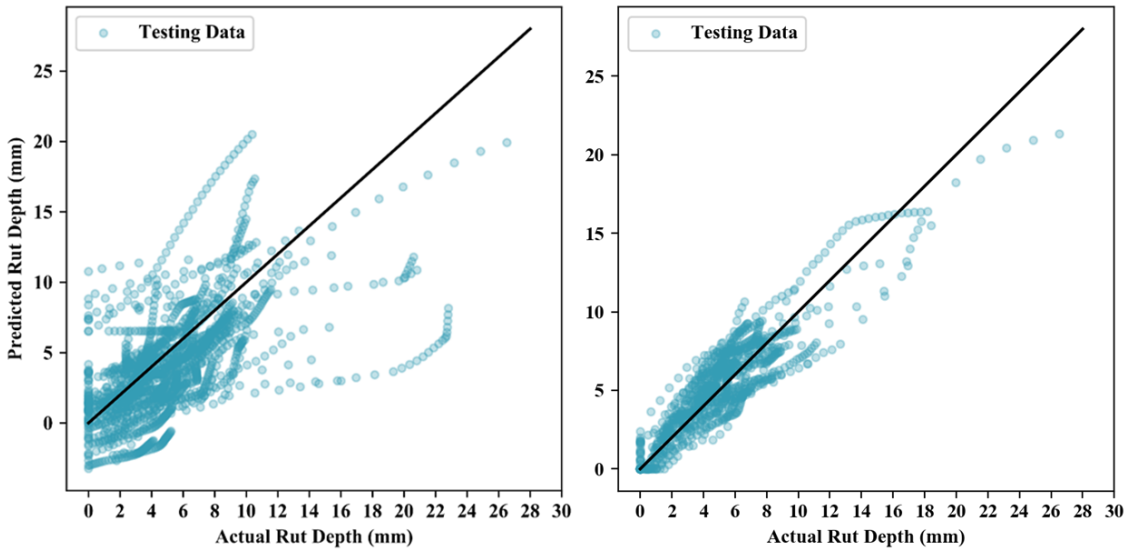

a) Before Improvements **b) After Improvements**

Figure 27: Model performance comparison: a) Before improvements and b) After improvements.

6.1.3 NN Model Evaluation

6.1.3.1 Comparison with Multiple Linear Regression Results

The model developed using NN is evaluated against a model developed based on traditional multivariate linear regression (MLR) techniques and relying on the same dataset (Figure 28). Fitting the data using an MLR model results in a low coefficient of determination (R^2) of 0.28 for the testing and training datasets. The MSE for the testing dataset is 8.49 mm^2, while that for the training dataset is 7.84 mm^2. Additionally, the MAE is 2.07 and 2.03 mm for testing and training. The overall performance of the MLR model is poor as expected due to its inability to model the complex interactions between the features affecting rutting. This provides strong evidence regarding the superiority of the NN rutting prediction model and therefore justifies its selection (Figure 28).

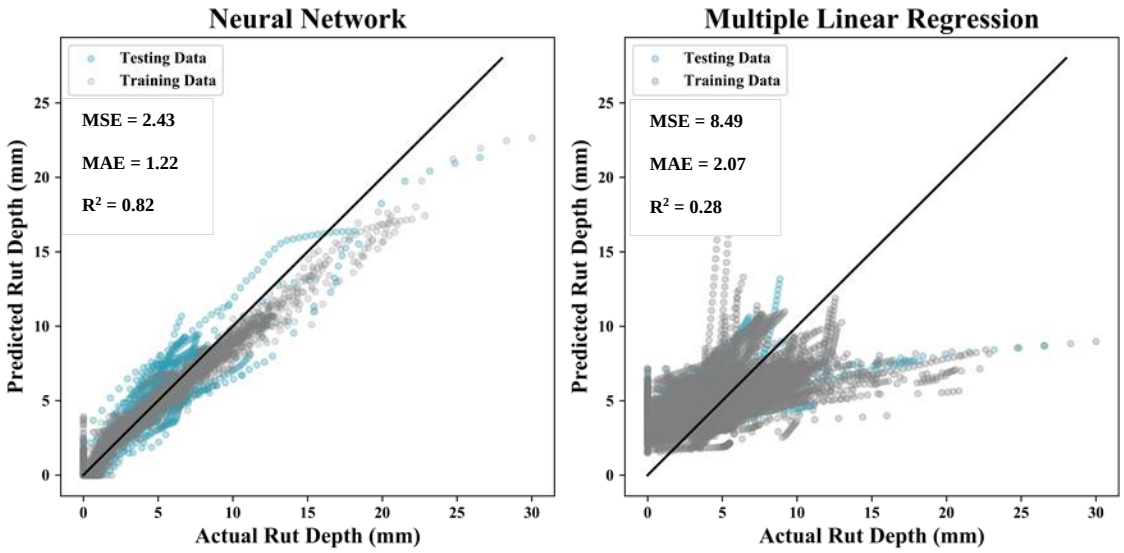

Figure 28: Comparison between MLR and NN modeling methods for predicting rutting depth.

6.1.3.2 Comparison with the Current State-of-Practice

To date, the M-E rutting prediction models that are incorporated in Pavement-ME are the most common due to their ability to generalize to different climates and material properties as opposed to other models that are developed using location-specific data. The M-E model was developed based on 334 data points and had an R^2 of 0.57 [56]. Therefore, the developed NN model having an R^2 exceeding 0.9 improves rutting prediction by 45%. Additionally, it is worth noting that the developed NN model requires a total of 29 inputs that fall into three main categories compared to the M-E model that requires more than 80 inputs. For the M-E model to provide acceptable prediction, meticulous laboratory testing of materials and traffic assessments are essential. In contrast, the developed NN model works using simple inputs that can be attained at a low cost and minimal efforts. In addition to the Pavement-ME models, the obtained NN model is also superior to the available HDM-4 rutting prediction models which have a low coefficient of determination of 0.42 [134]. It is not until local calibration efforts are conducted that the HDM-4 models start performing comparably to the developed NN model [26]. Similarly, the cumulative rutting prediction model reported by Austroads was developed using 144 data points and has an R^2 of 0.44 [135].

On the other hand, it is not possible to compare the results with other NN models that are available in the literature mainly due to the difference in the adopted sampling methods. As discussed previously in section 5.1 and as demonstrated in Figure 16 and Table 11, the sampling method has a significant impact on the performance of the model. The second sampling method, which is considered more representative, adds restrictions to the model; thus, resulting in increased errors. Most studies that employ NNs for similar applications, utilize the first sampling method which results in slightly

better performance in contrast to this study which uses a more challenging approach. However, if the dataset developed in this study is used with the first sampling method, comparable results to the literature are obtained, as provided in Table 11.

Overall, this model delivers significantly better results due to its ability to model the different input interactions while requiring simplistic and limited inputs unlike the other available models which exhibit relatively higher errors, require local calibration, and involve meticulous materials laboratory testing and traffic assessments.

6.2 Model Interpretation

6.2.1 Permutation Importance Analysis

The developed model is also utilized to identify the significant factors affecting rutting depth to provide decision-makers with guidance regarding the most critical features so that they prioritize their collection. The importance of the different features is evaluated using the Permutation Feature Importance method which measures the importance of any feature by calculating the increase in errors as a result of shuffling or permuting the features' values [136]. Figure 29 shows the feature importance of all the studied variables. It is observed that the local climate and traffic conditions are the highest contributors to rutting prediction. Familiarity with the local construction technologies is also important for performing accurate rutting predictions where construction variability was the second most influential factor. Regarding material properties, aggregate gradation characteristics are amongst the most important variables for all AC layers. Particularly, the percentage passing #4 and #200 sieves as well as the NMAS are among the top 10 most contributing features. On the other hand, AC

thickness variables did not exhibit high importance. This is in line with common technical knowledge which attributes asphalt rutting to material and environmental factors rather than thickness. It can also be concluded that on average, the properties of the surface and binder layers contribute comparably to the rutting prediction, while the properties of the base layers are significantly less influential. Regarding subsurface layers, Figure 29 shows that the material types for base layers are more important than their thickness. As a result, municipalities can decide to focus their investments on collecting material information of the top asphalt layers as opposed to collecting data for the base and subgrade layers. While permutation importance analysis provides a general indication of the importance of the different features, it holds several limitations that may affect the results. The main limitation is that it does not take into account the correlation between the different features while it permutes one feature at a time. This is specifically critical when permuting base material properties which are categorical variables, or asphalt mix volumetric and gradation properties.

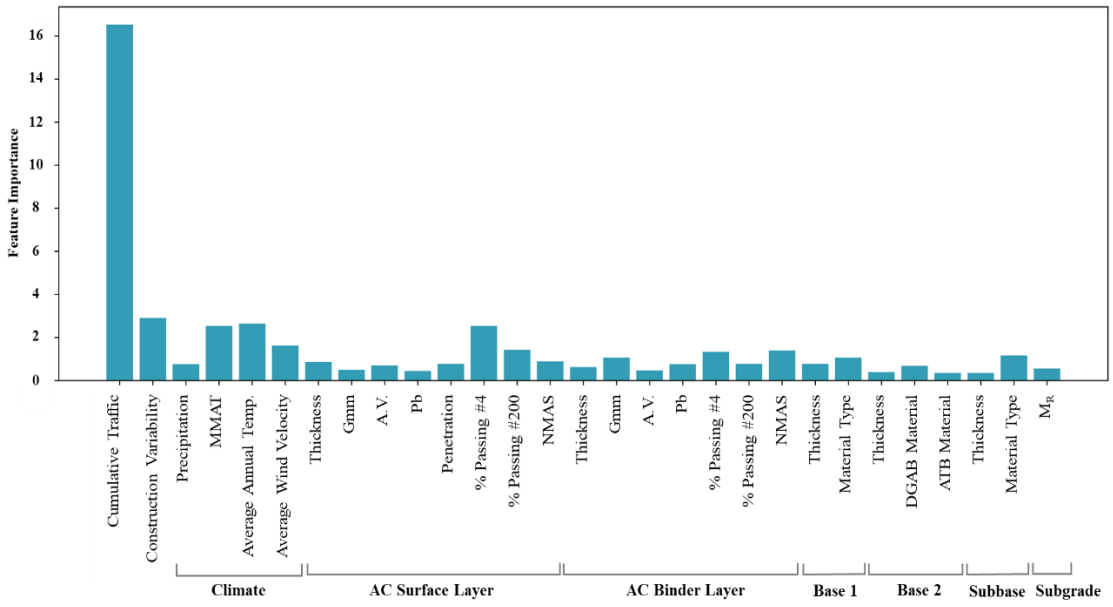

Figure 29: Feature Importance results.

6.2.2 Sensitivity Analysis

To further interpret the developed model, a detailed sensitivity analysis is conducted to quantify the effects of the different variables. Figure 30 shows the relationships between rutting depth and some of the key input variables. A reference input vector is generated based on the minimum, first, second, third, and fourth quantiles. Appendix B provides detailed documentation of the used values. Figure 30a complements the findings of section 6.2.1 regarding the importance of traffic for predicting rutting. It also mirrors the rutting mechanism as it starts with a high rate until the traffic reaches 5 million ESALs and slows down as rutting and the cumulative traffic increase (Figure 30a). This notable impact reflects an average elasticity value of 0.26. Another important variable is the construction variability which reflects the coefficient of variation of rutting depth on a road section. Figure 30b shows a significant decrease in rut depth as the C.O.V variable increases. While this may be a result of many factors,

the main reason for the decreasing trend is mathematical. The C.O.V is calculated as the standard deviation divided by the mean and as the value of the mean increases the C.O.V decreases and vice versa.

Additionally, the permutation importance analysis revealed the significant importance of climate-related variables, especially the average annual temperature and the wind velocity. As expected, rutting increases with temperature at an average rate of 0.95% for a 1% increase in temperature (Figure 30c). Similarly, the increase in wind velocity results in an increased rutting depth corresponding to an elasticity value of 0.63 (Figure 30d). This is inconsistent with previous research which suggests that the presence of high wind speeds contributes to cooling the pavement's surface through convention, thus reducing the accumulation of rutting. Therefore, the inconsistency may arise since the effect of wind speed was studied independently of temperature [127], [137].

The effect of the thickness of the different asphalt layers was also evaluated (Figure 30e). Rutting increases as the thickness of the surface AC layer increases until reaching 6 cm (2.5 in.) beyond which rutting becomes relatively insensitive to thickness. On the other hand, the thickness of the binder AC layer appears to affect rutting in a strictly increasing manner at an average elasticity of 0.26 as opposed to 0.07 for the surface layer (Figure 30e). This contradicts previous findings that discuss that thicker pavements generally develop higher rutting resistance [138].

In addition to thickness, the maximum specific gravity of the asphalt mixes used in both layers was studied. Rutting is relatively insensitive to the surface layer's G_{mm} but extremely susceptible to that of the binder layer (Figure 30f). A decreasing

relationship is obtained where rutting decreases by more than 4% for every 1% increase in G_{mm} (Figure 30f). While this was the highest obtained elasticity value, it is worth noting that a 1% increase in G_{mm} is considered a relatively high increase as compared to a 1% increase in traffic for example which is considered negligible. Other volumetric properties are also studied as shown in Figure 30g and Figure 30h. The rutting depth does not appear to be sensitive to the change in the percentage of air voids and binder content. Rutting remains constant as the percentage of air voids in the surface layer increases but increases slightly with the percentage of air voids in the binder layer (Figure 30g). On the other hand, an increase in the binder content in the surface AC layer results in an average reduction in the rut depth (Figure 30h). The effect of changing the binder content in the binder layer is not uniform, where the rut depth increases with P_b then decreases as it exceeds 4.5%. Comparing these trends with previous studies is not straightforward since no constant trends have been observed and documented regarding these factors [139].

The effect of the percentage of aggregates passing the #4 and the #200 sieves are compared (Figure 30i and Figure 30j). The effect of the percentage of material passing sieve #4 is highly significant for both AC layers. Regarding the surface AC layer, as the percentage passing the #4 sieve increases by 1%, the percentage of rutting increases by 0.72% (Figure 30i). Similarly, increasing the percentage passing the #200 sieve results in increasing the rut depth with an elasticity of 0.2 (Figure 30i). Generally, mixes with excessive fine-grained aggregates are more susceptible to rutting which might justify the increase in rutting associated with the increase in the percentage of aggregates passing the #4 and #200 sieves [17]. However, the analysis of the sensitivity of the rut depth with respect to the gradation of the binder layer reveals a lower

sensitivity than that of the surface layer (Figure 30h). Additionally, a negative relationship is observed between the percentage of aggregates passing the #4 sieve with an elasticity value corresponding to -0.29. On the other hand, the model is not sensitive to the percentage of aggregates passing the #200 sieve (Figure 30h).

Regarding the penetration grade of the asphalt binder, the rut depth tends to decrease slightly as the penetration increases to 75 .1 mm and then starts to increase as the binder becomes softer (Figure 30k). The overall elasticity of this variable is quantified as 0.3 which reflects a 0.3% increase in rutting as a response to a 1% increase in penetration (Figure 30k). However, the exact sensitivity of rutting to the penetration grade may be masked because agencies generally use binders that satisfy the penetration values specified in their materials specifications.

Finally, the properties of the base and subgrade layers were studied. The results show that rut depth is not significantly sensitive to the change in the base thicknesses, material types, and the subgrade resilient modulus. A negative relationship between rut depth and the total base thickness is expected since that thickness contributes the most to the structural rutting component (Figure 30l). However, the obtained positive correlation between rutting and the subgrade resilient modulus defies common engineering judgment (Figure 30n).

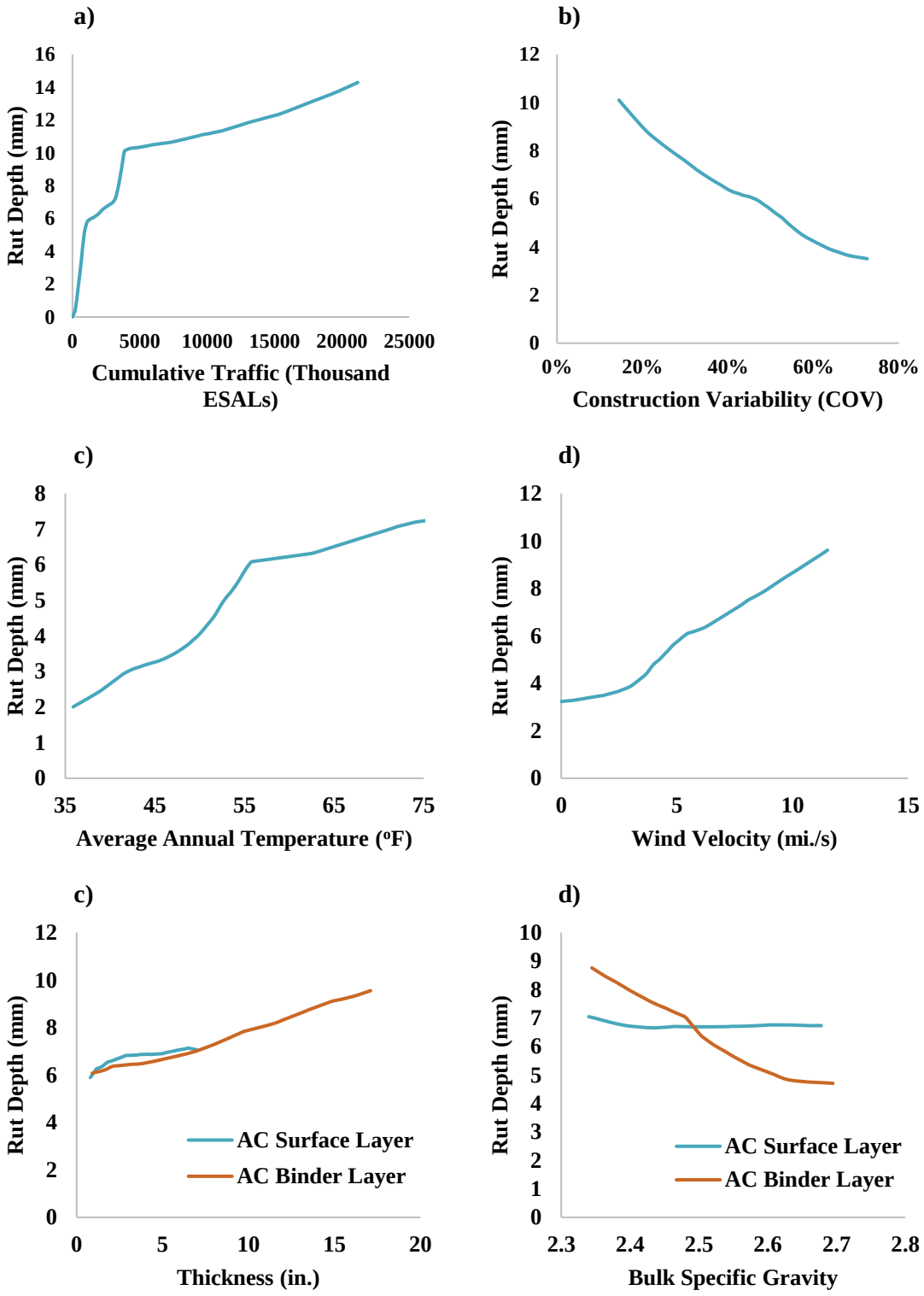
a)
Rut Depth (mm)
16
14
12
10
8
6
4
2
0
0
5000
10000
15000
20000
25000
Cumulative Traffic (Thousand ESALs)
b)
Rut Depth (mm)
12
10
8
6
4
2
0
0%
20%
40%
60%
80%
Construction Variability (COV)
c)
Rut Depth (mm)
8
7
6
5
4
3
2
1
0
35
45
55
65
75
Average Annual Temperature (ºF)
d)
Rut Depth (mm)
12
10
8
6
4
2
0
0
5
10
15
Wind Velocity (mi./s)
c)
Rut Depth (mm)
12
10
8
6
4
2
0
0
5
10
15
20
Thickness (in.)
AC Surface Layer
AC Binder Layer
d)
Rut Depth (mm)
10
9
8
7
6
5
4
3
2
1
0
2.3
2.4
2.5
2.6
2.7
2.8
Bulk Specific Gravity
AC Surface Layer
AC Binder Layer

g)

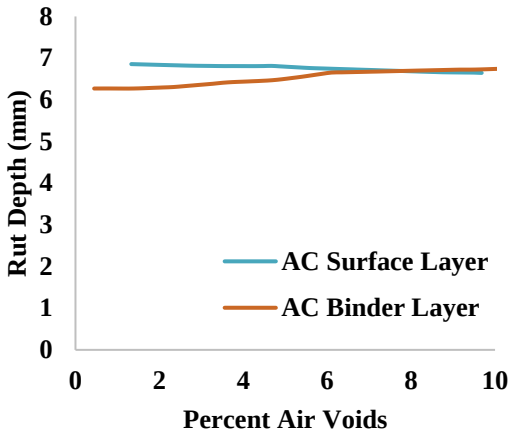
Rut Depth (mm)
0
1
2
3
4
5
6
7
8
0
2
4
6
8
10
Percent Air Voids
AC Surface Layer
AC Binder Layer

h)

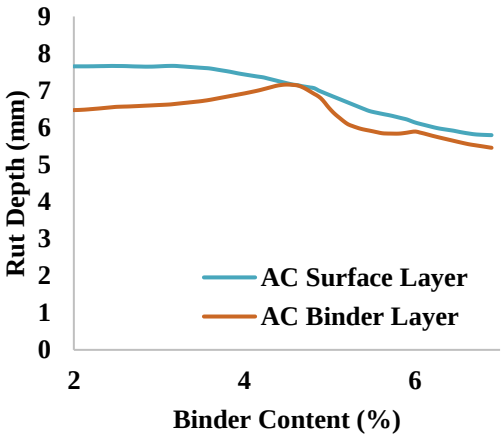
Rut Depth (mm)
0
1
2
3
4
5
6
7
8
9
2
4
6
Binder Content (%)
AC Surface Layer
AC Binder Layer

i)

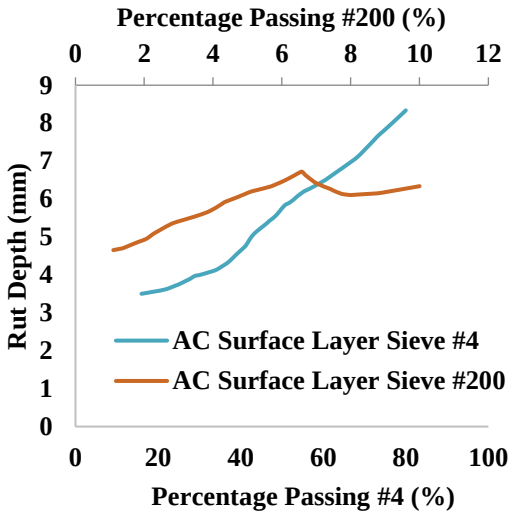
Percentage Passing #200 (%)
0
2
4
6
8
10
12
Rut Depth (mm)
0
1
2
3
4
5
6
7
8
9
0
20
40
60
80
100
Percentage Passing #4 (%)
AC Surface Layer Sieve #4
AC Surface Layer Sieve #200

j)

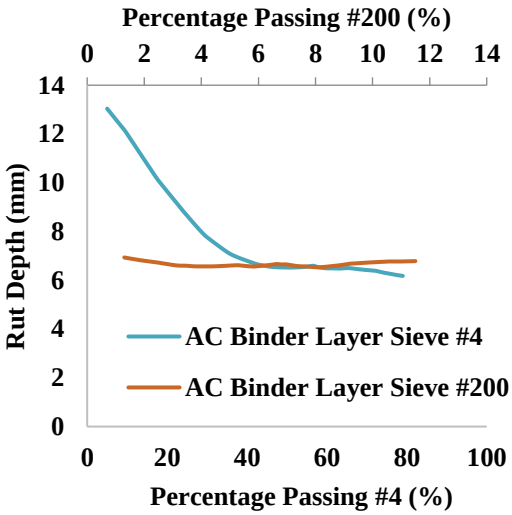
Percentage Passing #200 (%)
0
2
4
6
8
10
12
14
Rut Depth (mm)
0
2
4
6
8
10
12
14
0
20
40
60
80
100
Percentage Passing #4 (%)
AC Binder Layer Sieve #4
AC Binder Layer Sieve #200

k)

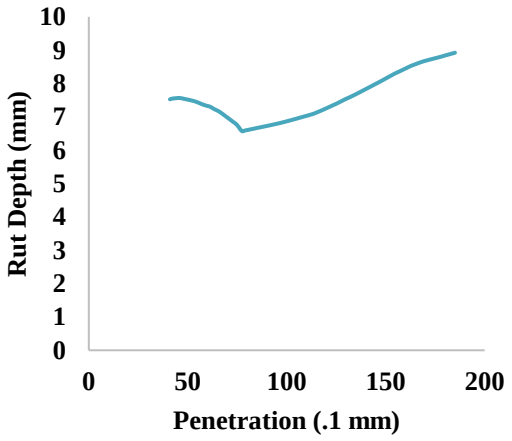
Rut Depth (mm)
0
1
2
3
4
5
6
7
8
9
10
0
50
100
150
200
Penetration (.1 mm)

l)

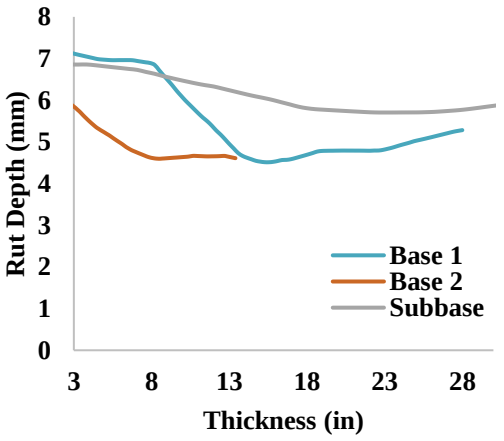
Rut Depth (mm)
0
1
2
3
4
5
6
7
8
3
8
13
18
23
28
Thickness (in)
Base 1
Base 2
Subbase

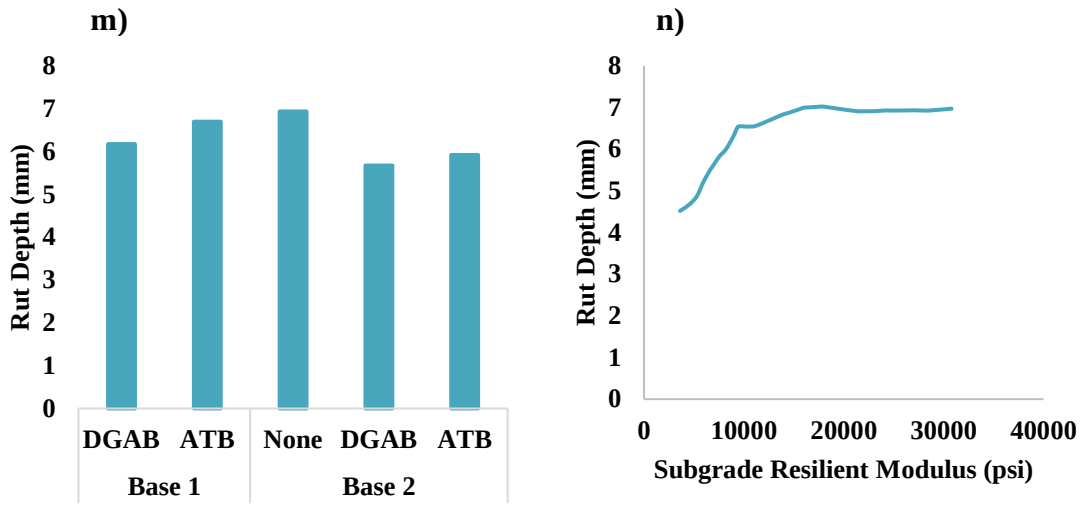

Figure 30: Sensitivity of rutting depth with respect to: a) Cumulative traffic, b) Construction variability, c) Average annual temperature, d) Wind velocity, e) Thickness of AC layers, f) Bulk specific gravity, g) Percent air voids, h) Binder content, i) Gradation od surface layer, j) Gradation of binder layer, k) Penetration, l) Thickness of base layers, m) Base material types, n) Subgrade resilient modulus.

The results of the sensitivity analysis are summarized in Figure 31 that presents the elasticity and the rank corresponding to all the continuous variables. The ranking scheme obtained from the sensitivity analysis resulted in a different order than that obtained from the permutation importance analysis (Figure 29). This is to be expected since both methods rank the different variables based on different metrics and a different methodology. The permutation importance relies on fitting a model for several permuted datasets and comparing the loss of accuracy, while the sensitivity analysis relies on the final trained and tuned model. Additionally, both methods do not explicitly account for collinearity in the models and therefore their results are not comprehensive.

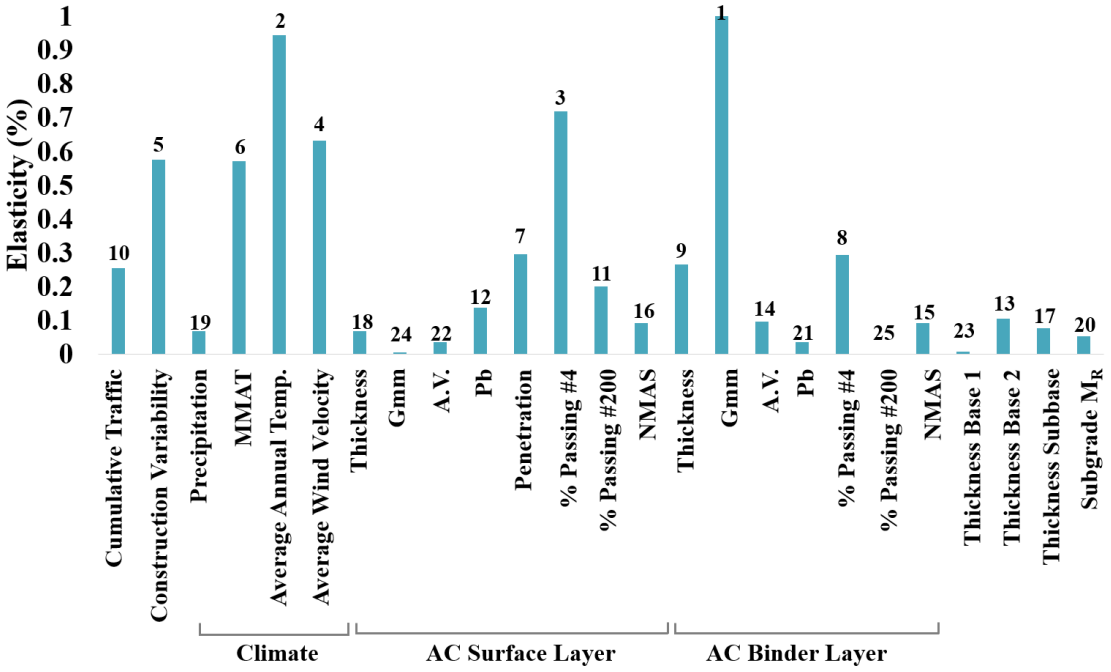

Figure 31: Sensitivity analysis results.

6.3 Family Models

Family models discussed herein are developed in accordance with the methodology described in section 4.5. It is worth noting that data was not available to develop family models for all combinations, therefore, only the 27 families will be provided. Figure 32 demonstrates all derived rutting prediction curves for different highway functional classes, climate zones, and rutting resistance capabilities. All the obtained family curves have a mathematical structure of a third-degree polynomial. While the freezing and non-freezing climate zones have similar deterioration trends for interstates in dry climates as observed in Figure 32a and Figure 32b, it is evident from Figure 32c and Figure 32d corresponding to wet regions that the effect of freezing is more pronounced. Figure 32c shows that the mix that is the least resistant to rutting reaches a rut depth value of approximately 11 mm after 20 years in a WF zone while a

higher depth of almost 22 mm is obtained for WNF zones as illustrated in Figure 32d. Similar conclusions can also be obtained if the different mix types are compared. Additional observations are made from analyzing the family curves for interstates regarding the effect of moisture where wet regions experience higher rutting values than dry regions.

In contrast, the conclusions obtained for interstates were reversed in the case of arterial roads where the freeze regions exhibit significantly higher rutting depths than non-freeze regions (Figure 32e, f, g, and h). Investigating the data reveals that regions located in a freeze zone tend to use softer binders for arterial roads compared to interstates. On average, binder grades having an average penetration of 75 .1mm is used for interstates in freezing regions compared to an average penetration of 100 .1mm for arterials in the same climatic regions. This justifies the higher rutting values in freeze regions (Figure 32e and g) as opposed to lower values in non-freeze regions (Figure 32f and h). Additionally, the effect of moisture conditions was not significant for arterials as opposed to interstates.

Limited data was available for determining family deterioration curves for collector roads. It is evident that collectors appear to have lower rutting depths compared to the other road functional classes as shown in Figure 32i and Figure 32j. This is inline with common engineering judgment since collector roads experience significantly lower truck volumes.

The percentage error for each curve was also obtained. This error describes how much the rutting measurements deviate from the prediction for each family. On average the error was equivalent to 16% and it ranged between 2% and 36%. This

reflects a significant variability in rutting within the same family which is attributed to the introduced simplifications.

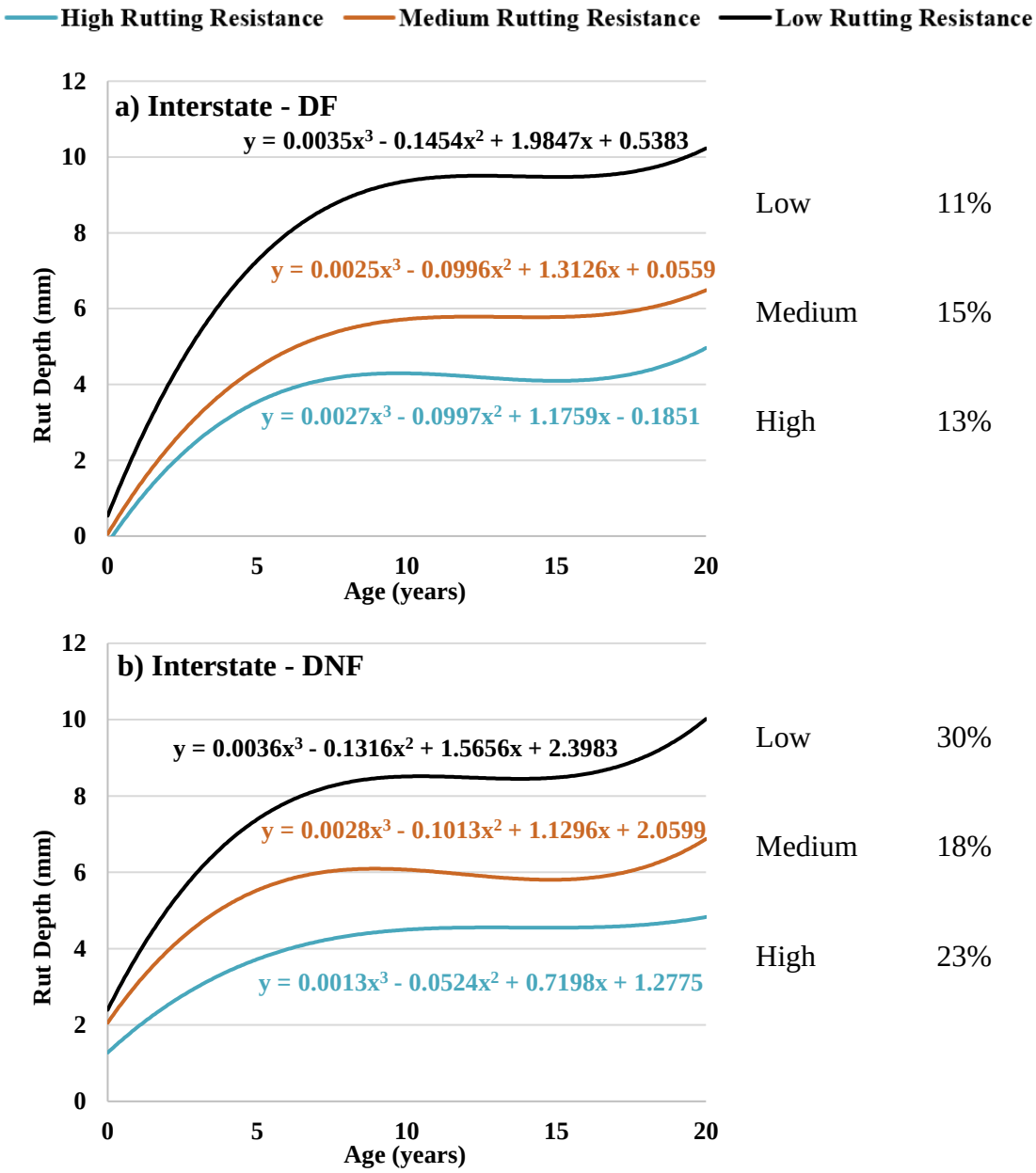

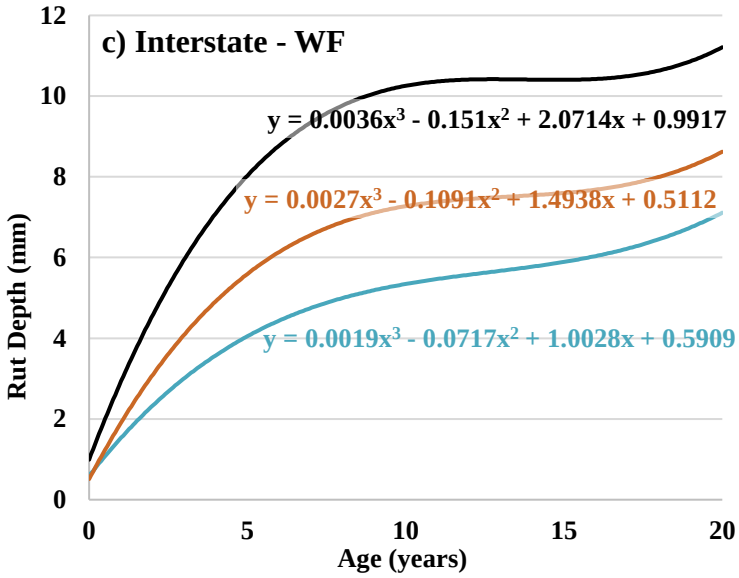

Low	32%
Medium	16%
High	17%

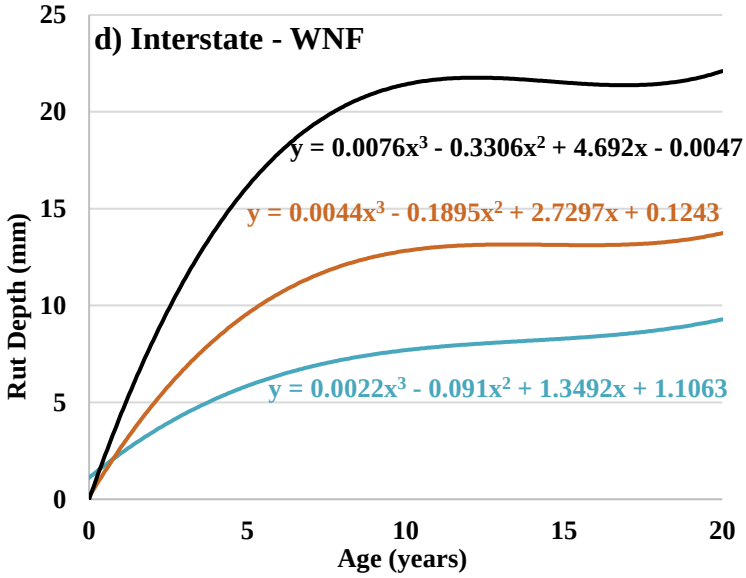

Low	17%
Medium	8%
High	19%

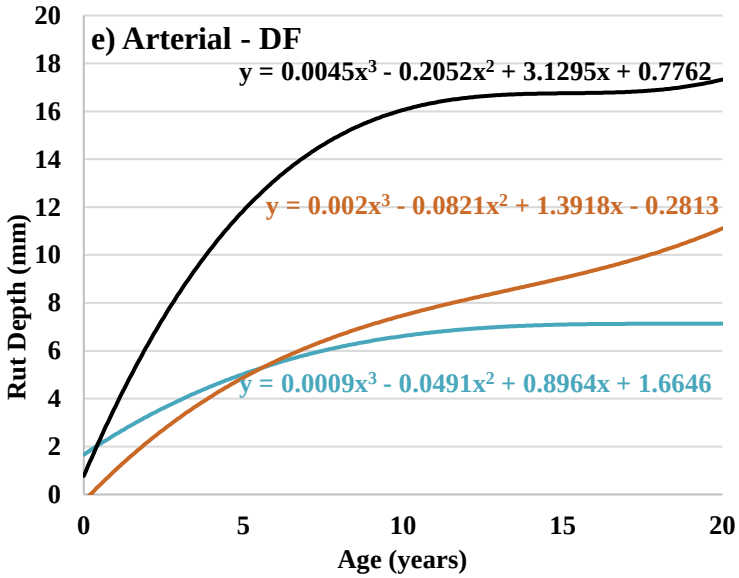

Low	12%
Medium	10%
High	3%

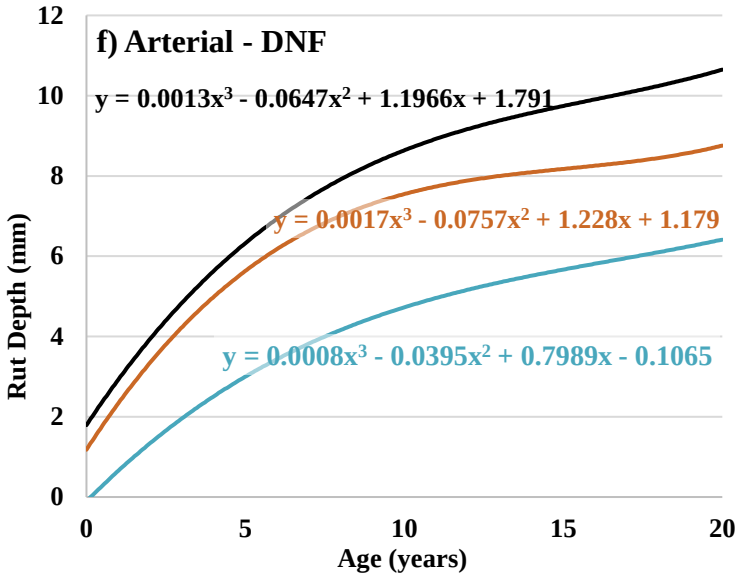

Low	5%
Medium	8%
High	20%

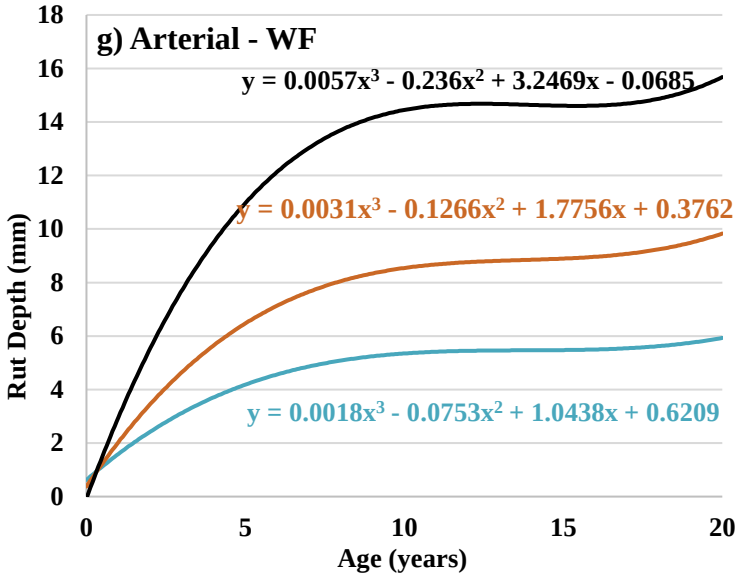

Low	15%
Medium	19%
High	20%

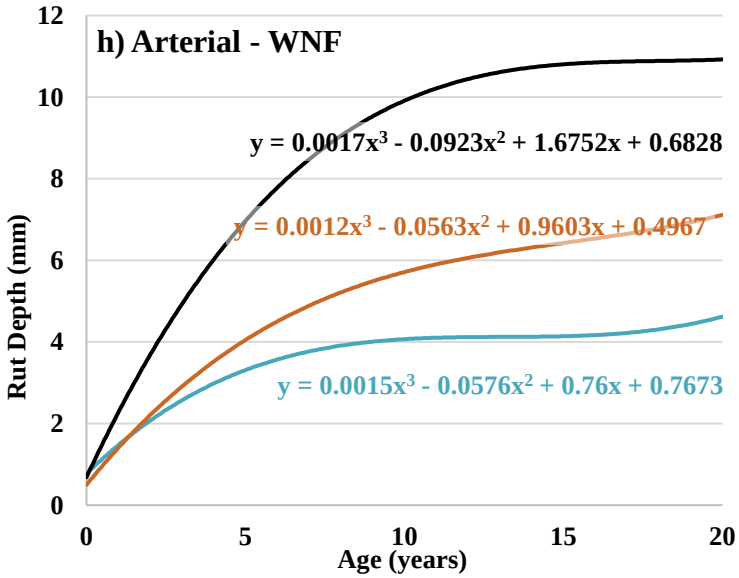

Low	8%
Medium	22%
High	11%

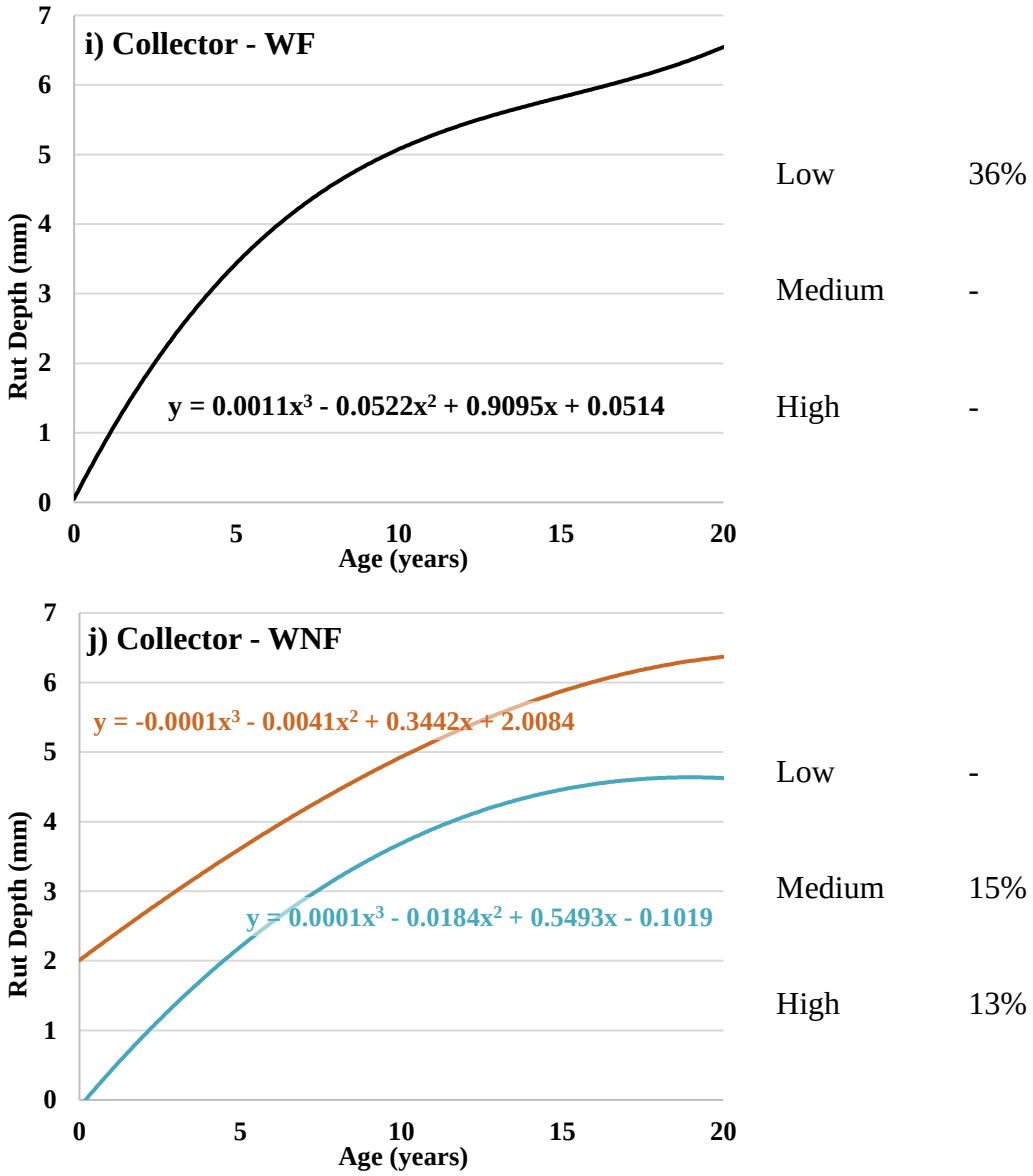

Figure 32: Family rutting prediction curves.

6.4 Ensemble Kalman Filter Framework

An EnKF framework is proposed to calibrate the family curves. To assess the robustness and applicability of the framework, sensitivity analysis is conducted by varying several contributing factors such as the effect of the ensemble size and initial guesses.

6.4.1 Numerical Example

A case study using rutting measurements collected over 14 years from SHRP section 112 in the State of Alabama is used to illustrate the proposed updating framework as well as perform sensitivity and convergence analysis. Alabama lies in a wet non-freeze (WNF) zone and the considered road section is part of an interstate. Additionally, the road is considered to have high resistance to rutting. As a result, the ODE corresponding to the family curve presented in Figure 32d is used as the dynamic model at the forecast step for predicting the progression of rutting. A time step of 0.01 years is selected for the dynamic propagation based on a sensitivity analysis study. Table 15 summarizes all the sources of uncertainty that apply.

6.4.2 Effect of the Ensemble Size

The sensitivity of the EnKF framework to the ensemble size is evaluated to obtain the optimal size that provides the required accuracy and efficiency. To that extent, the simulation is performed 100 times for every ensemble size to calculate the mean and standard deviation of the predicted parameters at the last update step.

Table 15: Quantified uncertainty in the EnKF framework.

Uncertainty Type		Error C.O.V.	Distribution	Quantification Method
Initial Guess Error		20%	Normal	Sensitivity Analysis
Model Error		20%	Normal	Family curves residuals
Process Noise		5%	Normal	Sensitivity Analysis
Measurement Error	Instrumental	2mm	Uniform [-2,2]	Literature Review
	Spatial Variability	20%	Normal	Variability in LTPP data

Figure 33 presents the results of the sensitivity analysis showing the deviation of the mean and standard deviation of the parameters across the different simulations. The variability between the means of the predicted parameters of the different simulation runs decreases as a function of the ensemble size. The variability achieved at an ensemble size of 10,000 is considered acceptable and it will be used for the subsequent simulations in this study.

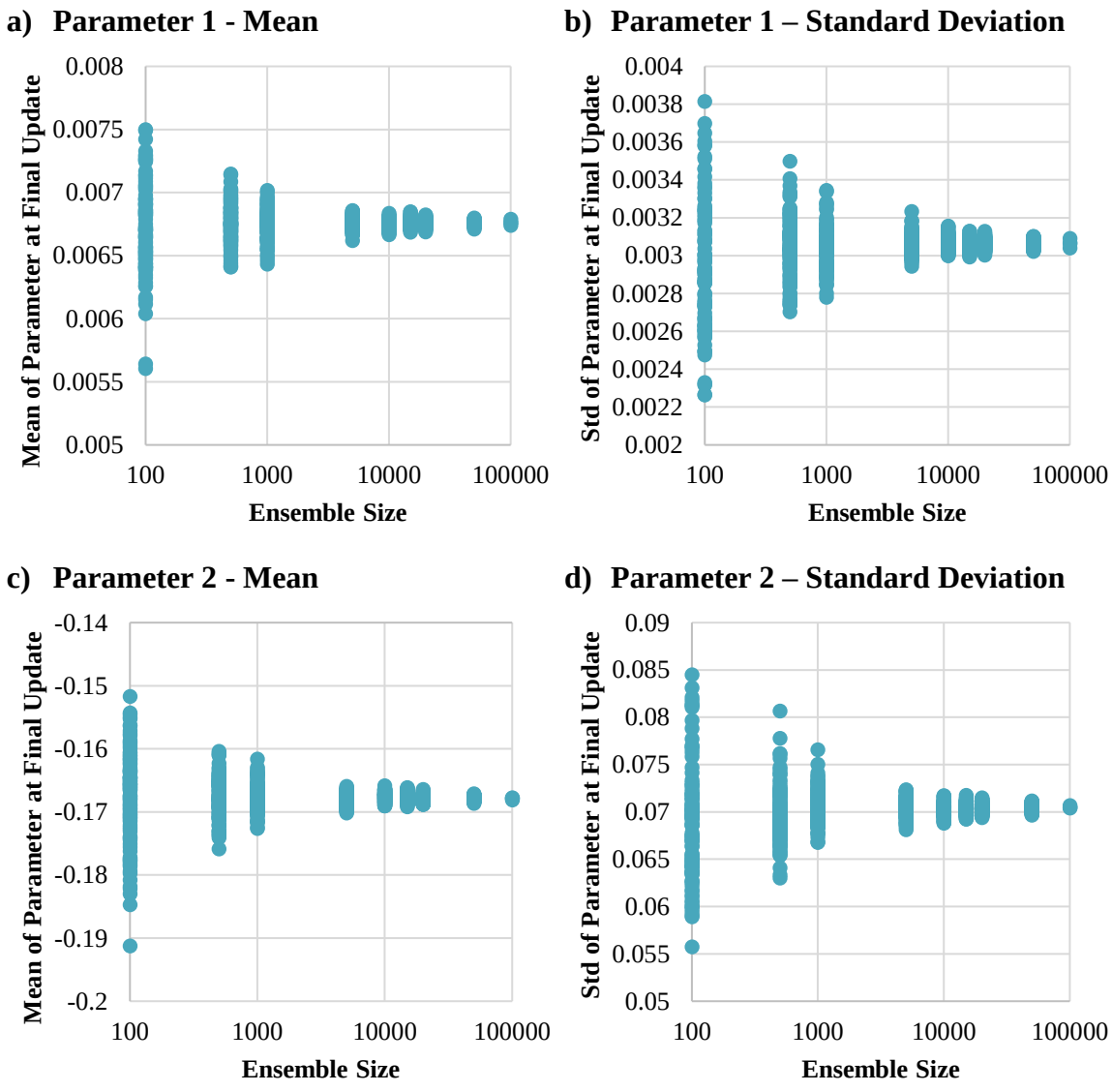

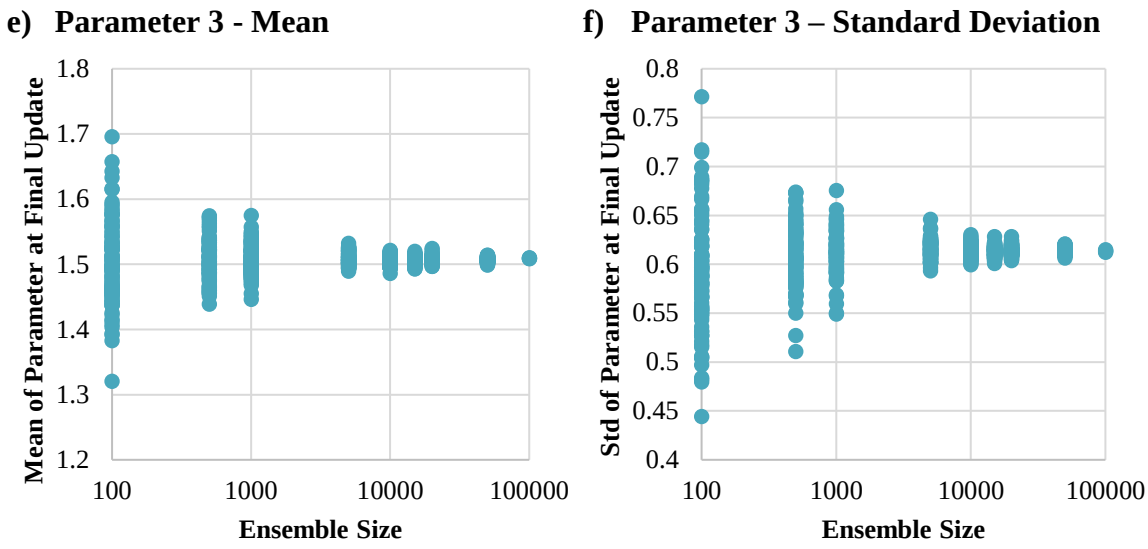

Figure 33: Mean and Std. of predicted parameters as a function of the Ensemble size.

6.4.3 Sensitivity to the Initial Guess

Sensitivity analysis is also conducted to evaluate the robustness of the framework and its ability to converge despite the selected initial states. This evaluation is essential since road agencies may not have sufficient information to select the ideal family curve. Therefore, the framework is assessed starting with initial state vectors corresponding to three different family curves as presented in Table 16.

Table 16: Different scenarios for the initial state vector.

Case	Pavement Family	Parameter 1	Parameter 2	Parameter 3
Base Case	Interstate – WNF – High Resistance	0.0066	-0.182	1.35
Incorrect Rutting Resistance	Interstate – WNF – Medium Resistance	0.0132	-0.379	2.73
Incorrect Climate Zone and Rutting Resistance	Interstate – DNF – Medium Resistance	0.0084	-0.203	1.13

Figure 34 shows the three different scenarios and illustrates how far their predictions are from the actual measurements. The EnKF framework is performed for each of the three cases. Monte Carlo simulations are then carried out to sample 1,000 realizations of the calibrated parameters. These realizations are propagated forward in time to obtain the mean and the standard deviation of the predicted rutting depths. Figures 35, 36, and 37 present the results of the mean parameters obtained at the end of different updates. An envelope representing one standard deviation away from the mean of the predictions corresponding to the final update is also shown. Figures 35a, 36a, and 37a show that the average prediction does not change significantly beyond the tenth update. It is also noted that even though the accuracy of the EnKF estimate varies between the three scenarios, the measurements remain almost within one standard deviation from the estimated mean.

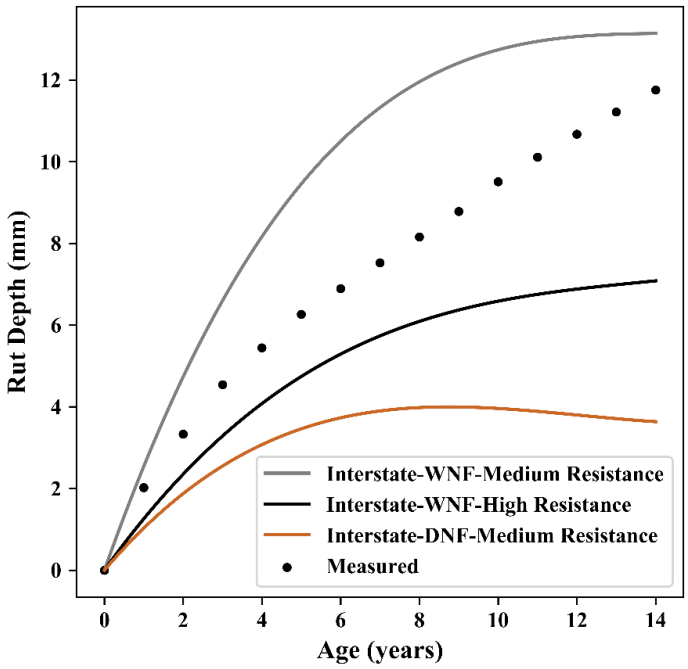

Figure 34: Example of different initial guesses.

Moreover, the figures present the average of the errors computed for all 1,000 simulations after each update and for the different initial guesses. Figures 35b, 36b and 37b reveal that sharp drops in the average prediction errors equivalent to approximately 58%, 52%, and 50% respectively occur after the second update. Beyond that, the initial prediction errors are further improved by 8%, 6%, and 11% for each initial guess respectively. Based on the results of Figures 35b, 36b, and 37b, the improvements in the average predictive performance of the three scenarios are consistent and comparable where the framework reduces the errors by 60% on average.

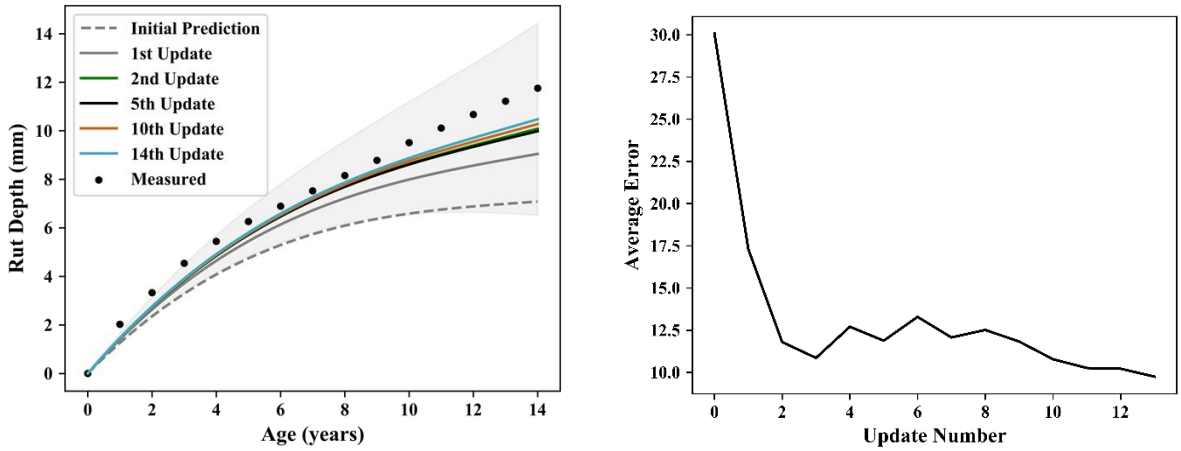

Figure 35: Base case results: a) Rut depth, and b) Model performance as a function of the number of EnKF updates

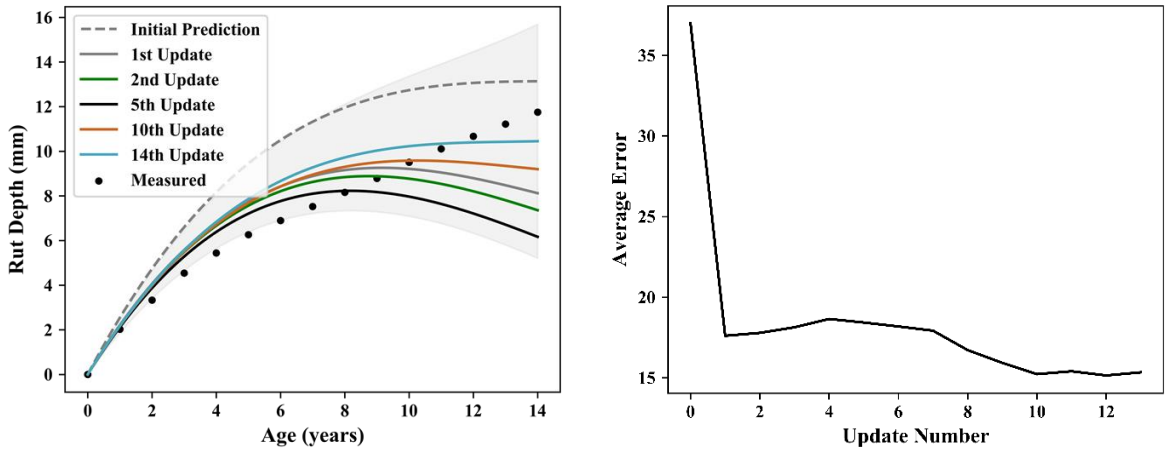

Figure 36: Incorrect rutting resistance case results: a) Rut depth, and b) Model performance as a function of the number of EnKF updates

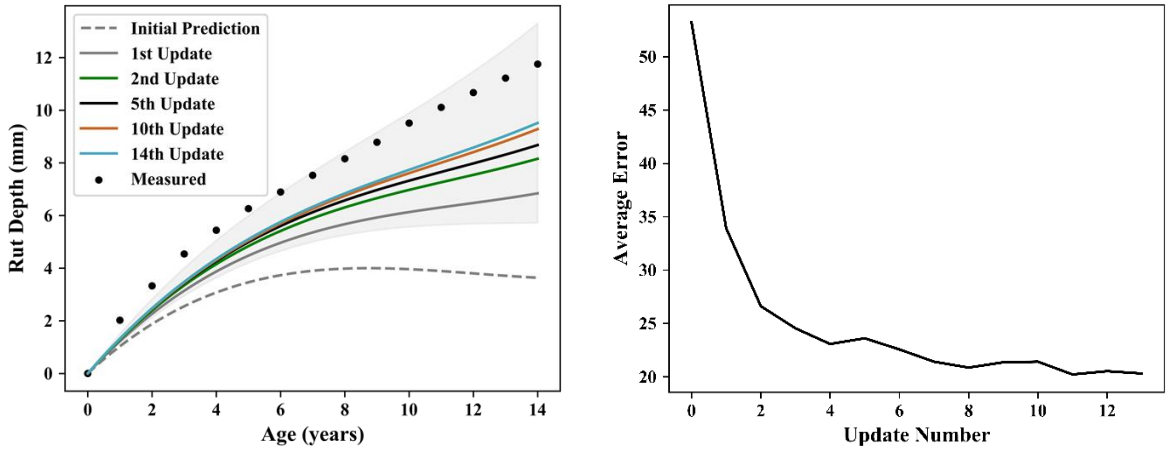

Figure 37: Incorrect Climate Zone and Rutting Resistance case results: a) Rut depth, and b) Model performance as a function of the number of EnKF updates

6.4.4 Discussion

While applying this framework, the data distributions of the updated parameters after every measurement are identified. The Chi-Squared test is used to identify the ideal distribution for each parameter. Table 17 shows the corresponding distribution of parameters after the final update. While the parameters were considered independent at the start on the EnKF framework, the calibrated states were correlated.

In fact, a correlation of -0.1 exists between parameters 1 and 2 and of -0.2 between parameters 2 and 3. Therefore, the covariance of the calibrated parameters should be considered for sampling realizations through Monte Carlo simulations (Table 17). One thousand realizations of the three parameters are sampled to study the variability in the predicted rutting depth.

Figure 38 shows the mean and standard deviation of the predictions after the final update as well as the measurements and their corresponding variability. The results show that the proposed framework achieves its objectives as it reduces the mismatch between the measurements and the predictions. Additionally, it allows for modeling and representing the uncertainties and overcoming the limitations associated with deterministic models. While the prediction interval which delineates where future observations may fall is relatively wide, the results are considered acceptable provided the high uncertainties associated with measuring and predicting rutting in asphalt pavements.

The power of the proposed methodology lies in its ability to provide accurate predictions that practitioners can employ in pavement management. In addition to obtaining a prediction curve, the framework can be used to develop maintenance schedules by providing engineers with the probability of reaching specific maintenance thresholds. In this application, rut depths of 6mm and 13mm are set as triggers for

Table 17: Calibrated model parameters distribution.

Parameters	Distribution	Mean	Covariance Matrix		
Parameter 1	Lognormal	0.00667	1.82 e-06	-3.94 e-06	-1.03 e-05
Parameter 2	Beta	-0.176	-3.94 e-06	1.10 e-03	-1.56 e-03
Parameter 3	Lognormal	1.54	-1.03 e-05	-1.56 e-03	4.02 e-02

milling and overlaying and removing the distressed area as suggested in AASHTO's Guide Specifications for Highway Construction [58]. This is reflected in Figure 39 which shows the probability of requiring milling or rehabilitation at each year. This concept can be interpreted on the project and network levels. On the project level, the outcome provides engineers with the probability that a road may require a certain treatment. On the network level, the outcome is interpreted as the percentage of the entire network that requires each treatment type. It is evident that at the 8th year of the pavement's life, 80% of the roads of the corresponding family will require milling. Beyond 8 years the percentage of pavements that require removing the rutted areas rises while that of pavements requiring milling is reduced.

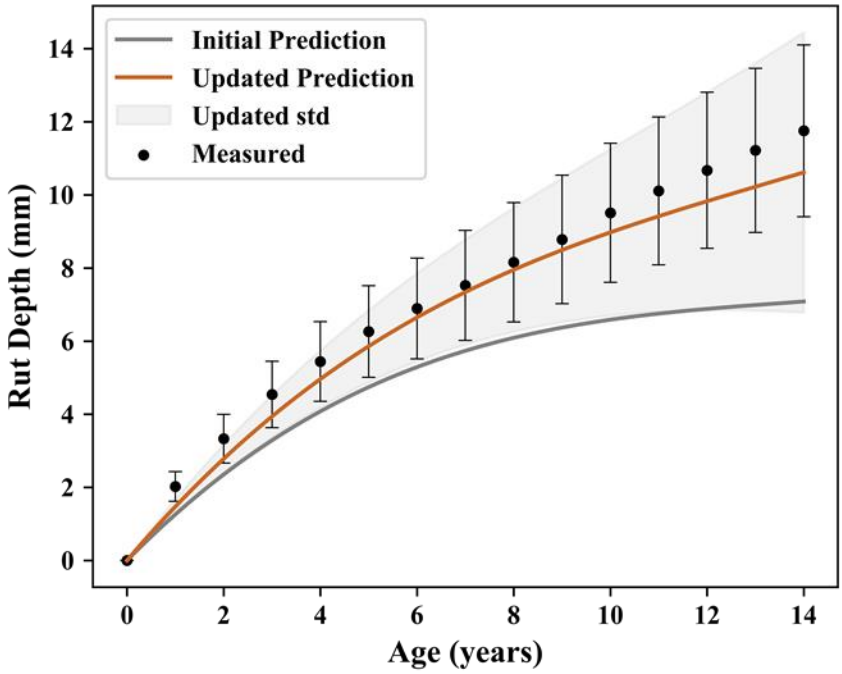

Figure 38: Calibrated rutting prediction model.

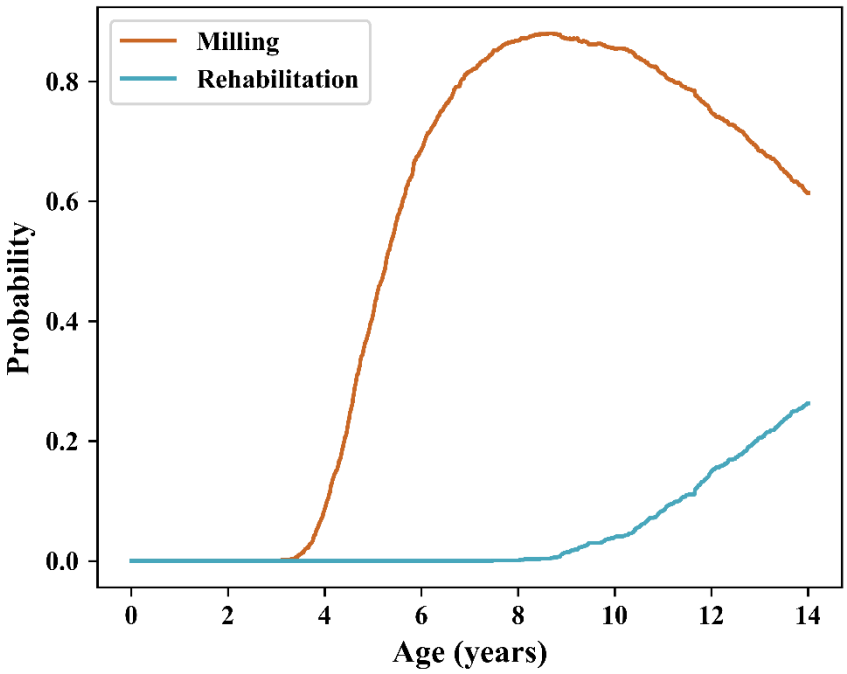

Figure 39: Probability of achieving maintenance triggers.

CHAPTER 7

USER INTERFACE

7.1 Introduction

Since the NN model does not have a mathematical form, a user-friendly interactive graphical user interface (GUI) is developed in order to deploy the final model. This tool can be made available to researchers and road agency personnel who are interested in predicting rutting performance. The GUI involves three main pages. The first is the home page where the user provides general information as shown in Figure 40.

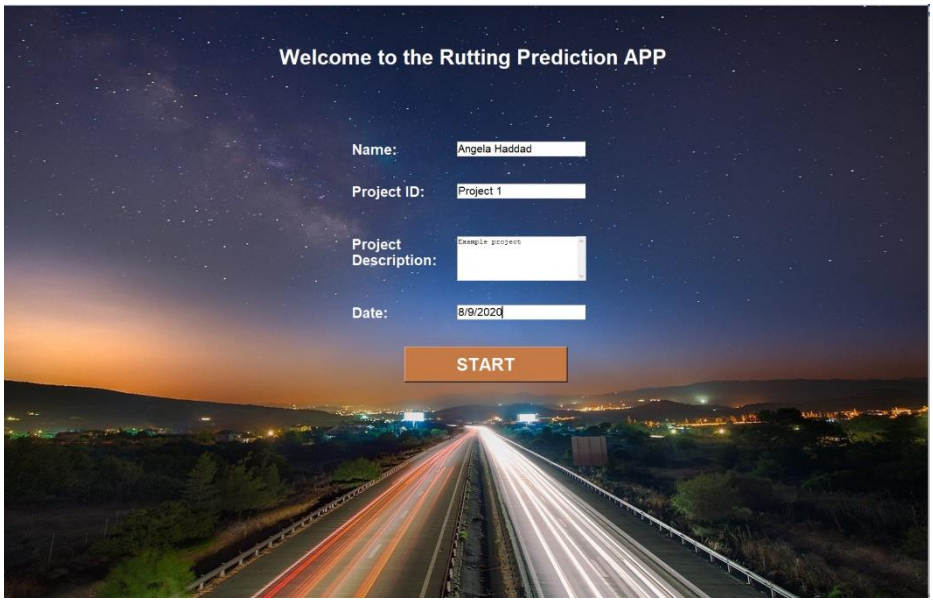

Figure 40: Home page interface for the developed GUI.

7.2 Inputs Interface

On the second page, the user enters all the inputs that are required to run the model (Figure 41a). For each input, the value and the unit used need to be included. For most inputs, the users have the liberty of selecting a specific input value or a categorical feature. When an accurate numerical value is unavailable for a specific input, it is substituted by a category that reflects a low, medium, or high estimate for that input (Figure 41b). The low, medium, and high levels are determined based on the data distribution where each category spans over approximately 33% of the data. Overall, the application requires the following inputs:

- Traffic inputs which include the average annual ESALs, the growth rate, and the growth trend which can be linear or compounded.
- Climate inputs which include the average annual precipitation, the average annual temperature (MAAT), the standard deviation of the monthly mean air temperature (MMAT), and the average wind velocity.
- Asphalt layer inputs which include the number of available layers (e.g., one or two) as well as thickness, maximum specific gravity, percentage of air voids, binder content, gradation, and binder penetration information,
- Base layer inputs which include the number of available layers (e.g., one or two), their thickness and material type (e.g., DGAB or ATB).
- Subbase layer inputs which include the number of available layers (e.g., zero or one), their thickness, and material type (e.g., DGAB or ATB).
- Subgrade layer inputs which include the resilient modulus value.
- Analysis period which reflects the number of years to predict for.

Also, for each input, an inquiry button is provided to specify the ranges of the data corresponding to each category and each input (Figure 41c). Additionally, the application allows the users to select between metric and imperial units to match their available data formats.

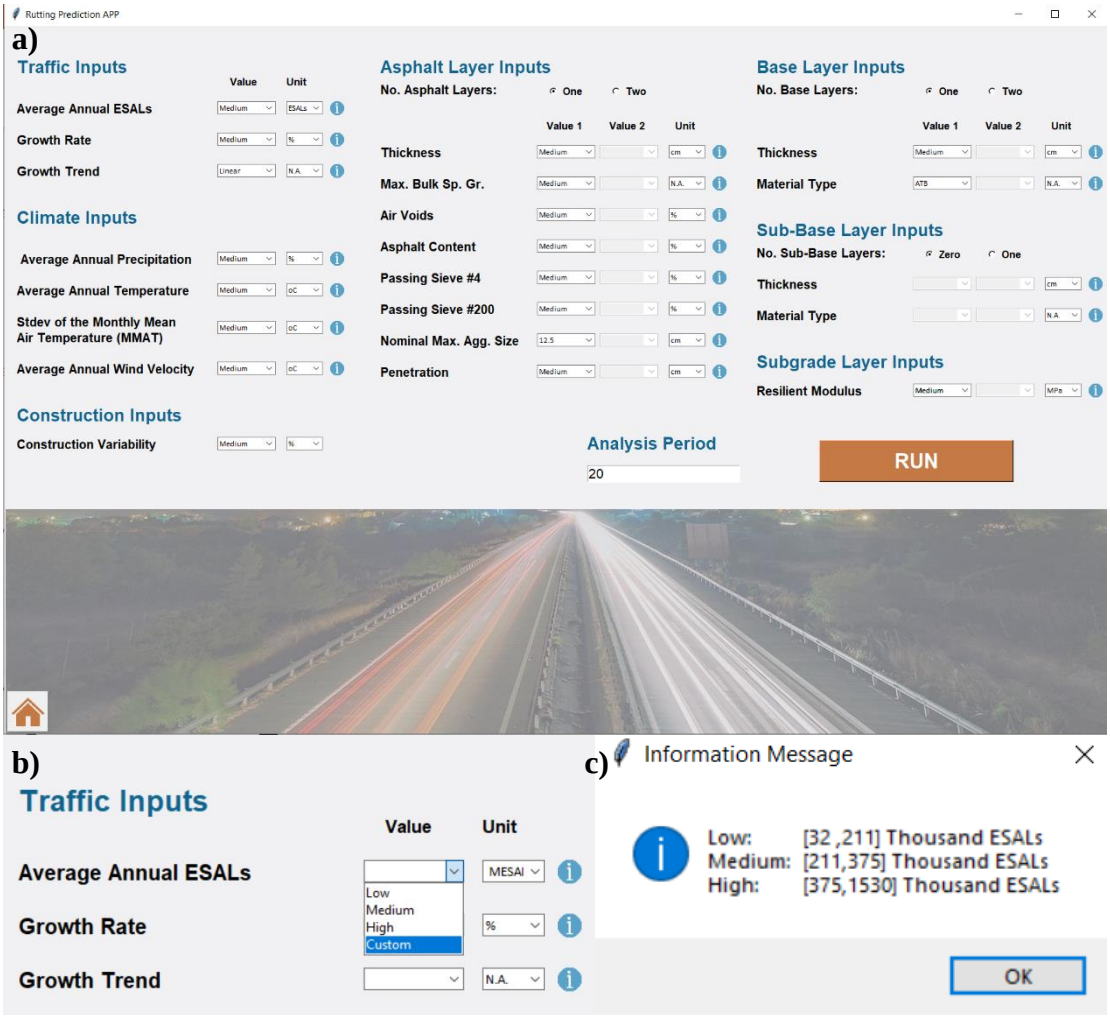

Figure 41: Inputs interface for the developed GUI: a) Overall interface, b) Example of inputs requirements and c) Inquiry button output.

7.3 Outputs Interface

In the third page, the user inputs are analyzed to provide the corresponding rutting prediction (Figure 42). If exact numerical values are used as inputs, a deterministic rutting curve is obtained. However, in cases where one or more inputs are categorical (i.e., low, medium, or high), a stochastic output that demonstrates the 95% confidence interval of the prediction is provided. When a categorical input is used instead of a numerical value, an algorithm that applies random sampling with replacement is employed to obtain a dataset of 100 random values of that input. For example, if the user inputs numerical values for all features expect the average annual ESALs where a medium category is selected, 100 random values ranging between the 33^{rd} and the 66^{th} percentile value are determined. These 100 values are combined with the other inputs and rutting is predicted a hundred times each year in order to obtain the confidence intervals. In case the user did not have numerical values for several inputs, the random sampling is conducted for each categorical input independently then the features are arbitrarily combined to obtain 100 predictions. Finally, the user can save and export the inputs and outputs into excel to conduct further analysis (Figure 43).

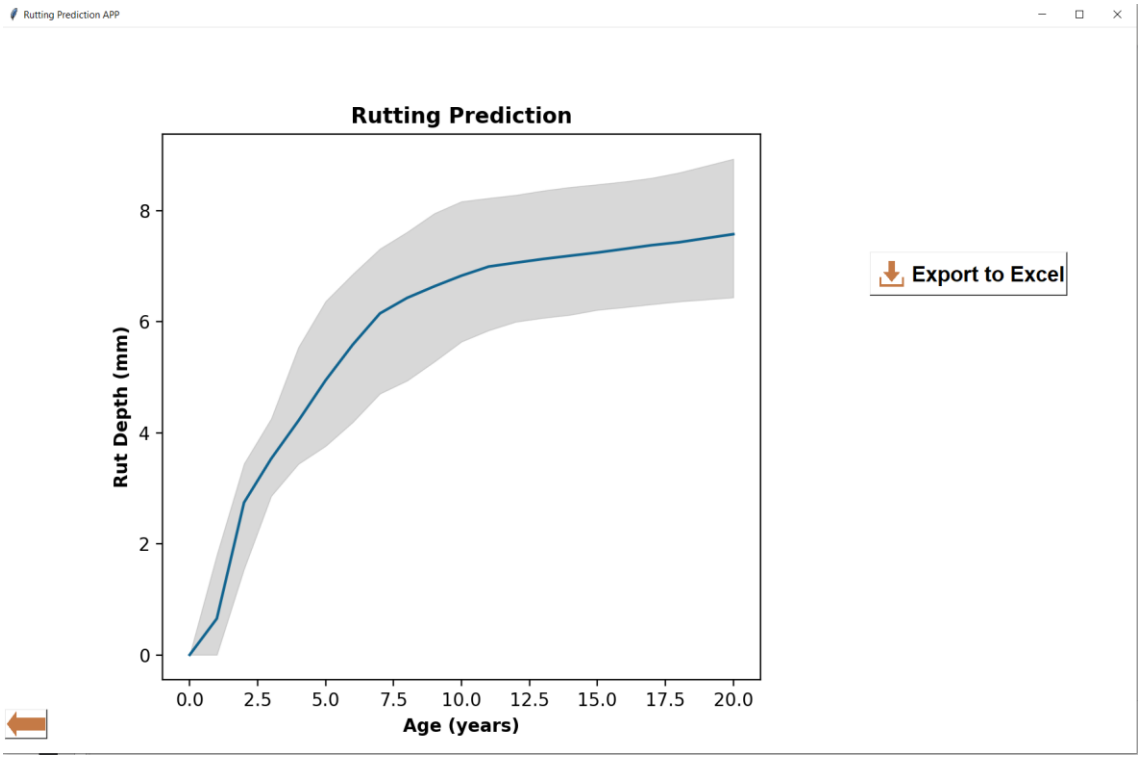

Figure 42: Outputs interface for the developed GUI.

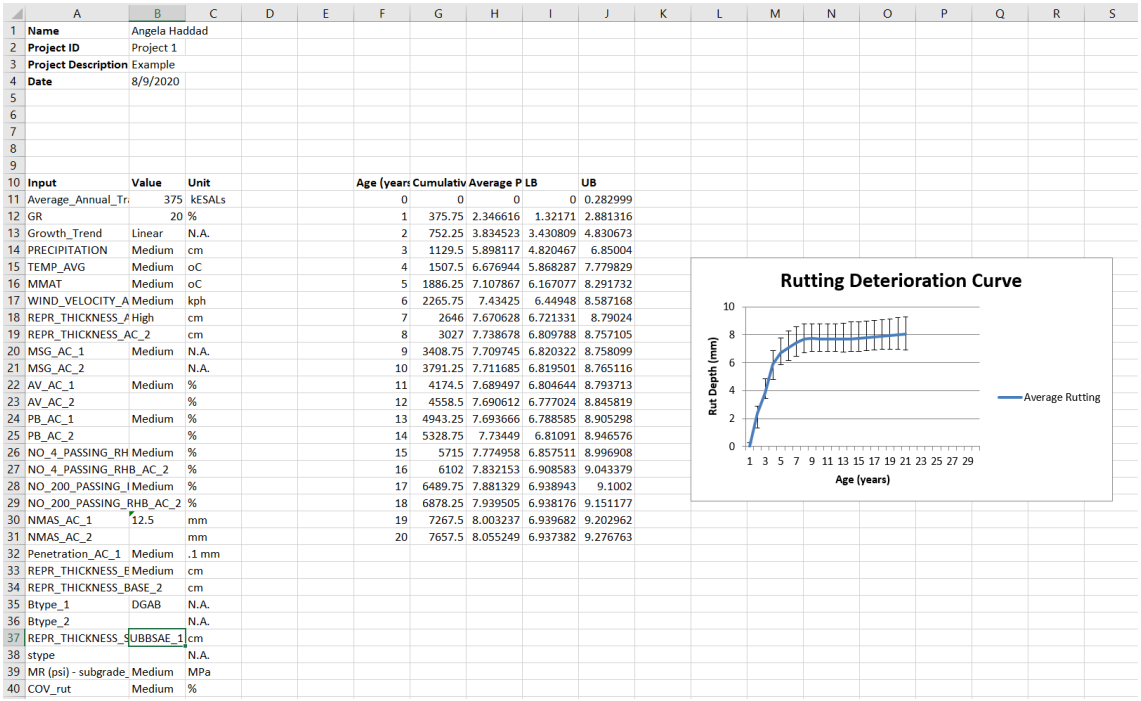

	A	B	C	D	E	F	G	H	I	J	K	L	M	N	O	P	Q	R	S
1	**Name**	Angela Haddad																	
2	**Project ID**	Project 1																	
3	**Project Description**	Example																	
4	**Date**	8/9/2020																	
5																			
6																			
7																			
8																			
9																			
10	**Input**	**Value**	**Unit**			**Age (years**	**Cumulativ**	**Average P**	**LB**	**UB**									
11	Average_Annual_Tr	375	kESALs			0	0	0	0	0.282999									
12	GR	20	%			1	375.75	2.346616	1.32171	2.881316									
13	Growth_Trend	Linear	N.A.			2	752.25	3.834523	3.430809	4.830673									
14	PRECIPITATION	Medium	cm			3	1129.5	5.898117	4.820467	6.85004									
15	TEMP_AVG	Medium	oC			4	1507.5	6.676944	5.868287	7.779829									
16	MMAT	Medium	oC			5	1886.25	7.107867	6.167077	8.291732									
17	WIND_VELOCITY_A	Medium	kph			6	2265.75	7.43425	6.44948	8.587168									
18	REPR_THICKNESS_A	High	cm			7	2646	7.670628	6.721331	8.79024									
19	REPR_THICKNESS_AC_2		cm			8	3027	7.738678	6.809788	8.757105									
20	MSG_AC_1	Medium	N.A.			9	3408.75	7.709745	6.820322	8.758099									
21	MSG_AC_2		N.A.			10	3791.25	7.711685	6.819501	8.765116									
22	AV_AC_1	Medium	%			11	4174.5	7.689497	6.804644	8.793713									
23	AV_AC_2		%			12	4558.5	7.690612	6.777024	8.845819									
24	PB_AC_1	Medium	%			13	4943.25	7.693666	6.788585	8.905298									
25	PB_AC_2		%			14	5328.75	7.73449	6.81091	8.946576									
26	NO_4_PASSING_RH	Medium	%			15	5715	7.774958	6.857511	8.996908									
27	NO_4_PASSING_RHB_AC_2		%			16	6102	7.832153	6.908583	9.043379									
28	NO_200_PASSING_I	Medium	%			17	6489.75	7.881329	6.938943	9.1002									
29	NO_200_PASSING_RHB_AC_2		%			18	6878.25	7.939505	6.938176	9.151177									
30	NMAS_AC_1	12.5	mm			19	7267.5	8.003237	6.939682	9.202962									
31	NMAS_AC_2		mm			20	7657.5	8.055249	6.937382	9.276763									
32	Penetration_AC_1	Medium	.1 mm																
33	REPR_THICKNESS_E	Medium	cm																
34	REPR_THICKNESS_BASE_2		cm																
35	Btype_1	DGAB	N.A.																
36	Btype_2		N.A.																
37	REPR_THICKNESS_S	UBBSAE_1	cm																
38	stype		N.A.																
39	MR (psi) - subgrade_	Medium	MPa																
40	COV_rut	Medium	%																

Figure 43: Output exported to Excel.

CHAPTER 8

CONCLUSIONS AND RECOMMENDATION

8.1 Summary of Findings and Contributions

Predicting the future overall pavement performance, specifically rutting, serves as a vital component in asset management systems. Prediction models available in research and practice exhibit numerous shortcomings related to generalization abilities, accuracy, and applicability. This thesis provided a framework to predict rutting depth that addresses the prevalent limitations while taking into account the data and resource scarcity existing in developing countries and local road agencies. A NN model that correlates the depth of rutting in asphalt concrete pavements to a set of climate, traffic, asphalt, base and subgrade properties was developed. This model was estimated on data extracted from the LTPP database. Feature selection and the reduction in the number of inputs required were achieved by correlation analysis and pilot studies. The model results are presented in what follows:

- The feature selection efforts reduced the number of required inputs from 51 to 29 variables. This results in the reduction of data collection efforts for model users.
- The data sampling method used to obtain the testing and training datasets is very critical and must be diligently addressed.
- The final model is a fully connected three-layered feedforward neural network having 128-32-8 nodes and has an R^2 of 0.83 and a root-mean-squared-error of 1.5 mm.

- The results of the NN model outperformed the MLR model estimated from the same dataset since NN models can deal with larger and more complex data sets.
- The presented NN model provides a major advance on current methods, which include the M-E models in Pavement-ME and the HDM-4 models, in terms of accuracy and simplicity of application.
- The model exhibits acceptable generalization abilities as it provides comparable accuracy to the locally calibrated models available in the literature.

Model development was followed by interpreting the relative contribution of the variables through permutation importance and sensitivity analyses. The objective of this effort was to identify the most critical variables to be considered in future data collection efforts. Most findings of these interpretations were consistent with research showing that cumulative traffic plays a central role in predicting rut depth. Climatic factors, especially temperature-related variables, also had a relatively high contribution to rutting prediction. Additionally, regarding pavement properties, the aggregates gradation variables were amongst the most contributing factors. Overall, the mix volumetric properties of the binder layer exhibited higher elasticities when compared to their counterparts in the surface layer. Finally, base and subgrade layers properties exhibited low importance which is broadly inline with expectations.

The model was further simplified to create a set of family curves corresponding to several traffic, climate, and performance categories. The family rutting curves would benefit agencies that cannot attain the inputs required for the NN model to initiate their pavement management systems. An EnKF framework was also proposed to overcome

the limitations of the family curves when new data becomes available. The main conclusions of the presented analyses and results are summarized as follows:

- A sensitivity analysis performed on the ensemble size revealed that a relatively large ensemble size of 10,000 is needed to attain sufficiently high accuracy in estimating the parameters.
- The presented framework calibrates the governing parameters of the rutting prediction models and reduces the mismatch between the measurements and predictions by 60% on average.
- The results were consistent among the three examined initial state scenarios and revealed that the accuracy of the predictions remains within tolerable limits while varying the initial states.
- The framework allows engineers to identify the rut depth and the probability of requiring maintenance and consequently enhances the efficiency of pavement management systems.

8.2 Limitations

A number of limitations are associated with this study. The first limitation corresponds to the used data. Although the extracted data covers a wide range of local conditions, it corresponds to the experience and technologies corresponding to one country and one main project (i.e., LTPP). This limitation can be addressed by using international data obtained from other databases, such as the Swedish and Australian long-term pavement performance studies, or a range of other DOT-specific data. Additionally, using a larger dataset can improve the model performance and provide further validation to the conclusions obtained in this thesis.

The results and conclusions of the sensitivity analysis were based on empirical studies which indicates that they are entirely dependent on the dataset and do not necessarily reflect scientific relationships. This justifies the conclusions that contradicted general expectations and engineering judgments in some cases.

While the reported family curves provide additional simplifications that can benefit agencies lacking data, they are subject to certain limitations. The family curves compromise the generalizability and accuracy of the NN model due to the introduction of significant simplifications. Therefore, these models exhibit relatively high errors that can be overcome by local calibration.

8.3 Recommendations for Future Research

Future work may consist of acquiring a larger and more diversified dataset to improve model performance and generalizability. The model features can be further evaluated to reduce the required inputs. Creating a larger dataset can assist in obtaining a comprehensive set of family curves and improve their accuracy. Future investigations can explore using reinforcement learning or other sequential data assimilation techniques to update the family curves. Additionally, the developed GUI can be enhanced to allow batch mode operations and to incorporate the EnKF framework. Finally, the scope of this research can be expanded to include all other distresses in order to achieve a comprehensive pavement management system. Such a system will allow agencies to select maintenance and rehabilitation treatments while simultaneously considering all distresses.

APPENDIX A

NEURAL NETWORK MODEL OUTPUTS

A.1 Correlation Analysis

Correlation analysis was conducted for identifying and eliminating highly correlated features as part of the feature selection efforts.

Table A. 1: Correlation matrix Part-1.

	Age	Cumulative Traffic	Construction Variability	Evaporation	Precipitation	MMAT	MAAT	Freeze Index	Avg. Wind Velocity	Cloud Cover	Average Surface Shortwave	T effective	Thickness - AC1	Gmb - AC1	Gmm - AC1	AV - AC1	Pb - AC1	Penetration - AC1	% Passing 11/2 in- AC1	% Passing 1in- AC1	% Passing 3/4 in- AC1	% Passing 1/2 in- AC1	% Passing 3/8 in- AC1	% Passing #4 - AC1	% Passing #10 - AC1
Age	1.0	0.4	0.0	0.2	0.2	0.2	0.1	0.1	0.3	0.0	0.0	0.1	0.1	0.0	0.0	0.0	0.0	0.1	0.0	0.0	0.1	0.1	0.1	0.1	0.2
Cumulative Traffic	0.4	1.0	0.2	0.0	0.0	0.1	0.0	0.1	0.2	0.0	0.0	0.1	0.0	0.3	0.3	0.1	0.0	0.1	0.0	0.0	0.1	0.0	0.0	0.1	0.1
Const. Variab.	0.0	0.2	1.0	0.2	0.2	0.1	0.0	0.0	0.1	0.1	0.1	0.0	0.1	0.2	0.1	0.2	0.0	0.2	0.1	0.1	0.1	0.1	0.1	0.0	0.1
Evapor.	0.2	0.0	0.2	1.0	0.9	0.4	0.2	0.1	0.3	0.5	0.4	0.3	0.7	0.0	0.0	0.1	0.2	0.1	0.1	0.2	0.4	0.4	0.4	0.3	0.4
Precip.	0.2	0.0	0.2	0.9	1.0	0.2	0.1	0.1	0.3	0.6	0.5	0.0	0.7	0.2	0.2	0.2	0.2	0.2	0.1	0.1	0.3	0.4	0.4	0.3	0.3
MMAT	0.2	0.1	0.1	0.4	0.2	1.0	0.8	0.8	0.4	0.1	0.5	0.6	0.2	0.0	0.2	0.2	0.1	0.5	0.1	0.1	0.1	0.2	0.2	0.3	0.4
MAAT	0.1	0.0	0.0	0.2	0.1	0.8	1.0	1.0	0.1	0.5	0.7	0.9	0.1	0.1	0.2	0.1	0.1	0.6	0.1	0.1	0.1	0.1	0.1	0.3	0.3
Freeze Index	0.1	0.1	0.0	0.1	0.1	0.8	1.0	1.0	0.2	0.5	0.7	0.8	0.0	0.1	0.3	0.0	0.1	0.6	0.1	0.0	0.2	0.0	0.1	0.3	0.3
Avg. Wind Velocity	0.3	0.2	0.1	0.3	0.3	0.4	0.1	0.2	1.0	0.0	0.1	0.2	0.1	0.1	0.3	0.0	0.0	0.2	0.0	0.0	0.3	0.2	0.2	0.0	0.2
Cloud Cover	0.0	0.0	0.1	0.5	0.6	0.1	0.5	0.5	0.0	1.0	0.9	0.5	0.4	0.1	0.0	0.2	0.5	0.3	0.2	0.0	0.4	0.3	0.2	0.0	0.1
Average Surface Shortwave	0.0	0.0	0.1	0.4	0.5	0.5	0.7	0.7	0.1	0.9	1.0	0.6	0.3	0.1	0.2	0.1	0.3	0.5	0.2	0.0	0.4	0.3	0.2	0.0	0.0
T effective	0.1	0.1	0.0	0.3	0.0	0.6	0.9	0.8	0.2	0.5	0.6	1.0	0.2	0.1	0.1	0.1	0.2	0.5	0.1	0.1	0.0	0.1	0.1	0.3	0.2
Thickness - AC1	0.1	0.0	0.1	0.7	0.7	0.2	0.1	0.0	0.1	0.4	0.3	0.2	1.0	0.1	0.2	0.1	0.2	0.1	0.1	0.1	0.2	0.4	0.3	0.2	0.2
Gmb - AC1	0.0	0.3	0.2	0.0	0.2	0.0	0.1	0.1	0.1	0.1	0.1	0.1	0.1	1.0	0.7	0.8	0.3	0.1	0.0	0.1	0.1	0.1	0.2	0.1	0.0
Gmm - AC1	0.0	0.3	0.1	0.0	0.2	0.2	0.2	0.3	0.3	0.0	0.2	0.1	0.2	0.7	1.0	0.2	0.5	0.0	0.0	0.1	0.1	0.2	0.2	0.2	0.2
AV - AC1	0.0	0.1	0.2	0.1	0.2	0.2	0.1	0.0	0.0	0.2	0.1	0.1	0.1	0.8	0.2	1.0	0.0	0.0	0.1	0.0	0.1	0.1	0.0	0.1	0.1

Table A. 1: Correlation matrix Part-1 (Continued).

	Age	Cumulative Traffic	Construction Variability	Evaporation	Precipitation	MMAT	MAAT	Freeze Index	Avg. Wind Velocity	Cloud Cover	Average Surface Shortwave	T effective	Thickness - AC1	Gmb - AC1	Gmm - AC1	AV - AC1	Pb - AC1	Penetration - AC1	% Passing 11/2 in- AC1	% Passing 1in- AC1	% Passing 3/4 in- AC1	% Passing 1/2 in- AC1	% Passing 3/8 in- AC1	% Passing #4 - AC1	% Passing #10 - AC1
Pb - AC1	0.0	0.0	0.0	0.2	0.2	0.1	0.1	0.1	0.0	0.5	0.3	0.2	0.2	0.3	0.5	0.0	1.0	0.1	0.0	0.0	0.1	0.3	0.4	0.3	0.4
Penetration - AC1	0.1	0.1	0.2	0.1	0.2	0.5	0.6	0.6	0.2	0.3	0.5	0.5	0.1	0.1	0.0	0.0	0.1	1.0	0.2	0.0	0.0	0.0	0.0	0.1	0.1
% Passing 11/2 in- AC1	0.0	0.0	0.1	0.1	0.1	0.1	0.1	0.1	0.0	0.2	0.2	0.1	0.1	0.0	0.0	0.1	0.0	0.2	1.0	0.6	0.2	0.2	0.2	0.2	0.2
% Passing 1in- AC1	0.0	0.0	0.1	0.2	0.1	0.1	0.1	0.0	0.0	0.0	0.0	0.1	0.1	0.1	0.1	0.0	0.0	0.0	0.6	1.0	0.3	0.3	0.3	0.3	0.2
% Passing 3/4 in- AC1	0.1	0.1	0.1	0.4	0.3	0.1	0.1	0.2	0.3	0.4	0.4	0.0	0.2	0.1	0.1	0.1	0.1	0.0	0.2	0.3	1.0	0.7	0.5	0.2	0.1
% Passing 1/2 in- AC1	0.1	0.0	0.1	0.4	0.4	0.2	0.1	0.0	0.2	0.3	0.3	0.1	0.4	0.1	0.2	0.1	0.3	0.0	0.2	0.3	0.7	1.0	0.9	0.6	0.4
% Passing 3/8 in - AC1	0.1	0.0	0.1	0.4	0.4	0.2	0.1	0.1	0.2	0.2	0.2	0.1	0.3	0.2	0.2	0.0	0.4	0.0	0.2	0.3	0.5	0.9	1.0	0.7	0.5
% Passing #4 - AC1	0.1	0.1	0.0	0.3	0.3	0.3	0.3	0.3	0.0	0.0	0.0	0.3	0.2	0.1	0.2	0.1	0.3	0.1	0.2	0.3	0.2	0.6	0.7	1.0	0.9
% Passing #10 - AC1	0.2	0.1	0.1	0.4	0.3	0.4	0.3	0.3	0.2	0.1	0.0	0.2	0.2	0.0	0.2	0.1	0.4	0.1	0.2	0.2	0.1	0.4	0.5	0.9	1.0
% Passing #40 - AC1	0.1	0.1	0.1	0.4	0.3	0.6	0.5	0.5	0.1	0.0	0.1	0.4	0.2	0.2	0.1	0.3	0.1	0.3	0.1	0.2	0.1	0.4	0.5	0.7	0.8
% Passing #80 - AC1	0.1	0.1	0.2	0.4	0.4	0.6	0.4	0.4	0.2	0.1	0.1	0.3	0.2	0.2	0.0	0.3	0.1	0.2	0.1	0.2	0.1	0.4	0.4	0.5	0.6
% Passing #200 - AC1	0.0	0.3	0.1	0.0	0.3	0.0	0.2	0.2	0.3	0.1	0.2	0.1	0.0	0.5	0.5	0.3	0.2	0.1	0.0	0.1	0.0	0.1	0.1	0.0	0.1
Thickness - AC2	0.1	0.1	0.0	0.4	0.4	0.1	0.0	0.0	0.1	0.3	0.3	0.2	0.5	0.3	0.2	0.3	0.1	0.0	0.1	0.1	0.2	0.2	0.1	0.1	0.1
Gmb - AC2	0.1	0.2	0.1	0.4	0.5	0.2	0.1	0.0	0.2	0.3	0.2	0.2	0.6	0.6	0.5	0.5	0.1	0.1	0.1	0.1	0.2	0.2	0.1	0.1	0.1
Gmm - AC2	0.1	0.2	0.1	0.5	0.6	0.0	0.1	0.2	0.2	0.3	0.3	0.1	0.7	0.5	0.5	0.3	0.1	0.1	0.1	0.1	0.2	0.2	0.1	0.1	0.1
AV - AC2	0.1	0.0	0.2	0.5	0.4	0.0	0.0	0.1	0.0	0.3	0.4	0.1	0.6	0.1	0.0	0.2	0.2	0.0	0.1	0.1	0.3	0.3	0.3	0.1	0.0
Pb - AC2	0.0	0.2	0.0	0.5	0.5	0.2	0.0	0.0	0.0	0.6	0.4	0.0	0.5	0.1	0.1	0.1	0.5	0.0	0.1	0.1	0.3	0.4	0.4	0.2	0.2
% Passing 11/2 in - AC2	0.1	0.2	0.0	0.6	0.5	0.2	0.1	0.0	0.1	0.4	0.3	0.3	0.7	0.3	0.1	0.3	0.2	0.0	0.2	0.2	0.3	0.4	0.3	0.2	0.1
% Passing 1in - AC2	0.1	0.2	0.0	0.6	0.6	0.3	0.1	0.1	0.2	0.5	0.4	0.2	0.6	0.2	0.1	0.3	0.3	0.0	0.1	0.2	0.3	0.4	0.3	0.1	0.2
% Passing 3/4 in - AC2	0.1	0.1	0.1	0.5	0.5	0.3	0.2	0.1	0.1	0.4	0.3	0.2	0.4	0.2	0.0	0.3	0.2	0.1	0.1	0.1	0.3	0.4	0.3	0.2	0.2
% Passing 1/2 in - AC2	0.1	0.1	0.1	0.5	0.5	0.4	0.3	0.2	0.1	0.4	0.3	0.3	0.5	0.2	0.0	0.3	0.2	0.1	0.1	0.1	0.3	0.4	0.3	0.2	0.3
% Passing 3/8 in - AC2	0.1	0.2	0.1	0.5	0.5	0.4	0.2	0.2	0.1	0.4	0.3	0.2	0.5	0.2	0.0	0.3	0.2	0.1	0.1	0.1	0.3	0.4	0.4	0.3	0.3
% Passing #4 - AC2	0.2	0.1	0.1	0.5	0.5	0.4	0.2	0.2	0.2	0.4	0.3	0.2	0.5	0.1	0.1	0.2	0.3	0.2	0.1	0.1	0.3	0.3	0.3	0.3	0.3
% Passing #10 - AC2	0.1	0.1	0.1	0.5	0.4	0.5	0.4	0.3	0.1	0.4	0.1	0.4	0.5	0.1	0.1	0.3	0.3	0.2	0.1	0.1	0.2	0.4	0.3	0.4	0.4
% Passing #40 - AC2	0.1	0.1	0.0	0.5	0.4	0.6	0.5	0.4	0.1	0.3	0.0	0.5	0.5	0.2	0.1	0.4	0.2	0.3	0.1	0.1	0.2	0.4	0.3	0.3	0.3
% Passing #80 - AC2	0.1	0.2	0.0	0.5	0.4	0.5	0.4	0.3	0.1	0.3	0.1	0.4	0.5	0.3	0.0	0.4	0.2	0.3	0.1	0.1	0.3	0.4	0.3	0.2	0.2

Table A. 1: Correlation matrix Part-1 (Continued).

	Age	Cumulative Traffic	Construction Variability	Evaporation	Precipitation	MMAT	MAAT	Freeze Index	Avg. Wind Velocity	Cloud Cover	Average Surface Shortwave	T effective	Thickness - AC1	Gmb - AC1	Gmm - AC1	AV - AC1	Pb - AC1	Penetration - AC1	% Passing 11/2 in- AC1	% Passing 1in- AC1	% Passing 3/4 in- AC1	% Passing 1/2 in- AC1	% Passing 3/8 in- AC1	% Passing #4 - AC1	% Passing #10 - AC1
% Passing #200 - AC2	0.0	0.2	0.1	0.4	0.5	0.2	0.1	0.0	0.1	0.3	0.2	0.2	0.5	0.4	0.3	0.3	0.0	0.1	0.1	0.1	0.3	0.3	0.2	0.0	0.0
Equivalent – Base	0.0	0.2	0.1	0.2	0.1	0.1	0.1	0.1	0.1	0.0	0.1	0.2	0.3	0.1	0.0	0.1	0.1	0.0	0.1	0.1	0.1	0.2	0.2	0.1	0.0
Thickness – Base 1	0.0	0.1	0.0	0.1	0.1	0.1	0.1	0.1	0.1	0.0	0.0	0.1	0.1	0.1	0.0	0.1	0.0	0.0	0.1	0.0	0.0	0.1	0.0	0.1	0.1
MR - Base 1	0.0	0.2	0.1	0.3	0.3	0.1	0.0	0.0	0.0	0.1	0.1	0.1	0.2	0.0	0.1	0.0	0.0	0.1	0.1	0.1	0.0	0.1	0.1	0.1	0.1
Thickness – Base 2	0.0	0.1	0.1	0.0	0.1	0.1	0.0	0.0	0.2	0.1	0.1	0.1	0.0	0.1	0.1	0.2	0.1	0.1	0.1	0.1	0.0	0.0	0.0	0.0	0.0
MR - Base 2	0.0	0.1	0.1	0.1	0.0	0.1	0.1	0.0	0.1	0.1	0.0	0.1	0.2	0.1	0.0	0.2	0.1	0.0	0.1	0.1	0.1	0.0	0.1	0.0	0.0
Thickness - Subbase	0.1	0.1	0.0	0.1	0.0	0.2	0.1	0.1	0.1	0.1	0.1	0.1	0.1	0.2	0.0	0.3	0.1	0.1	0.1	0.1	0.3	0.2	0.1	0.0	0.1
MR – Subbase	0.1	0.1	0.0	0.1	0.0	0.2	0.1	0.1	0.2	0.0	0.1	0.1	0.1	0.2	0.0	0.2	0.1	0.0	0.1	0.1	0.2	0.2	0.1	0.0	0.1
MR (psi) – subgrade	0.1	0.0	0.1	0.0	0.0	0.3	0.2	0.2	0.1	0.0	0.1	0.1	0.0	0.0	0.3	0.1	0.1	0.0	0.0	0.0	0.0	0.2	0.2	0.2	0.2

Table A. 2: Correlation matrix Part-2.

	% Passing #40 - AC1	% Passing #80 - AC1	% Passing #200 - AC1	Thickness - AC2	Gmb - AC2	Gmm - AC2	AV - AC2	Pb - AC2	% Passing 11/2 in- AC2	% Passing 1in- AC2	% Passing 3/4 in- AC2	% Passing 1/2 in- AC2	% Passing 3/8 in- AC2	% Passing #4 - AC2	% Passing #10 - AC2	% Passing #40 - AC2	% Passing #80 - AC2	% Passing #200 - AC2	Equivalent_Base	Thickness - Base 1	MR - Base 1	Thickness - Base 2	MR - Base 2	Thickness - Subbase	MR - Subbase	MR (psi) - subgrade
Age	0.1	0.1	0.0	0.1	0.1	0.1	0.1	0.0	0.1	0.1	0.1	0.1	0.1	0.2	0.1	0.1	0.1	0.0	0.0	0.0	0.0	0.0	0.0	0.1	0.1	0.1
Cumulative Traffic	0.1	0.1	0.3	0.1	0.2	0.2	0.0	0.2	0.2	0.2	0.1	0.1	0.2	0.1	0.1	0.1	0.2	0.2	0.2	0.1	0.2	0.1	0.1	0.1	0.1	0.0
Const. Variab.	0.1	0.2	0.1	0.0	0.1	0.1	0.2	0.0	0.0	0.0	0.1	0.1	0.1	0.1	0.1	0.0	0.0	0.1	0.1	0.0	0.1	0.1	0.1	0.0	0.0	0.1
Evapor.	0.4	0.4	0.0	0.4	0.4	0.5	0.5	0.5	0.6	0.6	0.5	0.5	0.5	0.5	0.5	0.5	0.5	0.4	0.2	0.1	0.3	0.0	0.1	0.1	0.1	0.0
Precip.	0.3	0.4	0.3	0.4	0.5	0.6	0.4	0.5	0.5	0.6	0.5	0.5	0.5	0.5	0.4	0.4	0.4	0.5	0.1	0.1	0.3	0.1	0.0	0.0	0.0	0.0
MMAT	0.6	0.6	0.0	0.1	0.2	0.0	0.0	0.2	0.2	0.3	0.3	0.4	0.4	0.4	0.5	0.6	0.5	0.2	0.1	0.1	0.1	0.1	0.1	0.2	0.2	0.3
MAAT	0.5	0.4	0.2	0.0	0.1	0.1	0.0	0.0	0.1	0.1	0.2	0.3	0.2	0.2	0.4	0.5	0.4	0.1	0.1	0.1	0.0	0.0	0.1	0.1	0.1	0.2
Freeze Index	0.5	0.4	0.2	0.0	0.0	0.2	0.1	0.0	0.0	0.1	0.1	0.2	0.2	0.2	0.3	0.4	0.3	0.0	0.1	0.1	0.0	0.0	0.0	0.1	0.1	0.2

Table A. 2: Correlation matrix Part-2 (Continued).

	% Passing #40 - AC1	% Passing #80 - AC1	% Passing #200 - AC1	Thickness - AC2	Gmb - AC2	Gmm - AC2	AV - AC2	Pb - AC2	% Passing 11/2 in- AC2	% Passing 1in- AC2	% Passing 3/4 in- AC2	% Passing 1/2 in- AC2	% Passing 3/8 in- AC2	% Passing #4 - AC2	% Passing #10 - AC2	% Passing #40 - AC2	% Passing #80 - AC2	% Passing #200 - AC2	Equivalent_Base	Thickness - Base 1	MR - Base 1	Thickness - Base 2	MR - Base 2	Thickness - Subbase	MR - Subbase	MR (psi) - subgrade
Avg. Wind Velocity	0.1	0.2	0.3	0.1	0.2	0.2	0.0	0.0	0.1	0.2	0.1	0.1	0.1	0.2	0.1	0.1	0.1	0.1	0.1	0.1	0.0	0.2	0.1	0.1	0.2	0.1
Cloud Cover	0.0	0.1	0.1	0.3	0.3	0.3	0.3	0.6	0.4	0.5	0.4	0.4	0.4	0.4	0.4	0.3	0.3	0.3	0.0	0.0	0.1	0.1	0.1	0.1	0.0	0.0
Average Surface Shortwave	0.1	0.1	0.2	0.3	0.2	0.3	0.4	0.4	0.3	0.4	0.3	0.3	0.3	0.3	0.1	0.0	0.1	0.2	0.1	0.0	0.1	0.1	0.0	0.1	0.1	0.1
T effective	0.4	0.3	0.1	0.2	0.2	0.1	0.1	0.0	0.3	0.2	0.2	0.3	0.2	0.2	0.4	0.5	0.4	0.2	0.2	0.1	0.1	0.1	0.1	0.1	0.1	0.1
Thickness - AC1	0.2	0.2	0.0	0.5	0.6	0.7	0.6	0.5	0.7	0.6	0.4	0.5	0.5	0.5	0.5	0.5	0.5	0.5	0.3	0.1	0.2	0.0	0.2	0.1	0.1	0.0
Gmb - AC1	0.2	0.2	0.5	0.3	0.6	0.5	0.1	0.1	0.3	0.2	0.2	0.2	0.2	0.1	0.1	0.2	0.3	0.4	0.1	0.1	0.0	0.1	0.1	0.2	0.2	0.0
Gmm - AC1	0.1	0.0	0.5	0.2	0.5	0.5	0.0	0.1	0.1	0.1	0.0	0.0	0.0	0.1	0.1	0.1	0.0	0.3	0.0	0.0	0.1	0.1	0.0	0.0	0.0	0.3
AV - AC1	0.3	0.3	0.3	0.3	0.5	0.3	0.2	0.1	0.3	0.3	0.3	0.3	0.3	0.2	0.3	0.4	0.4	0.3	0.1	0.1	0.0	0.2	0.2	0.3	0.2	0.1
Pb - AC1	0.1	0.1	0.2	0.1	0.1	0.1	0.2	0.5	0.2	0.3	0.2	0.2	0.2	0.3	0.3	0.2	0.2	0.0	0.1	0.0	0.0	0.1	0.1	0.1	0.1	0.1
Penetration - AC1	0.3	0.2	0.1	0.0	0.1	0.1	0.0	0.0	0.0	0.0	0.1	0.1	0.1	0.2	0.2	0.3	0.3	0.1	0.0	0.0	0.1	0.1	0.0	0.1	0.0	0.0
% Passing 11/2 in- AC1	0.1	0.1	0.0	0.1	0.1	0.1	0.1	0.1	0.2	0.1	0.1	0.1	0.1	0.1	0.1	0.1	0.1	0.1	0.1	0.1	0.1	0.1	0.1	0.1	0.1	0.0
% Passing 1in- AC1	0.2	0.2	0.1	0.1	0.1	0.1	0.1	0.1	0.2	0.2	0.1	0.1	0.1	0.1	0.1	0.1	0.1	0.1	0.1	0.0	0.1	0.1	0.1	0.1	0.1	0.0
% Passing 3/4 in- AC1	0.1	0.1	0.0	0.2	0.2	0.2	0.3	0.3	0.3	0.3	0.3	0.3	0.3	0.3	0.2	0.2	0.3	0.3	0.1	0.0	0.0	0.0	0.1	0.3	0.2	0.0
% Passing 1/2 in- AC1	0.4	0.4	0.1	0.2	0.2	0.2	0.3	0.4	0.4	0.4	0.4	0.4	0.4	0.3	0.4	0.4	0.4	0.3	0.2	0.1	0.1	0.0	0.0	0.2	0.2	0.2
% Passing 3/8 in - AC1	0.5	0.4	0.1	0.1	0.1	0.1	0.3	0.4	0.3	0.3	0.3	0.3	0.4	0.3	0.3	0.3	0.3	0.2	0.2	0.0	0.1	0.0	0.1	0.1	0.1	0.2
% Passing #4 - AC1	0.7	0.5	0.0	0.1	0.1	0.1	0.1	0.2	0.2	0.1	0.2	0.2	0.3	0.3	0.4	0.3	0.2	0.0	0.1	0.1	0.1	0.0	0.0	0.0	0.0	0.2
% Passing #10 - AC1	0.8	0.6	0.1	0.1	0.1	0.1	0.0	0.2	0.1	0.2	0.2	0.3	0.3	0.3	0.4	0.3	0.2	0.0	0.0	0.1	0.1	0.0	0.0	0.1	0.1	0.2
% Passing #40 - AC1	1.0	0.9	0.2	0.1	0.3	0.2	0.0	0.2	0.2	0.2	0.3	0.4	0.4	0.4	0.5	0.6	0.4	0.2	0.2	0.1	0.1	0.1	0.0	0.2	0.1	0.3
% Passing #80 - AC1	0.9	1.0	0.4	0.1	0.3	0.1	0.1	0.2	0.2	0.2	0.3	0.3	0.4	0.3	0.4	0.5	0.4	0.3	0.2	0.1	0.2	0.1	0.1	0.3	0.2	0.3
% Passing #200 - AC1	0.2	0.4	1.0	0.0	0.3	0.3	0.1	0.1	0.0	0.1	0.1	0.1	0.1	0.1	0.1	0.0	0.1	0.4	0.1	0.0	0.2	0.1	0.1	0.1	0.0	0.1
Thickness - AC2	0.1	0.1	0.0	1.0	0.7	0.7	0.5	0.5	0.7	0.7	0.5	0.5	0.5	0.6	0.5	0.5	0.6	0.6	0.0	0.1	0.0	0.2	0.1	0.1	0.1	0.1
Gmb - AC2	0.3	0.3	0.3	0.7	1.0	0.9	0.3	0.4	0.8	0.7	0.5	0.5	0.6	0.5	0.5	0.6	0.7	0.8	0.2	0.1	0.1	0.1	0.0	0.2	0.1	0.1
Gmm - AC2	0.2	0.1	0.3	0.7	0.9	1.0	0.5	0.3	0.8	0.6	0.4	0.4	0.5	0.4	0.4	0.5	0.5	0.7	0.2	0.1	0.2	0.1	0.1	0.1	0.1	0.2
AV - AC2	0.0	0.1	0.1	0.5	0.3	0.5	1.0	0.6	0.7	0.6	0.5	0.5	0.5	0.5	0.5	0.4	0.4	0.4	0.1	0.0	0.1	0.0	0.1	0.1	0.1	0.1
Pb - AC2	0.2	0.2	0.1	0.5	0.4	0.3	0.6	1.0	0.7	0.8	0.8	0.8	0.8	0.8	0.7	0.6	0.6	0.5	0.1	0.0	0.0	0.1	0.1	0.2	0.1	0.1
% Passing 11/2 in - AC2	0.2	0.2	0.0	0.7	0.8	0.8	0.7	0.7	1.0	0.9	0.8	0.8	0.8	0.8	0.8	0.8	0.8	0.8	0.1	0.1	0.1	0.1	0.0	0.2	0.2	0.0
% Passing 1in - AC2	0.2	0.2	0.1	0.7	0.7	0.6	0.6	0.8	0.9	1.0	0.8	0.8	0.8	0.8	0.8	0.7	0.7	0.7	0.1	0.1	0.1	0.2	0.1	0.2	0.1	0.0
% Passing 3/4 in - AC2	0.3	0.3	0.1	0.5	0.5	0.4	0.5	0.8	0.8	0.8	1.0	1.0	0.9	0.8	0.8	0.8	0.7	0.6	0.0	0.0	0.0	0.2	0.1	0.3	0.2	0.0
% Passing 1/2 in - AC2	0.4	0.3	0.1	0.5	0.5	0.4	0.5	0.8	0.8	0.8	1.0	1.0	0.9	0.9	0.8	0.8	0.7	0.6	0.1	0.0	0.0	0.2	0.1	0.3	0.2	0.1

Table A. 2: Correlation matrix Part-2 (Continued).

	% Passing #40 - AC1	% Passing #80 - AC1	% Passing #200 - AC1	Thickness - AC2	Gmb - AC2	Gmm - AC2	AV - AC2	Pb - AC2	% Passing 11/2 in- AC2	% Passing 1in- AC2	% Passing 3/4 in- AC2	% Passing 1/2 in- AC2	% Passing 3/8 in- AC2	% Passing #4 - AC2	% Passing #10 - AC2	% Passing #40 - AC2	% Passing #80 - AC2	% Passing #200 - AC2	Equivalent_Base	Thickness - Base 1	MR - Base 1	Thickness - Base 2	MR - Base 2	Thickness - Subbase	MR - Subbase	MR (psi) - subgrade
% Passing 3/8 in - AC2	0.4	0.4	0.1	0.5	0.6	0.5	0.5	0.8	0.8	0.8	0.9	0.9	1.0	0.9	0.8	0.8	0.8	0.7	0.1	0.0	0.1	0.2	0.1	0.4	0.3	0.1
% Passing #4 - AC2	0.4	0.3	0.1	0.6	0.5	0.4	0.5	0.8	0.8	0.8	0.8	0.9	0.9	1.0	0.9	0.8	0.7	0.6	0.0	0.1	0.0	0.2	0.1	0.2	0.2	0.0
% Passing #10 - AC2	0.5	0.4	0.1	0.5	0.5	0.4	0.5	0.7	0.8	0.8	0.8	0.8	0.8	0.9	1.0	0.9	0.8	0.6	0.0	0.1	0.0	0.2	0.2	0.2	0.2	0.1
% Passing #40 - AC2	0.6	0.5	0.0	0.5	0.6	0.5	0.4	0.6	0.8	0.7	0.8	0.8	0.8	0.8	0.9	1.0	0.9	0.6	0.1	0.1	0.0	0.2	0.2	0.4	0.3	0.1
% Passing #80 - AC2	0.4	0.4	0.1	0.6	0.7	0.5	0.4	0.6	0.8	0.7	0.7	0.7	0.8	0.7	0.8	0.9	1.0	0.8	0.2	0.1	0.1	0.2	0.1	0.4	0.3	0.1
% Passing #200 - AC2	0.2	0.3	0.4	0.6	0.8	0.7	0.4	0.5	0.8	0.7	0.6	0.6	0.7	0.6	0.6	0.6	0.8	1.0	0.2	0.0	0.2	0.2	0.1	0.3	0.2	0.1
Equivalent – Base	0.2	0.2	0.1	0.0	0.2	0.2	0.1	0.1	0.1	0.1	0.0	0.1	0.1	0.0	0.0	0.1	0.2	0.2	1.0	0.0	0.5	0.5	0.5	0.4	0.4	0.2
Thickness – Base 1	0.1	0.1	0.0	0.1	0.1	0.1	0.0	0.0	0.1	0.1	0.0	0.0	0.0	0.1	0.1	0.1	0.1	0.0	0.0	1.0	0.1	0.5	0.4	0.1	0.0	0.0
MR - Base 1	0.1	0.2	0.2	0.0	0.1	0.2	0.1	0.0	0.1	0.1	0.0	0.0	0.1	0.0	0.0	0.0	0.1	0.2	0.5	0.1	1.0	0.2	0.1	0.1	0.0	0.1
Thickness – Base 2	0.1	0.1	0.1	0.2	0.1	0.1	0.0	0.1	0.1	0.2	0.2	0.2	0.2	0.2	0.2	0.2	0.2	0.2	0.5	0.5	0.2	1.0	0.9	0.1	0.1	0.0
MR - Base 2	0.0	0.1	0.1	0.1	0.0	0.1	0.1	0.1	0.0	0.1	0.1	0.1	0.1	0.1	0.2	0.2	0.1	0.1	0.5	0.4	0.1	0.9	1.0	0.1	0.1	0.0
Thickness - Subbase	0.2	0.3	0.1	0.1	0.2	0.1	0.1	0.2	0.2	0.2	0.3	0.3	0.4	0.2	0.2	0.4	0.4	0.3	0.4	0.1	0.1	0.1	0.1	1.0	0.9	0.2
MR – Subbase	0.1	0.2	0.0	0.1	0.1	0.1	0.1	0.1	0.2	0.1	0.2	0.2	0.3	0.2	0.2	0.3	0.3	0.2	0.4	0.0	0.0	0.1	0.1	0.9	1.0	0.1
MR (psi) – subgrade	0.3	0.3	0.1	0.1	0.1	0.2	0.1	0.1	0.0	0.0	0.0	0.1	0.1	0.0	0.1	0.1	0.1	0.1	0.2	0.0	0.1	0.0	0.0	0.2	0.1	1.0

A.1. Weight Matrix of the Final Model

The results of the NN are a set of matrices defining the connection weights of the neuros and their biases. At each neuron (k) in the hidden layer, the inputs (X_i), that are normalized, are multiplied by the input connection weights (W_{ik}^{L}) and added to the neuron's bias factor (B_k^L). A Dense layer performs the following operation at each layer $L : h = W_{ik}^{L} X_i + B_k^L$. The value is adjusted using the ReLU activation function to calculate the value of $\widehat{H}_k$, the output of each hidden neuron. Similar computations are applied to the latter value to ultimately calculate the rut depth. The weights and biases of the final model are summarized in the following tables.

Table A. 2: Weight matrix for the first hidden layer W_{ik}^{1}.

Hidden Layer 1	Input Layer																												
	0	**1**	**2**	**3**	**4**	**5**	**6**	**7**	**8**	**9**	**10**	**11**	**12**	**13**	**14**	**15**	**16**	**17**	**18**	**19**	**20**	**21**	**22**	**23**	**24**	**25**	**26**	**27**	**28**
0	0.52	-0.14	0.29	-0.18	0.00	0.02	0.11	0.29	0.12	-0.07	0.28	0.01	-0.21	0.06	0.14	0.22	0.06	0.05	-0.24	0.02	0.20	0.20	-0.02	0.11	0.21	-0.31	0.06	0.54	-0.07
1	0.31	-0.16	0.06	-0.25	0.08	-0.25	-0.39	-0.34	0.01	0.38	0.10	-0.30	-0.01	-0.05	-0.16	0.17	0.27	0.15	-0.26	-0.27	-0.51	0.32	-0.41	0.32	-0.04	-0.11	0.03	0.34	-0.05
2	0.06	-0.47	-0.09	-0.02	0.36	0.34	0.08	-0.03	-0.03	-0.03	0.11	0.05	0.13	-0.15	0.12	-0.08	-0.16	0.39	-0.44	-0.19	0.03	-0.33	0.28	-0.32	-0.38	-0.30	-0.01	0.49	0.06
3	0.18	0.38	-0.08	-0.27	-0.35	-0.24	-0.07	-0.15	-0.12	-0.17	0.39	0.19	-0.21	-0.16	0.13	-0.02	-0.14	0.01	0.16	0.14	-0.51	0.18	-0.06	-0.08	0.31	0.02	0.00	-0.42	0.17
4	0.04	-0.02	-0.03	-0.06	0.53	0.06	-0.26	0.02	0.33	0.00	-0.04	-0.18	0.15	0.24	-0.22	-0.08	0.19	0.16	-0.47	0.05	0.06	-0.11	-0.21	0.00	0.06	-0.10	0.23	-0.12	-0.11
5	0.16	-0.34	-0.16	-0.13	-0.20	0.21	-0.20	-0.43	-0.24	-0.57	0.32	0.27	0.29	-0.06	0.17	-0.45	-0.23	0.20	-0.07	0.09	-0.08	-0.07	0.23	-0.39	0.29	-0.14	-0.03	0.17	0.04
6	0.10	0.43	0.18	-0.09	-0.14	0.32	0.33	-0.31	0.15	-0.05	0.17	0.03	-0.34	0.31	-0.45	0.38	-0.42	-0.48	0.00	0.02	0.03	0.16	0.45	-0.19	0.03	-0.24	-0.12	0.37	-0.48
7	0.24	-0.09	0.04	-0.26	-0.07	-0.17	0.04	-0.34	-0.11	-0.39	0.23	0.18	0.41	-0.16	-0.33	-0.16	0.51	-0.28	0.39	0.23	-0.09	0.08	0.03	-0.09	0.11	-0.01	0.44	-0.39	-0.03
8	0.50	0.07	-0.01	-0.15	0.39	0.16	-0.05	0.27	0.13	-0.07	0.23	0.32	0.22	0.29	-0.35	0.00	0.18	0.19	0.24	0.20	-0.34	0.20	-0.25	-0.40	0.30	0.16	0.00	0.25	-0.01
9	0.11	-0.57	0.05	-0.35	-0.28	-0.02	0.10	0.22	0.17	0.10	-0.05	-0.01	-0.06	0.28	0.20	-0.09	-0.06	0.03	-0.11	0.00	0.23	-0.03	0.14	-0.02	0.41	0.34	0.18	0.14	-0.13
10	0.02	-0.14	0.21	-0.20	0.12	0.15	-0.11	0.05	0.28	0.08	-0.05	-0.25	-0.16	0.08	0.22	-0.14	-0.37	-0.19	-0.53	-0.29	-0.06	0.01	0.03	-0.25	0.09	-0.17	-0.26	0.32	0.05
11	-0.04	-0.27	0.08	0.28	0.28	0.15	-0.08	-0.22	0.06	0.14	0.25	0.05	0.41	0.13	-0.30	-0.14	-0.16	-0.02	-0.12	0.23	-0.32	-0.20	-0.46	0.10	-0.24	-0.01	-0.43	0.36	-0.06
12	-0.92	-0.06	0.33	-0.18	0.36	0.08	-0.33	-0.05	-0.24	-0.04	0.27	0.14	0.24	-0.23	0.00	0.17	0.25	-0.39	0.00	-0.29	0.04	0.15	-0.25	0.27	0.14	-0.11	-0.30	-0.11	-0.69
13	-0.02	0.05	-0.14	0.48	-0.05	-0.18	-0.12	0.20	0.19	-0.16	-0.18	0.48	-0.05	0.13	-0.43	-0.29	-0.25	0.28	-0.01	0.07	0.02	0.05	-0.31	-0.22	0.20	0.13	-0.43	0.09	0.02
14	0.01	-0.18	-0.34	-0.08	-0.20	0.26	-0.08	-0.22	-0.15	0.20	0.10	0.02	0.44	0.05	0.30	-0.10	0.27	0.10	-0.18	0.25	0.03	-0.05	0.17	0.14	-0.22	-0.20	0.08	-0.21	-0.23
15	0.11	-0.33	0.04	-0.26	-0.11	0.10	-0.08	-0.03	0.03	-0.13	-0.12	-0.12	0.10	0.11	0.31	-0.33	-0.36	0.06	-0.39	-0.44	-0.06	-0.03	0.50	-0.12	-0.07	-0.28	-0.18	0.41	0.01
16	0.04	-0.18	0.21	0.09	0.11	0.13	0.04	-0.03	-0.07	0.08	0.30	-0.10	0.26	-0.03	-0.16	-0.15	0.19	0.22	0.13	-0.01	-0.22	0.18	-0.35	-0.40	0.16	0.33	0.18	0.02	0.00
17	-1.23	-0.11	-0.03	-0.36	0.11	-0.12	0.03	0.20	-0.41	0.28	0.31	-0.18	-0.15	-0.25	-0.45	0.28	0.26	0.13	0.06	-0.21	0.06	-0.49	0.16	-0.10	-0.15	-0.26	0.55	-0.11	0.19
18	0.11	-0.51	-0.03	-0.39	0.11	0.07	0.03	0.13	-0.28	0.23	0.10	-0.27	0.09	-0.20	-0.07	0.11	0.32	0.06	0.00	-0.16	0.37	-0.27	0.15	-0.13	-0.31	-0.15	0.02	0.58	0.04
19	0.23	0.00	0.21	0.10	0.41	0.17	0.06	-0.03	-0.12	-0.34	0.36	0.24	0.27	0.00	-0.03	-0.29	0.06	0.39	0.03	0.14	-0.32	0.16	-0.05	-0.01	-0.03	0.07	0.08	0.16	0.01
20	0.27	0.01	0.10	-0.13	-0.02	-0.03	0.06	0.03	-0.04	-0.27	-0.01	0.17	-0.14	-0.11	0.01	-0.09	-0.04	0.09	-0.36	0.39	-0.27	-0.02	0.37	0.13	0.04	-0.01	-0.14	-0.15	0.01
21	0.15	-0.21	0.51	-0.02	0.26	-0.16	-0.17	-0.34	-0.16	0.35	-0.09	-0.52	-0.07	-0.11	-0.15	0.10	-0.02	0.44	-0.57	0.27	-0.39	0.24	0.14	-0.07	0.07	0.05	0.18	0.23	-0.12

Table A. 1: Weight matrix for the first hidden layer W_{ik}^{1} (Continued).

Hidden Layer 1	Input Layer																												
	0	**1**	**2**	**3**	**4**	**5**	**6**	**7**	**8**	**9**	**10**	**11**	**12**	**13**	**14**	**15**	**16**	**17**	**18**	**19**	**20**	**21**	**22**	**23**	**24**	**25**	**26**	**27**	**28**
22	0.01	-0.27	-0.08	0.10	-0.20	0.25	0.08	-0.08	0.11	0.18	-0.03	-0.22	0.01	-0.36	0.08	-0.36	0.25	0.00	0.05	0.27	-0.33	0.47	0.23	0.31	-0.06	0.01	0.13	-0.19	-0.23
23	0.04	-0.27	-0.39	-0.31	0.15	-0.12	0.09	0.10	0.03	-0.26	0.00	-0.22	0.10	-0.41	0.27	-0.33	-0.27	0.11	-0.55	-0.26	0.00	0.03	0.32	0.00	-0.26	-0.40	-0.06	0.16	0.16
24	0.14	-0.01	0.01	0.07	0.16	0.17	0.06	-0.28	0.02	-0.14	0.42	0.06	0.18	0.14	0.06	0.17	0.49	0.13	0.21	0.01	-0.06	0.33	-0.14	0.42	-0.21	0.05	0.04	0.06	-0.01
25	0.10	-0.37	-0.16	-0.16	0.09	-0.41	0.09	-0.02	0.31	-0.14	-0.15	-0.16	0.02	0.02	0.04	0.07	0.21	0.04	-0.57	0.03	-0.22	0.13	0.17	-0.05	-0.03	-0.12	-0.08	-0.08	0.37
26	0.19	-0.01	-0.05	-0.03	0.13	0.05	-0.25	0.06	-0.36	-0.03	0.18	-0.11	-0.05	0.04	0.09	0.02	-0.21	0.25	-0.17	-0.40	-0.26	0.00	0.21	-0.49	-0.02	-0.43	-0.27	0.15	-0.02
27	0.00	-0.31	-0.53	-0.55	0.02	-0.13	-0.02	0.08	0.12	-0.01	0.02	-0.11	0.58	0.08	-0.19	0.18	-0.23	-0.05	-0.49	-0.16	-0.17	0.16	-0.08	-0.18	0.40	0.02	-0.06	0.15	-0.03
28	0.15	-0.30	0.05	-0.06	-0.33	-0.17	-0.13	-0.54	0.21	-0.30	-0.09	-0.21	-0.01	-0.29	0.08	-0.01	-0.14	0.06	-0.45	-0.03	-0.10	-0.38	0.09	-0.09	-0.14	-0.34	-0.06	0.08	0.09
29	0.12	0.27	0.04	0.46	0.19	0.23	-0.09	-0.33	-0.25	0.14	-0.05	0.01	-0.16	-0.39	-0.15	-0.33	0.20	-0.14	-0.04	0.45	-0.09	-0.06	0.25	-0.07	-0.11	0.00	0.29	-0.17	-0.04
30	0.33	0.51	-0.17	-0.19	-0.12	-0.18	0.16	-0.27	0.19	-0.57	0.02	-0.23	-0.50	-0.23	0.22	0.34	-0.47	0.33	0.30	0.30	0.16	-0.19	-0.07	0.07	0.00	0.02	-0.08	-0.10	-0.23
31	0.04	-0.13	-0.46	-0.04	-0.12	-0.41	-0.06	0.12	0.09	0.10	-0.15	-0.33	0.23	-0.16	0.21	-0.22	0.27	-0.24	-0.30	-0.11	0.25	-0.09	0.07	0.17	-0.06	-0.29	-0.02	-0.19	0.04
32	0.20	0.39	-0.17	-0.28	0.10	-0.13	0.05	-0.46	0.15	-0.12	-0.21	-0.44	-0.20	-0.25	0.33	-0.01	-0.26	-0.10	0.16	0.33	-0.03	-0.35	-0.06	-0.11	-0.14	0.04	-0.09	-0.45	0.07
33	0.57	-0.26	0.07	-0.03	-0.10	-0.28	0.17	-0.40	0.04	0.22	-0.41	-0.03	0.33	0.51	-0.20	-0.01	0.43	0.34	0.47	-0.11	0.11	-0.22	0.09	0.08	0.15	-0.33	-0.06	0.22	-0.26
34	-0.26	-0.24	0.20	0.10	0.35	0.24	-0.29	0.38	-0.19	0.07	-0.12	0.03	0.14	-0.15	-0.30	0.23	0.22	-0.17	0.22	0.00	0.19	0.35	-0.15	0.04	0.19	0.13	0.08	-0.13	0.32
35	-0.02	0.31	0.07	-0.04	-0.23	-0.23	0.49	0.09	0.28	-0.35	-0.07	-0.29	-0.72	0.24	-0.14	0.02	-0.27	0.59	0.19	0.29	-0.05	0.28	0.53	0.05	-0.16	-0.14	-0.21	0.43	-0.27
36	0.11	-0.49	-0.10	0.23	-0.06	-0.07	0.07	-0.09	-0.06	0.26	-0.04	0.02	-0.01	-0.26	0.04	0.01	-0.14	-0.05	0.34	0.55	0.24	0.01	0.38	-0.16	0.27	0.20	-0.06	0.32	-0.07
37	0.06	0.31	0.10	-0.10	-0.16	-0.33	0.31	-0.16	-0.38	0.05	-0.21	0.05	-0.33	-0.18	0.06	0.11	-0.30	0.17	-0.08	-0.11	-0.01	-0.15	-0.32	0.24	0.05	-0.05	0.42	-0.06	0.34
38	0.10	-0.10	0.07	-0.34	0.31	0.05	0.19	-0.06	0.18	-0.33	-0.13	-0.27	0.32	-0.01	0.23	0.05	0.23	0.03	0.07	-0.11	-0.27	0.15	0.03	-0.10	0.16	0.00	0.19	-0.09	-0.05
39	-0.15	0.16	-0.25	0.07	0.02	-0.26	-0.05	0.23	-0.35	0.15	-0.26	0.04	-0.05	0.00	-0.26	0.04	-0.09	0.27	-0.11	0.41	0.29	0.21	-0.36	0.00	0.32	-0.15	0.14	0.00	0.38
40	0.59	0.00	0.25	-0.01	-0.11	0.04	-0.01	-0.35	0.29	-0.17	-0.07	0.27	-0.08	0.04	-0.41	0.12	-0.21	0.06	0.20	0.09	0.15	0.05	-0.31	0.08	0.33	0.28	0.30	0.11	-0.02
41	0.16	0.25	-0.09	0.09	0.10	0.25	-0.01	-0.12	0.11	-0.12	0.18	0.43	-0.15	-0.27	0.14	-0.17	0.23	-0.11	0.30	0.17	0.26	0.18	0.24	0.08	0.04	-0.08	0.19	-0.12	0.16
42	0.94	0.10	-0.24	0.36	0.31	0.20	0.00	-0.01	-0.01	0.16	-0.29	0.35	-0.25	0.02	-0.14	-0.39	0.18	0.13	-0.07	0.03	-0.02	-0.11	0.00	-0.05	-0.13	-0.07	-0.07	0.19	-0.09
43	0.22	-0.23	-0.27	-0.03	0.24	0.06	0.23	-0.15	-0.03	0.11	-0.02	0.49	0.18	0.21	0.27	0.01	-0.26	-0.21	0.14	0.18	0.11	-0.10	0.46	-0.31	0.06	-0.08	-0.14	0.15	0.12
44	0.25	-0.33	-0.45	0.01	-0.02	-0.09	0.19	0.50	0.10	0.10	-0.03	-0.12	0.28	-0.18	0.27	-0.08	0.00	-0.06	0.18	0.02	0.38	-0.30	0.03	0.06	-0.01	-0.10	-0.33	0.08	-0.10

Table A. 1: Weight matrix for the first hidden layer W_{ik}^{1} (Continued).

Hidden	Input Layer																												
Layer 1	0	1	2	3	4	5	6	7	8	9	10	11	12	13	14	15	16	17	18	19	20	21	22	23	24	25	26	27	28
45	0.12	-0.28	-0.07	0.05	0.09	0.11	-0.31	-0.06	-0.20	0.10	-0.02	-0.45	0.45	-0.20	-0.13	0.21	0.02	0.67	0.08	-0.08	-0.05	-0.12	-0.24	0.06	-0.36	-0.09	-0.17	-0.03	-0.01
46	0.51	-0.25	-0.22	-0.20	0.49	0.01	-0.13	0.06	0.09	-0.21	-0.41	-0.48	0.15	0.04	-0.05	0.09	-0.07	0.17	-0.27	-0.16	0.16	0.23	-0.07	-0.02	0.28	0.14	-0.08	-0.01	0.00
47	0.12	-0.34	-0.33	-0.35	0.36	-0.17	-0.27	0.41	0.35	0.06	-0.15	0.28	0.10	0.17	-0.51	-0.34	-0.14	-0.09	-0.15	0.12	0.42	-0.24	-0.15	-0.22	-0.26	0.14	0.41	0.00	0.20
48	0.42	0.57	0.26	0.04	-0.01	-0.18	-0.15	0.26	-0.20	0.01	-0.25	0.15	-0.02	-0.13	-0.40	0.35	0.00	-0.16	0.04	-0.18	-0.01	0.08	0.17	-0.13	-0.20	-0.20	0.26	-0.26	-0.42
49	-1.04	0.26	-0.03	-0.09	0.62	-0.50	0.05	-0.06	0.17	-0.12	-0.09	0.00	-0.08	-0.20	0.07	0.03	-0.01	0.60	-0.05	0.27	0.24	-0.11	0.18	0.07	-0.17	-0.15	-0.05	-0.31	-0.05
50	0.05	-0.28	0.08	-0.34	0.14	0.27	0.09	0.34	0.41	-0.18	-0.21	0.50	-0.25	0.15	-0.18	0.09	-0.14	0.16	-0.07	0.25	0.35	-0.29	0.30	-0.18	-0.17	0.16	0.11	0.08	0.09
51	0.18	0.27	-0.12	-0.06	0.24	0.13	0.13	0.05	0.42	-0.35	-0.01	0.49	0.15	0.00	0.10	-0.06	-0.19	0.00	0.22	0.23	0.41	-0.21	0.31	0.04	-0.05	-0.01	0.04	-0.15	0.04
52	0.04	-0.09	0.20	-0.04	-0.15	-0.32	-0.09	0.24	0.02	0.18	-0.25	-0.34	-0.12	-0.19	-0.20	0.26	-0.29	0.46	-0.41	0.11	-0.21	0.03	-0.29	-0.22	0.34	0.08	-0.18	0.03	-0.09
53	-0.01	0.07	0.39	0.44	0.06	-0.27	0.02	-0.13	-0.16	-0.27	0.18	-0.14	0.18	-0.08	-0.11	-0.41	-0.21	0.13	0.08	-0.27	0.01	0.13	-0.02	-0.28	0.32	-0.05	-0.10	-0.36	0.02
54	0.32	0.01	0.05	-0.14	0.46	-0.30	-0.24	-0.12	-0.28	0.09	0.53	-0.56	-0.03	-0.07	-0.12	0.04	-0.21	-0.11	0.24	-0.17	-0.33	0.41	0.15	0.02	0.09	0.03	0.28	0.05	-0.27
55	0.55	0.47	0.35	-0.15	0.09	-0.22	-0.32	0.37	-0.19	-0.22	-0.06	0.42	-0.10	0.17	-0.39	0.40	0.18	0.03	0.09	0.02	0.23	0.00	-0.36	0.00	0.32	0.30	0.18	0.07	-0.49
56	-0.02	-0.15	-0.08	0.22	0.21	0.33	0.17	-0.21	0.02	-0.13	0.33	0.16	0.46	0.19	0.30	0.00	0.11	0.13	-0.01	-0.04	-0.02	0.00	0.19	0.13	-0.29	-0.22	0.29	-0.31	0.02
57	-0.90	0.13	0.51	-0.36	0.24	0.02	-0.56	-0.15	0.03	0.04	0.37	0.29	0.19	-0.47	-0.02	0.24	0.17	0.09	-0.21	-0.01	0.19	0.36	0.14	0.04	0.14	-0.15	0.17	-0.33	-0.10
58	0.41	0.22	0.17	0.19	0.18	-0.06	-0.02	-0.11	-0.09	0.01	-0.04	0.29	0.07	0.39	0.00	-0.11	0.18	-0.17	0.44	-0.21	0.00	0.09	-0.13	-0.16	0.27	0.15	0.03	-0.23	-0.24
59	-1.67	0.00	-0.05	-0.03	0.00	0.14	-0.17	-0.32	0.30	-0.01	-0.31	-0.12	0.19	0.04	-0.12	0.34	-0.21	0.12	-0.06	0.04	-0.03	0.23	0.09	0.16	-0.15	-0.04	-0.13	-0.01	-0.10
60	0.05	0.09	0.36	0.33	-0.30	-0.27	-0.05	-0.30	0.05	0.08	0.33	-0.29	0.02	0.06	-0.10	-0.20	-0.31	-0.07	0.23	0.12	0.03	0.12	0.09	0.07	0.10	-0.07	-0.24	-0.41	-0.14
61	-1.78	-0.07	-0.04	0.07	0.00	-0.06	0.07	0.08	0.12	0.14	-0.18	-0.13	-0.12	0.04	-0.17	0.06	-0.19	0.13	-0.01	0.20	-0.03	-0.08	0.02	0.00	-0.11	-0.05	0.17	-0.01	0.10
62	0.06	-0.15	0.05	0.16	0.16	0.59	0.07	-0.16	0.28	-0.27	0.14	0.31	0.16	0.00	0.00	-0.13	0.33	0.26	0.23	0.23	0.27	-0.15	-0.15	-0.22	0.29	-0.25	-0.24	0.34	-0.06
63	0.09	0.18	-0.02	0.15	0.02	-0.24	0.16	0.01	-0.20	0.26	-0.08	-0.24	-0.48	-0.33	0.18	0.21	-0.02	-0.06	-0.24	0.38	-0.14	-0.16	0.40	0.36	-0.44	-0.24	-0.24	0.02	0.00
64	0.06	-0.35	-0.08	-0.32	0.40	0.04	0.04	0.05	0.19	-0.13	-0.04	-0.25	0.31	-0.01	-0.25	0.21	-0.17	0.37	-0.38	-0.32	-0.40	0.11	-0.29	-0.18	0.13	0.13	0.08	0.19	0.17
65	0.07	0.00	-0.30	0.07	0.01	-0.25	-0.22	0.09	0.17	0.22	-0.20	-0.44	0.07	-0.22	-0.06	0.14	-0.26	-0.15	-0.33	-0.12	0.22	-0.44	-0.18	0.11	0.07	-0.22	-0.31	0.21	-0.03
66	0.15	-0.25	-0.27	-0.15	0.02	0.24	0.11	0.05	-0.22	-0.20	0.29	0.33	0.22	-0.44	-0.09	-0.19	0.43	0.29	-0.13	0.26	-0.22	0.00	-0.07	-0.13	0.12	0.08	-0.18	0.13	0.06
67	0.05	-0.29	0.05	-0.35	-0.21	-0.05	0.17	-0.11	-0.12	0.14	-0.02	-0.05	-0.12	0.07	0.38	-0.17	0.17	-0.17	-0.47	0.14	-0.07	0.30	0.03	0.45	0.07	0.20	-0.13	0.05	-0.07

Table A. 1: Weight matrix for the first hidden layer W_{ik}^{1} (Continued).

Hidden Layer 1	Input Layer																												
	0	**1**	**2**	**3**	**4**	**5**	**6**	**7**	**8**	**9**	**10**	**11**	**12**	**13**	**14**	**15**	**16**	**17**	**18**	**19**	**20**	**21**	**22**	**23**	**24**	**25**	**26**	**27**	**28**
68	-1.77	0.03	-0.04	0.02	0.01	-0.14	0.03	-0.11	0.00	-0.10	0.03	-0.02	0.09	-0.07	0.00	0.07	0.05	0.13	-0.06	-0.06	0.01	-0.02	0.01	0.00	-0.02	0.01	0.08	-0.04	0.00
69	0.76	0.19	-0.07	-0.32	0.11	-0.07	0.02	0.02	-0.13	-0.22	-0.14	0.23	0.16	-0.03	-0.39	-0.06	0.25	0.08	0.24	-0.31	-0.32	-0.10	0.01	-0.39	0.02	0.08	0.00	0.12	-0.15
70	-1.75	0.05	-0.08	-0.31	-0.19	-0.17	-0.14	-0.03	-0.29	0.04	-0.18	0.16	0.25	0.19	-0.01	-0.05	-0.01	0.31	-0.24	-0.09	0.09	0.04	0.16	-0.09	-0.05	-0.04	0.24	-0.25	0.07
71	0.22	0.05	0.09	-0.03	0.06	0.28	-0.25	0.13	0.07	-0.03	0.23	0.22	-0.29	-0.09	-0.32	-0.27	0.25	0.03	0.31	0.41	-0.21	0.11	-0.06	-0.22	0.01	-0.06	-0.10	0.29	-0.02
72	0.08	-0.07	-0.41	-0.47	0.00	0.12	-0.16	0.08	0.12	0.06	-0.21	0.18	0.34	0.23	-0.07	0.48	0.16	0.34	-0.61	0.00	-0.03	0.14	-0.03	0.16	0.03	0.07	-0.06	0.21	-0.13
73	0.11	0.35	-0.01	-0.14	0.23	0.48	-0.14	-0.36	0.22	-0.06	0.17	0.32	0.42	-0.16	-0.04	0.06	-0.12	-0.07	-0.21	-0.01	-0.47	-0.01	-0.12	-0.02	-0.44	-0.23	0.15	0.02	0.16
74	-1.84	0.02	-0.23	-0.20	-0.16	-0.09	0.12	0.28	-0.12	0.07	0.07	-0.02	-0.45	-0.05	-0.13	-0.06	-0.16	0.00	-0.02	0.21	0.13	0.07	0.12	-0.08	-0.04	-0.09	0.11	0.05	-0.17
75	-1.62	-0.06	0.18	-0.10	0.43	-0.10	0.03	-0.28	0.32	0.41	-0.06	-0.09	-0.19	-0.34	0.10	0.27	-0.14	0.29	0.12	0.09	-0.02	-0.03	-0.20	0.03	0.09	0.05	0.14	0.17	0.12
76	0.49	0.19	0.01	0.10	0.04	0.27	0.15	0.12	0.40	-0.08	-0.44	-0.35	-0.41	-0.23	-0.28	0.12	-0.43	0.09	-0.03	-0.48	-0.15	0.48	0.17	-0.02	0.05	0.09	-0.08	-0.20	-0.37
77	-0.23	0.10	0.07	-0.03	-0.20	-0.11	-0.10	-0.29	0.20	0.08	0.21	-0.11	0.14	-0.14	-0.11	-0.06	-0.17	0.06	0.13	0.07	0.14	0.22	0.21	0.13	-0.15	0.00	-0.19	0.57	0.48
78	0.32	0.05	0.15	-0.13	0.16	-0.33	0.08	0.14	-0.08	0.10	-0.02	0.16	0.30	0.30	-0.02	0.09	0.38	0.08	-0.06	0.13	0.28	0.01	-0.17	0.00	-0.33	0.08	-0.19	-0.07	0.12
79	0.04	-0.34	-0.28	0.13	-0.21	-0.11	0.03	-0.14	0.15	0.23	-0.27	0.18	0.23	0.09	0.41	0.14	-0.17	-0.21	0.07	0.01	0.06	0.34	0.41	0.23	0.11	-0.09	0.17	0.14	-0.07
80	0.28	-0.12	-0.07	-0.15	-0.22	-0.21	-0.01	0.12	0.39	-0.04	0.26	0.04	0.19	0.16	-0.05	-0.26	-0.15	0.05	0.35	0.01	0.27	-0.17	0.04	0.05	-0.03	-0.04	0.10	-0.36	-0.02
81	-0.48	-0.21	0.15	-0.24	-0.02	0.12	-0.22	-0.03	-0.08	0.09	-0.17	0.18	0.09	0.08	0.36	-0.01	0.41	-0.32	-0.35	-0.40	-0.24	-0.07	0.28	-0.18	-0.08	0.16	-0.32	-0.31	-0.30
82	0.30	-0.03	0.01	-0.33	0.29	0.06	-0.36	-0.06	0.28	-0.15	-0.33	0.08	-0.14	0.09	-0.12	0.03	-0.05	-0.15	-0.19	-0.05	-0.21	0.03	0.04	-0.34	0.01	-0.34	0.04	0.48	0.25
83	0.14	0.02	-0.15	-0.01	0.14	-0.16	-0.26	0.11	0.25	-0.08	0.00	-0.04	0.26	0.08	-0.64	0.24	0.06	-0.05	0.19	-0.24	0.53	-0.33	-0.56	-0.29	0.20	0.30	0.35	-0.10	-0.06
84	0.07	-0.45	-0.11	0.24	0.42	0.44	0.14	0.13	-0.08	0.01	-0.17	0.21	0.12	-0.03	0.12	-0.14	0.18	-0.09	0.05	0.16	0.30	-0.29	0.48	-0.07	-0.50	-0.36	-0.03	0.21	0.29
85	0.05	0.51	0.03	-0.09	0.16	-0.56	-0.26	0.00	-0.01	0.04	-0.17	0.42	0.27	0.05	0.33	-0.33	0.54	0.25	-0.08	-0.20	-0.22	-0.33	0.21	-0.49	0.08	0.16	0.52	0.01	-0.01
86	0.12	-0.32	-0.09	-0.33	0.09	-0.24	-0.18	0.04	-0.42	0.16	0.28	0.00	-0.11	-0.12	-0.08	-0.22	-0.05	0.08	-0.39	0.20	-0.42	0.47	-0.07	-0.02	0.25	0.09	-0.23	0.20	-0.22
87	0.59	-0.13	-0.05	-0.04	0.48	-0.10	0.11	-0.23	-0.01	0.21	0.28	-0.34	0.33	0.15	-0.06	-0.06	0.22	0.06	0.32	0.31	-0.41	0.38	0.15	0.18	-0.15	-0.03	0.25	-0.18	0.07
88	-1.31	0.04	-0.13	-0.18	0.31	-0.20	0.17	-0.12	-0.01	0.33	0.24	-0.36	-0.06	-0.16	-0.10	0.34	-0.02	-0.01	0.36	-0.16	-0.07	-0.05	-0.01	0.11	-0.11	-0.06	-0.06	0.24	-0.14
89	0.42	0.04	-0.22	-0.50	-0.07	-0.32	-0.06	0.24	0.25	-0.12	0.30	0.27	0.34	-0.08	-0.16	-0.39	-0.06	0.02	0.25	0.33	-0.10	-0.18	0.13	-0.12	0.01	0.03	-0.03	0.25	-0.22
90	0.13	-0.24	0.21	0.17	0.18	0.41	0.15	-0.22	0.12	-0.16	0.00	0.20	0.31	-0.08	0.01	0.06	0.05	-0.02	0.32	0.09	0.33	-0.16	0.32	0.02	-0.16	-0.22	-0.02	0.24	0.00

Table A. 1: Weight matrix for the first hidden layer W_{ik}^{1} (Continued).

Hidden Layer 1	Input Layer																												
	0	**1**	**2**	**3**	**4**	**5**	**6**	**7**	**8**	**9**	**10**	**11**	**12**	**13**	**14**	**15**	**16**	**17**	**18**	**19**	**20**	**21**	**22**	**23**	**24**	**25**	**26**	**27**	**28**
91	0.03	-0.12	0.16	-0.33	-0.08	0.21	0.17	-0.36	-0.07	-0.02	-0.09	0.13	-0.08	0.09	0.26	0.20	-0.19	-0.24	0.03	0.09	0.25	-0.28	0.50	-0.46	-0.15	0.07	0.18	0.13	0.03
92	-0.03	0.25	-0.02	0.04	0.24	0.22	-0.03	-0.08	0.29	-0.10	0.13	0.29	0.07	0.14	-0.08	-0.14	0.00	-0.15	0.04	0.27	0.24	-0.29	0.05	-0.01	-0.12	-0.34	-0.20	-0.04	0.07
93	0.24	-0.12	0.11	-0.26	-0.10	-0.02	0.22	-0.18	0.08	-0.01	0.06	0.01	-0.01	-0.06	0.29	0.01	0.19	0.20	-0.44	-0.22	0.42	-0.31	-0.12	0.04	-0.35	-0.16	0.13	0.29	0.25
94	0.09	0.08	-0.13	0.35	0.31	-0.04	-0.07	0.14	-0.24	0.00	0.15	-0.35	0.08	-0.48	-0.13	-0.03	0.31	0.43	-0.05	-0.07	-0.36	0.02	-0.38	-0.07	0.10	0.09	-0.01	-0.25	-0.15
95	0.03	-0.63	-0.34	-0.22	0.10	0.01	0.06	-0.25	0.22	-0.12	-0.10	0.07	0.37	-0.24	-0.16	0.38	-0.03	0.40	-0.22	-0.12	0.34	-0.22	-0.11	0.06	0.01	-0.04	0.23	0.15	0.09
96	0.10	0.16	-0.30	0.07	0.02	0.48	0.15	-0.04	0.12	-0.10	-0.30	0.37	-0.17	-0.41	-0.32	0.29	0.12	-0.09	0.44	-0.09	0.17	-0.11	0.20	-0.46	-0.13	0.17	0.06	0.06	0.04
97	-1.77	-0.01	0.05	-0.15	-0.20	0.04	0.03	0.06	0.05	0.05	-0.06	-0.13	0.00	-0.05	-0.06	-0.02	-0.04	-0.02	0.12	0.04	0.07	0.03	0.01	-0.03	0.03	0.03	-0.05	0.06	-0.04
98	0.04	0.42	0.34	0.45	0.07	-0.17	0.07	-0.08	-0.02	-0.11	-0.22	0.39	0.01	0.08	-0.34	-0.09	0.09	0.00	0.20	-0.02	0.22	0.13	-0.37	0.18	-0.12	0.04	-0.15	-0.03	0.02
99	0.12	-0.31	0.34	-0.34	0.35	0.01	-0.06	0.02	-0.19	0.54	0.12	-0.26	-0.02	0.11	-0.02	0.00	-0.33	-0.15	-0.18	0.00	0.16	-0.11	0.19	-0.47	0.16	0.03	0.29	0.33	0.01
100	0.17	-0.03	0.44	-0.43	-0.30	-0.20	-0.02	0.17	-0.01	0.45	0.24	0.20	0.07	0.45	-0.02	0.04	0.18	-0.06	0.17	-0.09	-0.12	0.37	-0.37	0.20	0.45	0.42	-0.04	0.39	-0.21
101	0.67	-0.09	-0.26	-0.26	0.24	0.09	0.28	-0.13	-0.03	-0.02	-0.09	0.39	0.18	-0.23	0.20	0.36	0.30	-0.34	0.43	0.00	0.04	0.02	0.39	-0.12	-0.02	-0.08	0.01	0.07	-0.02
102	0.02	-0.14	0.14	0.27	-0.03	0.07	0.16	-0.14	0.00	0.49	0.02	-0.03	0.02	-0.02	0.00	0.18	0.05	-0.17	-0.13	-0.03	-0.06	-0.18	-0.01	-0.04	-0.11	0.02	-0.21	-0.31	-0.05
103	-0.45	-0.18	-0.10	-0.23	-0.06	-0.18	0.18	-0.15	-0.10	-0.13	-0.06	0.05	-0.48	0.57	-0.31	-0.11	-0.06	0.07	0.10	0.09	-0.33	-0.34	-0.18	0.15	-0.25	-0.01	0.35	0.10	0.14
104	0.21	-0.09	0.00	0.13	0.02	-0.40	-0.42	-0.04	0.00	-0.17	-0.10	0.00	0.20	0.31	-0.20	0.07	0.26	0.34	-0.12	-0.03	-0.13	0.24	-0.56	0.16	-0.19	0.16	0.18	-0.27	0.14
105	0.48	0.10	-0.33	0.16	0.09	-0.17	-0.11	-0.03	0.22	-0.08	-0.22	-0.15	-0.39	-0.01	-0.17	-0.07	-0.05	0.29	-0.03	-0.01	-0.24	-0.02	0.22	-0.23	-0.41	0.26	-0.02	-0.11	0.16
106	0.05	-0.02	-0.12	0.21	0.01	0.32	0.04	-0.11	0.16	-0.10	-0.29	0.32	-0.10	-0.47	-0.31	-0.21	0.05	-0.16	0.02	0.36	0.18	-0.19	-0.07	-0.03	-0.19	0.04	-0.14	0.10	0.19
107	0.31	0.10	0.30	-0.22	0.15	-0.11	0.06	0.00	-0.29	0.04	0.32	-0.09	0.01	-0.16	0.03	0.16	0.02	0.26	0.52	0.09	0.07	0.33	0.38	-0.05	-0.09	-0.18	0.17	0.19	-0.16
108	-0.02	-0.30	0.35	0.40	0.46	0.36	0.22	-0.14	0.08	-0.04	-0.26	0.44	0.16	0.27	0.06	-0.24	-0.12	-0.08	-0.20	-0.08	0.19	-0.29	0.48	-0.04	-0.49	-0.15	0.26	0.22	0.19
109	-1.50	0.04	0.08	-0.39	0.08	-0.15	0.09	-0.01	-0.05	0.22	-0.01	-0.22	0.28	-0.26	-0.05	0.00	0.20	-0.17	0.05	-0.01	0.12	0.23	0.01	0.10	0.22	-0.13	-0.20	-0.04	-0.38
110	0.22	-0.39	0.21	-0.05	0.28	-0.04	-0.39	-0.36	0.49	0.07	-0.22	-0.37	0.02	0.27	-0.06	-0.02	-0.22	0.17	-0.58	-0.23	-0.01	-0.23	-0.20	0.07	0.01	0.02	0.00	0.48	0.13
111	0.11	-0.14	0.02	-0.25	0.00	-0.23	0.04	0.32	0.13	0.04	0.12	0.11	-0.07	0.05	-0.22	0.10	0.14	0.24	-0.38	-0.01	0.45	-0.67	-0.15	-0.02	-0.12	-0.10	0.28	-0.09	-0.02
112	-0.06	0.14	0.17	0.03	-0.31	-0.20	0.09	-0.24	0.08	0.03	-0.09	0.10	0.21	-0.28	-0.31	-0.39	-0.19	-0.05	0.09	0.24	-0.01	-0.03	0.13	0.04	-0.41	0.05	-0.21	0.17	-0.20
113	0.07	-0.19	0.28	-0.09	0.38	0.31	0.11	0.09	0.02	0.15	-0.31	0.03	0.08	0.10	0.08	0.05	-0.02	-0.05	-0.13	-0.17	0.33	-0.29	0.46	-0.20	-0.60	-0.13	0.11	0.42	0.14

Table A. 1: Weight matrix for the first hidden layer W_{ik}^{1} (Continued).

Hidden Layer 1	Input Layer																												
	0	**1**	**2**	**3**	**4**	**5**	**6**	**7**	**8**	**9**	**10**	**11**	**12**	**13**	**14**	**15**	**16**	**17**	**18**	**19**	**20**	**21**	**22**	**23**	**24**	**25**	**26**	**27**	**28**
114	-1.28	-0.14	0.17	-0.10	-0.19	0.38	-0.18	-0.14	0.05	-0.09	0.28	-0.09	0.26	0.06	-0.12	0.12	0.13	-0.23	-0.05	-0.14	-0.20	-0.13	0.20	-0.12	-0.21	0.10	-0.18	0.26	-0.20
115	0.13	0.04	0.04	-0.01	0.21	0.24	-0.10	-0.06	0.17	-0.27	0.07	0.21	0.17	0.23	0.13	0.07	0.06	0.03	0.02	-0.21	0.22	-0.54	0.25	-0.24	-0.23	-0.30	-0.22	0.31	0.21
116	0.02	-0.33	-0.47	0.21	-0.43	-0.20	-0.13	-0.26	0.02	0.30	-0.32	0.25	-0.34	-0.13	-0.13	0.24	0.11	0.04	0.00	0.31	0.19	-0.33	-0.13	0.20	0.24	0.30	-0.08	-0.12	0.00
117	-0.91	0.25	-0.12	-0.45	-0.28	0.08	-0.32	-0.17	0.00	0.07	0.37	-0.11	0.51	0.00	-0.05	0.27	0.09	0.20	0.11	0.20	0.19	-0.17	0.15	-0.03	-0.05	0.16	0.16	0.29	0.34
118	0.32	-0.02	-0.04	0.34	0.07	-0.46	0.05	-0.03	-0.23	0.03	-0.01	-0.17	0.16	0.15	0.00	-0.32	0.29	0.15	0.09	0.29	0.10	-0.23	0.03	0.22	-0.20	0.12	-0.42	-0.34	-0.10
119	0.04	-0.25	-0.15	-0.35	0.17	0.03	0.13	0.07	0.02	0.05	0.01	-0.04	0.07	0.00	-0.30	0.02	0.29	-0.46	-0.21	0.25	0.03	0.18	0.36	0.07	0.12	-0.03	-0.09	-0.17	-0.06
120	0.12	0.15	-0.11	0.27	0.12	0.20	0.17	-0.01	0.11	0.07	-0.15	0.46	-0.15	-0.25	0.17	-0.20	-0.02	-0.27	-0.22	0.39	-0.43	0.20	0.19	0.06	-0.11	-0.04	-0.10	0.26	0.03
121	0.89	-0.35	-0.32	-0.26	-0.34	-0.03	-0.34	0.04	0.10	0.17	-0.04	0.10	-0.31	0.31	-0.02	-0.33	0.03	-0.14	0.40	0.35	-0.34	0.27	0.26	0.22	-0.22	-0.07	0.28	0.20	0.25
122	-0.01	-0.02	0.11	0.06	-0.07	0.38	0.06	-0.15	-0.31	0.08	-0.04	0.36	0.10	0.15	0.32	-0.28	-0.29	-0.33	0.26	-0.07	-0.07	0.17	0.29	-0.33	0.36	-0.01	-0.19	0.21	0.01
123	0.13	-0.33	-0.39	0.14	-0.01	0.17	0.10	-0.10	0.43	-0.24	-0.16	0.45	0.27	-0.21	-0.11	-0.03	-0.25	0.20	-0.10	-0.18	0.29	-0.13	-0.05	-0.26	0.22	-0.08	-0.24	0.17	0.11
124	0.02	0.16	-0.08	0.26	0.08	0.26	0.10	0.02	0.23	-0.15	-0.13	0.38	-0.06	-0.32	-0.15	-0.31	-0.24	-0.08	-0.24	0.05	-0.32	0.11	-0.06	-0.21	0.09	0.13	-0.12	0.26	0.13
125	-1.67	-0.01	-0.01	-0.51	-0.72	-0.13	0.14	0.14	-0.07	-0.10	-0.12	-0.06	-0.16	-0.06	-0.08	-0.20	0.11	0.00	0.22	0.04	0.17	-0.04	0.02	0.00	-0.01	-0.02	-0.10	0.07	0.02
126	0.01	-0.22	-0.24	0.33	-0.21	-0.06	-0.09	-0.13	0.03	0.16	0.04	0.24	0.05	0.29	0.16	0.08	-0.07	0.01	0.06	0.16	0.31	-0.20	0.00	0.20	0.05	-0.10	-0.16	0.04	-0.05
127	0.21	0.25	-0.16	0.11	0.35	0.28	0.03	-0.10	-0.35	-0.14	0.03	-0.06	-0.19	-0.45	0.09	0.00	0.22	0.04	0.31	-0.21	-0.28	0.00	-0.04	-0.07	-0.24	-0.06	0.15	-0.33	0.20

Table A. 2: Biases matrix for the first hidden layer B_k^1.

Hidden Layer 1 Biases																										
k	**0**	**1**	**2**	**3**	**4**	**5**	**6**	**7**	**8**	**9**	**10**	**11**	**12**	**13**	**14**	**15**	**16**	**17**	**18**	**19**	**20**	**21**	**22**	**23**	**24**	**25**
B_k	-0.46	-0.22	-0.32	-0.46	-0.52	-0.32	-0.31	-0.38	-0.29	-0.65	-0.34	-0.47	-0.34	-0.38	-0.40	-0.39	-0.32	-0.11	-0.26	-0.50	-0.26	-0.46	-0.38	-0.51	-0.18	-0.43
k	**26**	**27**	**28**	**29**	**30**	**31**	**32**	**33**	**34**	**35**	**36**	**37**	**38**	**39**	**40**	**41**	**42**	**43**	**44**	**45**	**46**	**47**	**48**	**49**	**50**	**51**
B_k	-0.42	-0.51	-0.48	-0.52	-0.71	-0.47	-0.37	-0.10	-0.25	-0.40	-0.53	-0.48	-0.51	-0.24	0.02	-0.42	0.04	-0.13	-0.13	-0.21	-0.13	-0.60	-0.29	-0.41	-0.18	-0.10
k	**52**	**53**	**54**	**55**	**56**	**57**	**58**	**59**	**60**	**61**	**62**	**63**	**64**	**65**	**66**	**67**	**68**	**69**	**70**	**71**	**72**	**73**	**74**	**75**	**76**	**77**
B_k	-0.50	-0.44	-0.69	-0.31	-0.32	-0.40	-0.14	-0.76	-0.46	-0.79	-0.53	-0.31	-0.54	-0.44	-0.64	-0.41	-1.09	-0.02	-0.53	-0.62	-0.34	-0.12	-0.47	-0.42	-0.26	-0.30
k	**78**	**79**	**80**	**81**	**82**	**83**	**84**	**85**	**86**	**87**	**88**	**89**	**90**	**91**	**92**	**93**	**94**	**95**	**96**	**97**	**98**	**99**	**100**	**101**	**102**	**103**
B_k	-0.42	-0.36	-0.26	-0.34	-0.48	-0.50	-0.49	-0.38	-0.61	-0.16	-0.37	-0.20	-0.15	-0.50	-0.23	-0.25	-0.37	-0.29	-0.37	-1.04	-0.14	-0.34	-0.46	-0.06	-0.29	-0.11
k	**104**	**105**	**106**	**107**	**108**	**109**	**110**	**111**	**112**	**113**	**114**	**115**	**116**	**117**	**118**	**119**	**120**	**121**	**122**	**123**	**124**	**125**	**126**	**127**		
B_k	-0.34	-0.35	-0.53	-0.29	-0.37	-0.51	-0.39	-0.42	-0.44	-0.70	-0.39	-0.36	-0.57	-0.18	-0.37	-0.36	-0.47	0.01	-0.48	-0.37	-0.29	-0.85	-0.46	-0.18		

Table A. 3: Weight matrix for the second hidden layer W_{ik}^{2}.

Hidden Layer 1	Hidden Layer 2																														
	0	**1**	**2**	**3**	**4**	**5**	**6**	**7**	**8**	**9**	**10**	**11**	**12**	**13**	**14**	**15**	**16**	**17**	**18**	**19**	**20**	**21**	**22**	**23**	**24**	**25**	**26**	**27**	**28**	**29**	**30**	**31**
0	0.02	-0.02	0.02	-0.09	-0.11	-0.05	-0.10	0.08	-0.02	0.00	-0.07	-0.01	0.04	0.11	-0.04	0.07	-0.02	-0.25	0.02	-0.05	0.05	-0.19	0.23	0.02	0.07	-0.09	-0.05	-0.03	0.08	-0.03	-0.09	-0.15
1	0.06	0.19	0.06	0.01	-0.04	0.04	-0.04	-0.01	0.01	0.09	0.13	-0.11	0.01	0.09	0.05	0.16	0.20	-0.25	0.06	-0.11	-0.05	-0.28	-0.02	0.05	-0.08	0.05	-0.03	0.02	0.00	0.10	0.19	-0.15
2	0.07	0.02	-0.06	-0.15	0.18	-0.01	0.06	-0.10	0.00	-0.05	-0.31	0.07	-0.11	0.12	-0.02	-0.05	0.15	-0.35	0.15	0.07	0.15	0.10	-0.04	-0.01	0.07	0.13	0.00	0.03	0.09	0.23	0.00	-0.08
3	0.02	0.09	-0.03	0.02	-0.14	0.07	0.03	-0.13	-0.07	0.01	-0.03	0.09	-0.06	0.00	0.09	0.08	-0.10	0.05	0.03	0.05	-0.08	-0.01	0.04	0.16	-0.52	-0.01	0.15	0.01	0.10	0.01	0.01	-0.01
4	-0.02	-0.10	-0.08	0.09	0.00	0.09	0.01	-0.08	0.00	-0.01	-0.15	0.25	-0.05	0.09	0.32	0.08	0.16	-0.08	0.12	0.19	0.02	0.04	0.16	0.23	-0.08	0.06	-0.09	0.08	0.12	0.17	0.19	0.00
5	0.11	-0.15	-0.05	-0.05	0.15	0.05	-0.01	-0.08	0.14	0.04	-0.21	0.13	0.01	0.12	0.00	-0.09	0.02	0.05	0.07	0.01	0.18	0.12	0.01	-0.04	0.02	-0.04	0.05	0.00	-0.07	0.00	0.04	0.07
6	0.09	-0.16	-0.17	-0.03	-0.05	-0.04	-0.30	-0.07	-0.01	-0.16	0.27	-0.08	0.02	-0.11	-0.22	-0.01	0.02	0.04	0.06	-0.01	-0.15	0.03	-0.12	-0.08	0.06	-0.09	-0.39	-0.02	-0.11	-0.14	-0.11	-0.05
7	-0.04	0.05	-0.05	-0.06	0.07	0.07	-0.03	-0.05	-0.04	-0.10	-0.19	0.13	0.00	0.06	-0.04	0.04	-0.04	0.03	0.06	0.10	-0.01	0.04	0.11	-0.06	0.08	0.08	0.06	0.02	0.03	0.14	0.06	-0.02
8	0.05	0.09	-0.26	-0.10	0.02	-0.06	-0.11	-0.14	0.04	-0.35	0.20	0.09	-0.04	0.03	0.01	0.09	0.03	-0.18	0.11	0.07	-0.03	-0.30	0.07	0.21	-0.07	0.09	0.07	0.16	0.02	-0.09	-0.02	-0.19
9	0.11	-0.01	0.06	0.03	0.06	0.07	0.12	-0.08	0.12	0.00	-0.20	0.18	0.07	0.06	-0.04	0.01	0.09	-0.06	0.03	0.07	0.02	-0.15	0.05	0.06	0.14	0.05	0.06	0.03	0.02	0.08	0.25	-0.22
10	0.02	0.00	0.00	0.00	0.12	0.03	0.11	0.12	-0.02	0.05	-0.28	0.11	0.08	0.00	0.00	-0.01	0.13	-0.01	-0.02	0.13	-0.08	-0.04	0.09	0.00	0.12	0.02	0.12	-0.07	-0.02	0.04	0.18	-0.08
11	0.05	0.22	-0.16	0.13	0.22	-0.01	0.13	-0.09	0.03	-0.12	-0.15	-0.09	0.01	-0.02	0.13	-0.10	0.12	0.21	0.09	0.13	-0.01	0.11	0.06	0.15	0.01	0.01	0.03	-0.15	0.19	-0.04	0.08	0.06
12	-0.10	-0.37	0.07	0.20	0.00	-0.11	-0.37	0.07	0.05	-0.08	-0.02	-0.03	0.02	-0.10	-0.14	-0.06	-0.48	-0.13	-0.08	-0.06	0.08	0.13	-0.31	-0.07	-0.55	-0.06	-0.11	-0.10	-0.07	-0.28	-0.15	0.06
13	0.00	0.21	-0.14	0.02	0.01	-0.05	0.19	-0.02	0.05	-0.14	0.17	0.04	-0.10	0.03	-0.05	0.11	0.21	0.12	0.04	0.16	0.14	-0.01	0.08	-0.08	-0.22	0.19	0.24	0.06	-0.01	0.08	0.11	0.06
14	0.01	0.14	-0.14	-0.02	0.10	-0.03	-0.14	-0.08	-0.01	-0.29	0.17	0.16	0.14	0.09	-0.04	0.00	-0.06	0.08	0.18	0.02	-0.06	0.04	-0.06	-0.03	-0.06	0.08	0.15	0.09	0.05	0.04	0.12	0.06

Table A. 3: Weight matrix for the second hidden layer W_{ik}^{2} (Continued).

Hidden Layer 1	Hidden Layer 2																														
	0	1	2	3	4	5	6	7	8	9	10	11	12	13	14	15	16	17	18	19	20	21	22	23	24	25	26	27	28	29	30	31
15	0.16	0.03	0.10	0.03	0.14	-0.02	0.03	-0.35	0.09	0.01	-0.07	-0.01	-0.09	0.00	-0.01	0.22	0.04	0.00	0.08	0.07	0.03	0.02	-0.07	0.10	-0.08	0.13	0.16	0.15	0.23	-0.05	-0.02	-0.05
16	0.00	-0.03	-0.13	-0.01	0.03	0.14	0.01	-0.19	0.00	-0.11	-0.02	0.03	0.18	-0.02	0.02	0.06	-0.01	0.08	-0.08	0.08	-0.01	0.10	0.11	0.07	-0.10	-0.01	-0.06	0.18	0.04	0.04	0.00	-0.07
17	-0.02	-0.05	0.07	0.14	-0.07	-0.03	-0.43	-0.19	-0.08	-0.06	-0.16	-0.45	0.08	-0.13	-0.49	0.05	-0.24	0.02	-0.13	-0.08	-0.30	0.12	-0.15	0.05	-0.05	-0.18	-0.99	-0.03	-0.04	-0.27	-0.08	0.17
18	0.08	0.09	-0.03	-0.24	-0.11	0.17	0.09	-0.05	0.11	0.16	-0.50	0.12	-0.02	-0.02	0.13	0.08	-0.01	-0.15	0.01	0.00	-0.06	0.03	-0.07	0.09	-0.04	0.12	0.10	0.04	0.13	0.15	0.04	-0.10
19	-0.09	0.17	-0.15	-0.02	0.14	0.11	-0.03	0.01	0.03	-0.21	-0.02	0.02	0.00	0.07	-0.02	0.02	0.13	0.06	-0.05	0.04	0.10	-0.01	0.15	0.04	0.13	0.12	0.01	-0.07	-0.02	0.00	0.21	0.00
20	-0.07	-0.04	-0.08	-0.02	0.03	0.00	0.08	0.13	0.02	-0.09	0.03	-0.07	0.02	0.08	0.02	0.07	-0.04	-0.19	-0.14	-0.03	0.05	0.04	0.01	-0.05	0.01	0.00	-0.03	-0.05	-0.06	0.06	-0.12	-0.02
21	0.05	-0.04	0.10	-0.07	0.02	0.07	0.15	-0.14	0.02	0.12	-0.33	0.13	-0.13	0.01	0.18	0.08	0.09	-0.43	-0.02	0.08	0.09	-0.19	0.14	0.00	0.00	-0.01	0.15	0.03	0.04	-0.06	-0.03	-0.25
22	0.08	0.03	0.08	0.04	0.12	-0.01	0.00	0.03	0.04	0.00	-0.39	0.06	0.07	-0.03	0.07	0.13	0.00	-0.03	0.00	0.01	0.10	-0.05	-0.05	-0.04	-0.04	0.00	0.01	0.02	-0.10	0.14	0.11	0.01
23	0.10	0.02	0.04	0.04	0.18	0.06	0.00	-0.10	0.10	0.07	-0.21	-0.15	0.17	0.23	-0.10	0.05	-0.07	-0.24	0.21	0.00	0.19	-0.07	0.21	0.01	-0.12	0.18	-0.05	0.01	-0.09	-0.03	0.13	0.06
24	0.04	-0.09	-0.13	0.00	0.15	0.02	-0.04	-0.02	0.18	-0.11	-0.15	0.01	0.00	0.10	-0.02	0.00	-0.17	0.06	0.06	-0.04	0.14	0.03	0.03	-0.02	-0.05	0.12	-0.01	-0.02	-0.01	-0.06	0.16	0.05
25	-0.10	0.02	0.07	0.14	0.06	-0.13	0.04	0.01	0.03	-0.04	-0.12	0.04	0.15	-0.01	0.02	-0.12	-0.05	-0.05	0.06	-0.08	-0.01	0.00	0.24	-0.05	-0.13	0.11	-0.04	0.08	0.04	-0.12	-0.08	0.02
26	0.04	0.09	-0.06	-0.24	0.11	0.15	0.03	-0.02	0.01	-0.09	0.26	-0.04	0.01	-0.11	-0.07	-0.08	0.00	0.13	0.02	0.05	0.16	0.14	0.19	0.12	0.21	-0.01	-0.04	0.10	0.00	0.14	0.13	0.01
27	-0.03	-0.03	-0.17	-0.03	0.04	0.08	0.06	0.02	0.12	-0.15	-0.33	0.02	0.18	-0.12	0.19	0.07	-0.18	0.12	0.17	0.12	0.14	0.08	-0.12	0.06	-0.29	0.22	-0.01	-0.09	0.14	0.07	0.17	0.10
28	0.00	0.12	0.19	0.09	-0.04	-0.02	0.05	0.06	0.00	0.12	-0.04	0.00	0.08	0.01	0.18	0.26	0.10	-0.10	-0.06	0.00	0.12	-0.16	0.08	0.02	-0.11	0.13	0.18	0.13	0.00	0.07	-0.15	-0.01
29	0.02	0.19	-0.02	0.03	0.11	0.11	-0.01	-0.06	0.02	0.17	0.06	0.08	0.25	0.08	0.10	0.00	0.07	0.04	0.01	0.02	0.10	-0.02	0.20	-0.03	0.03	0.06	0.02	0.05	0.17	0.05	0.00	0.05
30	-0.15	-0.24	0.11	-0.22	-0.09	-0.21	-0.15	-0.12	-0.05	0.22	-0.05	-0.06	-0.22	-0.17	-0.22	-0.32	-0.33	-0.15	-0.22	-0.22	-0.08	-0.35	-0.26	-0.18	-0.01	-0.26	-0.03	-0.28	-0.13	-0.11	-0.19	-0.38

Table A. 3: Weight matrix for the second hidden layer W_{ik}^{2} (Continued).

Hidden Layer 1	Hidden Layer 2																														
	0	1	2	3	4	5	6	7	8	9	10	11	12	13	14	15	16	17	18	19	20	21	22	23	24	25	26	27	28	29	30	31
31	0.23	0.09	0.10	0.12	0.06	-0.02	-0.15	0.01	0.16	0.20	-0.10	0.14	0.03	-0.14	0.03	0.03	0.04	0.05	0.04	0.19	-0.13	-0.10	0.18	0.10	0.10	0.19	-0.03	-0.03	0.04	0.00	0.02	-0.05
32	-0.01	-0.06	-0.01	-0.05	-0.04	-0.10	-0.09	-0.05	-0.03	-0.01	-0.07	0.01	-0.25	-0.23	-0.05	-0.29	-0.15	-0.05	-0.12	-0.04	-0.16	-0.08	-0.12	0.01	-0.12	-0.08	-0.05	-0.09	-0.03	0.05	-0.16	-0.18
33	-0.01	0.00	0.08	-0.03	-0.03	0.07	0.01	-0.12	0.02	0.06	0.05	0.03	0.03	-0.01	-0.03	-0.16	0.04	-0.15	0.00	0.08	0.03	-0.45	-0.24	0.00	-0.09	0.00	-0.26	-0.08	0.00	-0.04	-0.01	-0.42
34	0.04	-0.08	-0.01	-0.03	-0.13	-0.10	-0.10	0.01	-0.01	0.01	-0.31	-0.04	-0.02	-0.02	-0.05	-0.21	-0.18	0.05	-0.03	-0.20	0.02	0.10	0.08	-0.13	-0.08	-0.05	-0.04	-0.01	0.02	-0.02	-0.02	-0.05
35	-0.12	-0.20	0.12	0.12	-0.10	-0.25	-0.44	-0.08	-0.10	0.18	-0.20	-0.14	-0.23	-0.21	-0.18	-0.75	-0.39	0.07	-0.15	-0.33	-0.25	-0.33	-0.62	-0.23	0.13	-0.08	-0.71	-0.27	-0.20	-0.64	-0.08	-0.27
36	0.13	0.08	-0.23	0.03	0.07	0.02	-0.16	-0.11	0.04	-0.42	-0.02	0.06	0.03	-0.02	0.15	0.07	0.05	0.11	0.09	-0.05	0.03	-0.05	0.10	0.11	0.13	0.22	0.01	0.14	-0.05	0.02	-0.04	-0.09
37	-0.15	-0.10	0.03	-0.03	-0.06	-0.09	-0.11	-0.09	-0.08	0.14	0.03	0.09	0.06	-0.07	-0.17	-0.07	0.11	-0.05	-0.08	-0.09	-0.10	-0.20	-0.05	-0.04	-0.05	0.01	-0.30	-0.15	-0.17	-0.18	-0.02	-0.28
38	0.24	-0.08	-0.08	-0.18	0.02	0.02	0.15	-0.03	0.01	-0.07	-0.22	0.23	0.03	0.02	0.01	0.16	-0.02	0.09	-0.04	0.01	-0.01	0.04	-0.11	0.08	0.14	0.05	0.02	-0.07	-0.02	0.08	0.09	0.09
39	-0.07	-0.07	0.17	-0.12	-0.06	0.02	-0.10	-0.17	0.07	0.17	0.04	0.03	-0.04	-0.10	-0.02	-0.12	-0.03	0.04	-0.05	-0.10	0.03	-0.02	-0.20	-0.03	-0.10	0.01	-0.27	-0.03	0.01	-0.17	0.02	-0.11
40	-0.06	-0.01	0.03	-0.19	0.06	0.01	-0.01	-0.04	-0.01	-0.04	0.00	0.03	0.15	-0.06	-0.01	0.00	-0.01	-0.44	0.00	0.08	-0.10	-0.53	-0.09	0.03	-0.10	0.03	-0.03	0.01	-0.08	-0.03	0.06	-0.33
41	0.05	-0.06	0.05	0.04	0.03	0.10	0.06	0.06	0.03	0.10	-0.06	-0.06	-0.03	0.01	-0.02	0.00	0.11	-0.08	0.02	0.17	0.07	-0.03	0.02	0.00	-0.08	0.03	0.04	0.02	0.08	0.13	-0.06	-0.05
42	0.13	-0.01	0.02	-0.24	0.07	0.00	0.01	-0.07	0.02	0.03	0.06	0.02	-0.01	-0.01	0.01	0.06	-0.08	-0.59	-0.08	-0.05	-0.11	-0.52	0.03	-0.01	0.10	-0.02	0.00	0.00	0.00	-0.05	-0.06	-0.54
43	0.00	-0.16	-0.23	-0.09	0.10	0.11	-0.10	-0.19	0.05	-0.23	0.18	0.00	-0.05	0.03	-0.01	0.02	0.00	-0.14	0.11	0.13	0.01	0.03	0.11	0.14	0.11	0.01	0.00	0.07	-0.11	0.00	0.04	-0.01
44	-0.10	-0.07	-0.03	-0.08	-0.02	0.02	-0.03	-0.09	-0.01	-0.05	0.11	0.00	0.09	0.07	-0.07	-0.08	0.01	-0.02	0.13	0.06	0.05	-0.13	-0.06	-0.02	0.07	-0.01	-0.05	0.01	0.15	-0.06	0.07	-0.32
45	-0.06	-0.08	-0.24	-0.22	-0.06	0.06	-0.04	-0.05	0.01	-0.23	0.04	0.03	-0.13	0.05	0.09	0.13	0.02	0.01	0.01	-0.07	0.06	0.03	-0.02	0.08	-0.09	0.11	-0.01	0.04	0.07	0.01	0.00	-0.11
46	0.06	0.05	-0.14	-0.20	-0.09	0.01	0.05	0.07	0.03	-0.04	0.01	0.04	-0.14	-0.07	0.02	-0.03	0.06	-0.30	-0.06	0.01	0.18	-0.25	-0.06	0.12	-0.04	0.09	0.07	-0.01	0.02	-0.11	-0.01	-0.31

Table A. 3: Weight matrix for the second hidden layer W_{ik}^{2} (Continued).

Hidden Layer 1	Hidden Layer 2																														
	0	1	2	3	4	5	6	7	8	9	10	11	12	13	14	15	16	17	18	19	20	21	22	23	24	25	26	27	28	29	30	31
47	0.13	0.08	-0.21	-0.08	0.02	0.15	0.04	-0.03	0.01	-0.18	0.00	0.08	-0.27	-0.11	0.02	-0.08	-0.03	-0.08	0.24	0.06	-0.03	0.05	-0.15	0.00	0.09	-0.01	0.03	0.23	-0.04	0.15	-0.04	-0.03
48	0.06	0.00	-0.06	-0.18	0.04	-0.02	0.06	0.04	0.00	-0.07	0.05	-0.33	0.06	-0.06	-0.21	-0.07	-0.12	0.04	-0.08	0.00	0.04	-0.08	-0.27	-0.02	-0.09	-0.03	-0.13	-0.08	-0.07	-0.03	0.11	-0.31
49	-0.15	-0.55	0.16	-0.08	-0.17	-0.16	-0.32	0.08	-0.17	0.21	-0.07	-0.07	-0.20	-0.29	-0.24	-0.36	-0.42	-0.05	-0.29	-0.02	-0.16	-0.02	-0.34	-0.13	-0.06	-0.30	-0.41	-0.19	-0.16	-0.23	-0.20	0.04
50	0.06	0.12	-0.12	-0.14	-0.07	0.02	0.00	0.21	0.11	-0.22	0.01	0.14	0.04	0.17	-0.06	0.02	-0.01	-0.01	0.07	0.00	-0.03	0.18	0.07	0.07	0.11	-0.15	-0.09	0.00	0.12	-0.05	-0.01	-0.07
51	0.04	-0.09	-0.20	-0.06	-0.02	0.16	0.07	0.14	0.06	-0.23	0.07	-0.13	0.13	0.00	-0.01	0.11	0.12	-0.08	0.05	0.01	-0.02	0.00	0.04	0.01	-0.05	0.01	0.00	-0.01	-0.01	0.01	0.02	-0.08
52	-0.06	0.14	-0.02	-0.16	-0.02	0.09	0.00	0.02	0.02	-0.04	0.06	-0.17	0.18	0.18	0.06	0.03	0.02	-0.17	0.01	-0.01	0.15	-0.44	-0.09	-0.03	-0.30	0.05	0.04	0.03	0.06	0.04	-0.08	-0.43
53	-0.09	0.08	0.07	-0.05	0.07	-0.03	-0.02	-0.14	-0.05	0.01	-0.13	0.03	0.04	0.01	0.20	0.21	0.18	0.05	0.12	0.00	-0.03	0.16	-0.09	0.01	-0.10	0.14	-0.05	0.00	0.05	0.14	0.03	0.27
54	0.18	0.01	-0.25	-0.08	0.12	0.16	0.02	0.09	0.10	-0.19	0.01	0.01	-0.08	0.14	0.07	-0.13	0.12	-0.04	0.03	-0.07	0.13	-0.09	-0.04	0.03	0.14	0.20	0.10	0.16	0.27	0.03	0.21	-0.09
55	-0.07	-0.09	-0.07	-0.07	-0.08	0.07	0.04	0.01	0.01	-0.06	-0.08	-0.20	-0.03	-0.08	0.07	-0.42	-0.50	-0.09	0.04	0.00	0.16	-0.14	-0.25	0.07	-0.56	-0.07	-0.10	-0.03	0.11	-0.10	-0.01	-0.07
56	0.12	0.06	-0.07	0.09	-0.02	0.11	0.07	0.00	0.08	-0.16	-0.22	0.04	-0.07	0.11	0.07	-0.04	-0.05	0.12	-0.07	0.08	0.10	0.16	0.13	0.00	0.13	0.17	0.12	0.08	0.00	-0.13	0.02	0.10
57	-0.05	-0.36	0.11	-0.04	-0.13	-0.02	-0.28	0.12	-0.03	0.12	-0.01	-0.03	-0.03	-0.29	-0.33	-0.15	-0.30	0.21	-0.13	-0.02	0.01	-0.09	-0.35	-0.03	-0.30	-0.08	-0.22	-0.09	-0.03	-0.26	-0.06	-0.02
58	0.04	0.01	0.04	0.02	-0.08	0.04	0.14	0.03	0.02	-0.11	0.09	0.00	0.17	0.01	-0.01	0.02	-0.02	-0.21	-0.08	-0.09	0.10	-0.16	0.07	0.04	-0.21	0.00	0.05	-0.05	0.07	0.00	0.16	0.02
59	-0.35	-0.33	0.46	0.02	-0.19	-0.37	-0.48	-0.08	-0.20	0.36	-0.06	-0.34	-0.30	-0.53	-0.24	-0.46	-0.38	0.25	-0.34	-0.14	-0.33	0.33	-0.13	-0.49	-0.33	-0.40	-0.19	-0.39	-0.15	-0.42	-0.46	0.34
60	0.02	0.07	0.01	-0.07	-0.02	-0.03	0.05	-0.11	-0.02	0.00	-0.17	0.05	0.12	0.13	0.03	-0.01	0.10	0.07	-0.02	-0.03	0.01	0.17	0.05	0.13	0.01	-0.06	0.02	0.02	0.07	-0.01	-0.07	0.11
61	-0.49	-0.40	0.16	0.44	-0.48	-0.38	-0.48	-0.11	-0.37	0.11	0.13	-0.62	-0.49	-0.53	-0.64	-0.48	-0.73	0.36	-0.41	-0.40	-0.44	0.46	-0.50	-0.30	-0.07	-0.46	-0.48	-0.52	-0.31	-0.38	-0.45	0.28
62	0.13	0.02	-0.02	0.02	0.02	0.19	0.09	0.02	0.07	-0.07	-0.47	0.00	0.04	0.02	-0.05	-0.03	0.10	0.03	0.05	0.00	-0.02	0.08	0.00	0.06	-0.05	0.11	-0.01	-0.01	0.17	0.27	0.07	0.04

Table A. 3: Weight matrix for the second hidden layer W_{ik}^{2} (Continued).

Hidden Layer 1	Hidden Layer 2																														
	0	1	2	3	4	5	6	7	8	9	10	11	12	13	14	15	16	17	18	19	20	21	22	23	24	25	26	27	28	29	30	31
63	0.04	0.15	0.00	-0.16	-0.05	-0.02	-0.25	-0.02	-0.03	0.03	-0.19	0.04	0.11	0.11	-0.14	0.13	0.09	-0.25	-0.01	0.06	-0.08	-0.34	-0.02	0.08	0.05	-0.25	-0.24	0.15	-0.01	0.01	0.05	-0.17
64	0.22	0.07	-0.10	-0.10	0.06	0.12	0.14	0.04	-0.01	0.00	-0.36	0.10	0.10	0.06	0.07	0.06	0.22	-0.21	0.14	0.19	0.11	0.00	0.19	0.18	-0.03	0.07	0.22	0.11	0.21	0.10	0.01	-0.03
65	0.01	0.04	0.03	-0.02	0.12	0.13	0.05	0.00	0.09	0.20	-0.26	-0.07	-0.03	0.07	0.05	0.17	0.01	-0.07	0.08	0.00	0.04	-0.31	-0.05	0.02	0.00	-0.01	0.12	0.03	0.05	0.02	0.01	-0.08
66	0.05	0.01	-0.13	0.04	0.07	-0.04	0.05	-0.09	-0.02	-0.23	-0.39	0.08	0.12	-0.03	0.19	-0.02	0.18	0.08	0.24	0.10	-0.04	0.11	0.10	-0.02	0.02	-0.07	0.06	0.01	0.18	0.02	0.01	0.06
67	0.12	0.10	-0.09	0.00	0.07	0.09	-0.14	0.16	0.04	-0.15	-0.07	0.07	0.06	-0.06	0.21	-0.01	0.09	-0.07	0.11	0.06	-0.03	0.03	0.17	0.04	-0.01	0.12	0.13	0.02	0.08	-0.08	0.10	0.10
68	-0.88	-0.50	0.89	1.10	-0.85	-0.72	-0.70	1.03	-0.74	1.00	-0.06	-0.48	-0.71	-0.64	-0.71	-0.64	-0.55	0.67	-0.70	-0.69	-0.35	0.75	-0.82	-0.94	-0.37	-1.04	-0.94	-0.73	-0.75	-0.72	-0.69	1.17
69	0.08	-0.07	0.06	-0.09	-0.04	0.03	0.00	0.07	-0.04	-0.08	0.13	0.00	-0.06	-0.10	0.07	-0.11	0.16	-0.33	0.01	0.06	-0.02	-0.51	0.14	0.03	0.00	0.07	0.02	-0.03	0.09	0.01	0.05	-0.29
70	-0.11	-0.72	0.18	0.24	-0.29	-0.11	-0.87	0.26	-0.09	0.15	0.02	-0.26	-0.43	-0.58	-0.88	-0.87	-0.71	0.19	-0.20	-0.18	-0.15	0.16	-0.96	-0.10	-0.27	-0.36	-1.07	-0.12	-0.10	-0.65	0.02	0.25
71	0.07	0.05	0.01	-0.01	0.12	-0.04	0.14	-0.08	0.00	-0.18	0.02	0.20	0.02	0.07	0.10	0.07	0.18	0.08	0.22	0.04	0.05	-0.04	0.18	0.01	0.09	0.13	0.14	0.19	0.01	0.04	0.00	0.10
72	0.00	0.03	-0.36	-0.06	0.06	0.04	0.01	0.02	0.09	-0.23	0.11	0.13	0.15	-0.12	0.14	-0.08	-0.08	0.03	0.09	0.09	0.06	-0.03	-0.16	0.27	0.03	0.10	-0.02	0.08	0.12	0.26	-0.02	0.00
73	0.09	-0.03	-0.02	-0.03	-0.10	0.07	-0.05	0.05	-0.03	-0.17	0.07	0.10	-0.05	-0.04	0.03	0.11	0.19	-0.02	-0.03	0.00	-0.03	0.02	0.05	0.01	0.01	0.05	0.09	0.09	-0.07	0.06	0.01	-0.01
74	-0.17	0.01	0.28	0.12	-0.07	-0.09	-0.50	-0.09	0.10	-0.13	0.11	-0.57	0.00	-0.11	-0.60	-0.24	-0.07	0.20	-0.24	-0.03	-0.33	0.08	-0.46	-0.15	0.18	-0.29	-0.82	-0.12	-0.13	-0.35	-0.26	0.33
75	-0.03	-0.18	-0.04	0.14	-0.33	-0.11	-0.52	0.02	-0.29	-0.14	-0.01	-0.35	-0.16	-0.11	-0.50	-0.15	-0.09	0.08	-0.13	-0.02	-0.28	0.14	-0.60	-0.03	0.09	-0.34	-0.48	-0.05	0.00	-0.34	-0.15	0.16
76	-0.12	-0.02	-0.02	-0.01	0.00	-0.02	0.06	0.03	0.00	-0.14	-0.06	-0.01	-0.18	-0.11	0.06	-0.36	-0.40	0.05	-0.04	-0.09	-0.14	0.07	-0.35	-0.05	-0.16	-0.01	0.07	0.00	-0.05	0.03	0.01	-0.19
77	0.01	0.00	0.21	0.04	0.03	-0.08	-0.16	0.05	0.01	0.14	-0.34	-0.12	-0.10	-0.14	-0.13	-0.23	-0.22	-0.02	-0.19	-0.29	-0.13	0.00	-0.07	-0.08	-0.33	-0.05	0.02	-0.02	-0.15	-0.03	0.04	0.01
78	0.05	0.07	-0.28	0.02	0.05	-0.06	0.03	-0.26	0.09	-0.43	-0.02	-0.10	-0.06	0.03	-0.20	-0.17	-0.04	-0.01	0.03	0.02	-0.12	0.01	0.02	-0.03	-0.01	0.10	-0.11	-0.04	-0.09	0.00	0.02	-0.07

Table A. 3: Weight matrix for the second hidden layer W_{ik}^{2} (Continued).

Hidden Layer 1	Hidden Layer 2																														
	0	1	2	3	4	5	6	7	8	9	10	11	12	13	14	15	16	17	18	19	20	21	22	23	24	25	26	27	28	29	30	31
79	0.04	0.21	0.01	-0.06	0.11	-0.03	-0.02	-0.02	0.06	-0.01	-0.37	0.17	0.00	0.09	0.07	0.07	0.04	-0.06	-0.05	0.02	-0.01	-0.03	-0.07	-0.01	-0.08	0.10	-0.19	0.00	0.06	-0.04	0.01	0.02
80	-0.03	0.08	0.02	-0.07	0.05	0.02	-0.02	-0.09	0.15	0.01	-0.03	-0.05	0.07	-0.03	-0.06	0.11	0.06	0.09	0.10	0.13	0.01	-0.04	0.13	-0.12	-0.01	0.07	-0.09	-0.03	0.03	0.02	0.02	-0.05
81	-0.07	-0.09	0.20	0.28	0.09	-0.09	-0.02	-0.06	0.02	0.10	-0.03	0.06	-0.02	-0.22	0.01	-0.28	-0.33	0.25	-0.04	0.00	-0.33	0.10	-0.28	-0.09	-0.34	-0.13	-0.25	-0.08	-0.11	-0.09	-0.07	0.01
82	0.00	-0.07	-0.13	-0.10	0.19	-0.01	-0.01	0.03	0.05	-0.05	-0.06	0.12	-0.10	0.01	-0.01	0.16	0.11	-0.03	0.02	-0.01	0.00	-0.03	0.03	0.02	0.14	0.01	-0.06	-0.07	0.10	0.18	0.05	-0.03
83	0.06	-0.03	-0.03	-0.07	0.28	0.13	0.00	-0.09	0.18	0.09	-0.04	-0.04	0.23	0.11	-0.14	0.00	-0.28	-0.01	0.06	0.10	0.27	-0.03	-0.08	0.07	-0.45	0.06	-0.01	0.02	0.22	-0.06	0.19	0.09
84	0.05	0.01	0.04	0.06	0.04	0.22	0.13	0.08	0.15	0.04	0.01	-0.07	0.14	0.01	0.24	-0.03	0.14	-0.16	0.21	0.08	-0.01	0.11	0.06	0.03	0.05	0.12	0.06	0.17	0.06	-0.03	-0.09	0.06
85	0.00	-0.24	-0.02	0.03	-0.28	-0.10	-0.05	0.08	-0.18	-0.05	-0.17	-0.03	-0.12	-0.41	0.00	-0.45	-0.23	0.06	-0.07	0.00	-0.44	-0.15	-0.36	-0.06	-0.10	-0.16	-0.52	-0.16	0.05	-0.48	0.12	-0.18
86	0.07	-0.02	-0.10	-0.09	0.07	0.12	0.06	-0.08	0.15	-0.19	-0.66	-0.07	0.08	0.11	0.06	-0.02	-0.04	0.10	0.08	0.11	0.14	0.16	-0.03	0.10	-0.04	0.06	0.04	0.01	0.20	0.13	0.04	0.06
87	0.09	0.06	-0.17	-0.15	-0.06	0.01	0.04	-0.38	0.06	-0.31	0.02	-0.14	0.00	0.15	-0.01	0.05	0.05	-0.06	0.08	0.01	-0.11	-0.14	0.05	-0.09	0.05	-0.10	0.01	0.05	0.14	-0.01	0.07	-0.13
88	-0.01	-0.15	0.11	0.09	-0.08	-0.27	-0.06	0.32	-0.10	0.22	-0.05	-0.32	-0.21	-0.05	-0.31	-0.34	-0.28	0.19	-0.14	-0.16	-0.23	0.25	-0.32	-0.02	0.11	-0.15	-0.39	-0.12	-0.13	-0.32	-0.14	0.14
89	0.03	0.04	0.09	-0.12	0.10	-0.03	0.10	0.06	0.00	0.08	0.08	-0.01	0.05	0.10	0.15	0.09	-0.10	-0.04	-0.03	0.00	0.09	-0.17	-0.01	-0.04	0.05	0.06	0.11	-0.14	0.00	-0.06	0.06	-0.13
90	0.03	0.16	-0.08	-0.10	-0.02	0.02	0.11	0.15	0.01	-0.17	-0.14	-0.01	-0.02	0.05	-0.01	0.13	0.06	0.02	0.09	-0.06	-0.01	-0.04	-0.13	0.04	-0.02	-0.02	0.05	0.08	0.13	-0.04	-0.01	-0.01
91	0.13	0.15	-0.11	-0.18	0.16	0.02	0.13	-0.03	0.07	0.09	-0.39	0.02	-0.05	-0.09	-0.06	0.15	0.05	-0.09	0.09	0.21	-0.04	-0.03	0.06	0.11	0.00	-0.17	-0.04	0.21	0.02	0.11	0.00	-0.12
92	-0.03	0.02	-0.13	0.02	0.13	0.06	0.09	0.07	0.07	-0.12	0.06	0.11	0.06	0.03	0.10	0.05	0.01	-0.02	0.12	0.21	0.01	0.08	0.08	0.03	0.00	0.08	-0.04	0.02	0.06	-0.08	-0.02	0.04
93	0.02	-0.04	0.10	-0.04	0.02	0.12	0.01	-0.15	0.00	0.05	-0.05	-0.07	-0.04	-0.06	-0.05	0.04	0.10	-0.15	-0.07	0.04	-0.03	-0.24	0.10	0.09	0.17	0.01	-0.08	0.06	-0.12	0.01	-0.04	-0.19
94	0.08	0.00	-0.20	-0.01	0.02	-0.17	0.09	-0.20	0.11	0.05	0.00	0.24	0.04	-0.01	-0.10	0.16	0.01	-0.01	0.14	0.11	-0.06	0.01	-0.13	-0.01	-0.28	0.15	-0.01	0.16	-0.09	0.14	0.01	-0.05

Table A. 3: Weight matrix for the second hidden layer W_{ik}^{2} (Continued).

Hidden Layer 1	Hidden Layer 2																														
	0	**1**	**2**	**3**	**4**	**5**	**6**	**7**	**8**	**9**	**10**	**11**	**12**	**13**	**14**	**15**	**16**	**17**	**18**	**19**	**20**	**21**	**22**	**23**	**24**	**25**	**26**	**27**	**28**	**29**	**30**	**31**
95	-0.04	0.01	-0.10	-0.17	0.04	0.05	0.15	-0.03	0.08	-0.31	-0.40	0.20	0.00	0.06	0.04	0.09	-0.12	-0.07	0.04	0.09	-0.02	0.17	0.26	0.25	-0.09	0.01	-0.01	0.16	0.05	-0.09	0.18	-0.02
96	0.03	0.15	-0.02	0.03	0.07	-0.01	-0.09	0.09	-0.02	-0.05	0.11	0.03	0.04	0.01	0.02	0.13	0.12	-0.04	0.11	0.08	-0.05	-0.04	0.00	0.10	0.01	0.08	-0.04	0.03	-0.02	0.03	-0.06	-0.03
97	-0.83	-0.71	0.32	0.75	-0.98	-0.69	-0.83	0.48	-0.83	0.72	0.11	-0.67	-0.94	-0.68	-0.78	-0.86	-0.62	1.01	-0.73	-0.68	-0.57	1.13	-0.81	-0.68	0.02	-1.12	-0.97	-0.86	-0.70	-0.72	-0.74	0.93
98	-0.09	-0.12	0.00	0.00	0.19	-0.01	-0.07	-0.02	0.17	-0.07	0.08	-0.13	0.00	0.13	0.06	0.01	0.08	-0.03	0.02	-0.08	-0.06	0.05	0.05	0.04	-0.50	0.00	0.18	0.11	0.06	0.06	-0.02	0.05
99	0.00	-0.02	0.01	-0.18	-0.01	-0.04	-0.09	-0.23	-0.02	0.01	-0.27	0.15	0.05	0.11	0.07	0.13	0.05	0.09	0.03	0.06	0.05	0.04	-0.08	0.03	-0.03	0.11	0.21	-0.12	-0.02	0.06	0.09	-0.05
100	0.13	-0.07	-0.02	0.03	0.00	0.03	0.26	0.02	0.00	-0.04	0.00	-0.01	0.10	0.05	-0.02	-0.09	-0.15	-0.15	0.06	0.00	0.04	-0.22	0.05	0.01	0.01	0.01	-0.25	0.12	0.06	0.21	0.10	-0.18
101	0.02	0.06	-0.15	-0.16	-0.01	-0.06	-0.07	-0.01	-0.05	-0.13	0.04	0.08	-0.11	0.07	0.03	0.02	-0.01	-0.19	-0.09	0.03	0.04	-0.20	-0.05	0.08	0.14	-0.03	0.00	-0.04	-0.03	0.09	0.05	-0.16
102	-0.12	-0.10	-0.06	-0.10	-0.10	-0.10	0.00	0.32	-0.06	-0.14	0.01	0.10	0.07	-0.02	0.06	0.08	0.14	0.25	0.01	-0.09	0.10	0.07	-0.08	-0.01	0.01	-0.04	0.11	-0.05	-0.12	0.05	0.04	-0.25
103	0.02	0.02	0.04	-0.06	-0.13	-0.11	0.00	0.01	-0.10	0.02	0.15	-0.06	-0.16	0.02	-0.08	-0.28	-0.11	0.03	0.00	-0.10	-0.10	-0.15	-0.24	0.01	-0.02	-0.03	-0.26	-0.01	-0.09	-0.17	0.01	-0.11
104	0.14	0.08	-0.14	-0.02	0.11	0.12	-0.02	-0.11	-0.04	-0.12	0.03	-0.17	0.01	0.07	-0.09	-0.07	-0.02	0.01	0.01	0.04	-0.13	-0.08	-0.10	0.02	-0.16	-0.05	-0.04	0.11	-0.01	0.14	0.12	-0.03
105	-0.10	-0.06	0.02	-0.12	-0.02	-0.01	-0.02	-0.02	0.03	-0.06	-0.07	-0.01	-0.12	-0.09	0.00	-0.36	-0.35	-0.13	-0.06	-0.19	-0.07	-0.26	-0.19	-0.06	-0.16	-0.07	0.11	0.01	-0.04	-0.03	-0.02	-0.23
106	0.06	0.20	-0.14	0.07	0.02	0.11	0.23	0.06	0.08	-0.18	0.06	-0.03	0.15	0.32	0.01	0.19	0.10	0.09	0.04	0.18	0.04	0.09	0.05	0.07	0.15	0.09	-0.03	-0.02	0.16	0.00	0.14	0.15
107	0.09	-0.01	-0.05	-0.11	0.02	-0.12	0.04	-0.11	-0.01	-0.05	0.12	0.14	0.18	-0.08	0.08	0.04	-0.15	-0.07	0.15	0.08	0.08	-0.05	0.18	0.09	-0.06	-0.02	0.03	-0.09	-0.07	0.04	-0.04	-0.14
108	0.08	0.25	-0.20	-0.15	0.18	0.08	-0.12	-0.14	0.07	-0.14	-0.22	-0.04	0.13	0.01	-0.01	0.21	0.10	0.00	0.01	0.04	-0.09	0.24	0.11	0.20	0.07	-0.11	0.21	0.00	0.19	0.04	0.20	0.09
109	-0.19	-0.44	0.16	0.18	-0.12	-0.28	-0.49	-0.26	0.02	0.33	0.15	-0.31	-0.15	-0.32	-0.50	-0.46	-0.68	0.32	-0.28	-0.09	-0.01	0.26	-0.77	-0.25	-0.05	-0.10	-0.44	-0.28	-0.29	-0.65	-0.28	0.15
110	0.00	0.05	0.04	0.11	-0.10	0.00	0.12	-0.04	0.02	0.01	-0.04	0.05	-0.08	-0.01	0.16	0.03	0.12	-0.27	0.07	0.02	0.15	-0.38	0.05	0.02	0.10	-0.02	0.03	0.15	0.02	0.17	0.08	-0.22

Table A. 3: Weight matrix for the second hidden layer W_{ik}^{2} (Continued).

Hidden Layer 1	Hidden Layer 2																														
	0	**1**	**2**	**3**	**4**	**5**	**6**	**7**	**8**	**9**	**10**	**11**	**12**	**13**	**14**	**15**	**16**	**17**	**18**	**19**	**20**	**21**	**22**	**23**	**24**	**25**	**26**	**27**	**28**	**29**	**30**	**31**
111	0.05	0.09	0.12	-0.08	0.07	-0.01	-0.14	-0.06	0.09	0.16	-0.30	0.01	-0.02	0.22	-0.07	0.10	0.16	-0.24	0.04	0.06	0.03	-0.34	0.01	0.01	0.04	0.06	-0.09	-0.10	0.19	0.11	-0.03	-0.18
112	0.00	-0.02	0.09	0.14	0.00	-0.04	0.21	0.12	-0.03	0.15	0.10	0.14	0.04	0.05	0.08	0.02	0.23	-0.02	-0.04	-0.16	0.10	0.05	-0.03	-0.03	0.01	0.06	0.27	0.05	-0.07	0.19	-0.13	0.04
113	0.19	0.30	-0.30	-0.38	0.29	0.18	0.05	-0.14	0.18	-0.01	-0.30	0.01	0.23	0.24	0.20	0.02	0.20	-0.02	0.28	0.12	0.13	0.01	0.00	0.26	0.00	0.04	0.13	0.24	0.18	0.09	0.11	-0.04
114	-0.11	-0.02	0.29	-0.01	-0.03	0.00	-0.08	-0.20	0.08	0.39	0.01	-0.10	0.06	-0.02	0.02	-0.02	-0.06	0.10	0.00	-0.04	-0.32	0.10	0.11	-0.16	-0.34	0.05	-0.27	0.03	-0.21	-0.11	-0.07	0.13
115	0.07	0.13	0.16	-0.01	-0.04	0.07	0.21	0.03	0.06	0.19	0.12	-0.09	0.18	0.04	-0.07	-0.03	0.03	0.03	0.10	0.13	0.00	-0.04	0.01	0.09	0.09	0.01	0.12	0.18	0.15	0.08	0.05	-0.07
116	0.03	0.12	-0.06	-0.04	0.17	0.13	-0.05	-0.04	-0.01	-0.02	-0.24	0.01	0.01	0.15	0.02	0.07	0.03	0.04	-0.05	0.09	0.11	-0.13	-0.12	0.03	0.26	-0.10	-0.12	0.00	0.03	-0.03	0.04	-0.08
117	-0.16	-0.06	0.09	0.13	-0.02	0.00	-0.47	-0.10	-0.01	0.03	0.13	-0.22	-0.07	-0.15	-0.33	-0.03	-0.52	0.04	-0.10	-0.06	-0.15	0.10	-0.04	-0.07	-0.35	-0.23	-0.48	-0.06	-0.14	-0.25	-0.10	0.02
118	-0.01	0.01	-0.12	-0.16	-0.06	-0.08	0.07	-0.19	-0.03	-0.13	0.06	0.10	-0.01	-0.02	0.01	-0.05	0.11	-0.09	-0.03	0.03	0.07	-0.04	0.04	0.07	-0.10	-0.08	-0.03	0.03	0.02	0.05	-0.10	-0.04
119	0.01	0.08	-0.12	-0.06	0.04	-0.01	0.07	0.15	0.09	-0.38	-0.23	0.02	-0.14	-0.10	0.11	-0.19	-0.04	0.13	0.03	0.08	0.08	0.02	0.10	0.04	-0.11	0.04	-0.08	0.12	0.02	0.05	-0.02	0.04
120	0.06	-0.03	-0.18	0.06	0.12	0.05	0.15	0.08	0.09	-0.07	-0.04	0.02	0.05	0.03	0.04	0.03	0.23	0.06	0.14	-0.04	0.09	0.07	-0.02	0.01	0.11	0.10	0.17	0.16	0.00	-0.11	0.09	0.09
121	-0.04	0.00	-0.04	-0.15	-0.02	-0.05	-0.03	-0.33	0.02	-0.16	0.00	-0.07	0.06	0.03	0.02	0.07	-0.12	-0.29	0.06	0.00	0.04	-0.48	-0.02	0.11	0.06	-0.04	-0.07	0.02	0.03	0.07	-0.08	-0.45
122	0.04	0.10	-0.06	0.07	0.09	0.01	0.19	-0.21	0.08	0.22	-0.17	0.11	0.10	0.02	0.08	-0.07	-0.14	0.10	0.14	0.02	0.08	0.06	0.11	0.14	-0.15	0.16	-0.12	0.17	-0.05	0.10	0.03	0.15
123	0.10	0.04	-0.26	-0.06	-0.07	-0.06	-0.04	0.01	0.02	-0.37	0.08	0.16	-0.01	0.18	-0.01	0.11	0.11	-0.13	0.00	-0.03	-0.10	-0.05	0.03	0.02	0.11	0.04	-0.11	0.01	-0.03	-0.08	0.03	-0.10
124	-0.05	0.07	-0.23	0.05	0.13	-0.01	0.13	0.16	0.08	-0.18	-0.03	0.02	-0.06	0.22	0.23	-0.01	0.02	0.08	0.09	-0.01	0.09	0.03	0.02	0.00	0.05	0.02	0.05	0.04	0.20	0.10	0.16	0.07
125	-0.55	-0.62	0.60	0.31	-0.65	-0.73	-0.51	0.65	-0.27	0.41	0.34	-0.49	-0.64	-0.53	-0.40	-0.83	-0.58	0.39	-0.57	-0.73	-0.26	0.36	-0.71	-0.43	-0.03	-0.83	-0.86	-0.63	-0.72	-0.79	-0.67	0.47
126	0.05	-0.02	0.00	0.04	0.11	0.08	0.12	-0.08	0.09	-0.07	-0.14	0.22	-0.18	0.00	0.11	0.09	-0.09	0.15	0.02	0.08	0.13	0.15	-0.04	0.01	0.11	-0.10	-0.04	-0.01	0.12	0.01	-0.01	-0.03

Table A. 3: Weight matrix for the second hidden layer W_{ik}^{2} (Continued).

Hidden Layer 1	Hidden Layer 2																													
	0	**1**	**2**	**3**	**4**	**5**	**6**	**7**	**8**	**9**	**10**	**11**	**12**	**13**	**14**	**15**	**16**	**17**	**18**	**19**	**20**	**21**	**22**	**23**	**24**	**25**	**26**	**27**	**28**	**29**	**30**	**31**
127	-0.01	0.00	-0.04	0.00	-0.01	0.01	0.07	0.12	0.04	-0.19	0.09	0.01	0.06	0.01	0.05	0.06	-0.08	-0.10	-0.02	-0.05	0.19	-0.02	-0.02	0.00	0.00	0.00	0.04	-0.01	0.10	0.09	0.05	-0.09

Table A. 4: Table A. 5: Biases matrix for the second hidden layer B_{k}^{2}.

k	**0**	**1**	**2**	**3**	**4**	**5**	**6**	**7**	**8**	**9**	**10**	**11**	**12**	**13**	**14**	**15**	**16**	**17**	**18**	**19**	**20**	**21**	**22**	**23**	**24**	**25**
B_k	0.04	-0.02	0.07	-0.16	-0.01	-0.03	-0.02	0.14	-0.08	0.03	-0.11	-0.05	-0.08	0.02	0.01	0.02	-0.07	0.00	-0.06	-0.01	-0.09	-0.13	-0.05	-0.01	0.04	-0.01
k	**26**	**27**	**28**	**29**	**30**	**31**																				
B_k	0.03	-0.04	0.02	0.00	-0.01	-0.30																				

Table A. 6: Weight matrix for the third hidden layer W_{ik}^{3}.

Hidden Layer 2	Hidden Layer 3							
	0	**1**	**2**	**3**	**4**	**5**	**6**	**7**
0	0.14	-0.07	-0.08	-0.12	0.09	-0.27	-0.07	-0.36
1	0.19	-0.05	-0.18	0.00	0.45	0.16	-0.09	-0.19
2	-0.70	0.17	-0.37	0.20	-0.63	-0.06	0.43	0.27
3	-0.67	0.36	0.22	0.21	-0.43	0.10	-0.11	0.31
4	0.13	-0.24	-0.07	-0.03	0.28	-0.21	0.08	-0.20
5	0.16	-0.04	-0.14	-0.04	0.33	-0.25	-0.32	-0.08
6	0.33	-0.28	0.07	-0.11	0.59	-0.07	-0.12	-0.01
7	-0.48	0.19	0.19	0.08	-0.70	0.17	0.16	0.12
8	0.28	-0.18	-0.15	-0.16	0.05	-0.28	-0.20	-0.19
9	-0.71	0.19	0.35	0.00	-0.77	0.21	-0.18	0.18
10	-0.63	0.07	0.00	0.05	-0.59	0.02	0.16	0.10
11	0.31	-0.10	-0.06	-0.10	0.33	-0.10	-0.06	-0.06
12	0.34	-0.21	-0.10	-0.23	0.26	-0.15	-0.13	-0.28
13	0.32	0.02	-0.10	-0.01	0.41	-0.24	0.13	-0.11
14	0.26	-0.12	-0.12	-0.32	0.36	-0.13	0.01	-0.15
15	0.72	-0.10	-0.03	-0.17	0.48	-0.13	-0.26	-0.21
16	0.71	0.08	0.20	0.10	0.49	0.11	-0.07	0.04
17	-0.48	-0.01	0.05	0.03	-0.72	0.04	0.10	0.32
18	0.08	-0.19	-0.04	0.02	0.26	0.00	-0.09	-0.09
19	0.35	-0.12	-0.09	-0.18	0.09	-0.47	-0.12	-0.38

Table A. 6: Weight matrix for the third hidden layer W_{ik}^{3} (Continued).

Hidden Layer 2	Hidden Layer 3							
	0	**1**	**2**	**3**	**4**	**5**	**6**	**7**
20	0.37	-0.11	-0.05	-0.29	0.21	-0.13	-0.13	-0.05
21	-0.57	0.44	-0.23	0.19	-0.98	0.26	-0.10	0.11
22	0.77	0.07	-0.31	-0.16	0.63	-0.07	-0.10	-0.12
23	0.12	-0.06	-0.12	-0.04	0.15	-0.26	-0.20	-0.11
24	0.68	-0.15	-0.12	-0.15	0.48	-0.06	-0.08	-0.10
25	0.43	-0.06	-0.18	-0.26	0.26	-0.17	-0.01	-0.22
26	0.79	0.01	-0.14	0.00	0.88	-0.01	0.10	0.05
27	0.44	-0.18	-0.12	-0.21	0.17	-0.34	0.08	-0.06
28	0.15	-0.11	-0.06	-0.12	0.18	-0.28	-0.12	-0.12
29	0.57	-0.11	-0.02	-0.17	0.30	-0.08	-0.24	-0.02
30	0.20	-0.13	-0.19	-0.17	0.14	-0.16	-0.21	-0.44
31	-0.69	0.04	0.43	0.16	-1.10	-0.11	0.40	0.03

Table A. 7: Biases matrix for the third hidden layer B_{k}^{3}

k	**0**	**1**	**2**	**3**	**4**	**5**	**6**	**7**
B_k	0.72	0.46	0.36	0.35	0.57	0.38	0.00	0.40

Table A. 8: Weight matrix for the output layer W_{ik}^{4}.

Hidden Layer 3	Output
	0
0	0.39
1	-0.39
2	-0.69
3	-0.51
4	0.42
5	-0.70
6	-0.61
7	-0.35

Table A. 9: Biases matrix for the output layer B_{k}^{4}

k	**0**
Bk	4.86

APPENDIX B

PROFILE SENSITIVITY ANALYSIS

B.1. Sensitivity Inputs

The inputs required to perform Profile sensitivity analysis require the data for five quantiles including: minimum, the 25% percentile, the 50% percentile, the 75% percentile, and the maximum. These values are listed in Table B. 1.

Table B. 1: Input considerations for Profile sensitivity analysis.

Input	Mean	Stdv	Min.	25%	50%	75%	Max.
Cumulative Traffic (Thousand ESALs)	1896.6	2177	0	493	1192	2471	21173
Construction Variability	37%	12%	14%	28%	35%	44%	73%
Precipitation (in.)	37.2	14.8	7.4	26.7	43.0	49.5	65.0
MMAT (^{o}F)	14.7	3.7	6.8	12.4	15.3	17.2	24.6
MAAT (^{o}F)	60.0	10.4	35.9	51.9	62.1	67.3	75.3
Avg. Wind Velocity (mi./s)	5.5	2.3	0.0	4.5	6.6	6.8	11.5
Thickness - AC1 (in.)	2.3	1.1	0.8	1.6	1.9	2.4	7.0
Gmm - AC1	2.5	0.1	2.3	2.4	2.5	2.5	2.7
AV - AC1 (%)	6.2	3.0	1.3	3.9	5.8	7.8	19.7
Pb - AC1 (%)	4.9	0.9	2.0	4.5	4.8	5.4	7.4
Penetration - AC 1 (.1mm)	77.2	22.9	41.0	62.0	71.0	87.0	185.0
% Passing #4 - AC1	57.0	10.2	16.0	52.5	57.6	63.0	80.0
% Passing #200 - AC1	5.5	1.3	1.1	4.4	5.8	6.5	10.0
NMAS - AC1 (mm)	-	-	9.5	12.5	12.5	19.0	25.0
Thickness - AC2 (in.)	4.2	2.2	0.9	2.5	3.6	5.2	17.1
Gmm - AC2	2.5	0.1	2.3	2.4	2.5	2.5	2.7
AV - AC2 (%)	5.9	2.9	0.4	3.5	5.7	7.7	23.8
Pb - AC2 (%)	4.7	0.8	2.0	4.1	4.8	5.2	6.9
% Passing #4 - AC2	52.3	11.0	5.0	45.8	52.0	60.0	79.0

Table B. 1: Input considerations for Profile sensitivity analysis.

Input	Mean	Stdv	Min.	25%	50%	75%	Max.
% Passing #200 - AC2	5.6	1.5	1.3	4.8	5.5	6.8	11.5
NMAS - AC2 (mm)	17.8	4.7	9.5	12.5	19.0	19.0	25.0
Thickness - Base 1 (in.)	7.9	4.0	0.0	4.1	8.0	10.9	28.0
Material Type - Base 1 (0-DGAB, 1-ATB)	-	-	0	-	-	-	1
Thickness - Base 2 (in.)	2.4	3.3	0.0	0.0	0.0	4.0	13.4
Material Type - Base 2 (0-None, 1-DGAB)	-	-	0	-	-	-	1
Material Type - Base 2 (0-DGAB, 1-ATB)	-	-	0	-	-	-	1
Thickness - Subbase (in.)	5.1	6.9	0.0	0.0	4.0	8.0	54.0
Material Type - Subbase (0-None, 1-DGAB)	-	-	0	-	-	-	1
M_R - Subgrade (psi)	10560	3204	3606	8454	10421	12564	30791

B.2. Sensitivity Inputs

Results of the sensitivity analysis include two indices: the sensitivity value and the elasticity value. For input sensitivity and elasticity are calculated over several values. The summary statistics of all these computations are provided in Table B. 2 and Table B. 3.

Table B. 2: Sensitivity values outputs statistics.

Input	Sensitivity					
	Min	25%	50%	75%	Avg.	Max
Cumulative Traffic (Thousand ESALs)	0.000	0.000	0.000	0.000	0.001	0.008
Construction Variability	-20.608	-14.032	-11.905	-7.968	-11.351	-2.876
Precipitation (in.)	-0.056	-0.021	-0.012	-0.007	-0.016	0.002
MMAT (^{o}F)	0.021	0.154	0.241	0.304	0.235	0.535
MAAT (^{o}F)	0.033	0.065	0.079	0.174	0.133	0.432
Avg. Wind Velocity (mi./s)	0.087	0.356	0.604	0.653	0.554	1.295

Table B. 2: Sensitivity values outputs statistics (Continued).

Input	Sensitivity					
	Min	**25%**	**50%**	**75%**	**Avg.**	**Max**
Thickness - AC1 (in.)	-0.148	0.031	0.141	0.278	0.188	1.148
Gmm - AC1	-4.801	-0.835	-0.014	0.729	-0.233	2.735
AV - AC1 (%)	-0.205	-0.057	-0.032	0.006	-0.016	0.272
Pb - AC1 (%)	-1.341	-0.651	-0.275	-0.127	-0.357	0.092
Penetration - AC 1 (.1mm)	-0.076	-0.008	-0.003	0.002	-0.011	0.008
% Passing #4 - AC1	0.018	0.052	0.077	0.101	0.076	0.168
% Passing #200 - AC1	-0.898	0.117	0.272	0.378	0.189	0.673
NMAS - AC1 (mm)	0.032	0.032	0.033	0.084	0.050	0.084
Thickness - AC2 (in.)	0.026	0.163	0.207	0.277	0.215	0.354
Gmm - AC2	-29.276	-14.295	-12.537	-9.149	-11.570	-1.053
AV - AC2 (%)	-0.238	0.033	0.056	0.081	0.039	0.148
Pb - AC2 (%)	-2.868	-0.528	0.097	0.243	-0.208	0.605
% Passing #4 - AC2	-0.248	-0.196	-0.056	-0.015	-0.093	0.024
% Passing #200 - AC2	-0.223	-0.114	-0.002	0.070	-0.015	0.173
NMAS - AC2 (mm)	-0.070	-0.070	-0.059	0.019	-0.037	0.019
Thickness - Base 1 (in.)	-0.467	-0.105	-0.010	0.067	-0.075	0.121
Thickness - Base 2 (in.)	-0.455	-0.291	-0.157	-0.009	-0.168	0.061
Thickness - Subbase (in.)	-0.101	-0.041	0.012	0.018	-0.008	0.055
M_R - Subgrade (psi)	0.000	0.000	0.000	0.000	0.000	0.001

Table B. 3: Elasticity values outputs statistics.

Input	Elasticity						Rank
	Min	**25%**	**50%**	**75%**	**Avg.**	**Max**	
Cumulative Traffic (Thousand ESALs)	4.0%	15.2%	25.6%	42.8%	36.9%	297.5%	9
Construction Variability	-173%	-112%	-57%	-43%	-78%	-23%	5
Precipitation (in.)	-32%	-9%	-7%	-2%	-8%	1%	18
MMAT (^{o}F)	4%	36%	57%	73%	57%	116%	6
MAAT (^{o}F)	30%	67%	95%	262%	159%	485%	2
Avg. Wind Velocity (mi./s)	0%	28%	63%	73%	53%	108%	4
Thickness - AC1 (in.)	-14%	2%	7%	11%	6%	20%	17
Gmm - AC1	-170%	-29%	-1%	28%	-7%	96%	24

Table B. 3: Elasticity values outputs statistics (Continued.

Input	Elasticity						Rank
	Min	25%	50%	75%	Avg.	Max	
AV - AC1 (%)	-34%	-14%	-4%	2%	-6%	17%	21
Pb - AC1 (%)	-108%	-62%	-14%	-5%	-33%	7%	11
Penetration - AC 1 (.1mm)	-97%	-14%	-3%	6%	-15%	26%	22
% Passing #4 - AC1	9%	39%	72%	91%	67%	145%	3
% Passing #200 - AC1	-88%	8%	20%	26%	11%	48%	10
NMAS - AC1 (mm)	5%	5%	9%	17%	11%	17%	15
Thickness - AC2 (in.)	1%	12%	27%	40%	26%	46%	8
Gmm - AC2	-1094%	-572%	-412%	-359%	-442%	-60%	1
AV - AC2 (%)	-30%	2%	10%	17%	8%	23%	13
Pb - AC2 (%)	-209%	-56%	4%	12%	-23%	39%	20
% Passing #4 - AC2	-61%	-40%	-29%	-12%	-26%	21%	7
% Passing #200 - AC2	-21%	-5%	0%	9%	2%	24%	25
NMAS - AC2 (mm)	-9%	-10%	-9%	0%	-6%	0%	14
Thickness - Base 1 (in.)	-106%	-18%	-1%	28%	-5%	57%	23
Thickness - Base 2 (in.)	-35%	-23%	-11%	-1%	-11%	14%	12
Thickness - Subbase (in.)	-28%	-7%	8%	13%	4%	30%	16
M_R - Subgrade (psi)	-10%	0%	5%	19%	12%	76%	19

REFERENCES

[1] F. Finn, “Pavement management systems--Past, present, and future,” *Public Roads*, vol. 62, no. 1, 1998.

[2] K. Ozbay and R. Laub, “Models for pavement deterioration using LTPP,” 2001.

[3] ASCE, “2017 infrastructure report card,” 2017.

[4] ASCE., “2013 report card for America’s infrastructure,” 2013.

[5] TRIP, “The Interstate Highway System turns 60: Challenges to Its Ability to Continue to Save Lives, Time and Money,” Washington, DC., 2016.

[6] H. Pérez-Acebo, A. Linares-Unamunzaga, R. Abejón, and E. Rojí, “Research trends in pavement management during the first years of the 21st century: A bibliometric analysis during the 2000–2013 period,” *Appl. Sci.*, vol. 8, no. 7, p. 1041, 2018.

[7] W. R. Hudson, R. Haas, and R. D. Pedigo, “Pavement Management System Development,” 1979.

[8] K. A. Zimmerman and P. V Ram, “Pavement Management’s Role in an Asset Management World,” in *9th International Conference on Managing Pavement Assets*, 2015.

[9] 112th Congress, “Moving Ahead for Progress in the 21st Century Act (MAP-21),” *LAW 112–141*, p. 141, 2012.

[10] FHWA, “Transportation Asset Management Plan Development Processes Certification and Recertification Guidance,” Washington, D.C., 2018.

[11] J. A. Prozzi and S. M. Madanat, “Development of pavement performance models by combining experimental and field data,” *J. Infrastruct. Syst.*, vol. 10, no. 1, pp. 9–22, 2004.

[12] N. Li, R. Haas, and W.-C. Xie, “Investigation of relationship between deterministic and probabilistic prediction models in pavement management,” *Transp. Res. Rec.*, vol. 1592, no. 1, pp. 70–79, 1997.

[13] Z. Alyami, D. Mizutani, K. Kaito, and S. Tighe, “A dynamic optimal model for pavement asset management and PPP projects,” in *Pavement and Asset Management: Proceedings of the World Conference on Pavement and Asset Management (WCPAM 2017), June 12-16, 2017, Baveno, Italy*, 2019, p. 175.

[14] C.-Y. Chu and P. L. Durango-Cohen, “Estimation of dynamic performance models for transportation infrastructure using panel data,” *Transp. Res. Part B Methodol.*, vol. 42, no. 1, pp. 57–81, 2008.

[15] A. S. Wolters and K. A. Zimmerman, “Current practices in pavement performance modeling project 08-03 (C07): task 4 report final summary of

findings.," Pennsylvania. Dept. of Transportation. Bureau of Planning and Research, 2010.

[16] Advanced Research Associates, "AASHTO guide for design of pavement structure," *NCHRP 1-37A Proj. Natl. Res. Counc.*, no. July, 2002.

[17] A. R. Archilla and S. Madanat, "Development of a Pavement Rutting Model from Experimental Data," *J. Transp. Eng.*, vol. 126, no. 4, pp. 291–299, 2000.

[18] O. S. El-Haggan, "Evaluation of Rutting Behavior of Density Deficient Asphalt Mixtures," 2003.

[19] Y. Zhang, X. Luo, Y. Deng, S. Hou, X. Shi, and R. L. Lytton, "Evaluation of Rutting Potential of Flexible Pavement Structures using Energy-based Pseudo Variables," *Constr. Build. Mater.*, vol. 247, p. 118391, 2020.

[20] K. P. George, A. S. Rajagopal, and L. K. Lim, "Models for Predicting Pavement Deterioration," *Transp. Res. Rec.*, no. 1215, 1989.

[21] A. S. Wolters and K. A. Zimmerman, "Current Practices in Pavement Performance Modeling," 2010.

[22] K. P. George, "MDOT pavement management system: prediction models and feedback system," Mississippi. Dept. of Transportation, 2000.

[23] N. Li, "Development of a probabilistic based, integrated pavement management system," UWSpace, 1997.

[24] H. L. Von Quintus, *Calibration of Rutting Models for Structural and Mix Design*, vol. 719. Transportation Research Board, 2012.

[25] L. Yao, Q. Dong, J. Jiang, and F. Ni, "Establishment of Prediction Models of Asphalt Pavement Performance based on a Novel Data Calibration Method and Neural Network," *Transp. Res. Rec.*, p. 0361198118822501, 2019.

[26] D. T. Thube, "Artificial Neural Network (ANN) Based Pavement Deterioration Models for Low Volume Roads in India," *Int. J. Pavement Res. Technol.*, vol. 5, no. 2, pp. 115–120, 2012.

[27] J. Yang, J. J. Lu, M. Gunaratne, and Q. Xiang, "Overall Pavement Condition Forecasting Using Neural Networks—An Application to Florida Highway Network," in *82nd annual meeting of the transportation research board*, 2003.

[28] X. Huang, J. Zhang, and H. Li, "Development of a Mechanics Model for Three-Phase Permanent Deformation of Asphalt Mixture Under Repeated Load," in *87th Annual Meeting of the Transportation Research Board*, 2007.

[29] AASHTO, *Pavement Management Guide*, Second Edi. Washington, D.C: American Association of State Highway and Transportation Officials, 2012.

[30] A. M. G. Ribeiro, S. D. Capitão, and R. G. Correia, "Deciding on maintenance of small municipal roads based on GIS simplified procedures," *Case Stud. Transp. Policy*, vol. 7, no. 2, pp. 330–337, 2019.

[31] W. Zheng, F. Gerardo, F. Adelino, and P.-S. L. de, "Framework for

Multiobjective Optimization of Physical Highway Assets Investments," *J. Transp. Eng.*, vol. 138, no. 12, pp. 1411–1421, Dec. 2012.

[32] A. Wolters, K. Zimmerman, K. Schattler, and A. Rietgraf, "Implementing pavement management systems for local agencies—State-of-the-art/state-of-the-practice synthesis," 2011.

[33] M. Y. Shahin, "Components of a Pavement Maintenance Management System," *Transp. Res. Rec.*, no. 781, 1980.

[34] U. Rusmanto, Syafi'i, and D. Handayani, "Structural and Functional Prediction of Pavement Condition (A Case Study on South Arterial Road, Yogyakarta)," in *AIP Conference Proceedings*, 2018, vol. 1977, no. 1, p. 40014.

[35] R. Haas and W. R. Hudson, *Pavement Asset Management*. John Wiley & Sons, Inc., 2015.

[36] L. M. Pierce, G. McGovern, and K. A. Zimmerman, "Practical Guide for Quality Management of Pavement Condition Data Collection," United States Federal Highway Administration, Washington, DC, 2013.

[37] S. Ercisli, "Development of Enhanced Pavement Deterioration Curves." Virginia Tech, 2015.

[38] AASHTO and TRIP, *Rough Roads Ahead: Fix them Now or Pay for it Later*. Washington D.C.: e American Association of State Highway and Transportation Officials, 2009.

[39] J. S. Miller and W. Y. Bellinger, "Distress identification manual for the long-term pavement performance program," United States. Federal Highway Administration. Office of Infrastructure Research and Development, 2014.

[40] W. L. Gramling, J. E. Hunt, and G. S. Suzuki, "Rational Approach to Cross-Profile and Rut Depth Analysis," *Transp. Res. Rec.*, vol. 1311, pp. 173–179, 1991.

[41] A. L. Simpson, "Measurement of Rutting in Asphalt Pavements," The University of Texas at Austin, 2001.

[42] A. L. Simpson, "Characterization of Transverse Profile," *Transp. Res. Rec.*, vol. 1655, no. 1, pp. 185–191, 1999.

[43] M. W. Witczak and M. M. El-Basyouny, "Appendix GG-1: Calibration of Permanent Deformation Models for Flexible Pavements," Washington D.C., 2004.

[44] F. Zhou and T. Scullion, "Discussion: Three Stages of Permanent Deformation Curve and Rutting Model," *Int. J. Pavement Eng.*, vol. 3, no. 4, pp. 251–260, 2002.

[45] K. Kaloush *et al.*, "Tertiary Flow Characteristics of Asphalt," *J. Assoc. Asph. Paving Technol.*, pp. 248–280, 2002.

[46] F. Alharbi, "Predicting Pavement Performance Utilizing Artificial Neural Network (ANN) Models," Iowa State University, 2018.

[47] H. Gong, Y. Sun, Z. Mei, and B. Huang, “Improving accuracy of rutting prediction for mechanistic-empirical pavement design guide with deep neural networks,” *Constr. Build. Mater.*, vol. 190, pp. 710–718, 2018.

[48] C. W. Schwartz, R. Li, H. Ceylan, S. Kim, and K. Gopalakrishnan, “Global Sensitivity Analysis of Mechanistic–Empirical Performance Predictions for Flexible Pavements,” *Transp. Res. Rec.*, vol. 2368, no. 1, pp. 12–23, 2013.

[49] N. Jackson and J. Puccinelli, “Long-Term Pavement Performance (LTPP) Data Analysis Support : National Pooled Fund Study TPF-5 (013),” 2006.

[50] G. Zou, J. Xu, and C. Wu, “Evaluation of factors that affect rutting resistance of asphalt mixes by orthogonal experiment design,” *Int. J. Pavement Res. Technol.*, vol. 10, no. 3, pp. 282–288, 2017.

[51] R. A. Tarefder, L. White, and M. Zaman, “Development and application of a rut prediction model for flexible pavement,” *Transp. Res. Rec.*, vol. 1936, no. 1, pp. 201–209, 2005.

[52] P. A. Serigos, J. A. Prozzi, B. H. Nam, and M. R. Murphy, “Field Evaluation of Automated Rutting Measuring Equipment,” Austin, TX, 2012.

[53] T. F. Fwa, L. Chu, and K. H. Tan, “Rational Procedure for Determination of Rut Depth Intervention Level in Network-Level Pavement Management,” *Transp. Res. Rec.*, vol. 2589, no. 1, pp. 59–67, Jan. 2016.

[54] F. T. F., P. H. R., and O. G. P., “Critical Rut Depth for Pavement Maintenance Based on Vehicle Skidding and Hydroplaning Consideration,” *J. Transp. Eng.*, vol. 138, no. 4, pp. 423–429, Apr. 2012.

[55] G. Y. Baladi, T. Dawson, G. Musunuru, M. Prohaska, and K. Thomas, “Pavement Performance Measures and Forecasting and the Effects of Maintenance and Rehabilitation Strategy on Treatment Effectiveness,” United States. Federal Highway Administration, 2017.

[56] AASHTO, *Mechanistic-Empirical Pavement Design Guide: A Manual of Practice*. Washington D.C.: American Association of State Highway and Transportation Officials, 2015.

[57] G. Jameson and K. G. Sharp, *Technical Basis of Austroads Pavement Design Guide*. Sydney, New South Wales Australia: AUSTROADS, 2004.

[58] AASHTO, *Guide Specifications for Highway Construction*, 9th Editio. American Association of State Highway and Transportation Officials (AASHTO), 2008.

[59] Caltrans, “Chapter A Flexible Pavement,” in *Caltrans Maintenance Manual*, Sacramento, CA: California Department of Transportation, 2014.

[60] ASTM International, “ASTM D6433-18, Standard Practice for Roads and Parking Lots Pavement Condition Index Surveys,” West Conshohocken, PA, 2018.

[61] ASTM International, “ASTM D6433-18, Standard Practice for Roads and Parking Lots Pavement Condition Index Surveys,” West Conshohocken, PA,

2018.

[62] IDOT, “Bureau of Local Roads and Streets Manual: Local Agency Pavement Preservation,” Illinois Department of Transportation, Springfield, Illinois, 2005.

[63] MDSHA, “Guide to Pavement Preservation,” 2011.

[64] NCDOT, “Digital Imagery Distress Evaluation Handbook,” Raleigh, NC, 2011.

[65] NDOT, “Fully-Compliant Transportation Asset Management Plan,” Carson City, Nevada, 2019.

[66] TxDOT, “Pavement Management Information System Rater’s Manual for Fiscal Year 2016,” Austin, Texas, 2015.

[67] Northwest Pavement Management Association, “Pavement Surface Condition Field Rating Manual for Asphalt Pavements,” Washington, D.C, 1999.

[68] Roadway Engineering Group, “ADOT Pavement Design Manual,” Phoenix, Arizona, 2017.

[69] BC MTI, *Pavement Surface Condition Rating Manual*, Fifth Edit. British Columbia Ministry of Transportation and Infrastructure, 2016.

[70] G. J. Chong, W. A. Phang, and G. A. WRONG, *Manual for Condition Rating of Flexible Pavements Distress Manifestations*. Ontario Ministry of Transportation, 2016.

[71] M. S. R. Amin, “The Pavement Performance Modeling: Deterministic vs. Stochastic Approaches,” in *Numerical methods for reliability and safety assessment*, Springer, 2015, pp. 179–196.

[72] R. B. Kulkarni and R. W. Miller, “Pavement Management Systems: Past, Present, and Future,” *Transp. Res. Rec.*, vol. 1853, no. 1, pp. 65–71, Jan. 2003.

[73] S. S. Jain, M. Parida, and D. T. Thube, “HDM-4 based optimal maintenance strategies for low-volume roads in India,” *Road Transp. Res. A J. Aust. New Zeal. Res. Pract.*, vol. 16, no. 4, p. 3, 2007.

[74] World Bank, “HDM-4: Deterioration of Bituminous Roads,” 2008.

[75] NDLI, “Modelling Road Deterioration and Maintenance Effects in HDM-4,” 1995.

[76] A. Bannour, M. El Omari, E. K. Lakhal, M. Afechkar, A. Benamar, and P. Joubert, “Optimization of the maintenance strategies of roads in Morocco: calibration study of the degradations models of the highway development and management (HDM-4) for flexible pavements,” *Int. J. Pavement Eng.*, vol. 20, no. 2, pp. 245–254, 2019.

[77] L. B. Abu-Ennab, “Developing pavement performance prediction models for the state of Arkansas,” University of Arkansas at Little Rock, 2015.

[78] L. Choummanivong and T. Martin, “Predicting Structural Deterioration of Pavements at a Network Level–Interim Models,” *Austroads Publ. No. AP–*

T159/10, ARRB., 2010.

[79] G. Dzotepe and K. Ksaibati, “Implementation of the mechanistic-empirical pavement design guide (MEPDG),” *Univ. Wyoming, Laramie, WY*, 2010.

[80] P. D. Hunt and J. M. Bunker, “Time series analysis of pavement roughness condition data for use in asset management,” 2003.

[81] L. E. (Concordia U. Amador-Jiménez and D. (University of N. B. Mrawira, “Bayesian Regression in Pavement Deterioration Modeling: Revisiting the AASHO Road Test Rut Depth Model,” *Infraestruct. Vial*, vol. 14, no. 25, pp. 28–35, 2012.

[82] P. Saha, K. Ksaibati, and R. Atadero, “Developing pavement distress deterioration models for pavement management system using Markovian probabilistic process,” *Adv. Civ. Eng.*, vol. 2017, 2017.

[83] K. A. Abaza, “Simplified staged-homogenous Markov model for flexible pavement performance prediction,” *Road Mater. Pavement Des.*, vol. 17, no. 2, pp. 365–381, 2016.

[84] M. Abambres and A. Ferreira, “Application of ANN in Pavement Engineering: State-of-Art,” *Available SSRN 3351973*, 2017.

[85] D. T. Thube, “Performance based maintenance management for rural roads,” Indian Institute of Technology Roorkee, 2006.

[86] F. Hong and J. A. Prozzi, “Updating pavement deterioration models using the Bayesian principles and simulation techniques,” in *1st Annual Inter-University Symposium on Infrastructure Management*, 2005.

[87] E. S. Park, R. E. Smith, T. J. Freeman, and C. H. Spiegelman, “A Bayesian approach for improved pavement performance prediction,” *J. Appl. Stat.*, vol. 35, no. 11, pp. 1219–1238, 2008.

[88] N. Li, R. Haas, and W.-C. Xie, “Development of a new asphalt pavement performance prediction model,” *Can. J. Civ. Eng.*, vol. 24, no. 4, pp. 547–559, 1997.

[89] F. Hong and J. A. Prozzi, “Estimation of pavement performance deterioration using Bayesian approach,” *J. Infrastruct. Syst.*, vol. 12, no. 2, pp. 77–86, 2006.

[90] M. I. Hossain, L. S. P. Gopisetti, and M. S. Miah, “International Roughness Index Prediction of Flexible Pavements Using Neural Networks,” *J. Transp. Eng. Part B Pavements*, vol. 145, no. 1, p. 4018058, 2018.

[91] G. E. Elkins, T. Thompson, B. Ostrom, and B. Visintine, “Long-Term Pavement Performance Information Management System User Guide,” McLean, VA., 2018.

[92] D. Aleksendric and P. Carlone, *Soft Computing in the Design and Manufacturing of Composite Materials: Applications to Brake Friction and Thermoset Matrix Composites*. Woodhead Publishing, 2015.

[93] M. Y. Rafiq, G. Bugmann, and D. J. Easterbrook, “Neural network design for

engineering applications," *Comput. Struct.*, vol. 79, no. 17, pp. 1541–1552, 2001.

[94] L. Liu, "A Methodology for Developing Performance-Related Specifications for Pavement Preservation Treatments." 2013.

[95] G. Dreyfus, *Neural networks: methodology and applications*. Springer Science & Business Media, 2005.

[96] M. S. Hasan, "Deterioration Prediction of concrete bridge components using artificial intelligence and stochastic methods," no. March, 2015.

[97] X. Yao, "Evolving artificial neural networks," *Proc. IEEE*, vol. 87, no. 9, pp. 1423–1447, 1999.

[98] I. Goodfellow, Y. Bengio, and A. Courville, *Deep learning*. MIT press, 2016.

[99] H. Ceylan, M. B. Bayrak, and K. Gopalakrishnan, "Neural networks applications in pavement engineering: A recent survey," *Int. J. Pavement Res. Technol.*, vol. 7, no. 6, pp. 434–444, 2014.

[100] A. Géron, *Hands-On Machine Learning with Scikit-Learn, Keras, and TensorFlow: Concepts, Tools, and Techniques to Build Intelligent Systems*. O'Reilly Media, 2019.

[101] J. D. Olden and D. A. Jackson, "Illuminating the 'black box': a randomization approach for understanding variable contributions in artificial neural networks," *Ecol. Modell.*, vol. 154, no. 1–2, pp. 135–150, 2002.

[102] I. Guyon and A. Elisseeff, "An introduction to variable and feature selection," *J. Mach. Learn. Res.*, vol. 3, no. Mar, pp. 1157–1182, 2003.

[103] S. Kaushik, "Introduction to Feature Selection methods with an example (or how to select the right variables?)," *Anal. Vidhya*, 2016.

[104] A. Zheng and A. Casari, *Feature engineering for machine learning: principles and techniques for data scientists*. " O'Reilly Media, Inc.," 2018.

[105] P. Terence, T. Kerem, C. Christopher, and H. Jeremy, "Beware default random forest importances." 2018.

[106] L. Bertino, G. Evensen, and H. Wackernagel, "Sequential data assimilation techniques in oceanography," *Int. Stat. Rev.*, vol. 71, no. 2, pp. 223–241, 2003.

[107] W. Slika and G. Saad, "An Ensemble Kalman Filter Approach for Service Life Prediction of Reinforced Concrete Structures Subject to Chloride-Induced Corrosion," *Constr. Build. Mater.*, vol. 115, pp. 132–142, 2016.

[108] E. Di Lorenzo, S. Zedler, I. Hoteit, R. Milliff, and B. Cornuelle, "Theory and Applications of Variational, Sequential and Bayesian Hierarchical Methods in Data Assimilation," *AGU Fall Meet. Abstr.*, Dec. 2008.

[109] G. Evensen, "Sequential data assimilation for nonlinear dynamics: the ensemble Kalman filter," in *Ocean Forecasting*, Springer, 2002, pp. 97–116.

[110] D. T. Pham, "Stochastic methods for sequential data assimilation in strongly

nonlinear systems," *Mon. Weather Rev.*, vol. 129, no. 5, pp. 1194–1207, 2001.

[111] G. Evensen, "The Ensemble Kalman Filter: Theoretical Formulation and Practical Implementation," *Ocean Dyn.*, vol. 53, no. 4, pp. 343–367, 2003.

[112] S. Gillijns, O. B. Mendoza, J. Chandrasekar, B. L. R. De Moor, D. S. Bernstein, and A. Ridley, "What is the ensemble Kalman filter and how well does it work?," in *2006 American Control Conference*, 2006, pp. 6-pp.

[113] M. M. El-Basyouny, *Calibration and Validation of Asphalt Concrete Pavements Distress Models for 2002 Design Guide*. Arizona State University, 2004.

[114] W. S. Cleveland and S. J. Devlin, "Locally weighted regression: an approach to regression analysis by local fitting," *J. Am. Stat. Assoc.*, vol. 83, no. 403, pp. 596–610, 1988.

[115] Fugro Consultants Inc. and Arizona State University, "NCHRP Report 704: A Performance-Related Specification for Hot-Mixed Asphalt," Washington, 2011.

[116] FHWA, *Traffic Data Computation Method: Pocket Guide*. Washington, D.C: U.S. Department of Transportation, Federal Highway Administration, Office of Highway Policy Information, 2018.

[117] Y. H. Huang, *Pavement Analysis and Design*. Pearson Education, 2012.

[118] D. Andrei, M. W. Witczak, C. W. Schwartz, and J. Uzan, "Harmonized Resilient Modulus Test Method for Unbound Pavement Materials," *Transp. Res. Rec.*, vol. 1874, no. 1, pp. 29–37, 2004.

[119] A. Gelman and J. Hill, Eds., "Missing-data imputation," in *Data Analysis Using Regression and Multilevel/Hierarchical Models*, Cambridge: Cambridge University Press, 2006, pp. 529–544.

[120] M. A. Hall, "Correlation-based feature selection for machine learning," 1999.

[121] J. Moolayil, "Tuning and Deploying Deep Neural Networks BT - Learn Keras for Deep Neural Networks: A Fast-Track Approach to Modern Deep Learning with Python," J. Moolayil, Ed. Berkeley, CA: Apress, 2019, pp. 137–159.

[122] K. He, X. Zhang, S. Ren, and J. Sun, "Deep Residual Learning for Image Recognition," in *2016 IEEE Conference on Computer Vision and Pattern Recognition (CVPR)*, 2016, pp. 770–778.

[123] X. Zhang, X. Chen, L. Yao, C. Ge, and M. Dong, "Deep Neural Network Hyperparameter Optimization with Orthogonal Array Tuning," in *International Conference on Neural Information Processing*, 2019, pp. 287–295.

[124] A. Fisher, C. Rudin, and F. Dominici, "Model class reliance: Variable importance measures for any machine learning model class, from the" rashomon" perspective," *arXiv Prepr. arXiv1801.01489*, vol. 68, 2018.

[125] M. Gevrey, I. Dimopoulos, and S. Lek, "Review and Comparison of Methods to Study the Contribution of Variables in Artificial Neural Network Models," *Ecol. Modell.*, vol. 160, no. 3, pp. 249–264, 2003.

[126] M. Cao, N. F. Alkayem, L. Pan, and D. Novák, “Advanced Methods in Neural Networks-Based Sensitivity Analysis with their Applications in Civil Engineering,” *Artif. neural networks Model. Appl. Rijeka, Croat. IntechOpen*, pp. 335–353, 2016.

[127] C. W. Schwartz *et al.*, “Evaluation of Long-Term Pavement Performance (LTTP) Climatic Data for Use in Mechanistic-Empirical Pavement Design Guide (MEPDG) Calibration and Other Pavement Analysis,” Turner-Fairbank Highway Research Center, 2015.

[128] K. H. McGhee, “Automated Pavement Distress Collection Techniques,” 2004, vol. 334.

[129] D. Wang, A. Cannone Falchetto, M. Goeke, W. Wang, T. Li, and M. P. Wistuba, “Influence of Computation Algorithm on the Accuracy of Rut Depth Measurement,” *J. Traffic Transp. Eng. (English Ed.*, vol. 4, no. 2, pp. 156–164, 2017.

[130] K. Jeyapalan, J. K. Cable, and R. Welper, “Iowa DOT Evaluation of the PASCO Road Survey System,” 1987.

[131] R. R. Picard and K. N. Berk, “Data Splitting,” *Am. Stat.*, vol. 44, no. 2, pp. 140–147, May 1990.

[132] F. J. Massey, “The Kolmogorov-Smirnov Test for Goodness of Fit,” *J. Am. Stat. Assoc.*, vol. 46, no. 253, pp. 68–78, Mar. 1951.

[133] H. Zou and T. Hastie, “Regularization and Variable Selection via the Elastic Net,” *J. R. Stat. Soc. Ser. B (statistical Methodol.*, vol. 67, no. 2, pp. 301–320, 2005.

[134] W. D. O. Paterson, *Road Deterioration and Maintenance Effects: Models for Planning and Management*. 1987.

[135] R. Wix, I. Espada, A. Rooke, and T. Martin, “Guide to Asset Management – Technical Information Part 15: Technical Supplements,” 2018.

[136] A. Altmann, L. Toloşi, O. Sander, and T. Lengauer, “Permutation importance: a corrected feature importance measure,” *Bioinformatics*, vol. 26, no. 10, pp. 1340–1347, 2010.

[137] R. B. Mallick, D. Singh, and A. Veeraragavan, “Extension of Asphalt Pavement Life by Reduction of Temperature,” *Transp. Dev. Econ.*, vol. 2, no. 1, p. 7, 2016.

[138] A. Sotil, *Use of the Dynamic Modulus E Test as Permanent Deformation Performance Criteria for Asphalt Pavement Systems*. Arizona State University, 2005.

[139] Z. Weiguang, S. Shihui, W. Shenghua, C. Xiao, X. Jiayue, and M. L. N., “Effects of In-Place Volumetric Properties on Field Rutting and Cracking Performance of Asphalt Pavement,” *J. Mater. Civ. Eng.*, vol. 31, no. 8, p. 4019150, Aug. 2019.